Time-Resolved Fluorescence Spectroscopy of Crude Petroleum Oils

Peter Owens B.Sc. M.Sc.

School of Chemistry

Presented for the degree of Ph.D.
of the National University of Ireland, Galway

Submitted March 2009

Supervisor:
Dr. A.G. Ryder, School of Chemistry

Head of School: ***Prof. P. V. Murphy***

Abstract

Characterisation of crude oil properties in real-time by spectroscopic methods has been a major challenge to the oil industry. While current methods can show the presence of oil, a quantitative determination of oil physical and chemical properties has yet to be found. Also the mechanisms of oil photophysics are far from being fully understood. This thesis seeks to address these issues by two principle objectives. First, the determination of fluorescence lifetimes for crude oils by the Frequency Domain method and second, the analysis of the effects of dilution and temperature on the photophysical properties of crude oils.

As a primary objective, a Frequency Domain (FD) method was developed to measure the fluorescence lifetimes of a series of crude oils. Analysis of the average lifetimes was made based on how many decay terms and the type of fitting model used. Correlations were made between the bulk chemical data for the oils and average lifetimes from distribution and discrete models. The FD method was then applied to the analysis of Hydrocarbon Fluid Inclusions (HCFI) where individual inclusions could be isolated and the average lifetime determined for the included oils. Comparisons were made between the lifetimes for the bulk oils and HCFI.

The second objective of the thesis was to examine the effects of dilution and temperature on the photophysical behaviour of crude petroleum oils. Comparisons were made between lifetimes over the range of temperatures sampled and differences between dilute and neat average lifetime values gave estimations of quenching effects. Lifetimes were monitored over a range of temperatures and were found to follow a simple Arrhenius-like behaviour. A modified Stern-Volmer quenching model could be applied to the crude oil lifetime data showing the presence of both static and dynamic quenching and the calculated quenching rate constants have been found to vary linearly with oil type. Neat and dilute oils also followed a reverse Eyring

behaviour allowing calculation of activation enthalpy and entropy values. Although the theory for the Arrhenius, Eyring and Stern-Volmer models is based on single fluorophore systems, they were found to apply for a complex system of multiple emitting and interacting fluorophores. In the context of these simple models, the average lifetime calculated for crude oils represented an summation of the excited state processes.

Preface

The work presented in this thesis has been carried out in the School of Chemistry at the National university of Ireland Galway during the years 2006-2009. Figures and tables not referenced throughout the text represent diagrams or data produced during this thesis.

I would like to thank my supervisor Dr. Alan Ryder for his support and encouragement over the course of this research. Thanks also go to Dr. Martin Feely who provided insight into the geological realm and kindly provided the low temperature stage.

This thesis was financially supported by Science Foundation Ireland (SFI Grant number 05/RFP/GEO0002), which is gratefully acknowledged.

I would like to dedicate the work presented herein to my wife Vera, daughter Lilian and our new addition to the family, Ruairí.

Peter Owens

Anatomy Department, NUIG January 2010

Contents

List of Publications and Presentations

The work outlined in this has been published, in part, in the following manuscripts:

Publications

1. P. Owens, A.G. Ryder and N.J.F. Blamey (2008), Frequency Domain Fluorescence Lifetime Study of Crude Petroleum Oils, *Journal of Fluorescence*, 18(5):997–1006.

2. P. Owens and A.G. Ryder, "Low temperature lifetime study of crude petroleum oils," *manuscript in preparation.*

Co-authored Papers

1. Blamey N.J.F., Ryder A.G., Feely M., Dockery P., Owens P. (2008), The application of structured-light illumination microscopy to hydrocarbon-bearing fluid inclusions, *Geofluids* 8(2): 102 -112.

2. Blamey N.J.F., Ryder A.G., Owens P. and Feely M., "Accurate characterisation of hydrocarbon-bearing fluid inclusions using frequency domain fluorescence lifetime measurements", *Manuscript in preparation.*

Abstracts and Presentations

1. Owens P. and Ryder A.G.,"Dynamics of crude oil fluorescence revealed by low temperature time-resolved single photon counting studies", *XXII IUPAC Symposium on Photochemistry*, Gothenburg, Sweden, 28th July -1st August 2008.[Poster]

2. Owens P., Ryder A.G., Blamey N.J.F. and Feely M., "Low temperature fluorescence lifetime studies of crude petroleum oils", *Photonics Ireland*, Galway, 24-26th September 2007.[Poster]

3. Owens P., Ryder A.G. and Blamey N.J.F., "Frequency Domain Fluorescence Lifetime Study of Crude Petroleum Oils", *10th Conference on Methods and Applications of Fluorescence: Spectroscopy, Imaging and Probes*, Salzburg, Austria, 9 - 12 September 2007.[Poster]

4. Owens P., Ryder A.G. and Blamey N.J.F., "Analysis of Crude Petroleum Oils using Frequency Domain Fluorescence Lifetime Measurements", *59th Irish Universities Chemistry Research Colloquium*, Dublin City University 13th-15th June 2007.[Presentation]

5. Owens P., Blamey N.J.F. and Ryder A.G., "Application of multi-frequency phase and modulation fluorometry to lifetime analysis of petroleum oils", *Infocus Magazine*, number 5, pp. 88-89, 2007.

6. Owens P., Ryder A.G. and Blamey N.J.F., "Fluorescence lifetime study on crude petroleum oils using the frequency domain technique", *50th Annual Irish Geological Research Meeting, University of Ulster*, Coleraine, 23rd-25th February 2007.[Presentation]

7. Owens P., Blamey N.J.F. and Ryder A.G., "Application of multi-frequency phase and modulation fluorometry to lifetime analysis of bulk petroleum oils". *Microscopical Society of Ireland 30th Annual Symposium*, Galway, 30th Aug. -1st September 2006.[Poster]

Abbreviations

Abbrev	Definition
API	American Petroleum Institute
APD	Avalanche Photo Diode
ASTM	American Society for Testing and Materials
CCD	Charge coupled device
CFD	Constant Fraction Discriminator
CLSM	Confocal Laser Scanning Microscope
CMOS	Complimentary Metal Oxide Semi-Conductor
DAC	Diamond Anvil Cell
DASPI	trans-4-[4-(DimethylAmino)-Styryl]-1-methylPyridinium Iodide
EEM	Excitation-Emission Matrix
FCS	Fluorescence Correlation Spectroscopy
FD	Frequency Domain
FLIM	Fluorescence Lifetime Imaging
FRET	Fluorescence Resonance Energy Transfer
FWHM	Full Width Half Maximum
GC	Gas Chromatography
GOR	Gas Oil Ratio
HCFI	Hydro Carbon Fluid Inclusions
HOMO	Highest occupied molecular orbital
HPLC	High Performance Liquid Chromatography
HPTS	8-hydroxypyrene-1,3,6-trisulphonic acid trisodium salt
IRF	Instrument Response Function
LC	Liquid Chromatography
LUMO	Lowest unoccupied molecular orbital
MS	Mass Spectroscopy
MPLC	Medium Pressure Liquid Chromatography
NA	Numerical Aperture
NIR	Near Infra Red
PAH	Polycyclic Aromatic Hydrocarbon

PCA	Principle Components Analysis
PLS	Partial Least Squares
PM	Phase Modulation
PMT	Photo Multiplier Tube
PVT	Pressure Volume Temperature
RET	Resonance Energy Transfer
RF	Radio Frequency
RI	Refractive Index
SARA	Saturates Aromatics Resins Asphaltenes
SFS	Synchronous Fluorescence Spectra
SLI	Structured Light Illumination
SPA	N-(3-sulfopropyl) acridinium salt
TAC	Time to Amplitude Convertor
TCSPC	Time Correlated Single Photon Counting
TRES	Time Resolved Emission Spectra
TSFS	Total Synchronous Fluorescence Spectra
UV	Ultra-Violet
XRF	X-Ray Fluorescence

Chapter 1

Introduction

For many years chemists, physicists and geologists have strived to characterise the physical and chemical nature of crude oils. The main impetus for this development has been the oil industry but techniques developed in this area also have environmental applications such as determination of oil spill type and petroleum in waste water systems and soils [1]. Crude oil can be separated into subfractions by Liquid Chromatography and High Pressure Liquid Chromatography (HPLC) [2] and subsequent analysis of these fractions can be performed by Gas Chromatography (GC). Mass Spectrometry can also be used to give a detailed chemical fingerprint of the oil [3]. However these methods are destructive and time consuming, requiring separation of heavy crude oil constituents before analysis. Non-destructive analytical methods may provide an welcome alternative to these methods where fast analysis is required. For example, in the case of the oil industry, the pursuit of a real-time and in-situ analytical techniques for the determination of oil composition has been a major goal [4]. Knowledge of oil composition can be used to aid resource optimisation and exploitation, i.e., crude oils are formed with a wide variety of physical and chemical properties which determine whether they are economical to extract or what extraction method to use [4]. Optimisation of pipeline conditions and the distillation process is also critical to the oil industry; both of which are dependent on the properties of the crude oil. Heavy crude oils are often diluted with low molecular weight alkanes to improve pipeline flow conditions and the determination of distillation curves (showing the relationship between crude oil boiling point and the volume fraction distilled) of the crude oil can be then be used to optimise the delivery of

the diluted oil to the refinery [5]. Fluid and composition properties* are usually determined from laboratory studies on samples collected from the bottom of the well or at the surface but such experimental data are, however, not always available or very costly to obtain and so, their determination in real-time during test drilling is of key importance [6]. Estimates of viscosity and phase behaviour can be performed using empirical equations (Equations of State) but there is one major drawback; the composition of the crude oil has a major influence on the predicted properties and must be estimated if not available. To improve on traditional methods of analysis and predictions of equations of state, non-destructive spectroscopic techniques have been investigated as a means to quantitatively analyse crude oils because of their versatility, fast response and low cost.

1.1 Crude Oils

1.1.1 Formation

Crude oil and natural gas are the product of compression and heating of ancient organic materials over geological time frames [7, 8]. Today's oils are formed from the preserved remains of prehistoric plankton and algae, which had settled to a sea or lake bottom in large quantities under anoxic conditions. The remains of prehistoric terrestrial plants, on the other hand, tends to form coal (Figure 1.1). The

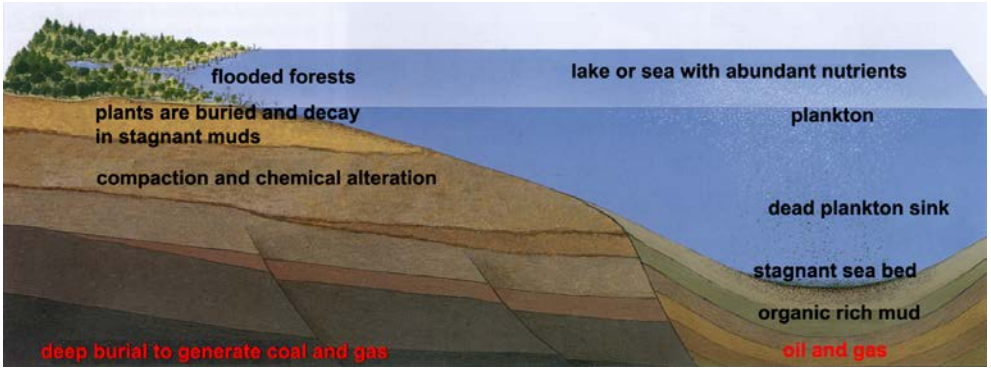

Figure 1.1: *Formation of crude oil from land and sea based sources.*

* Viscosity Pressure-Volume-Temperature (PVT) phase behaviour are commonly determined. PVT diagrams are specific to a crude oil and can be used for modeling the behaviour of the oil at any pressure and temperature; for example, what happens to the crude oil when brought from the reservoir to the surface [6].

temperature increases with depth within the Earth's crust, so that sediments, and the organic material they contain, heat up as they become buried under younger sediments. As the heat and pressure increase, organic materials such as lipids, proteins, carbohydrates, lignin and humic compounds that are present in the buried sediments combine to form high molecular weight hydrocarbons called *Kerogens* [8]. As burial continues and the material gets hotter, thermal cracking of kerogen results in the formation of oil. At higher temperatures the chains become shorter and light oil or gas is formed. If the temperature and pressure gets too high, the kerogen becomes carbonised to graphite and does not produce hydrocarbons [6].

Geologists often refer to the temperature range in which oil forms as an 'oil window' (from 50°C to 120°C). Below 50°C, oil does not form and the kerogen form remains, and from 120°C to 150°C, oil is converted to natural gas. Although this temperature range is found at different depths below the surface, a typical depth for the oil window is 2-4 km. Sometimes, oil which is formed at extreme depths may migrate and become trapped at much shallower depths; the Athabasca Oil Sands in Canada being one such example [7]. Three major phases in the transformation of organic matter after burial have been identified [8, 9]:

- **Diagenesis**: Occurs in the shallow subsurface at near normal temperatures and pressures. As the organic matter decomposes; carbon dioxide and water are expelled, leaving kerogen. The oxygen content is reduced, leaving the hydrogen to carbon ratio (H:C) unaltered.

- **Catagenesis**: Occurs in the deeper subsurface as burial continues and temperatures and pressures increase. Petroleum and hydrocarbon gases are formed from the thermal cracking of kerogen during catagenesis. In the early stages of catagenesis, formation of heavy molecules or *Bitumens* can occur. At later stages of catagenesis, gas formation occurs due to higher cracking temperatures. The H:C ratio declines with no significant change in the oxygen:carbon ratio.

- **Metagenesis**: At very high temperatures (higher than 160°C), gas evolution ceases and the H:C ratio declines until only carbon is left in the form of graphite.

Three types of kerogen are defined based on their source material. Type I is lacustrine algal in origin, the dominant compounds being lipids and their derivative fats, waxes and oils. The H:C ratio is ~ 1.5 indicating a high degree of aliphacity [10]. This type shows greater tendency to produce liquid hydrocarbons. Type II kerogen is predominantly planktonic in origin and although is rich in aliphatic compounds it has a lower H:C ratio than Type I kerogen. This type of kerogen also has a greater tendency to form petroleum. Type III kerogen, or humic kerogen has a much lower H:C ratio indicating a much higher degree of aromaticity. Humic kerogen is produced from the lignin of woody plants, which grow on land. If this type of kerogen is buried as peat, it can undergo diagenesis to coal. Otherwise, it tends to generate largely gas rather than oil.

Kerogens are noted by their high molecular weights and insolubility in organic solvents such as Toluene and Hexane. Because they are precursors to oil and gas, kerogen structure has long been the subject of investigation and to date realistic generalisations of structure have yet to be published. Molecular weights are estimated to range from $20,000$ g/mol for Type I kerogen to $26,000$ g/mol for Type III kerogen [11]. However each kerogen is formed under unique starting conditions and a general classification of kerogens is performed by describing gross kerogen composition and relating it to hydrocarbon generation.

There are a number of conditions that lead to the accumulation of oil in a reservoir:

- A sedimentary rock (called the source rock) rich in kerogenic material that is buried deep enough to generate the necessary pressure and temperature.
- A path to allow oil and gas to move upwards. This process is called *migration* and is subdivided into the processes of primary and secondary migration[†].
- A porous and permeable reservoir rock to contain the oil.

[†] *Primary migration* is the movement of oil and gas out of the source rocks into the permeable reservoir rocks, while *Secondary migration* is the movement of fluids within the permeable rocks that eventually leads to segregation of the oil and gas.

- A seal or cap-rock that prevents the oil from escaping to the surface.

1.1.2 Oil Maturity

In geochemical terms, the effect of heat or *thermal maturation* on kerogen and its subsequent transformation to oil is most important. Maturation processes involve cracking, isomerisation and aromatisation reactions, as well as alkylation and dealkylation of aromatic rings. These processes commence in the source rocks and continue during migration to the reservoir. Over the geological time frames (60-70 million years), maturation processes yield more thermodynamically stable small molecules as well as the transformation of saturated into aromatic hydrocarbons. The degree of maturity can be estimated by a number of methods such as the analysis of biomarker[‡] distribution and the distribution and abundance of saturated and aromatic hydrocarbons, i.e., compounds which generally constitute 95-98 % of crude oils [7, 13]. Another measure of the maturity of a crude oils is the relative density of a petroleum liquid or API gravity [14], given by the relation:

$$\text{API } gravity = \frac{141.5}{SG} - 131.5 \tag{1.1}$$

where SG is the specific gravity of the oil at 15.6°C or 60°F. Although mathematically API gravity has no units, it is nevertheless referred to as being in 'degrees'. The U.S. National Bureau of Standards in 1916 established the Baum scale as the standard for measuring specific gravity of liquids less dense than water. Unfortunately, hydrometers in the U.S. had been manufactured and distributed widely with a modulus of 141.5 instead of the Baum scale modulus of 140. The scale was so firmly established that by 1921 the remedy implemented by the American Petroleum Institute was to create the API Gravity scale recognising the scale that was actually being used [14].

[‡] Biomarkers are any organic compounds which are found in oil, bitumen, rocks and sediments that show little or no change in structure from their parent organic molecules in living organisms. These compounds are typically analyzed using gas chromatography or mass spectrometry, common examples of which are pristane, phytane, steranes and porphyrins. [12]

1.1.3 Chemical Composition

Crude oils consist of a large mixtures of aliphatic, aromatic, and high molecular weight organic compounds. Despite this multitude of components, the proportions of the elements in crude oils vary over fairly narrow limits. The carbon content normally is in the range 83-87%, and the hydrogen content varies between 10 and 14% (by weight) [14]. Varying small amounts of nitrogen, oxygen, sulfur and metals (Ni and V) are also found in crude oils [7]. A comparison between kerogen and crude oil in terms of elemental composition is shown in Table 1.1. During the process of thermal cracking of kerogen to oil, there is an increase in the % hydrogen and a corresponding decrease in Sulphur, Nitrogen and Oxygen.

Figure 1.2 shows the main constituents of crude oils in relation to their distillation fractions. The alkanes dominate the gasoline fraction of crude oils and are most abundant in highly mature oils. Moving from the gasoline fraction to the heavier fractions, there is a marked increase in amount of cycloalkanes, after which the aromatic content slowly rises until reaching the lubricating oil range. Note the absence of Alkenes and alkynes. These compounds are not found in crude oils as they are readily reduced to alkanes by H_2 or thiols by H_2S [7]. The residuum is the heaviest part of the crude at the bottom of a distillation tower. This residuum comprises of resins, waxes and asphaltenes and will be described in the next section.

Table 1.1: *Typical elemental composition of oil and kerogen (weight %). Reproduced from [7].*

	Oil	Kerogen
Carbon	84.5	79
Hydrogen	13	6
Sulphur	1.5	5
Nitrogen	0.5	2
Oxygen	0.5	8
Total	100	100

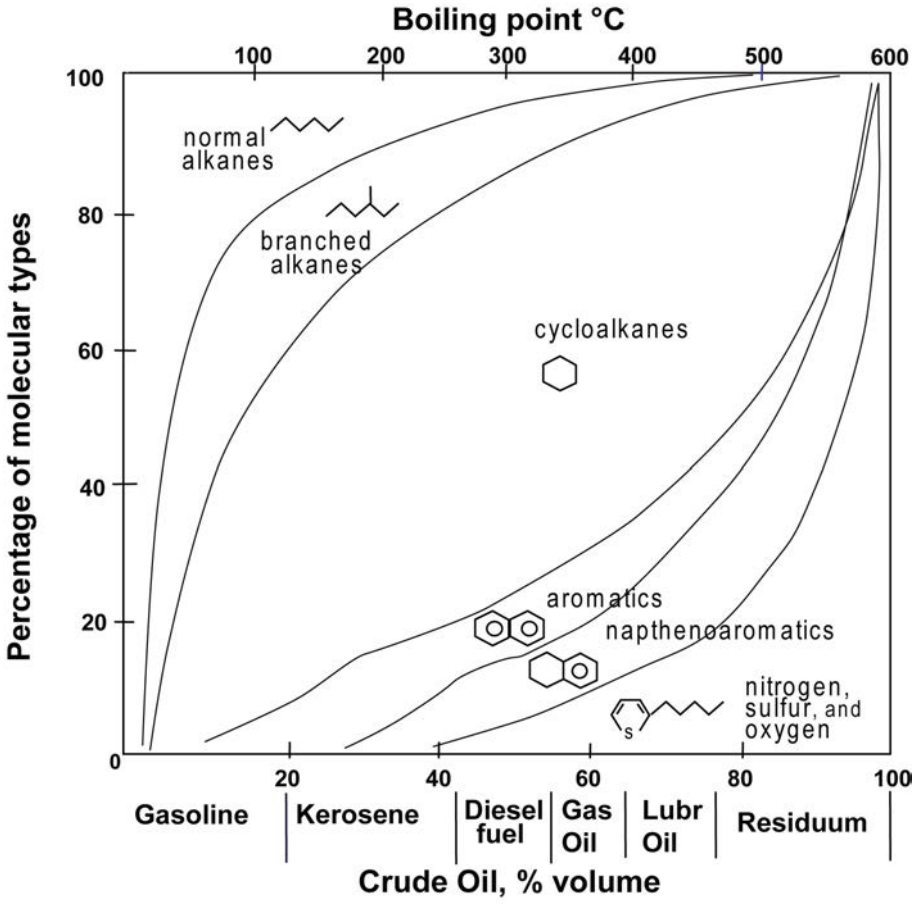

Figure 1.2: *Crude oil composition in terms of molecular structure. Adapted from [7]*

1.1.4 SARA Fractions

Refining of petroleum by distillation yields various fractions or 'cuts' based on where they separate in the distillation column. The C6- fraction consists of all pure hydrocarbon components (and non-hydrocarbons) with carbon numbers up to C5. These include all isomers in each carbon number range; the physical properties of each of the pure components are well understood. On the other hand, the C6+ fraction contains far more compounds due to multiple isomeric forms possible [15]. The C6+ group can be split into four major component classes based on differences in solubility and polarity. This is the basis for SARA analysis where saturates, aromatics, resins, and asphaltenes can be isolated [2, 16, 17]. The SARA fractions are as follows:

Saturates: The saturates (aliphatics) are non-polar hydrocarbons including straight and branched chain alkanes, as well as cycloalkanes (naphthenes). Cycloalkanes contain one or more rings, which may also have several alkyl side chains. Saturates are generally are the lightest fraction of the crude oil. The saturate consist primarily of straight-chain alkanes, mainly ranging from C_{20} to C_{30} [18].

Aromatics: The unsaturated aromatic fraction is common to all crude oils, yet rarely amount to more than 15% of the total oil content. They tend to be more concentrated in the heavy fractions of petroleum, such as gas oil, lubricating oil and the residuum (see Figure 1.2). The most common aromatics found in crude oil are simple derivatives of benzene such as toluene and xylene [19]. Aromatics may also contain alkyl chains and cycloalkane rings, along with additional aromatic rings which are termed Polycyclic Aromatic Hydrocarbons or PAH's. Not all PAH's are classed within the Aromatic fraction. High molecular weight PAH's such as chrysene and benzoperylene fall into the polar or asphaltene fractions respectively.

Polars/Resins: This fraction is comprised of polar molecules containing heteroatoms such as nitrogen, oxygen or sulphur. This fraction is defined by solubility, and one common definition is that it is the fraction soluble in light alkanes such as pentane and heptane, but insoluble in liquid propane [20]. Resins have a higher H:C ratio than asphaltenes, 1.2-1.7 compared to 0.9-1.2 for the asphaltenes [20]. Although resins are structurally similar to asphaltenes, they have lower molecular weights. Naphthenic acids[§] are commonly regarded as a part of the resin fraction.

Asphaltenes: The asphaltene fraction, is usually defined as the fraction of the crude oil which is insoluble in light alkanes such as pentane, hexane, or heptane [21]. Asphaltenes are soluble in aromatic solvents like toluene and benzene. Pure asphaltenes are non-volatile black solids, and contain the largest percentage of het-

[§] These acids are classified as monobasic carboxylic acids of the general formula RCOOH, where R represents a cycloalkane structure. The term 'naphthenic acid' is often used to account for all carboxylic acids present in crude oil, including acyclic and aromatic acids. Nearly all crude oils contain some naphthenic acids. These are extremely complicated mixtures and have been of interest due to the serious production problems related to their occurrence, causing corrosion problems at refineries when processed.

eroatoms (O, S, N) and organometallic constituents (Ni, V, Fe) in crude oils [22]. The chemistry of Asphaltenes is important to the oil industry as they have a negative impact in exploration, production, transportation, and refinement of crude oil. They can dramatically alter the viscosity of crude oils by precipitating out of solution at surface pressure, thus blocking pipelines [23].

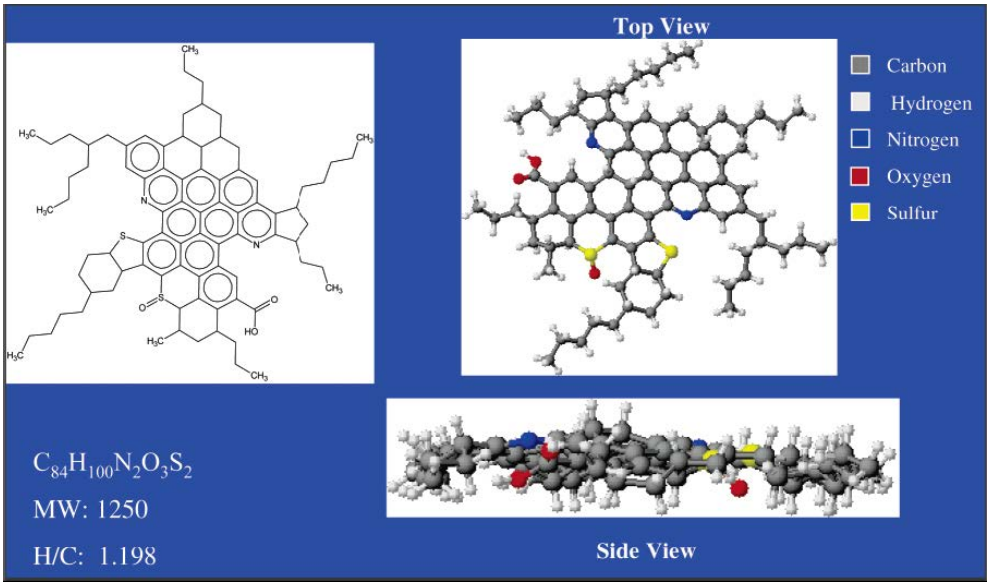

Figure 1.3: *Theoretical molecular structure for a petroleum asphaltene. In reality, Asphaltenes exist as an aggregation of high molecular weight PAH's. Reproduced from [15].*

The structure of the asphaltenes has also been the subject of several investigations, and is now believed to consist of polycyclic aromatic clusters, substituted with various alkyl side chains [22, 23]. Figure 1.3 shows a proposed hypothetical structure for an asphaltene molecule although current research [15] indicates that there is not just one structure, but a mixture of a broad spectrum of species. Evidence for this broad spectrum of components has come from molecular weight distributions determined by size exclusion chromatography. The molecular weight of asphaltene molecules has been difficult to measure due to the asphaltenes tendency to aggregate. Time resolved fluorescence depolarisation studies [21, 22, 24] and comparisons with PAH molecular orbital calculations [25] have shown that Asphaltene molecules possess 4-10 fused aromatic rings. Recently it has been possible to calculate diffusion coefficients and hydrodynamic radii for a range of coal and

petroleum asphaltenes by FCS experiments [26, 27], yielding molecular weight approximations. Non-aggregated Asphaltene molecular weights were found to be in the range of ~ 750 g/mol.

1.1.5 Separation of SARA fractions

Figure 1.4 shows a typical SARA fractionation from dead crude oil samples [28]. Asphaltenes are isolated as a separate fraction by precipitating with n-heptane (40:1). This is because their highly polar nature would cause irreversible adsorption and thus damage the LC column. Precipitated asphaltenes are separated by vacuum filtration, dried in an oven and weighed. The soluble compounds left after asphaltenes have precipitated is called the 'maltenes' fraction.

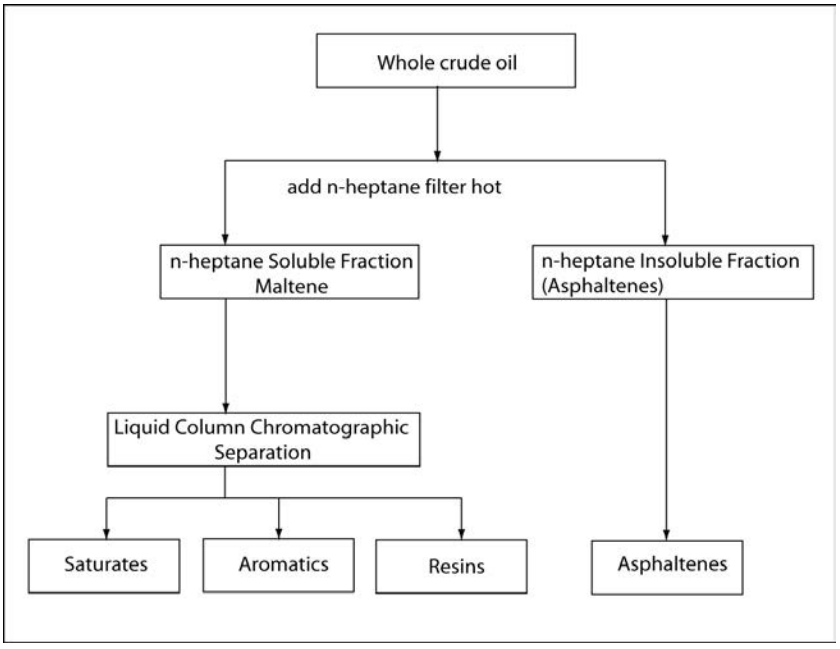

Figure 1.4: *SARA fractionation protocol for dead crude oils. Adapted from [28].*

Normal-phase LC elution can be performed on the maltenes in an open-column by a gravitational flow of solvent or by a force-flow using medium pressure (MPLC) to increase separation speed [17] (this technique was used to produce the fractionation data for the crude oil samples described in Chapter 2). Usually, saturates are eluted with an n-alkane such as n-hexane and the aromatics and resins/polars are eluted with solvents or solvent mixtures of higher eluotropic strengths such as

toluene, dichloromethane, acetone, or their mixtures with other solvents. For this, standard ASTM procedures for SARA separation are available [29, 30]. There are numerous variations on these SARA schemes that differ in the type of adsorbent and solvent elution scheme used.

For live crude oils, where information is required on the low molecular weight volatile fraction, distillation at 270° C which corresponds to the boiling point of alkanes containing 15 carbons or 'C15' can be performed. This distillation step separates the volatiles and the light fraction (< 270° C) from the rest of the crude oil components which can then be analysed by Gas Chromatography-Mass Spectrometry (GC-MS). The crude oil sample may be also be heated to constant weight at 60° C with flowing nitrogen to produce a volatile-free 'stable' oil, a process known as '*topping*'.

High performance liquid chromatography (HPLC) has been demonstrated to be a very efficient alternative to the standard ASTM procedures for SARA separation in terms of enhanced separation, greater efficiency and process automation [2, 31–33]. To separate the SARA fractions of the maltene, two chromatography columns are generally used [34, 35]. Figure 1.5 shows a typical chromatogram using modern HPLC based SARA analysis. To generate this chromatogram, a sample of asphaltene free crude oil diluted in hexane was injected into an amino-bonded silica precolumn in series with a silica column and using hexane as the mobile phase. The saturates, being weakly retained in the columns, are eluted first and recorded by refractive index (RI) detection. RI detection is used for the saturates due to their very low UV absorbance. The main bulk of the aromatic fraction (giving a strong UV response) was then eluted from the silica column and the residual heavy aromatics were collected by a dichloromethane backflush. The resin fraction remained in the amino precolumn and was desorbed by dichloromethane backflush. Typical retention times are shown in Figure 1.5.

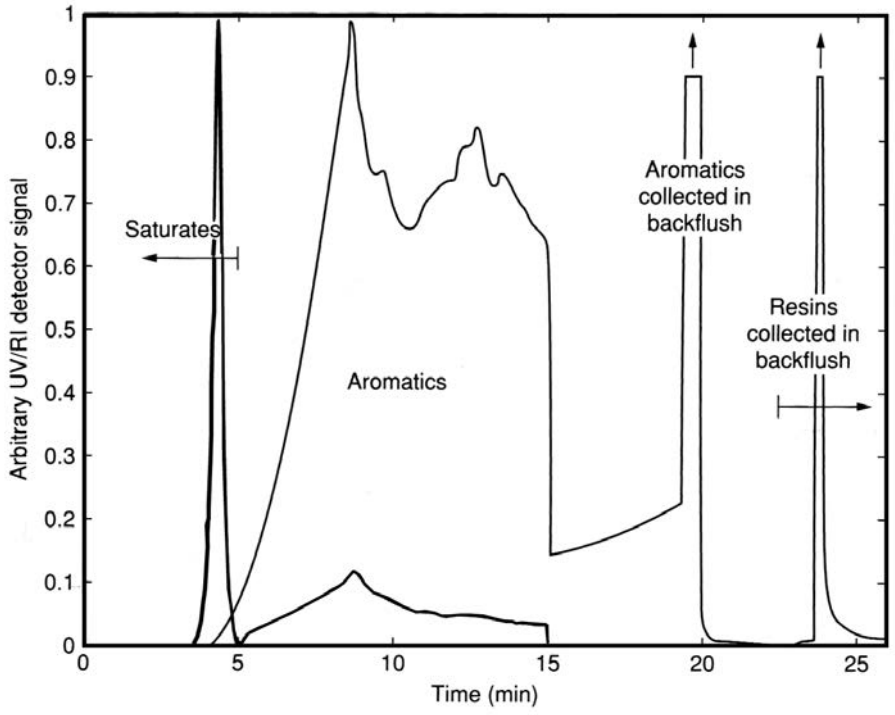

Figure 1.5: HPLC *Chromatogram from a typical* SARA *analysis. The bold line represents the* RI *signal, while the thin line represents the* UV *signal at 254nm. The maxima of the aromatic and resin peaks are cut for better visualisation. Reproduced from [35].*

In the case of complex mixtures covering a broad range of molecular weights and polarity, currently available chromatographic methods often have some limitations. Problems can arise from inadequate resolving power, low volatility, low solubility of the components in the chromatographic mobile phase, strong adsorption of sample components on the stationary phase, or low detector sensitivity. Thus, no single HPLC method can be utilised for all types of crude oils so specific methods must be developed. A particular crude oil may need specific solvents, detectors and columns [16]. Because of these limitations of HPLC, the OCLC method is still used regularly for the analysis of crude oils, particularly when separations of large quantities are required [33].

1.2 Fluorescence Spectroscopy

1.2.1 Fluorescence

If a molecule is promoted to an electronically excited state by the absorption of ultraviolet, visible, or near infrared radiation, luminescence or the emission of light from this state can occur when this excited molecule decays back to the ground state, or to a lower-lying excited electronic state [36]. Luminescent processes are subdivided into fluorescence and phosphorescence. The key characteristic of fluorescence spectroscopy is its high sensitivity, achieving limits of detection several orders of magnitude lower than many other analytical techniques. Limits of detection of 10^{-10} M or lower are possible for intensely fluorescent molecules. Under controlled conditions, single molecule (the ultimate limit of detection) may be reached. Because of the low detection limits, fluorescence is widely used for quantification of trace constituents of biological and environmental samples [37]. Also the use of fluorescent molecules or markers to detect non-fluorescent molecules is widespread and has numerous applications (such as molecular imaging and DNA sequencing) [38].

Fluorescence can be considered as a three-stage process that is best illustrated by a Perrin-Jablonski diagram (Figure 1.6 [36, 38]).

Stage 1: Excitation

Following light absorption, a molecule is excited from the ground state to one of the vibrational levels of an upper excited electronic state (S_1 or S_2). This is shown as a vertical transition which occur in the 10^{-15} s time frame, too short to significantly displace the nuclei (the Frank-Cordon principle [39]) or change the electronic spin-state from that of the ground state configuration.

Stage 2: Excited-State Transitions

The S_1 or S_2 excited state exists for a finite time with a subsequent partial dissipation of energy in the form of heat by rapid relaxation to the lowest vibrational level of S_1[¶], yielding a relaxed singlet excited state (S_1) from which fluorescence emission originates. This process is called internal conversion and occurs in 10^{-12} s or less. Since fluorescence lifetimes are typically near 10^{-9} s, internal conversion is generally complete prior to emission. Not all the molecules initially excited by

[¶] In a few rare exceptions emission occurs from the S_2 excited state e.g. Azulene.

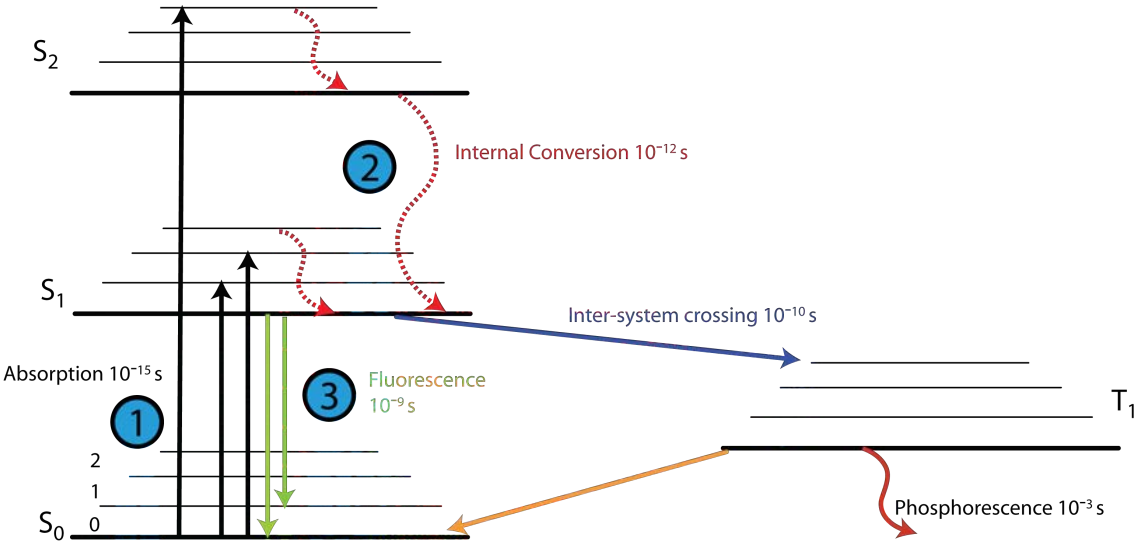

Figure 1.6: *Perrin-Jablonski diagram showing the electronic processes occurring in a fluorescent molecule after excitation by light. Here the singlet ground, first and second excited states are depicted by S_0, S_1, S_2 respectively. Each electronic energy level has a number of vibrational energy levels, depicted by* 0,1,2 *etc. Rotational energy levels are omitted from the diagram for clarity. The transitions between states are depicted as vertical lines to indicate the instantaneous nature of light absorption.*

absorption (Stage 1) return to the ground state (S_0) by fluorescence emission, instead returning to the ground state by non-radiative transitions. Internal conversion from S_1 to S_0 is also possible but is less efficient than conversion from S_2 to S_1, because of the larger energy gap between S_1 and S_0. Under certain conditions such as heavy atom spin-orbit[‖] coupling, molecules in the S_1 state can undergo a spin conversion to the first triplet state T_1 via the process of intersystem crossing. Emission from this state is termed phosphorescence and is typically of a much longer timescale than fluorescence due to $T_1 \longrightarrow S_0$ transitions being spin forbidden (or highly improbable) by the spin selection rule for electronic transitions ($\Delta S = 0$).

Stage 3: Fluorescence Emission

Fluorescence emission usually occurs from the lowest vibrational level of the S_1 state and can return to different vibrational levels of the ground state. The emission of a photon is as fast as the absorption ($\approx 10^{-15}$ s), but excited molecules stay in the

[‖] Intersystem crossing is in principal forbidden by quantum mechanics but coupling of the magnetic field generated by orbital motion and the electronic spin magnetic moment can lead to a conversion or flip of the spin state. This condition is enhanced by the presence of heavy atoms with high atomic numbers such as Br or Pb.

S_1 state for a certain time (from 10^{-12} to 10^6 s depending on the type of molecule and the medium used) before emitting a photon or undergoing other excited state transitions. This characteristic tim is called the *fluorescence lifetime*. Unless the fluorophore is irreversibly destroyed in the excited state (a phenomenon known as photobleaching), the same fluorophore can be repeatedly excited and detected. The fact that a single fluorophore can cycle between the ground and excited states many thousands of times (estimates of 10,000 to 40,000 cycles have been given [37]) is fundamental to the high sensitivity of fluorescence detection techniques [40].

1.2.2 Fluorescence Spectra

The phenomenon of fluorescence emission displays a number of general characteristics. As energy is lost due to internal conversion, the emitted photon is of lower energy and this results in a difference between the maximum of the first absorption band and the maximum of the fluorescence emission, called the *Stokes shift*. For single fluorophores, thermal relaxation usually leads to the lowest vibrational energy level of the S_1 state, and because of this, the same emission spectrum is generally observed irrespective of the excitation wavelength. This phenomenon is known as *Kasha's rule*. Because the differences between the vibrational levels are similar in the ground and excited states, and due to the Frank-Condon principle, the emission spectrum is typically a mirror image of the absorption spectrum of the $S_0 \longrightarrow S_1$ transition. Also, if a particular transition to a vibrational level of an excited state is of higher probability or intensity, then the reciprocal transition will also have the highest probability. The absorption and emission spectra of Anthracene, a typical aromatic hydrocarbon present in crude oil are shown in Figure 1.7. Incident photons of varying wavelength (and energies) initiate transitions to varying vibrational energy levels of S_1, giving rise to multiple peaks. Since the photons absorbed have a large number of vibrational and rotational energy levels, the discrete electronic transitions represented in Figure 1.6 are replaced by rather broad energy spectra called the fluorescence excitation spectrum and fluorescence emission spectrum, respectively.

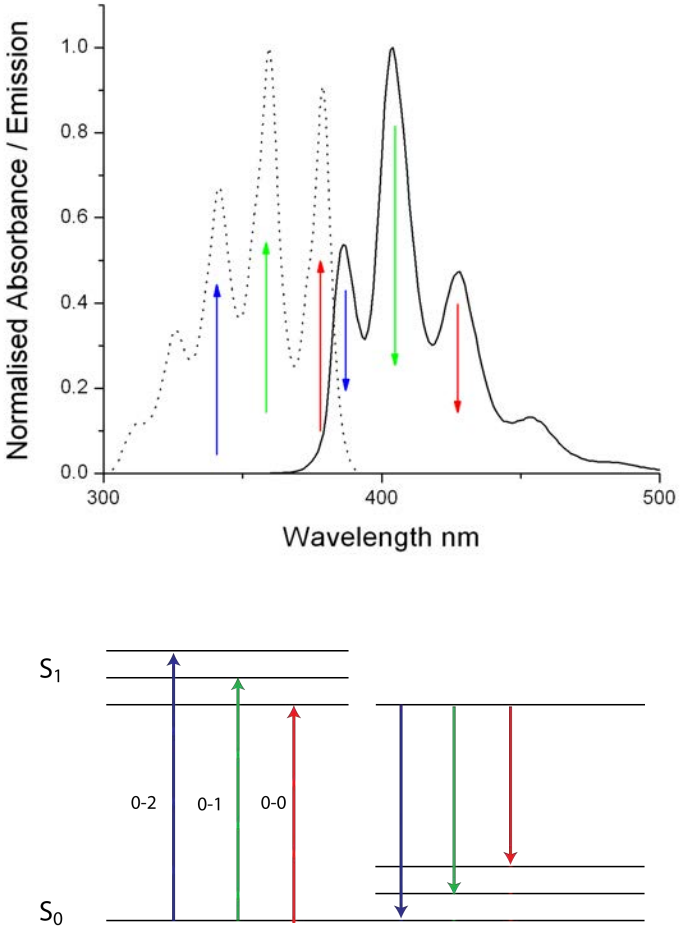

Figure 1.7: *Absorption (dash) emission and (solid) spectra for Anthracene (in Toluene). Excitation light source* 350 *nm. The numbers* 0,1 *and* 2 *refer to vibrational energy levels.*

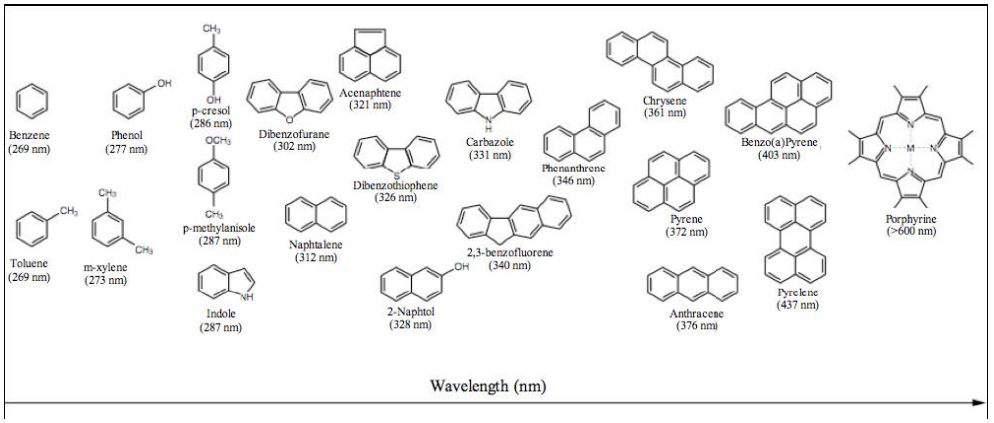

Figure 1.8: *Typical fluorophores present in crude oil and their emission maximum. Reproduced from [41].*

The peaks in the absorption spectrum correspond to transitions from the lowest vibrational level of the electronic ground state to different vibrational levels of the first electronic excited state, while the peaks observed in the fluorescence spectrum arise from transitions from the lowest vibrational level of the excited electronic state to the different vibrational levels of the ground state. As shown in Figure 1.7, there is some overlap of the absorption and emission spectra because at room temperature a small fraction of the molecules are in a vibrational level higher than 0. At cryogenic temperatures, this overlap would be reduced [37].

Larger molecules will typically have more complex electronic spectra, emitting at longer wavelengths. For example, in large PAH's, the degree of conjugation increases, the number of delocalised π orbitals increases. Increased delocalisation reduces the energy gap between the highest occupied molecular orbital (HOMO) and the lowest unoccupied molecular orbital (LUMO). Since the absorption energy is reduced, a shift of the absorption and emission to longer wavelengths occurs (Figure 1.8).

1.2.3 Kinetics of photophysical processes

Fluorescence quantum yield and lifetime are perhaps the two most important physical emission characteristics of a fluorophore [36]. Quantum yield (Equation 1.2) is defined as the number of emitted photons relative to the number of absorbed photons:

$$\phi = \frac{number\ of\ fluorescent\ events}{number\ of\ photons\ absorbed} = \frac{Intensity\ of\ fluorescence}{Intensity\ of\ light\ absorbed} = \frac{I_f}{I_{abs}} \quad (1.2)$$

To develop expressions for quantum yield and lifetime, consider the formation and decay of the excited state:

$$\begin{aligned} Absorption &: S + h\nu_{ex} \longrightarrow S^* & \upsilon_{abs} &= I_{abs} \\ Fluorescence &: S^* \longrightarrow S + h\nu_{em} & \upsilon_f &= k_f[S^*] \\ Internal\ conversion &: S^* \longrightarrow S & \upsilon_{ic} &= k_{ic}[S^*] \\ Intersystem\ crossing &: S^* \longrightarrow T^* & \upsilon_{isc} &= k_{isc}[S^*] \end{aligned}$$

where υ is the rate of each of the four processes listed, S is the ground state, S^* is the excited singlet state, T^* the excited triplet state, and $h\nu_{ex}$ and $h\nu_{ex}$ are the energies of the incident and fluorescent photons respectively. If the absorbance of the sample is low and the incident light intensity is relatively high, the steady-state approximation for the change in concentration of S^* can be given as:

$$\frac{d[S^*]}{dt} = I_{abs} - k_f[S^*] - k_{ic}[S^*] - k_{isc}[S^*] = I_{abs} - (k_f + k_{ic} + k_{isc})[S^*] = 0$$

it follows that:

$$I_{abs} = (k_f + k_{ic} + k_{isc})[S^*]$$

Bringing in the quantum yield term from Equation 1.2 yields:

$$\phi = \frac{k_f}{k_f + k_{ic} + k_{isc}} \tag{1.3}$$

In steady state experiments the sample is illuminated with a constant beam of light. Because of the short (typically nanosecond) timescale of fluorescence, a steady state is reached almost immediately. If the fluorophore is exposed to a pulse of light that generates the excited state, the intensity decays exponentially according to:

$$[S^*]_t = [S^*]_0 e^{-t/\tau}$$

where the average time that the excited state exists is given by the fluorescence lifetime, τ.

The observed fluorescence lifetime(τ) is comprised of the non-radiative (k_{ic}+k_{isc}) and the radiative (k_f) parts and is given by:

$$\tau = \frac{1}{k_f + k_{ic} + k_{isc}} = \frac{\phi}{k_f} \tag{1.4}$$

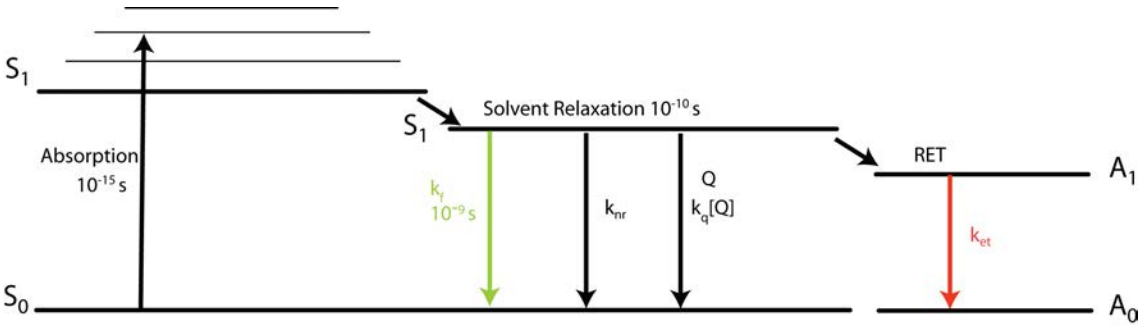

Figure 1.9: *Jablonski diagram with collisional quenching and resonance energy transfer (*RET*) of a fluorophore in solution. Solvent relaxation is also shown. The other non-radiative paths to the ground state apart from dynamic quenching and energy transfer is represented by* k_{nr}*.*

1.2.4 Quenching of fluorescence

Excluding photobleaching, the intensity of fluorescence can be decreased in a variety of mechanisms, collectively described as quenching. A wide variety of substances can act as quenchers of fluorescence, for example molecular oxygen quenches almost all known fluorophores [36]. The longer the lifetime in the absence of oxygen, the stronger the sensitivity to the presence of oxygen[**]. Heavy atoms such as halides are also efficient quenchers, providing a pathway for fluorophores to the triplet state by spin-orbit coupling (of the excited state and the fluorophore) [36]. Figure 1.9 shows an extended Jablonski diagram that incorporates quenching, energy transfer, and solvent relaxation[††].

Dynamic/Collisional Quenching: As molecules diffuse in solution, they can collide with each other. The collision of a fluorophore with another molecule known

[**] Oxygen can be removed from solution by degassing either by bubbling with Nitrogen (or Argon), or by the freeze-pump-thaw procedure.

[††] Figure 1.9 also includes the step down in energy due to relaxation or reorientation of the solvent molecules around the dipole moment of the excited state. Typically, a fluorophore has a larger dipole moment in the excited state than in the ground state. Following excitation the solvent dipoles can orient around the excited state fluorophore dipole which lowers the energy of the excited state. As the solvent polarity is increased, this effect becomes larger resulting in emission from lower energies (longer wavelengths). This is typically the case for $\pi - \pi^*$ transitions while the opposite is typically true for $n - \pi^*$ transitions. Polar fluorophores display a large sensitivity to solvent polarity while non-polar molecules are much less sensitive [38].

as a quencher (Q) can reduce the fluorescence intensity of the excited state S^*:

$$Quenching : S^* + Q \longrightarrow S + Q \qquad\qquad \upsilon_q = k_q[Q][S^*] \tag{1.5}$$

The excited fluorophore returns chemically unaltered to the ground state. The fluorescence quantum yield in the presence of a quencher (ϕ_q) is given by:

$$\phi_q = \frac{k_f}{k_f + k_{ic} + k_{isc} + k_q[Q]}$$

Using equation 1.4, the ratio of ϕ_q/ϕ is given by:

$$\phi_q/\phi = 1 + \tau k_q[Q] \tag{1.6}$$

which is the well-known *Stern-Volmer* equation. Because fluorescence intensity and lifetime are both proportional to the quantum yield, equation 1.6 can be written as

$$\frac{I_0}{I} = \frac{\tau_0}{\tau} = 1 + \tau_0 k_q[Q] \tag{1.7}$$

τ_0 is the lifetime in the absence of a quencher and k_q is the bimolecular quenching constant. The product of $\tau_0 k_q$ is the Stern-Volmer quenching constant and indicates the sensitivity of the fluorophore to the quencher. k_q reflects the efficiency of quenching or the accessibility of the fluorophores to a quencher.

Static Quenching: In some cases, fluorophores can form a stable complex with another molecule. If this ground-state is non-fluorescent, then the fluorophore has been statically quenched. In the case of static quenching the lifetime of the sample will not be reduced since those fluorophores which are not complexed, and hence are able to emit after excitation, will have normal excited state properties. The fluorescence of the sample is reduced since the quencher is essentially reducing the number of fluorophores which can emit (Figure 1.10).

When the complex absorbs light it immediately returns to the ground state

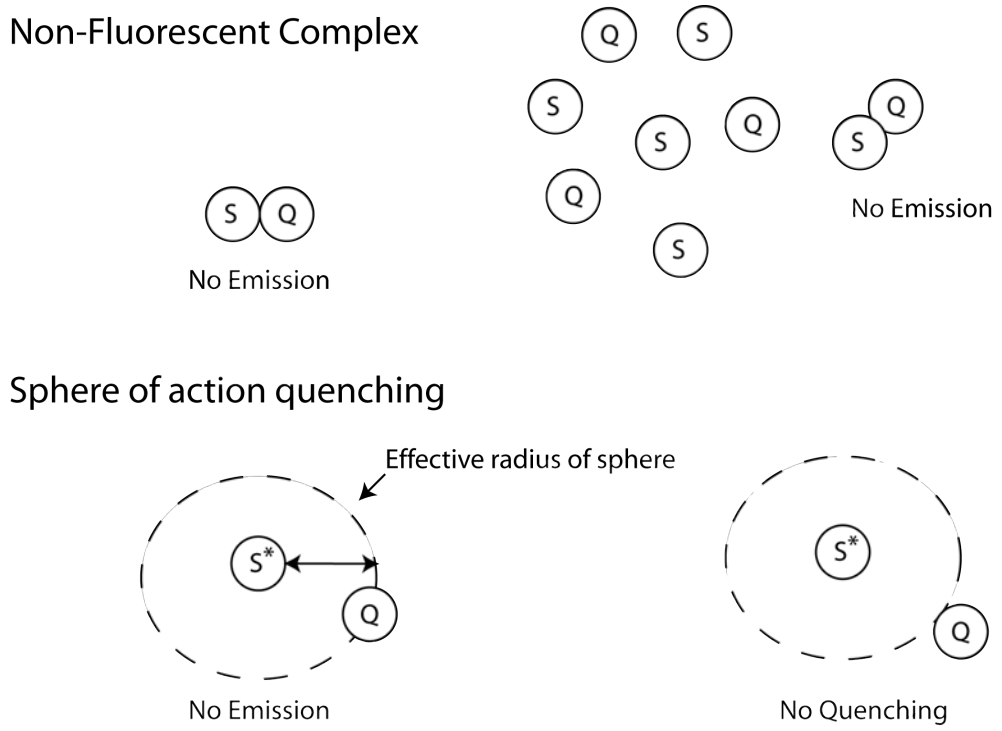

Figure 1.10: *Static quenching mechanisms. The fluorescence intensity can be reduced if the fluorophore forms a non-fluorescent ground-state complex with the quencher. Reduction of fluorescence intensity can also occur if a quencher is within a critical volume, or sphere of action, around the excited fluorophore.*

without emission of a photon. This form of static quenching is described by:

$$\frac{I_0}{I} = 1 + K_a[Q] \tag{1.8}$$

where K_a is the association constant of the complex.

In a Stern-Volmer plot for static quenching, the dependence of the intensity ratio on the quencher concentration is linear. Deviation from this linear behaviour can occur, yielding upward curving Stern-Volmer plots. These curved plots can be described by the 'Sphere of action' (SOA) model (Bottom part of Figure 1.10). In this model, fluorophores that are close to but not associated with quenchers have a high probability of being quenched before diffusing apart. If the fluorophore-quencher pair are close enough, quenching is immediate and they appear as dark or non-emitting complexes. The sphere of action describes the volume within which this probability of quenching is unity. The sphere of action is represented by the volume V_q around a fluorophore. If the quencher is outside this sphere, it will have no

effect on the fluorescence. As the quencher concentration increases the probability of SOA quenching increases. In SOA quenching, the fluorescence intensity is reduced by the quencher but the fluorescence decay is unaffected as the observed fluorescence only comes from the uncomplexed fluorophores in the sample. The action of SOA quenching can be described by:

$$\frac{I_0}{I} = exp(V_q N[Q]) \tag{1.9}$$

where I_0 is the incident light intensity, I is the fluorescence intensity and N is Avogadro's number[36, 38].

Comparison of dynamic and static quenching: The two mechanisms are compared in Figure 1.11.

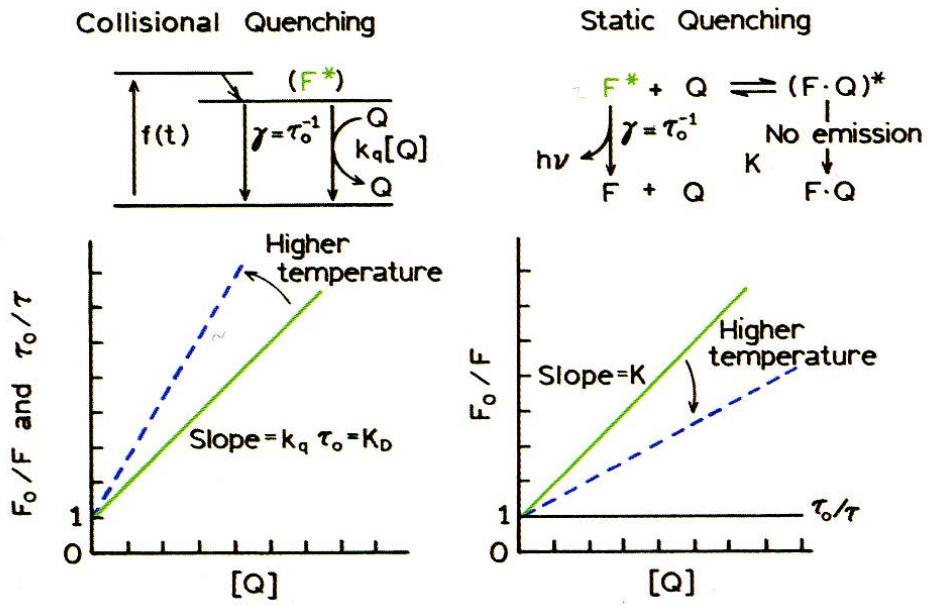

Figure 1.11: *Comparison of dynamic and static quenching. Reproduced from [36]*

For both dynamic and static quenching, the dependence of I_0/I on [Q] is linear and the two mechanisms can not be distinguished by intensity measurements alone. Lifetime measurements can be used to distinguish between dynamic and static quenching. For static quenching the lifetime remains unchanged as only the concentration of emitting fluorophores is reduced by formation of the complex and

the ratio of τ_0/τ is equal to 1. In contrast, for dynamic quenching $I_0/I = \tau_0/\tau$. The two mechanisms can also be distinguished by their differing dependence on temperature and viscosity. Higher temperatures result in faster diffusion rates and hence a greater degree of dynamic (collisonal) quenching. Higher temperatures will also typically result in the dissociation of weakly bound complexes, and therefore reduce the amount of static quenching.

Resonance Energy Transfer: Another mechanism that can quench the excited state is resonance energy transfer (RET) or Förster resonance energy transfer (FRET). Energy transfer is determined by number of factors [42]:

1. the extent of spectral overlap between the emission spectrum of a fluorophore, called the donor, and the absorption spectrum of another molecule, called the acceptor (Figure 1.12).

2. the distance between the donor and acceptor (1 to 10 nm).

3. their relative transition dipole orientations.

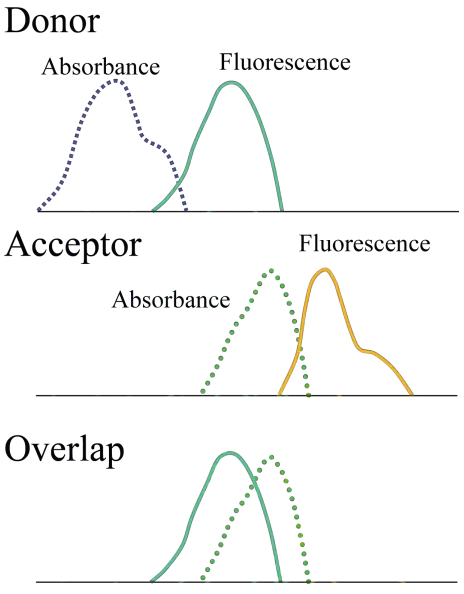

Figure 1.12: *RET requires the overlap of the emission band of the donor and the absorption band of the acceptor. When the donor molecule absorbs a photon, and there is an acceptor molecule close to the donor molecule, radiationless energy transfer can occur from the donor to the acceptor.*

The non-radiative process is described by:

$$Energy\ Transfer : S^* + Q \longrightarrow S + Q^* \qquad\qquad v_{et} = k_{et}[S^*]$$

The acceptor does not need to be fluorescent, but when it is, it's emission band will be observed at longer wavelength. It is important to note that RET does not involve emission of light by the donor, i.e., there is no emission and reabsorption of a photon in the RET processes. The distance at which energy transfer is 50% efficient (i.e., 50% of excited donors are deactivated by RET) is defined by the Förster radius (R_0). The magnitude of R_0 is dependent on the spectral properties of the donor and acceptor 'fluorophores. The Förster radius R_0 is given by:

$$R_0 = [8.8 \times 10^{23} \cdot \kappa^2 \cdot n^4 \cdot \phi \cdot J(\lambda)]^{1/6} \mathring{A} \tag{1.10}$$

where κ^2 is the dipole orientation factor, ϕ is the quantum yield of the donor in the absence of an acceptor, n is the refractive index, $J(\lambda)$ is the spectral overlap integral (see Figure 1.12). The spectral overlap is calculated from: $\int \epsilon_A(\lambda) \cdot F_D(\lambda) \cdot \lambda^4\ d\lambda\ cm^3\ M^{-1}$ where ϵ_A is the extinction coefficient of the acceptor and F_D is the fluorescence intensity of the donor as a fraction of the total integrated intensity.

The rate of energy transfer k_{et} is given by:

$$k_{et}(r) = \frac{1}{\tau_d}\left(\frac{R_0}{r}\right)^6 \tag{1.11}$$

where r is the distance between the donor and the acceptor molecules, and τ_d is the lifetime of the donor in the absence of energy transfer.

Non-Radiative Processes: If all the non-radiative processes (quenching, energy transfer etc) are taken into account, the expression for the observed fluorescence lifetime is then given as :

$$\tau = \frac{1}{k_f + k_{ic} + k_{isc} + k_q[Q] + k_{et}} = \frac{1}{k_f + k_{nr}} \tag{1.12}$$

where k_{nr} represents the sum of the non-radiative processes competing with the fluorescence decay.

1.2.5 Measuring fluorescence lifetimes

Fluorescence measurements can be broadly classified into two types: Steady-State and Time-Resolved. For steady-state measurements, the sample is illuminated with a continuous beam of light and the intensity of the emission spectrum is recorded. This fluorescence emission spectrum represents an average of the time-resolved processes occurring during an intensity decay. Temporal information such as lifetime can be recovered by using a pulsed or modulated light source, the essence of a time-resolved fluorescence measurement.

Two different time-resolved fluorescence techniques, *Pulse Fluorometry* and *Phase-Modulation fluorometry*, are commonly used to measure the fluorescence lifetimes [36, 38, 43]. In pulse fluorometry, one measures the sample emission following excitation by a short pulse of light and works in the *Time-Domain (*TD*)*. TD measurements are usually performed using the *Time Correlated Single Photon Counting* (TCSPC) method. In *Phase-Modulation fluorometry*, one measures the emission phase angle lag and modulation attenuation relative to the sinusoidally modulated excitation. This method works in the *Frequency-Domain (*FD*)*. Both TD and FD methods provide lifetime values, which will be the same for simple homogeneous fluorophores.

1.2.5.1 Time Domain Method

In the time-domain, if one excites a single fluorescent species with a short pulse of light, and if no photobleaching occurs, the decrease in fluorescence intensity($I(t)$) is described by an exponential decay law of the form:

$$I(t) = I_0 e^{-t/\tau} \tag{1.13}$$

This equation describes a single exponential decay where 63% of the intensity has decayed prior to $t = \tau$ and 37% has decayed at $t > \tau$. Figure 1.13 shows the simulated time domain decays for a range of single exponential fluorophores. In the case of mixtures of fluorophores, the intensity decay is not accurately described by a single exponential decay law. In these situations, the observed intensity decay may

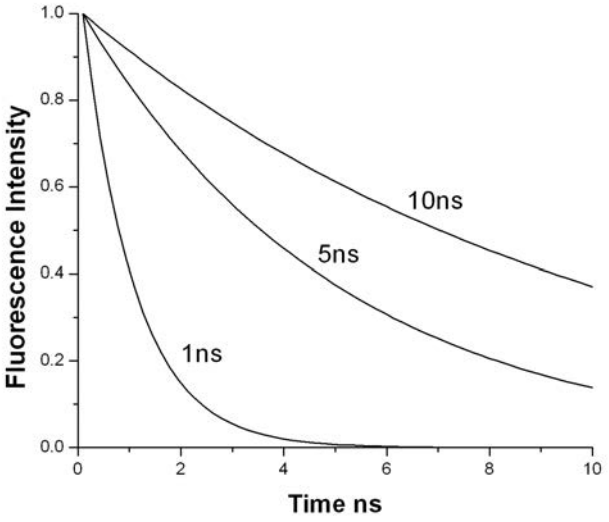

Figure 1.13: *Simulated time domain traces for a fluorophore that exhibits a* 1*,* 5*, and* 10 *ns excited-state lifetime.*

be fitted to a sum of exponentials:

$$I(t) = \sum_{i=0}^{n} \alpha_i e^{-t/\tau_i} \tag{1.14}$$

where α_i is the pre-exponential factor denoting the contribution to the total time-resolved decay of the component with lifetime τ_i. Figure 1.14 shows situation where there are two fluorophores with different lifetimes, one short and one long lifetime component. The fraction of the steady state intensity due to each component is given by:

$$f_i = \frac{\alpha_i \tau_i}{\sum_j \alpha_j \tau_j} \tag{1.15}$$

For TD experiments, the intensity of the decay (I(t)) is convolved with the Instrument Response Function (IRF). The IRF represents the response of the measurement system to the excitation pulse and can be generated by recording the output from a sample that scatters the excitation light or a fluorophore of very short lifetime. The convolution of the (IRF(t)) and the sample decay results in an observed

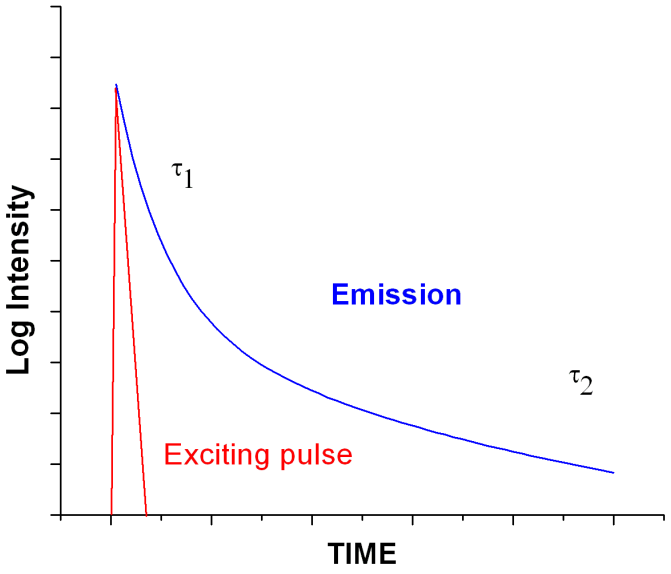

Figure 1.14: *Time-resolved decay of fluorescence intensity of a mixture of two species, the lifetimes of which are represented by τ_1 and τ_2.*

(N(t)) decay profile of the form:

$$N(t) = \int_0^n \mathrm{IRF}(t) I(t - t') dt' \tag{1.16}$$

where t' defines the variable time delays and the infinitesimally small time widths dt' of which I(t) is composed. The goal is then to extract I(t), and, in turn, the kinetic parameters from the experimental measurables (N(t) and IRF(t)). Numerous methods (such as Fourier and Laplace transforms) exist to extract I(t) from N(t) and IRF(t) [44]. The most common approach is to use a least-squares method in concert with an iterative reconvolution scheme [45, 46]. In this approach, a test model is selected (Equation 1.14), and then the convolution integral (Equation 1.16) is calculated based on an initial set of α_i and τ_i values and the measured IRF. The calculated response (C(t)) is compared with the observed data (N(t)) and the α_i and τ_i terms adjusted until a best fit is obtained. The quality of the fit is judged by the chi-squared (χ^2) (goodness of fit) test:

$$\chi^2 = \sum_{j=1}^{np} W_j \left[N(t) - C(t) \right]^2 \tag{1.17}$$

where np is the number of data points in the measured decay curve and W_j is a weighting factor. In the case of TCSPC methods, W_j follows Poisson statistics [44]‡‡.

Because χ^2 depends on the number of data points (the larger the number of data points the larger the value of χ^2), the reduced form of χ^2 is used. In this case:

$$\chi_r^2 = \frac{\chi^2}{n-p} = \frac{\chi^2}{\nu} \tag{1.18}$$

For a good fit, the value of χ_r^2 is expected to be close to unity. This is because each data point is expected to contribute to the deviation of χ^2, which is normalised by the summation term in Equation 1.17. Another diagnostic for the goodness of fit is the autocorrelation function [45]. This is given by Equation 1.19 where D_k is the deviation in the k^{th} data point and D_{k+j} is the deviation in the $(k+j)^{th}$ data point.

$$AC(t_j) = \frac{\left[\frac{1}{m}\sum_{k=1}^{m} D_k D_{k+j}\right]}{\left[\frac{1}{n}\sum_{k=1}^{n} D_k^2\right]} \tag{1.19}$$

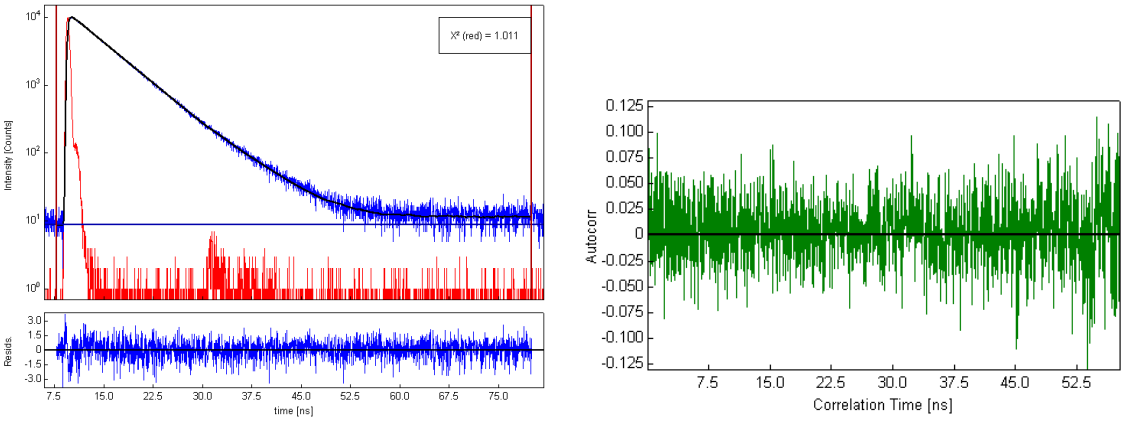

Figure 1.15: *Time domain intensity decay data for a dilute solution of* HPTS *dissolved in 0.2M phosphate buffer. Top: Time-resolved decay trace (blue) and* IRF *in red. The best fit to a mono-exponential decay function (black) is shown. The recovered residuals are given below. Bottom: The recovered autocorrelation function.* $\lambda_{ex} = 405$ *nm,* $\lambda_{em} = 510$ *nm,* $\tau = 5.4$ *ns,* $\chi_R^2 = 1.01$.

‡‡ A Poisson probability distribution is appropriate for counting experiments where the data represent the number of items or events observed per unit interval. For a Poisson distribution, the standard deviation is given by : $\sigma_j = \sqrt{N(t_j)}$ where σ_j is the standard deviation of each data point, $N(t_j)$ is the measured data [47].

The autocorrelation function gives the extent of the correlation between the deviations of the fitted and measured data in the k^{th} and $(k+j)^{th}$ channel. The calculation is normally performed for half the data channels (m=n/2). For a correct model, with an absence of systematic errors, the deviations are expected to be randomly distributed about zero. This randomness can be judged visually by plotting the autocorrelation value versus time. Figure 1.15 gives an example of a time-resolved decay trace of the pH-sensitive fluorophore HPTS (8-hydroxypyrene-1,3,6-trisulphonic acid trisodium salt) dissolved in 0.2M phosphate buffer. The decay (I(t)) is plotted in blue and the IRF(t) is plotted in red, along with the best fit (black line), The residuals determined by Equation 1.18 show a slight mismatch at $\sim$ 10ns but the autocorrelation trace is randomly distributed about zero. The fluorescence of HPTS is thus best described by a single exponential decay law with an excited-state lifetime of 5.4 ns lifetime which compares well with the literature values [48–50]. Calculations of TD lifetimes usually performed using deconvolution software.

1.2.5.2 Frequency Domain Method

In the FD method the sample is excited by a sinusoidally modulated light source and the resultant fluorescence emission occurs at the same frequency as the excitation (Figure 1.16). Due to the time delay between absorption and emission, the emission is phase shifted and demodulated [36, 51, 52]. The phase shift(ϕ_ω) where ω is the modulation frequency in radians/s ($\omega = 2\pi f$)) and demodulation of the emission depend on the relative values of the lifetime and the light modulation frequency which is illustrated in Figure 1.17 (a). In this case, a fluorophore of 5 ns lifetime is excited by light modulated at a range of frequencies from 2.5 to 250 MHz. As the light modulation frequency increases, the phase shift of the emission increases and the modulation of the emission decreases.

To explain the process of phase shift and demodulation further, in Figure 1.17 (b), a 10 ns mono-exponential decay is superimposed on the modulated excitation. For a modulation of 2.5 MHz, a full cycle is 400 ns long and on this timescale the intensity decay is very short. The emission resembles the excitation with a minimal shift in phase and demodulation. At 250 MHz, the cycle is 4 ns long. In this

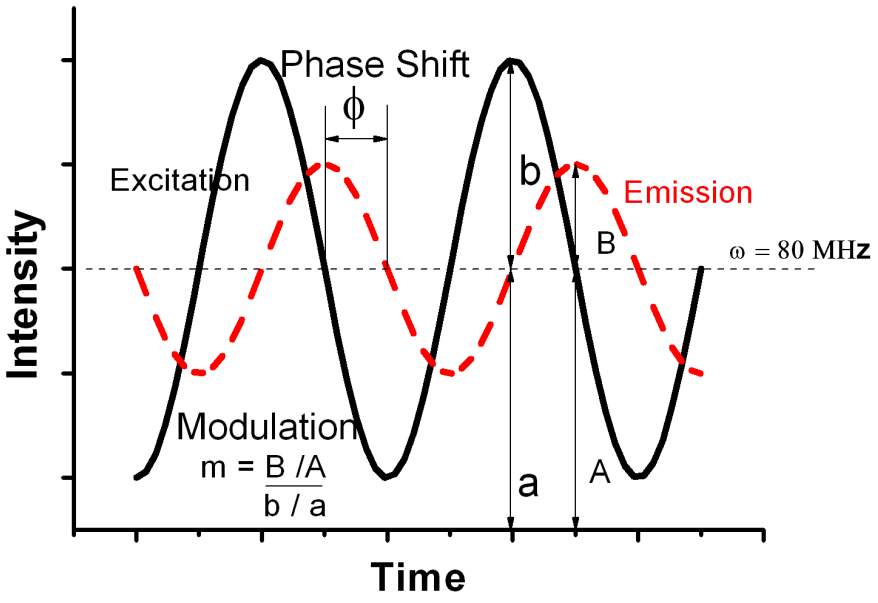

Figure 1.16: *On excitation of a fluorophore by a modulated light source the emission is shifted in phase by ϕ and demodulated according to the relationship for m shown.*

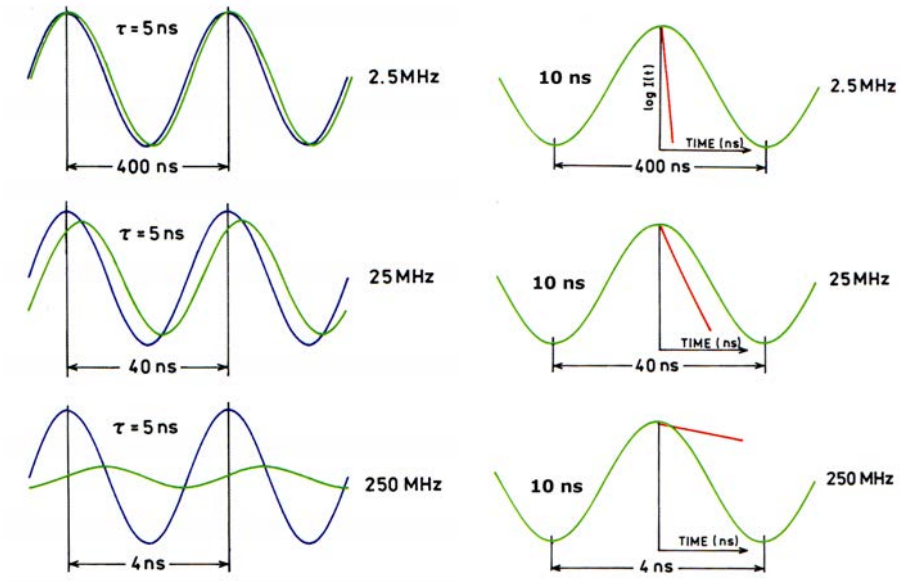

(a) (b)

Figure 1.17: *(a) Emission of a 5 ns decay time fluorophore in response to modulated excitation at 2.5, 25, and 250 MHz. (b) Comparison of a 10 ns decay with modulation frequencies of 2.5 to 250 MHz. Reproduced from [36].*

case, the molecules excited at the peak of the intensity continue to emit during the entire excitation cycle. The resultant averaging of the decay across the cycle gives an increasing phase shift and a greater demodulation of the emission signal. The influence of different lifetimes on the phase and demodulation responses is shown in the simulated FD curves in Figure 1.18. The phase and demodulation curves cross at low modulation frequencies for short lifetime fluorophores and at higher modulation frequencies for longer lifetime fluorophores. The cross-over point gives an indication of the optimal modulation frequency to be used to excite the sample as this is where the maximum rate of change in phase and demodulation occurs.

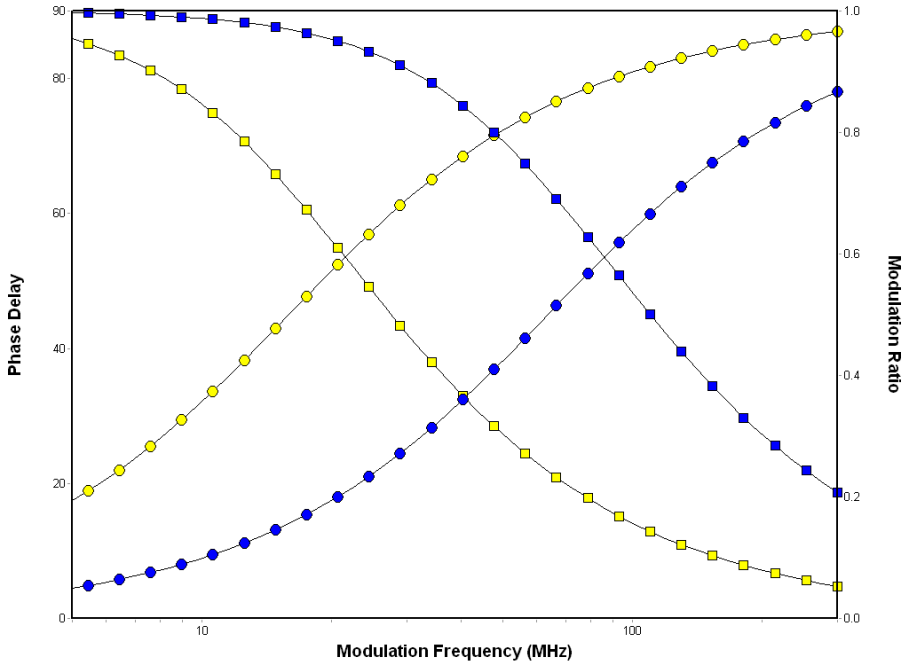

Figure 1.18: *Simulated FD data (square: modulation and circle: phase) for single exponential decays of lifetime* 2.5 *(yellow points) and* 10 *ns (blue points). The phase shift increases and the modulation decreases with increasing modulation frequency.*

The theory of the FD method are described in many publications [36, 53, 54] and the complete derivation is reproduced here. Referring back to Figure 1.16, if the excitation is sinusoidally modulated light, then:

$$I_0(t) = a + b \sin \omega t \tag{1.20}$$

where the ratio of the peak amplitude b to the base amplitude a,[§§] $b/a = m$ is termed the modulation of the incident light. As described above, the phase and modulation of the emission will be different but at the same frequency. The population of the excited state is:

$$N(t) = A + B\sin(\omega t - \phi) \tag{1.21}$$

The demodulation is given by the ratio of the amplitudes B/A and phase shift ϕ. Recall the single exponential intensity decay (Equation 1.13). Differentiating the single exponential intensity decay gives an expression for the time-dependent excited state population:

$$\frac{dN(t)}{dt} = -1/\tau N(t) + I_0(t) \tag{1.22}$$

Using $d/dx(\sin u) = \cos u \; du/dx$, the derivative of Equation 1.21 gives:

$$\frac{dN(t)}{dt} = \omega B\cos(\omega t - \phi) \tag{1.23}$$

Substitution of equation 1.23 into equation 1.22 yields:

$$\omega B\cos(\omega t - \phi) = -1/\tau[A + B\sin(\omega t - \phi)] + a + b\sin\omega t \tag{1.24}$$

If the sin and cos functions are expanded using the standard trigonometric identities i.e.:

$$Cosine\ Expansion : \cos(\alpha - \beta) = \cos\alpha\cos\beta + \sin\alpha\sin\beta$$
$$Sine\ Expansion : \sin(\alpha - \beta) = \sin\alpha\cos\beta - \sin\beta\cos\alpha$$

then the following relationships can be found by equating the constant terms and those terms in ϕ and ωt.

$$a - (1/\tau)A = 0 \tag{1.25}$$

[§§] This base amplitude is commonly called the *Direct Component (DC)* offset. This term comes from the function for a sinusoidal wave as opposed to the b term or *Alternate Component (AC)* part.

$$\omega \cos\phi - (1/\tau)\sin\phi = 0 \tag{1.26}$$

$$\omega \sin\phi + (1/\tau)\cos\phi = b/B \tag{1.27}$$

From Equation 1.26,

$$\tan\phi = \omega\tau_\phi \tag{1.28}$$

where τ_ϕ is the phase derived fluorescence lifetime. Squaring equations 1.26 and 1.27, addition of the terms and remembering the identity, $\cos^2\phi + \sin^2\phi = 1$, yields:

$$\omega^2 + (1/\tau)^2 = (b/B)^2 \tag{1.29}$$

From equation 1.25, $A = a\tau$, and if the demodulation of the excitation sinusoid is defined as by $m = \frac{B/A}{b/a}$ (see figure 1.16), then:

$$m = B/\tau b = \left[1 + \omega^2\tau_m^2\right]^{-1/2} \tag{1.30}$$

where τ_m is the modulation derived fluorescence lifetime.

Equations 1.28 and 1.30 provide the basis for the independent determination of a single lifetime based on a single frequency phase and modulation measurement value respectively. Figure 1.19 shows the result from a least squares regression fit of phase and modulation data obtained for the single fluorophore (HPTS) case. A single decay term fits the data giving a recovered lifetime of 5.4 ns.

In the case of a mixture of noninteracting fluorophores, each giving rise to a single exponential decay, then a composite sinusoidal emission waveform will result, which can be written in terms of the normalised sine and cosine fourier transforms of the multiple fluorophore intensity decay [55]:

$$P = \frac{\int_0^\infty I(t)\sin(\omega t)dt}{\int_0^\infty I(t)dt} \tag{1.31}$$

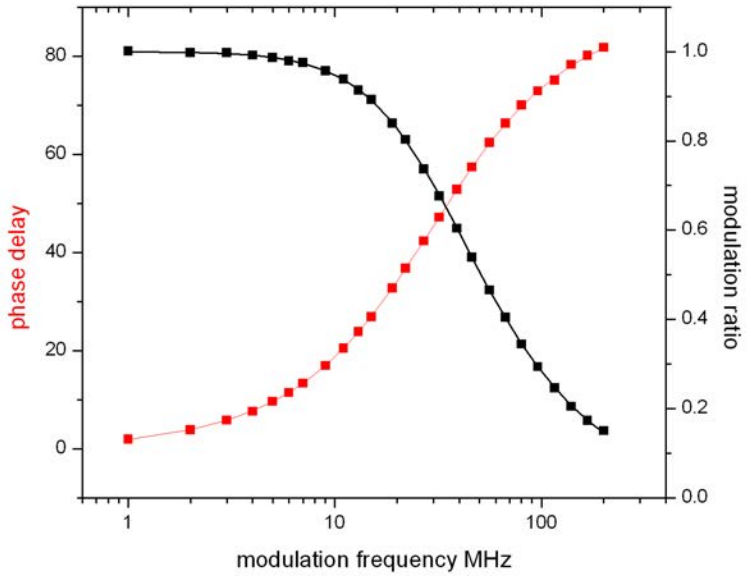

Figure 1.19: *Phase and Modulation data for the fluorophore HPTS and the associated least squares fitting line from a one decay term fit. Experimental details:* λ_{ex}*=405 nm,*λ_{em}*=465 to 500 nm, number of frequencies = 25, from 1 to 120* MHz*). Results:* $\tau = 5.4 \pm 0.1$ *ns,* χ^2_R *= 0.5.*

$$Q = \frac{\int_0^\infty I(t)\cos(\omega t)dt}{\int_0^\infty I(t)dt} \tag{1.32}$$

For a multi-exponential decay, the transforms are related to the pre-exponential factors and lifetimes by [52, 56]:

$$P = \sum_i \frac{\alpha_i \omega \tau_i^2}{1+\omega^2\tau_i^2} / \sum_i \alpha_i \tau_i \tag{1.33}$$

$$Q = \sum_i \frac{\alpha_i \tau_i}{1+\omega^2\tau_i^2} / \sum_i \alpha_i \tau_i \tag{1.34}$$

These transforms are related to the experimental parameters, i.e. phase and demodulation by:

$$\phi = \tan^{-1}(P/Q) \tag{1.35}$$

$$m = \frac{1}{\sqrt{P^2 + Q^2}} \tag{1.36}$$

The experimental data are compared by nonlinear regression to the values predicted from chosen model (single or multiple decay terms), and the parameters of the model adjusted to yield minimal deviations between the data and the prediction. The decay terms α_i and τ_i are varied to yield the best fit between the data and the calculated values according to the minimized χ_r^2 parameter which is given by [36]:

$$\chi_r^2 = 1/\nu \sum_{\omega} \left[\frac{\phi_\omega - \phi_{c\omega}}{\delta\phi} \right]^2 + 1/\nu \sum_{\omega} \left[\frac{m_\omega - m_{c\omega}}{\delta m} \right]^2 \tag{1.37}$$

where ν is the degrees of freedom (2 times the number of frequencies used in the experiment minus the number of variable parameters). The subscript c indicates the calculated values based on selected values for α_i and τ_i. $\delta\phi$ and δm are the uncertainties in the phase and modulation experimental data. The correct model is determined by the lowest value of χ_r^2.

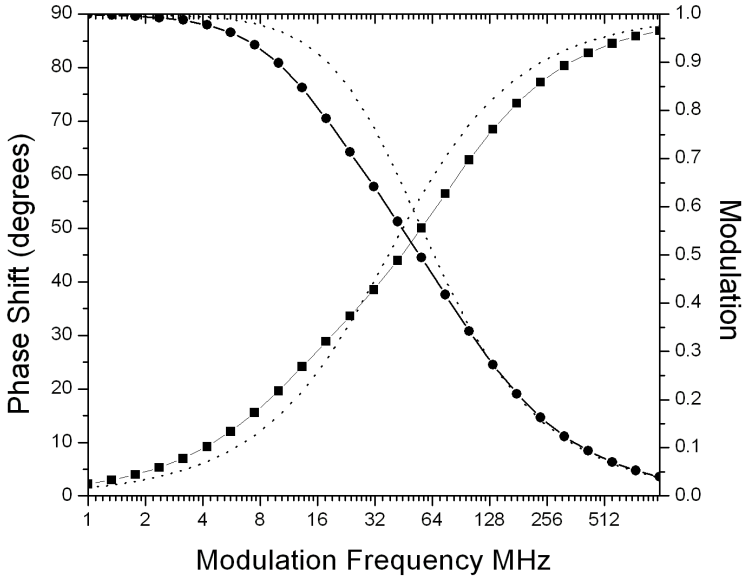

Figure 1.20: *Simulated data for a 50:50 mixture of two fluorophores of 2.5 and 10 ns. The dashed line shows the single decay fit. For two decay terms the solid line represents the model which gives a good fit to the data.*

Figure 1.20 shows the simulated phase and modulation response for a 50 : 50

mixture of two fluorophores of different lifetimes showing the difference between the single and double exponential fitting.

1.2.6 Average Lifetimes

For analysis of complex mixtures such as crude oils, the intensity based average lifetime, $\overline{\tau}$ is often used and is given by:

$$\overline{\tau}_{int} = \frac{\alpha_1\tau_1^2 + \alpha_2\tau_2^2 + \alpha_n\tau_n^2}{\alpha_1\tau_1 + \alpha_2\tau_2 + \alpha_n\tau_n} = f_1\tau_1 + f_2\tau_2 + f_n\tau_n = \sum_{i=1}^{n} f_i\tau_i \tag{1.38}$$

where f_i is the fractional contribution of the i^{th} component. In this expression, each decay time is weighted by its corresponding fractional intensity and thus this average lifetime is termed the *intensity averaged lifetime*. The intensity averaged lifetime can be defined as the average lifetime of a collection of different excited-state populations, where the lifetime of each population is weighted by the relative contribution of that population to the total fluorescence.

It is also possible to use the pre-exponential factors (i.e. the amplitudes) as weights and define the *amplitude averaged lifetime*:

$$\overline{\tau}_{amp} = \frac{\sum_{i=1}^{n} \alpha_i\tau_i}{\sum_{i=1}^{n} \alpha_i} = \sum_{i=1}^{n} \alpha_i\tau_i \tag{1.39}$$

where α_i are the fractional amplitudes which are defined as:

$$\alpha_i = \frac{\alpha_i}{\sum_{i=1}^{n} \alpha_i} \tag{1.40}$$

Since $\sum_{i=1}^{n} \alpha_i = 1$, the amplitude averaged lifetime reduces to:

$$\overline{\tau}_{amp} = \sum_{i=1}^{n} \alpha_i\tau_i \tag{1.41}$$

For heterogeneous decays, the intensity-based average lifetime is more accurate than the amplitude-based lifetime. However, there are cases where the amplitude

based average lifetime is more appropriate, for example, it has been used to calculate the efficiency of energy transfer [57].

1.2.7 Lifetime Distributions

There are a number of situations where a distribution of decay terms is expected instead of a set of discrete decay times [58–60]. For example, samples containing a mixture of interacting fluorophores, or where a fluorophore exists in a number of different but closely related environments, may be analysed as a distribution of decay times. The most common distributions used are the Gaussian, Lorentzian, and Stretched Exponential distributions [36]. Here, the α_i values are replaced by a distribution function $\alpha(\tau)$. The relationship to each lifetime is given by:

$$I(\tau, t) = \alpha(\tau)e^{-t/\tau} \tag{1.42}$$

The total decay is given by:

$$I(t) = \int_{\tau=0}^{\infty} \alpha(\tau)e^{-t/\tau}d\tau \tag{1.43}$$

where $\int \alpha(\tau) = 1.0$. The Gaussian $\alpha_G(\tau)$ and Lorentzian $\alpha_G(\tau)$ lifetime distributions are given by:

$$\alpha_G(\tau) = \frac{1}{\sigma\sqrt{2\pi}} exp\left\{-1/2\left(\frac{\tau - \overline{\tau}}{\sigma}\right)^2\right\} \tag{1.44}$$

$$\alpha_L(\tau) = \frac{1}{\pi}\frac{\Gamma/2}{(\tau - \overline{\tau})^2 + (\Gamma/2)^2} \tag{1.45}$$

where $\overline{\tau}$ is the central value of the distribution, σ is the standard deviation and Γ is the full width of the distribution at half maximum. For a Gaussian distribution the full width at half maximum is given by 2.345σ. When analysing lifetime distributions, each decay time component is associated with three variables, the amplitude α_i, the fractional contribution f_i, and the full width at half maximum or FWHM Γ. Consequently, a complex decay may be fit with fewer exponential components. The

Stretched Exponential or the Kohlrausch-Williams-Watts function takes the form:

$$I(t) = I_0 exp[(-t/\tau)^{\beta}] \tag{1.46}$$

where the exponent β or 'heterogeneity' parameter is related to the distribution of decay times, taking values from 0 to 1. For a single exponential decay, β would be equal to 1. The stretched exponential model has been applied to complex systems such as the generation of lifetime maps (FLIM) of biological tissue. It can be shown that superior signal-to-noise ratios of FLIM images can be obtained using the stretched exponential model although for complex materials a multi-exponential model was needed to reduce the noise adequately for image analysis [61, 62].

1.2.8 Experimental methods used to record lifetimes in the Time and Frequency Domains

The principle TD method used to determine fluorescence lifetimes is Time-Correlated Single Photon Counting (TCSPC) [63, 64]. This technique exploits the concept that the time-dependent probability distribution for emission of a single photon after an excitation event yields the actual intensity versus time distribution of *all* the photons emitted as a result of the excitation. By statistically sampling the random emission of photons following a large number of excitation events, a probability distribution is constructed [63].

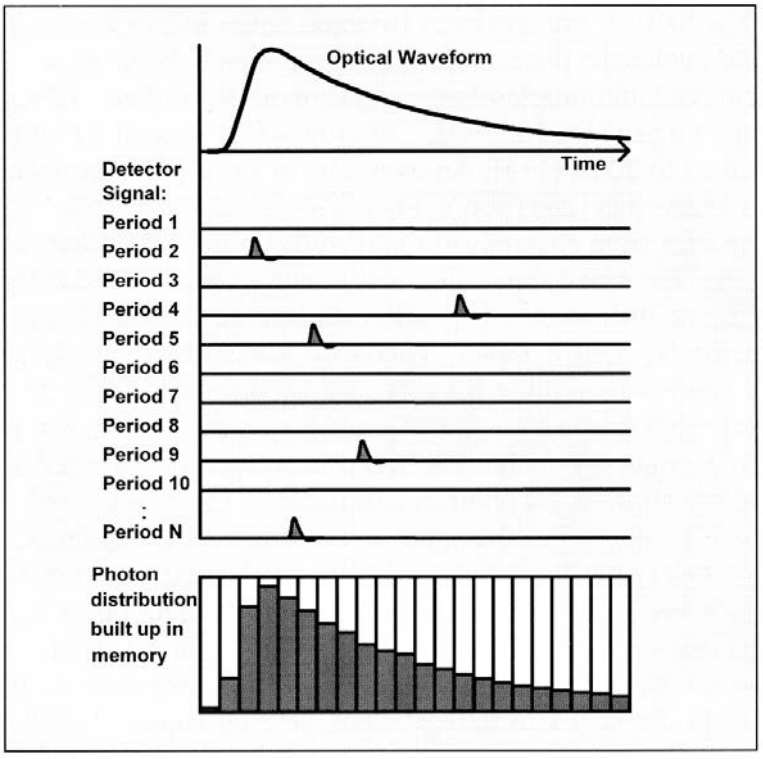

Figure 1.21: *General principle of* TCSPC. *The pulses in the middle panel represent the photons captured over the time interval. As each photon is counted a histogram is built up based on the accumulated counts versus arrival time. Reproduced from [64].*

Figure 1.21 presents a graphical representation of the principle behind TCSPC. The sample is excited with a short-duration pulse of light and the measurement conditions are adjusted so that the photon detection rate is typically 1 photon per 100 excitation pulses. The time between the excitation pulse and the arrival of observed photon is measured and the information is stored in a histogram. The x axis of the histogram is the arrival time and the y axis is the number of photons detected at each time. The resultant histogram therefore represents the decay profile of the fluorophore. The histogram is collected in a block of memory, where a memory block holds the photon counts for a corresponding time interval or channel. When sufficient counts have been collected the histogram memory can be read and be used for fluorescence lifetime calculation. In order to measure these very short time intervals, specialised electronics are necessary. A generalised schematic of the electronics for a typical TCSPC setup is given in Figure 1.22.

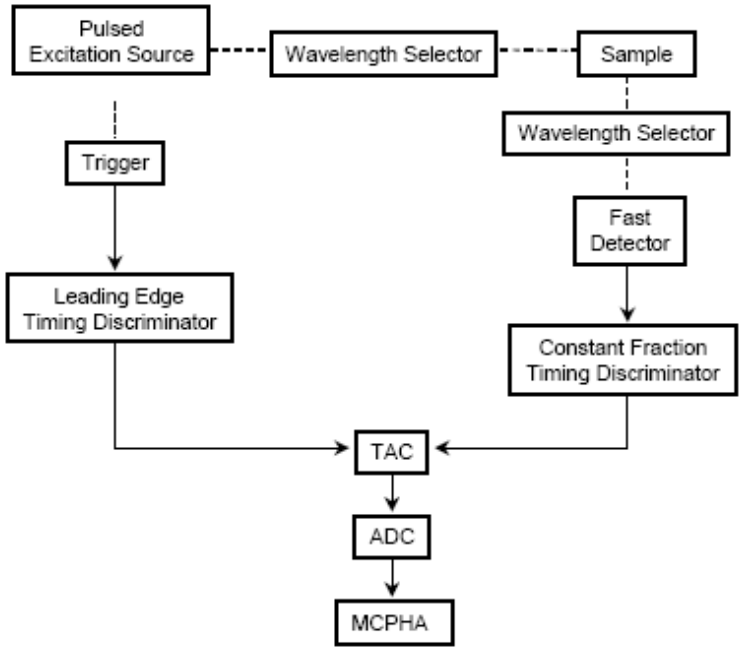

Figure 1.22: *Schematic of a typical* TCSPC *system. TAC: time to amplitude convertor, ADC: analog to digital convertor, MCPHA: multichannel pulse height analyser or Histogrammer. Reproduced from [43].*

The heart of the TCSPC system is the time-to-amplitude converter (TAC). It measures the elapsed time between the trigger from the pulsed light source and when the first emitted photon from the sample is detected [43]. Hence, the trigger pulse is time correlated with the time of generation of the optical pulse by the photomultiplier tube (PMT). After receiving the trigger pulse, the TAC then initiates the charging of a capacitor plate which is routed to the TAC start input via a discriminator. To avoid pulse height jitter common to PMTs, a Constant Fraction Discriminator (CFD) is used that triggers at a constant fraction of the pulse amplitude. Similarly, a second CFD is used to prevent fluctuations and drift in a reference signal from the excitation source. The output pulses are used as start/stop pulses of a time-to-amplitude converter (TAC). While the same optical pulse that triggered the TAC excites the fluorescent sample, the emission light intensity is adjusted so that only one photon (the 'stop' photon) is detected for every $100-200$ excitation events. The signal resulting from the detected photon stops the charging ramp in the TAC, which transmits a pulse. The amplitude of this pulse is proportional to the charge in the capacitor, and hence to the time difference between the start and stop pulses. The

TAC output pulse is given a numerical value within the analog-to-digital converter (ADC) and a count is stored in the data storage device (e.g. a multichannel pulse height analyzer or histogrammer; MCPHA) in an address corresponding to that number. Excitation and data storage are repeated again and again in this way until the histogram of the number of counts against address number (channel number) in the storage device represents the decay curve of the sample [63, 64].

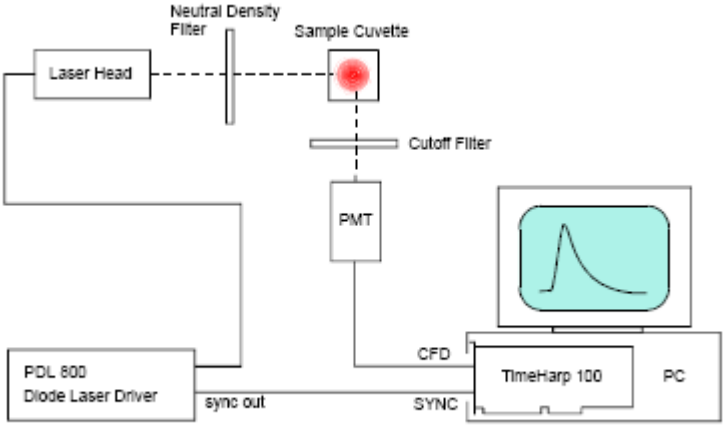

Figure 1.23: *A typical setup for fluorescence lifetime measurements with* TCSPC*. Reproduced from [65].*

Figure 1.23 shows a typical setup for fluorescence lifetime measurements with TCSPC. The light pulses controlled by the laser driver are directed at the sample cuvette, via the appropriate optics. A neutral density filter can be used to attenuate the light levels if necessary. Upon excitation, the fluorescent sample will emit light at a longer wavelength than that of the excitation light. The fluorescence emission is filtered out from scattered excitation light by means of an optical cutoff filter and directed to the detector (PMT or Avalanche Photo Diode (APD)). The electrical signal obtained from the detector is fed to the TCSPC electronics, now usually contained on a single PC board, placed in the computer. The laser driver also provides the electric synchronisation signal needed for the photon arrival time measurement. This signal is also fed to the TCSPC electronics via coaxial cable.

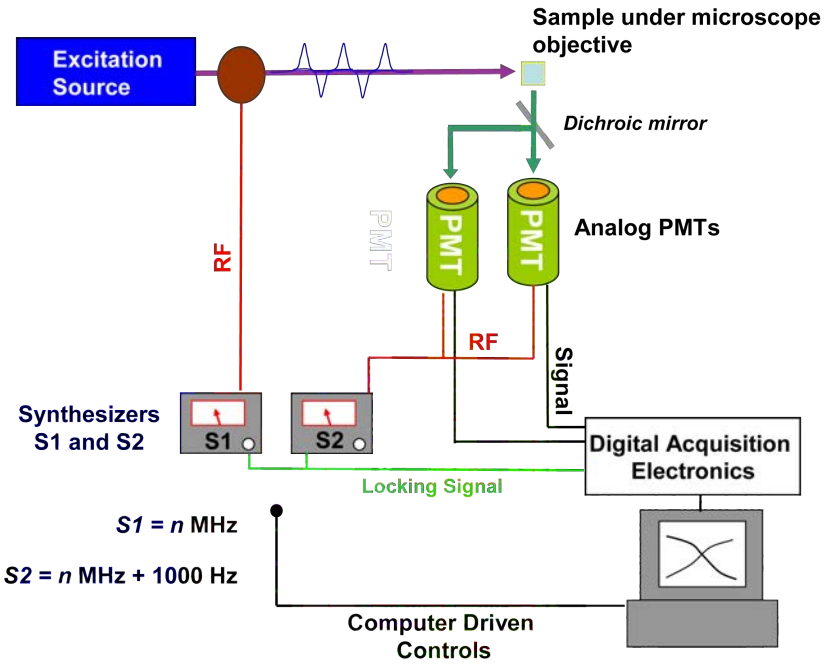

Figure 1.24: *Simplified schematic of a dual channel phase and modulation fluorometer.*

In the frequency domain (FD), the sample under study can be excited with sinusoidally, amplitude-modulated light over the MHz to GHz range [36, 43, 56]. The data acquisition system schematic used for FD measurements used in this work is illustrated in Figure 1.24. Two PMTs are available, enabling dual channel data collection. The two PMTs are gain modulated by an amplified radio frequency (RF) signal from a frequency synthesizer (S2), that is locked in phase to a second master oscillator used for laser diode source modulation (S1). The use of the *cross-correlation* technique is ubiquitous in FD measurements [43]. In this technique, the PMTs are modulated at the same frequency as the source (ω, from 1 to 200 MHz), plus a small offset frequency ($\Delta\omega$, $\sim$ 1000 Hz). This low frequency signal can then be filtered from the high frequency part so that it still contains the phase and modulation information but without interference from harmonics or noise. Consequently, the low frequency signal is analysed by software and processed to extract phase and modulation data. A reference sample of known lifetime is measured at a range of frequencies and the associated phase and modulation values are stored. The sample is then analysed using the same measurement conditions and comparison with the reference ϕ and modulation values yields a corrected phase and modulation value

at each frequency according to Equations 1.47 and 1.48 where the subscripts $corr$, $meas$ and ref represent the corrected, measured and reference phase and modulation values respectively:

$$\phi_{corr} = \phi_{meas} - \phi_{ref} + \arctan(\omega\tau_{ref}) \tag{1.47}$$

$$M_{corr} = \frac{M_{meas}}{M_{ref}} \times \frac{1}{\sqrt{[1 + (\omega\tau_{ref})^2]}} \tag{1.48}$$

In theory, for a single-exponential decay, one should observe the same lifetime using the observed ϕ and modulation at any given frequency [66]. However, for mixtures of components, ϕ is biased towards the faster decay components and the modulation is weighted toward the slower components. Hence, resolving separate fluorescence lifetime parameters for mixtures requires measurements at a range of frequencies to be statistically valid [51]. On the other hand, the multi-frequency cross-correlation technique is not constrained by the Poissonian single-photon detection limits of TCSPC, i.e., a small range of frequencies is usually sufficient to resolve separate fluorescence lifetimes.

1.2.9 Comparison between TD and FD

The main differences between TD and FD techniques are given in Table 1.2. Each method has its own advantages and disadvantages and are viewed as complimentary rather than competitive. Overall, the FD method is potentially more useful for complex fluid analysis, since the data analysis can be more straightforward and rapid than for TCSPC [36].

Table 1.2: *Comparison between the FD and TD techniques*

	Time Domain	Frequency Domain
1	Sample is excited with a pulse of light. The width of pulse is less than decay time of sample.	Sample is excited with intensity modulated light typically sine wave.
2	Visualisation of the fluorescence decay easy.	Variation of modulation and phase is conceptually more difficult to visualise.
3	High sensitivity using single photon technique very low levels of fluorescence detection possible.	Less sensitive for low levels of fluorescence.
4	De-convolution of the IRF from the decay curve is necessary.	No de-convolution necessary but a reference standard must be used.
5	Data analysis based on Poisson statistics is well defined.	Evaluation of the standard deviations of the phase shift and modulation ration is not easy.
6	Collection of a large number of photon events is necessary leading to longer acquisition times.	Small number of frequencies can sufficiently resolve heterogeneous decays leading to shorter acquisition times.
7	Relatively expensive equipment.	Equipment can be cheaper.

1.2.10 Fluorescence microscopy and Lifetime Imaging

Fluorescence based microscopy techniques have undergone major development in the last twenty years and continue to be at the forefront of modern biological research [37, 67]. The basic task of the fluorescence microscope is to allow excitation light to irradiate the sample and then to separate the fluorescence emission light from the excitation light, allowing only the emission light to reach the eye or detector. The excitation light is focussed on to the sample through an objective lens and the fluorescence emission is then observed through this same objective. This optical geometry is called *epi-fluorescence* and utilises a dichroic mirror (a mirror with significantly different reflection or transmission properties at two different wavelengths) to separate the excitation light from the fluorescence emission. A simplified block

diagram showing the operation of a fluorescence microscope is given in Figure 1.25. The dichroic beam splitter separates the reflected excitation light (purple) from the emission light from the sample (green). An emission filter then stops any stray emission light from reaching the eyepiece.

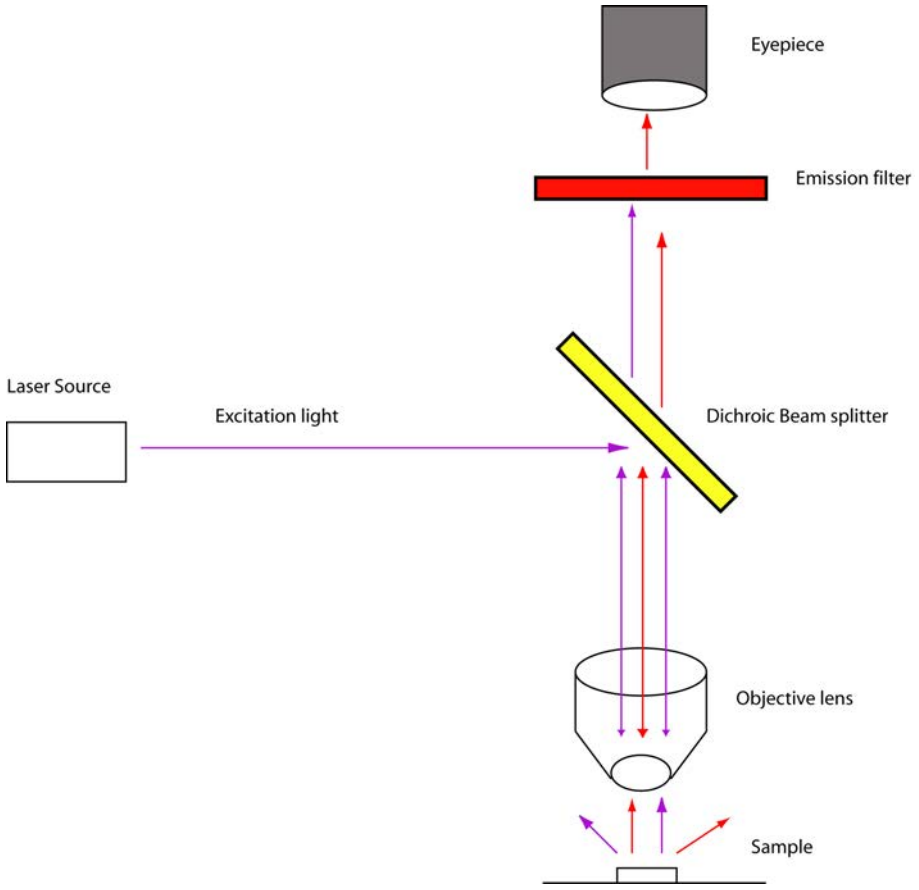

Figure 1.25: *Simplified block diagram of a fluorescence microscope.*

Fluorescence microscopy has been used in many applications across the sciences from biology (investigation of living cells and tissues), geology (fluorescence emission from fluid inclusions) [68] to chemistry (colloids, polymer blends and photodegradation studies) [69]. However the image obtained is often obscured by fluorescence occurring from parts of the sample that are out of the plane of focus. The problem is compounded by thicker samples (greater than $2\mu m$), which usually exhibit such

a high degree of fluorescence emission giving poor axial resolution[¶¶].

Confocal microscopy [70, 71] offers higher axial resolution over the conventional fluorescence microscope. The confocal approach uses a pinhole to eliminate out-of-focus light in samples whose thickness exceeds the immediate plane of focus. Contrast and definition are dramatically improved over conventional fluorescence microscope techniques due to the reduction in background fluorescence and improved signal-to-noise ratio. Figure 1.26 shows the principle of confocal operation. In some systems a pinhole can be used in the excitation beam allowing a unique point of the sample to be illuminated. As in conventional fluorescence microscopy, the excitation light is focussed onto the sample via the objective. The fluorescence emitted from the sample is separated from the incident light by a dichroic mirror and directed to the detector (Usually a PMT or APD). Fluorescence from out of focus planes above and below the sample point, will strike the pinhole wall and will not reach the detector. Because much of the out-of-focus light is restricted by the emission pinhole, high excitation energies may be needed to allow detection of weak fluorescence. At higher excitation energies, samples are more susceptible to photodamage and photobleaching but this can be partly counteracted by using a detector with high sensitivity and high numerical aperture objectives. The development of the Spinning-disk method*, based on the disk invented by Nipkow in 1884, has also partly alleviated the effects of high energy lasers on the sample [72].

[¶¶] The resolution of a microscope objective is defined as the smallest distance between two points on a specimen that can still be distinguished as two separate entities. In order to obtain effective image resolution, fluorescence microscopes require objectives with high numerical aperture (NA). The NA is a measure of the ability of the objective to gather light and resolve sample detail at a fixed object distance. However high NA objectives tend to have very small working distances so the lens must be placed very close to the sample. They have shallow depths of field and out of focus fluorescence can still be collected from the illuminated area. The maximum axial(xz) resolution of an objective is approximately equal to half the wavelength of the radiation used (i.e. $0.2 - 0.3\ \mu m$ for visible radiation). For samples thicker than this depth of field, the images are blurred by out of focus fluorescence.

* The Spinning disk method first invented by Nipkow in 1884, uses a disk with a series of pinhole apertures. The pinholes serve to both focus spots of light on the sample and also as the confocal pinholes. The arrangement of pinhole apertures on the disk is such that as the disk spins, the illumination spots scan the entire field of view of the microscope. The amount of excitation needed is reduced, thereby minimising photodamage and photobleaching.

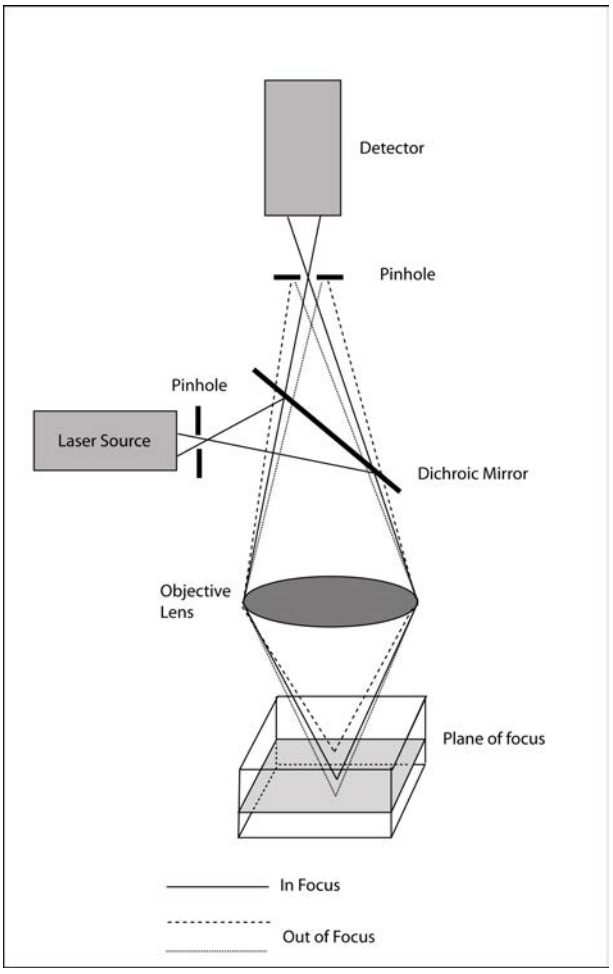

Figure 1.26: *Schematic showing the principle of confocal microscopy- Adapted from [73].*

Lateral(xy) and axial(z) resolution of confocal microscopy is greater than that of conventional optical microscopy by a factor of $1.4 - 2$ [73]. The improvement in confocal axial point spread functions over widefield microscopy is shown in Figure 1.27. Point spread functions are used to map the blurring or spread of photon intensity from the sample at the detector which comes from abberations of the optics and/or alignment issues.

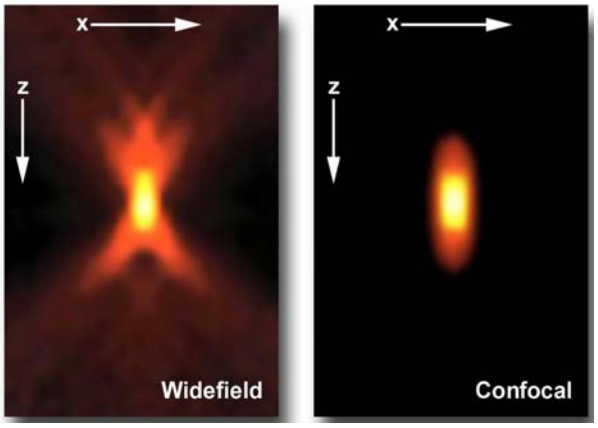

Figure 1.27: *Comparison of axial (x-z) point spread functions for widefield (left) and confocal (right) microscopy. Reproduced from [72].*

In confocal instruments the sample is scanned in the xy plane either by adjustment of the excitation light as it passes through the objective using a galvanometrically-controlled scanning mirror system or by movement of the sample stage. The sample is also scanned in the axial (z) direction using a motorised piezo controlled stage. Optical 2D sections can be then be obtained at different depths from the surface of the sample. A series of images is collected by coordinating incremental changes in the microscope/stage conditions with sequential image acquisition at each step.

The last decade has seen major advances in fluorescence/confocal microscopy such as imaging of protein localisation in living cells and being able to view the structure and function of living tissue [74]. These advances have mainly been due to the development of genetically encoded fluorophores such as Green Fluorescent Protein (GFP) and the invention of Multiphoton Microscopy***. Despite these advances, confocal methods (whether single or multi-photon) suffer from intensity-based steady-state artifacts. The measured fluorescence intensity is dependent upon a variety of environmental influences, such as quenching by other molecules, aggregation, energy transfer, and refractive index effects, and can thus be difficult to quantify or interpret. Coupling confocal microscopy with time resolved measurements has led to the development of Fluorescence Lifetime Imaging (FLIM) which

*** Utilising long wavelength , fast repetition rate lasers, two or more photons can be simultaneously absorbed by a fluorophore. The resultant emission still occurs from the same excited state as for standard fluorescence (one-photon) excitation. This leads to a localised excitation, minimised damage to the fluorophore (photobleaching) that has found many applications in biological imaging [75].

provides enhanced contrast according to the fluorescence lifetime measured at each point (pixel) of the image [76, 77]. The technique has found many applications in biology and medicine, examples of which are the mapping of cell parameters such as pH, ion concentrations or oxygen saturation by fluorescence quenching, scanning of tissue surfaces, and skin imaging [76–79]. The recording of lifetime based images constitutes a major challenge in data processing of an image 256 × 256 pixels in size (a typical image size). For every pixel there could be contributions of several fluorescent species, each one could be multi-exponential. Resolution of the decay relies on advanced computational methods and the use of 'global' analysis[‡] methods [80].

The technologies for FLIM can be divided into two categories: (i) confocal laser scanning or multiphoton excitation [75] FLIM, and (ii) wide-field camera-based FLIM [81]. FLIM can be recorded in time [82] and frequency domains [83, 84]. In a FD FLIM instrument, the principle of lifetime measurement is similar to that described in section 1.2.5.2 [85]. The phase, modulation and intensity values are recorded for each frequency at each point and the sample is scanned point by point until the desired range is achieved. The image of the sample is then built up pixel by pixel in terms of the calculated lifetimes from the phase and modulation measurements. Images can also be built up based on multiple frequency measurements [83]. Though more accurate in terms of lifetime, this approach lengthens the sample exposure time considerably leading to the possibility of photobleaching.

1.3 Spectroscopy of crude petroleum oils

1.3.1 Current spectroscopic techniques

From literature surveys of crude oil vibrational spectroscopy, Near Infra-red (NIR) and Infra-red (IR) spectroscopy are probably the most common methods in the analysis, identification and characterisation of crude oils [34, 86–93]. A preliminary investigation has also been made into the feasibility of Raman spectroscopy [94, 95].

[‡] Instead of analysing each pixel separately, all pixels are analysed simultaneously holding certain values as invariant or global. Generally the lifetimes are considered to be invariant and used as global parameters. This yields an image of the populations of each molecular species and the discrete lifetime values, dramatically improving in the accuracy and precision of FLIM data analysis.

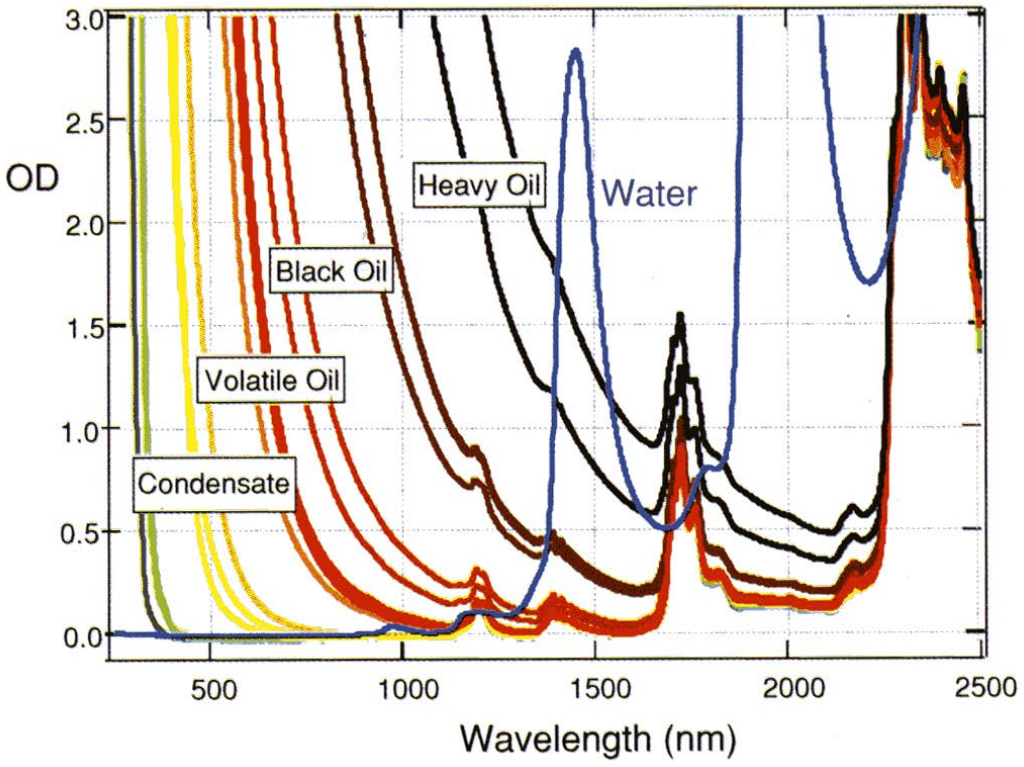

Figure 1.28: *Visible-*NIR *spectra of various crude oils and water. Both vibrational overtones and electronic absorption profiles are seen and water oil differentiation is possible. The* NIR *bands are similar for all oils yet the electronic absorption profile is very different. Reproduced from [96].*

NIR spectra (800-2500 nm) are typically very broad and complex and consist of overtones and combination bands of the fundamental molecular absorptions found in the mid infrared region. Though spectra can be acquired rapidly, it can be difficult to assign specific features to specific chemical components. However, utilising multivariate analytical methods, the technique has found uses in characterisation of crude oil physical and chemical properties [97]. Figure 1.28 shows both electronic absorption profiles and vibrational overtones covering the Visible to NIR regions of the electromagnetic spectrum for a series of crude oils [96]. The NIR spectra are dominated by -CH overtones, the first overtone occurring at $\sim$ 1700 nm and the second at $\sim$ 1300 nm. There is a marked overlap of the NIR peaks at these wavelengths. In contrast, as the oil density increases, containing more heavy aromatic compounds, the electronic absorption increases.

The colour of crude oils is due to the overlapping spectra of the many constituent

PAH's. It has been shown that this colouration is systematic, exhibiting a similar slope of the electronic absorption edge or 'Urbach Tail' [98]. When optical[†††] den-

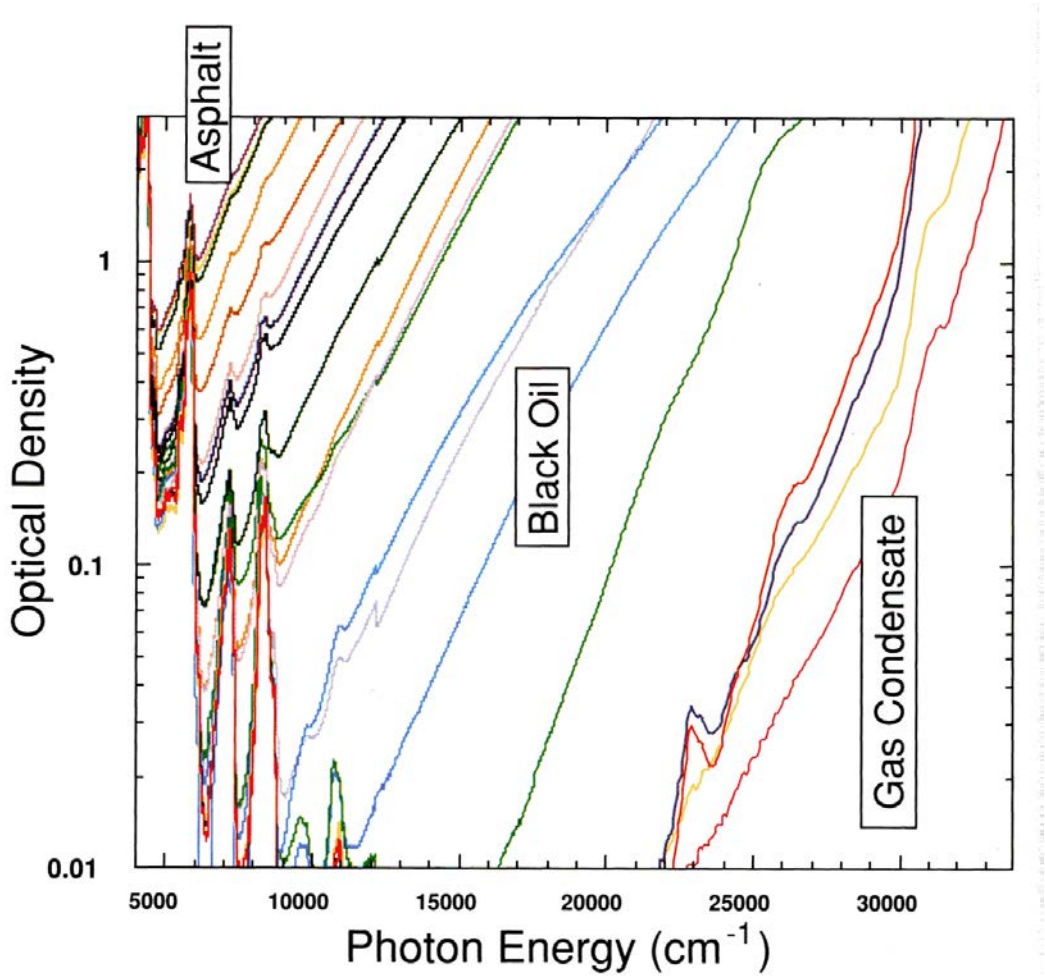

Figure 1.29: *In absorption spectra of crude oils the observed Urbach tail is similar but the spectral locations of where the tail occurs differ. Reproduced from [96].*

sity is plotted against photon energy an almost linear electronic absorption edge is observed (Figure 1.29) [96]. It is thought that this absorption spectrum directly reflects the population distribution of PAH's in crude oils and corresponds to an exponentially decreasing population of large PAH molecules [98].

[†††] The intensity of the incident light I_0 on a sample is reduced by its absorption (A) and how much scattering the sample induces yielding transmitted light of intensity I. Transmission of light is defined as $T = I/I_0$. The optical density (OD) of a sample is given by $A(OD) = -log\,(T)$. For homogeneous samples with no scattering, the Beer-Lambert law applies $A = \epsilon \cdot c \cdot l$ where ϵ is the extinction coefficient, c is the concentration and l is the optical pathlength through the sample. Both A and ϵ are a function of wavelength and the optical spectrum of a material is characterised by ϵ and the concentration. This situation is complicated when the heterogeneity of the sample is high.

Due to the similarity of the electronic absorption in the visible and ultra-violet regions [99], analysis of crude oils by UV-VIS has not received the same attention as given to NIR and IR methods. Recent studies on crude oil UV spectra [100, 101] have suggested that discrimination between heavy and light crude oils is possible when based on the ratio of absorption measured at 465 and 665 nm. However, dilution of the neat crude oils was necessary before analysis.

1.3.2 Crude Oil Fluorescence

Crude oil fluorescence originates from a multitude of different aromatic hydrocarbons and is strongly influenced by the chemical composition and physical properties of the oil. Much research (primarily for the oil industry) has been devoted to developing fluorescence based analytical methods, descriptions of which can be found in a number of recent reviews [1, 102, 103]. However, the use of fluorescence based methods for analysing crude oil is not a modern concept. UV induced fluorescence has been used to measure thermal alteration in kerogens in the '60's [104]. Geologists have been able to distinguish oil bearing fluid inclusions from aqueous fluid inclusions by examining fluorescence emission; a standard technique since the early '80s [105](See Section 1.6 for further information on fluid inclusions). More recently, emission spectra have been used to provide information on the nature of crude oil fluorescence [106–109] and also have been applied to oil spill identification and water quality control [110, 111].

Unfortunately, the wide range of chemical and physical characteristics found in crude oils introduces a high degree of complexity into any fluorescence based analysis method. In general, fluorescence emission from crude oils is governed by the complex interplay between energy transfer and quenching caused by the high concentrations of fluorophores and quenchers present in petroleum oils. For heavy oils, fluorescence emission is generally broad, has a large Stokes shift[‡‡‡], is weak, and has short lifetimes. Lighter oils tend to have a narrower emission band, a smaller Stokes shift, are more intense, and have longer lifetimes. Figure 1.30 shows three representative crude oils spanning the API range from light oils (high API gravity)

[‡‡‡] In reality, the Stokes Shift can not be exactly determined for crude oils. More practically it is represented by the shift in emission maximum from the absorption band edge.

to heavy oils (low API gravity).

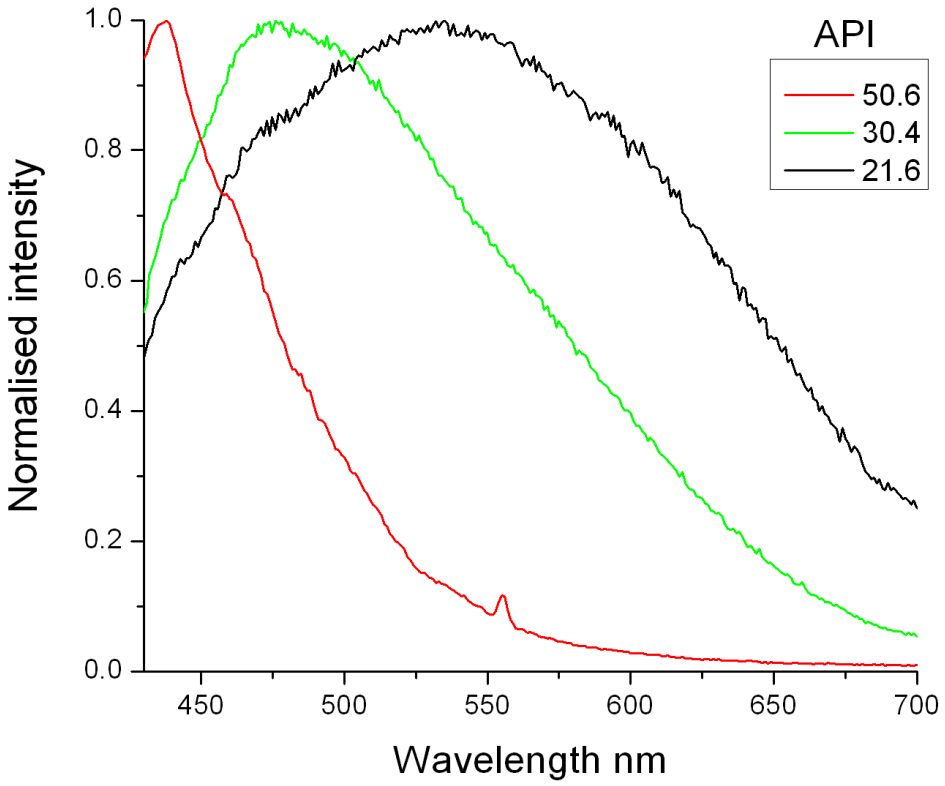

Figure 1.30: *Normalised steady state fluorescence emission spectra for a selection of crude petroleum oils excited at 405 nm. Reproduced from [112].*

Energy transfer processes result in red-shifted and spectrally broadened emission spectra, while quenching processes reduce emission intensity [108]. This can be seen in Figure 1.31 where the variation of red shift and intensity is shown for a series of oils of varying API gravity. Both deactivation processes lead to lower quantum yields and a decrease in the fluorescence lifetime. Therefore, the fluorescence spectrum will not only be determined by the emitting species present but also by the non-emitting species involved in the quenching and RET processes.

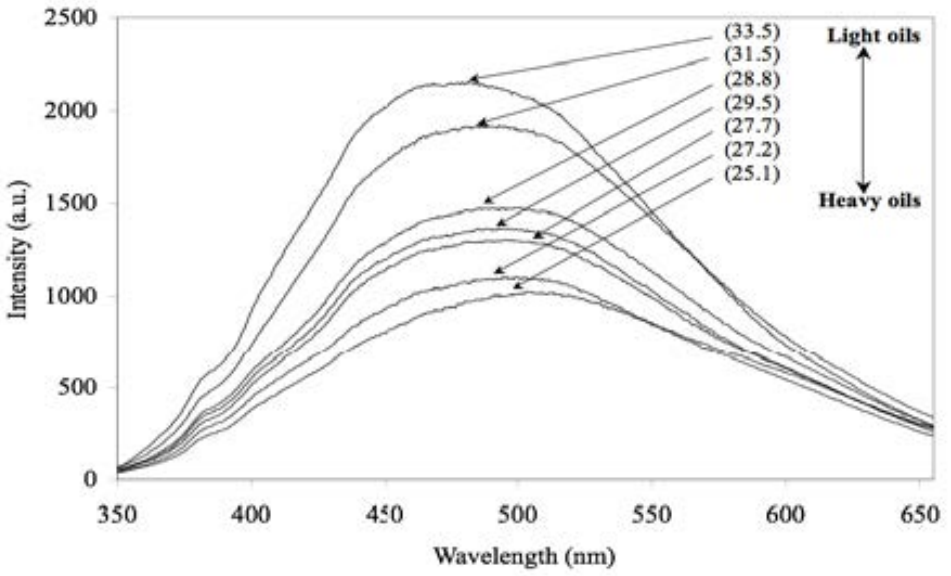

Figure 1.31: *Fluorescence emission spectra using* 337 *nm excitation for a range of petroleum samples with different API values. The emission intensity reduces as the oil density increases. Reproduced from [1].*

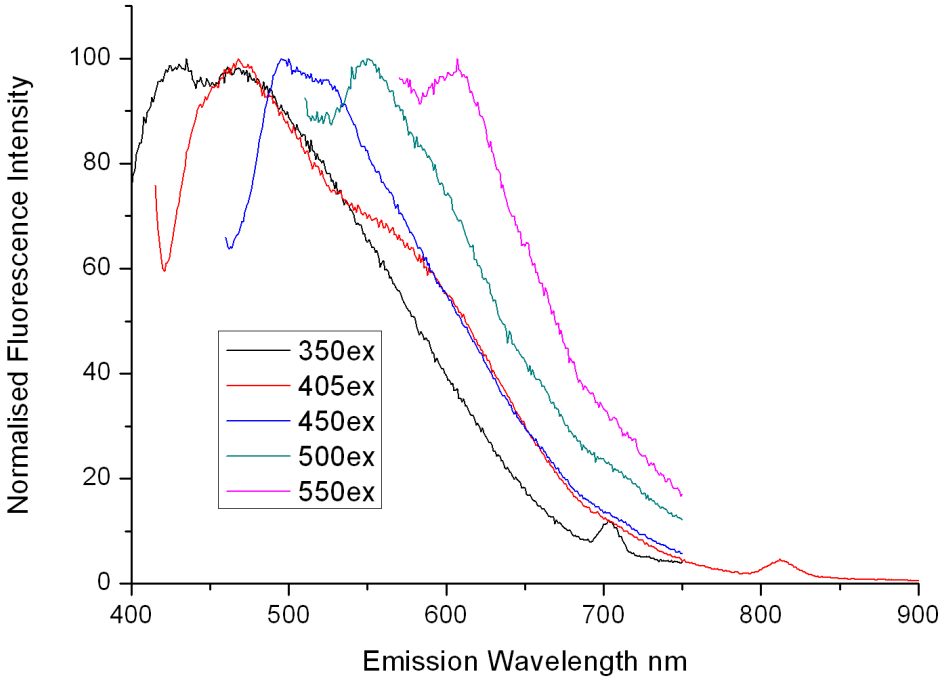

Figure 1.32: *Normalised emission spectra of a sample light crude oil resulting from a variety of excitation energies as given in the legend. Spectra recorded on a Cary Eclipse spectrofluorimeter.*

The balance between energy transfer and quenching is illustrated by Figure 1.32. Here the normalised emission spectra are given resulting from a range of excitation energies. As the excitation wavelength increases, the emission band is narrowed and the Stokes shift reduces. Fluorescence intensity is also reduced [113]. At short excitation wavelengths, smaller aromatic fluorophores with large HOMO-LUMO gaps are excited and can transfer energy to smaller bandgap molecules. For these short excitation wavelengths, energy transfer processes dominate. At longer excitation wavelengths, larger aromatic fluorophores with small HOMO-LUMO gaps are excited. There are fewer molecules with smaller bandgaps and the possibility of energy transfer is reduced. In this case, collisions between molecules results in quenching leading to a reduction in fluorescence intensity, A similar explanation in terms of singlet energies is given by Nicodem [114]. Excitation at short wavelengths excites components with high singlet energies, and these are easily quenched by the relatively higher concentration of components with lower singlet energies. Emission of these then shifts the spectrum to the red. Excitation at longer wavelengths can only excite components with lower singlet energies. These are inefficiently quenched due to the low concentration of components with low singlet energy and do not suffer such a large red shift. Furthermore, quenching efficiency may be a function of the proximity between the bandgap energy of the fluorophore and that of the quencher [115].

Multidimensional techniques such as Excitation-Emission Matrix (EEM) [117], Synchronous Fluorescence Spectroscopy (SFS) [118, 119] and Total Synchronous Fluorescence Spectroscopy(TSFS) [116, 120] have been used in an effort to provide more detailed spectroscopic fingerprinting of crude oils. Figure 1.33 shows normalised (to maximum intensity) TSFS plots obtained for a series of nine crude oils of varying API gravity. For these plots, the interval between the wavelength of excitation and the wavelength of emission is plotted against the excitation wavelength in an effort to improve on the resolution of contour plots obtained using SFS and EEM methods. A large variation in the TSFS plots is found which relates to the large compositional diversity of crude petroleum oils tested (API values from 50.6 to 12.8). Multivariate techniques have also been used to attempt classification of the data obtained by these methods with varying degrees of success [121, 122].

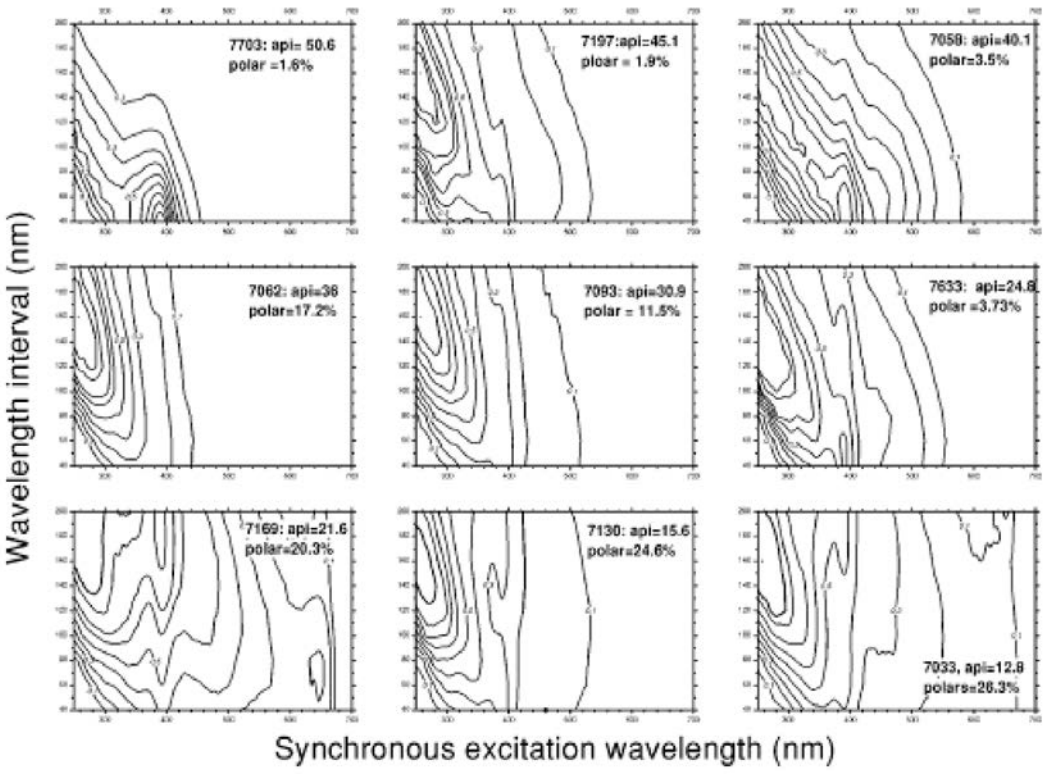

Figure 1.33: *Total Synchronous Fluorescence Spectra (TSFS) plots for 9 different crude petroleum oils recorded from 250 to 700 nm over a wavelength interval of 40 to 200 nm. Reproduced from [116].*

1.3.3 Crude Oil Dilution

In the oil industry, heavy crude oils (with viscosities of the order 10^3 cP) must be diluted to enable transportation by pipeline. The choice of solvent is critical as certain solvents (such as n-heptane) can cause precipitation of Asphaltenes. Condensates and Naphta (High API hydrocarbon) have been historically used for dilution; more recently organic solvents other than hydrocarbons (for example Methyl-tert-butyl Ether or Pentanol) have been proposed [5]. The stability of crude oil emulsions in water have also been investigated [123], which may lead to an alternative transportation mechanism in the future.

From a spectroscopic viewpoint, studies on the effect of dilution on the fluorescence emission of crude oils have been previously reported, based primarily on spectral comparisons [108]. The emission spectra of crude oils is the result of a combination of the emission from the multiple species that are present.

On dilution with light hydrocarbon solvents such as hexane or toluene, the fluo-

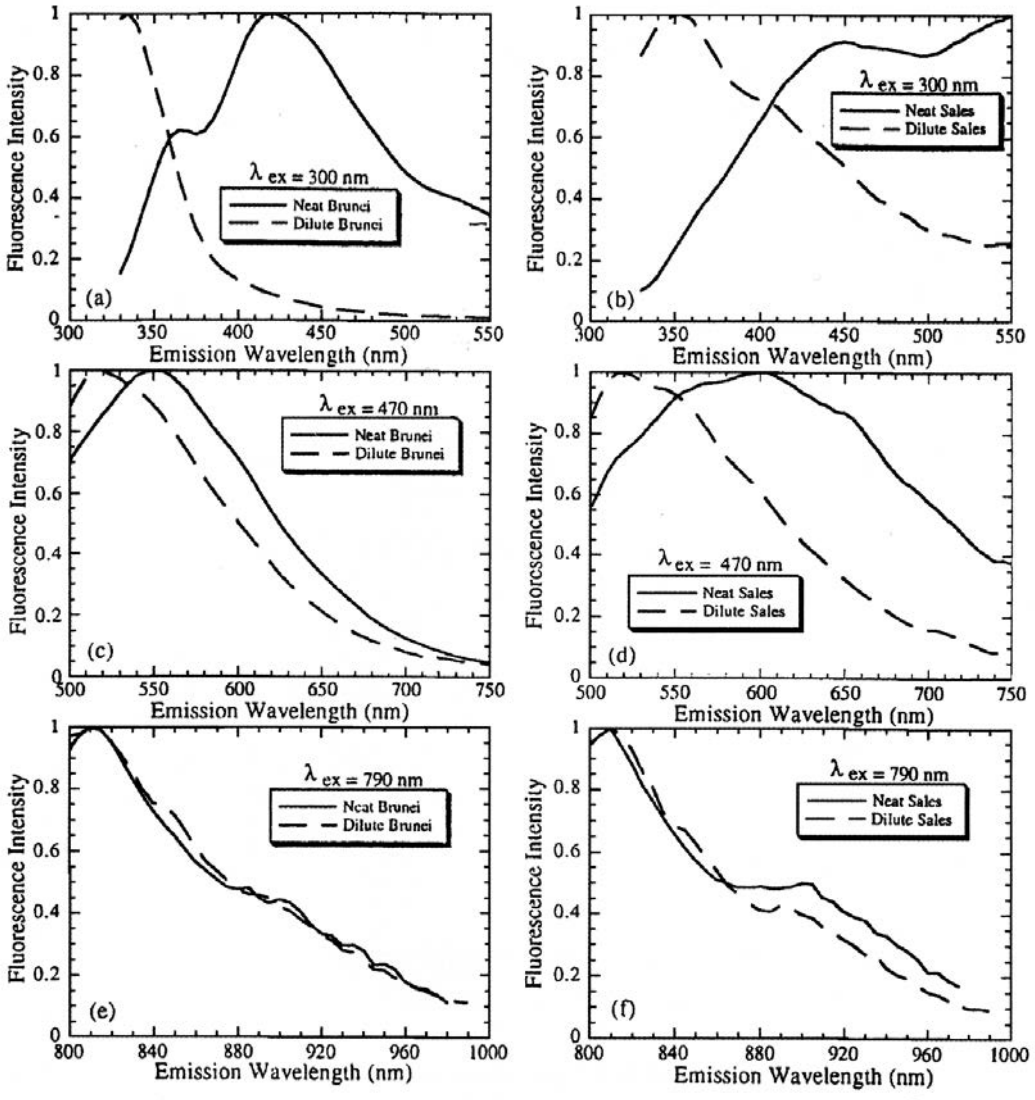

Figure 1.34: *Fluorescence emission spectra for neat and dilute solutions of a light (Brunei) and heavy (Sales) crude oil for* 300*,* 470 *and* 790 *nm emission wavelengths. Energy transfer produces large spectral differences between the neat and dilute solution at short wavelengths which decreases with increasing excitation wavelength. Reproduced from [108].*

rescence intensity of crude oils is increased and an increasing blue shift is observed as shown in Figure 1.34 [106, 108, 124, 125]. Dilution also increases the quantum yield which is due to the reduction in static and collisional quenching [113]. Diluted heavy oils have lower quantum yields compared to light oils due to the presence of a greater number of large red absorbing fluorophores. The comparison between neat and diluted crude oils has been used to study the effects of quenching and energy transfer processes on fluorescence spectra. Linear Stern-Volmer plots constructed

from quantum yield data implied that a simple collisional model applied. [108].

At short excitation wavelengths, large differences can be observed between neat and diluted oils. As the excitation wavelength increases, the blue shift between neat and dilute spectra reduces [108] which is shown in Figure 1.34. At 700 nm, there is no blue shift and the spectra of the neat and dilute oil are nearly identical. In [108] a method is described for determination of the percentage energy transfer from neat and dilute spectra. The ratio of the area under the normalized spectrum for the dilute solution is subtracted from the area under the spectrum for the neat crude oil solution. This area is then divided by the total area under the spectrum for the neat crude oil. This process yields the fractional change in the emission spectrum in going from the dilute to the neat limit, thus yielding the percent of energy transfer. The % energy transfer was found to be dependent on the excitation wavelength: for short wavelength excitation (300 nm), $\sim 90\%$ of the fluorescence emission from crude oils resulted from energy transfer. The value for % energy transfer reduced with increasing excitation wavelength.

1.3.4 Fluorescence Lifetime Analysis of crude oils

Crude oil emission spectra are relatively easy to acquire but can be adversely affected by instrumental factors such as excitation source intensity variation, stray light variation, detector spectral sensitivity variation, and also by the physical properties of sample such as opacity, geometry, turbidity, scattering properties, and photobleaching. In contrast, time-resolved fluorescence spectroscopy focuses on the temporal characteristics of fluorescent species which are less sensitive to steady-state artifacts [124, 126]. The fluorescence lifetime of crude oils has received attention from early pioneering work [127, 128] to an in-depth evaluation at the Nanoscale Biophotonics Laboratory [129–132].

The measured fluorescence lifetime for a crude oil includes contributions from all individual species and hence the fluorescence decay curves are complex. These complex decays can be fit to multi-exponential models leading to a determination of an average lifetime of the crude oil. However the value of the lifetime determined is very dependent on the experimental conditions and the calculation method used. At this laboratory, the intensity based average fluorescence lifetime $\overline{\tau}$) has been

used [126, 129, 132] as a means to providing a reproducible and standardised measurement for crude oils. Henceforth, lifetime as referenced in the text will mean the *intensity based average lifetime* unless otherwise noted. As crude oil fluorescence is a result of the complex interplay between quenching and energy transfer processes it follows that the lifetime will also be governed by this behaviour. The following observations are made between fluorescence lifetime and physical and chemical properties:

- Heavy oils (of API of $\leq$ 15) tend to have short lifetimes due to the high proportion of quenching species present. Light oils (of API of $\leq$ 15) have less quenching species (lower concentrations of emitting species) and thus yield longer lifetimes.

- Crude oil fluorescence lifetimes are dependent on the excitation wavelength. At short excitation wavelengths, collisional energy transfer is the dominant mechanism leading to longer average lifetimes. At longer excitation wavelengths, the light is absorbed by larger chromophores with smaller band gaps; collisional quenching is more prominent and non-radiative decay rates are higher, leading to shorter lifetimes [124].

- The fluorescence lifetimes of crude oils vary with emission wavelength. Two different well-defined trends were found for the variation of lifetime with the emission wavelength. For most crude oils, the lifetime increases from 550 to 650 nm and at longer wavelengths decreases. This 'curved' wavelength lifetime response is shown in Figure 1.35 where data is presented for nine oils of varying API gravity. The decrease at longer emission wavelengths ($>$ 650 nm) is due to the faster non-radiative decay and quenching rates of the smaller band gap fluorophores. Also, the maximum average lifetime is shifted to the red for heavy crude oils, which is in agreement with the shift of the emission spectra registered with steady state fluorescence. [126, 129]

- Diluted of crude oils results in reduced energy transfer and quenching effects leading generally to longer lifetimes than for neat oils [124].

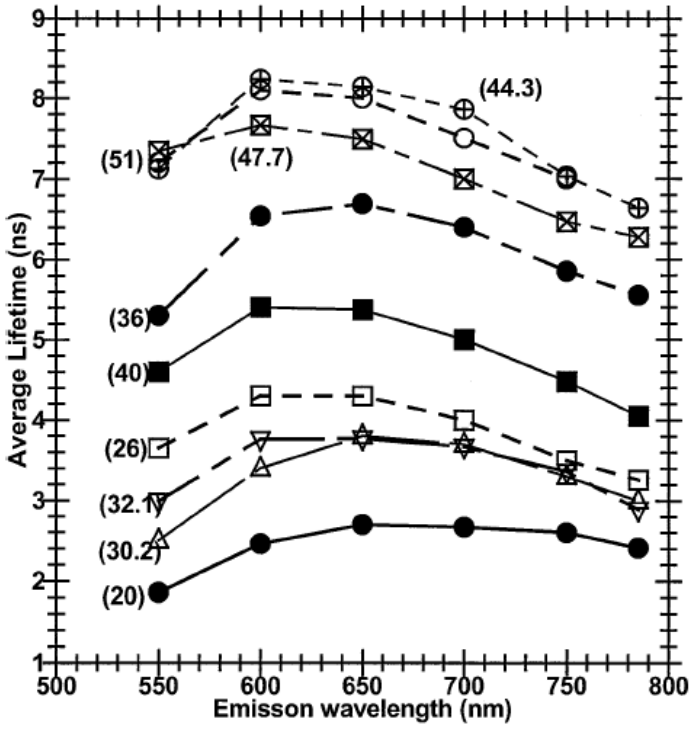

Figure 1.35: *Lifetime - Emission wavelength curves for nine crude oils using* 460 *nm excitation. Each curve represents a different oil with the* API *gravity being given in parentheses on the left-hand side of the plot.Reproduced from [126].*

- Correlations have been made between fluorescence lifetimes and chemical and physical parameters such as API gravity [116, 126, 129–132]. Lifetime is strongly negatively correlated with the polar concentrations and positively correlated with the corrected alkane concentration (Figure 1.36).

To date, studies involving fluorescence lifetimes of crude oils have been recorded using the time domain (TD) method [124, 127, 129, 132] and the frequency domain (FD) method [112, 133–135]. For the latter, studies were initially based on multi-frequency phase resolved measurements [§§§] on petroleum based lubricants, showing improved discrimination between samples by selective enhancement of spectral features as a function of the FD derived fluorescence lifetime [133–135]. Following McGown's [133] work on phase-resolved spectra, an investigation into lifetime distributions as a means to fingerprinting complex samples was made that led to Total

[§§§] In phase resolved fluorescence measurements, emission spectra from individual components in a heterogeneous sample can be derived using phase and modulation lifetimes [136] or using the raw phase angle and demodulation data [36].

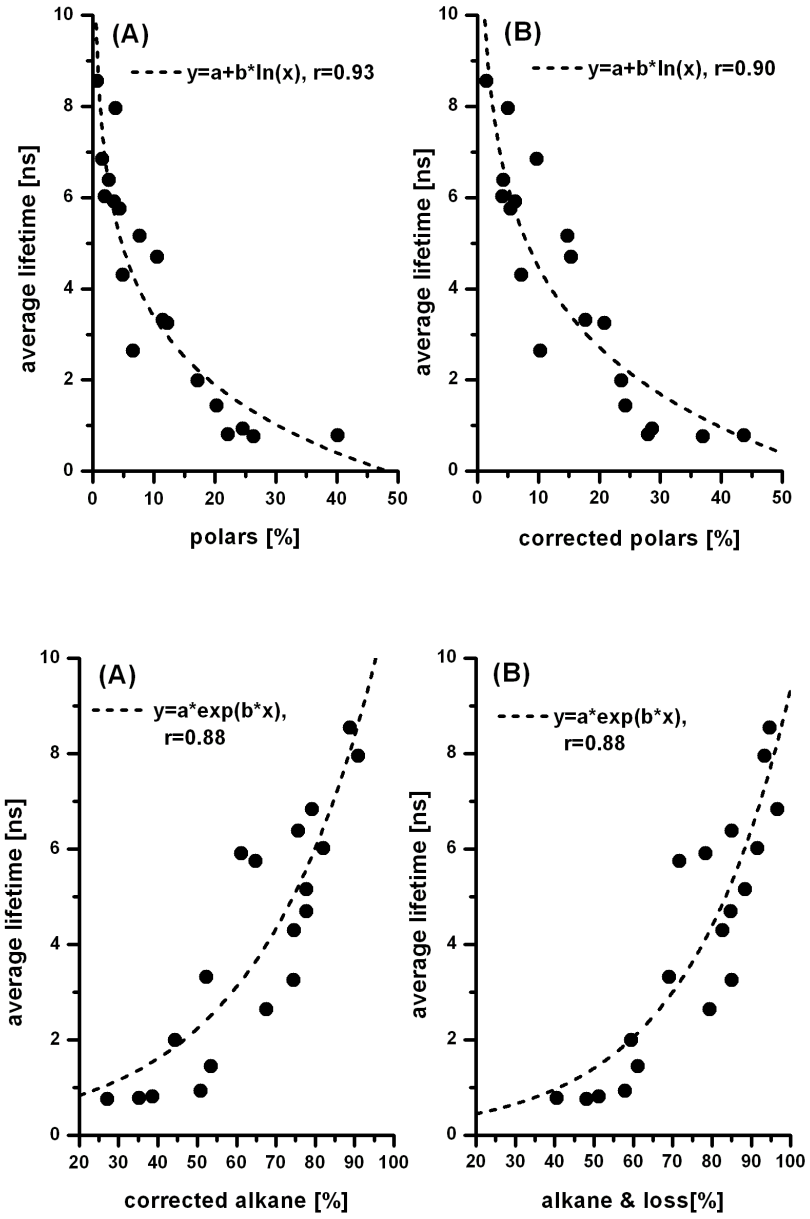

Figure 1.36: *Plot of average lifetime ($\bar{\tau}$) recorded at* 540 *nm versus polar and alkane concentration. The best logarithmic and exponential fits and the value of the correlation coefficient r for each concentration are also plotted. Reproduced from [131].*

Lifetime distribution analysis [137]. The authors postulated that the use of the distribution analysis model called the Maximum Entropy Model[¶¶¶] (MEM) [138], is more suitable for complex samples than using *a priori* methods such as the discrete exponential decay fitting, Gaussian, or Lorentzian distributions. These methods are termed *a priori* as they require the use of χ^2 and residuals to determine the best fit.

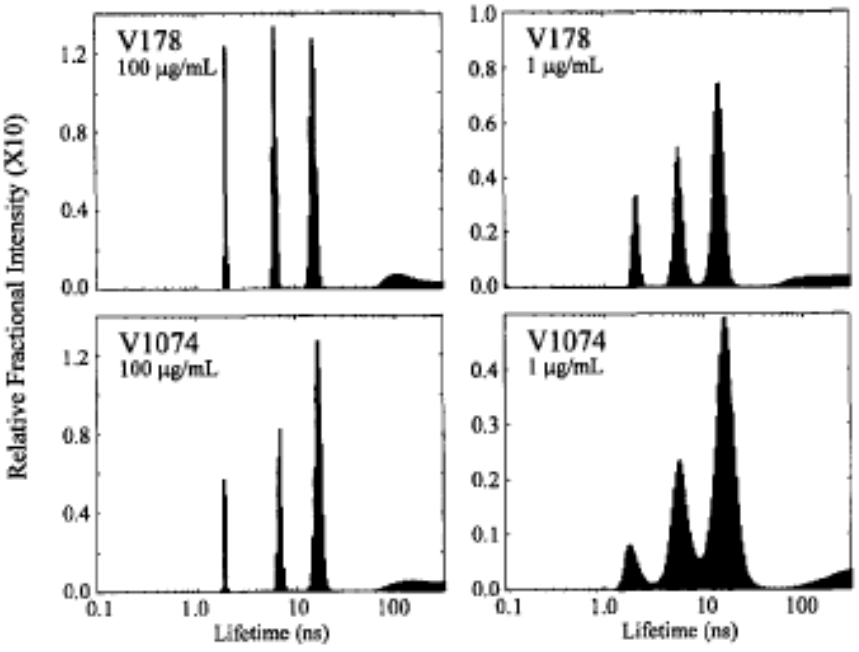

Figure 1.37: *Lifetime distributions from* TLDA *results for ethanolic solutions of two different coal liquids at concentrations of* 100μ *g/mL (left) and approximately* $1\mu g/mL$ *(right) [137].*

The MEM method was applied to the detection of fluorescence from coal derived liquids and humic materials (Figure 1.37), yet further characterisation of complex materials did not follow. More recently, the concept of frequency segmentation, i.e. analysing the frequency domain response of a sample in discrete frequency ranges or 'segments' [139] has found application in quenching studies of pyrene and dissolved humic materials [140]. This newly developed technique has been shown to provide more accurate lifetimes and improve resolution in samples that exhibit changing

[¶¶¶] The MEM technique starts with a broad lifetime window that covers the lifetime range of interest is evenly divided into closely spaced discrete exponential terms. The fitting process starts with a flat distribution and then varies the fractional intensity of each term to minimize the χ^2 value. Once a feasible set of models is obtained after χ^2 reaches the minimum, a unique solution is chosen by maximizing the Shannon-Jaynes entropy, $S = -\sum p_i log p_i$ where p_i is the factional intensity of term i.

fractional contributions over time due to photobleaching effects.

The accuracy of the average fluorescence lifetime can be described by a confidence interval, which can be determined by support plane analysis. However, there is a tendency in fitting algorithms to return an abnormally high long lifetime component when using multi-exponential fit models on crude oil decay curves [126], which can then in turn generate abnormally high average lifetimes. Despite the strong trends between lifetime data and physical and chemical parameters, quantitative correlations were not possible using intensity averaged lifetimes calculated from TCSPC data [131].

1.3.5 Fluorescence Energy Transfer and Quenching of PAH's and crude oils

Fluorescence quenching can be caused by a variety of processes such as molecular collisions, static effects, internal conversion and intersystem crossing effects which lead ultimately to a drop in quantum yield [36]. The quenching of fluorescence of aromatic hydrocarbons such as anthracene and perylene can occur by halogenated organic molecules and by molecular oxygen* where all observed quenching was predominantly diffusion based [142]. The oxygen quenching constants were shown to be largely independent of the aromatic hydrocarbon while for halogenated hydrocarbon quenchers, a large variation was found in rate constant which was dependent on the energy separation of excited electronic states. In motor oils, small aromatics such as nitrobenzene were found to behave as selective quenchers of fluorescence [119]. The analysis of quenching effects has the potential to be very useful technique in the analysis of PAH's and perhaps complex systems due to it's high sensitivity and selectivity. However, only a small number of fluorophore-quencher systems that have been studied in detail to date [143]. Although there are a large number of PAH molecules in crude oils, and a wide variety of quenching processes occurring, systematic quenching behaviour can still be shown [108, 124, 144].

* Molecular oxygen is a very efficient quencher of the electronically excited states of many organic molecules and displays a high solubility in aqueous solutions and organic solvents ($\sim 7.4 \times 10^{-3}$M in Toluene for example) [141]. This reaction is so efficient that it is usually diffusion limited [142]. Since crude oils contain large fluorescent PAH's, many of which have long lifetimes, they are thus highly susceptible to quenching by oxygen and for some applications, solutions must be deoxygenated.

In [124], the excited-state decay rate was given by:

$$\frac{1}{\tau_f} = k_f = k_{fo} + (k_e + k_q)[C] \tag{1.49}$$

where k_{fo} is the intrinsic fluorescence decay rate, k_e is the energy transfer rate, k_q is the quenching rate and [C] is the fluorophore concentration. Using equation 1.49 and lifetime data for a heavy crude oil it was shown that energy transfer and quenching mechanisms have a linear dependence with concentration. Also, the collisional decay rates as determined by the slope of the Stern-Volmer plot were found to decrease with increasing emission wavelength and vary with oil type, i.e, heavy oils had larger slopes compared to lighter oils [108, 124].

Fluorescence quenching of aromatic molecules in crude oils can occur in three ways:

- Diffusive quenching caused by the encounter of diffusing excited fluorophore and quencher molecules.
- Instantaneous quenching when a quencher molecule lays within a critical radius r_c containing n molecules around the fluorescent molecule. This is called sphere-of-action quenching.
- non-fluorescent complex formation.

The competing processes of fluorescence and quenching are:

$$\begin{aligned} A &\xrightarrow{h\nu} A^* \\ A^* &\xrightarrow{\tau_0^{-1}} A \\ A^* + Q &\xrightarrow{k_q} A + Q \end{aligned}$$

A^* and A are the excited and ground state fluorophore. Q is the quencher molecule, k_q is the quenching constant, and τ_0 is the unquenched fluorescence lifetime. The classic Stern-Volmer relationship for diffusion based quenching of molecules in solution is given by Equation **??**.

The Stern-Volmer equation predicts a linear dependence of I_0/I on the quencher

concentration and $K_{sv} = k_q \times \tau_0$. It is well known that certain quenching reactions lead to either positively or negatively curved Stern-Volmer plots of which numerous example are given by Lakowicz [36]. Positive curvature or deviation from Stern-Volmer behaviour has been modeled by a combined dynamic and static model and also by a sphere of action mechanism. Negative deviations have been modeled as resulting from fractional accessibility of a fluorophore to a quencher molecule. Quenching of single aromatic molecules by molecular oxygen or halohydrocarbons has been found to follow the diffusive model [142], showing linear plots of intensity versus quencher concentration. For complex mixtures containing multiple fluorophores, the quenching processes can be explained by the modified Stern-Volmer equations [38, 145]:

Static Quenching:

$$\frac{I}{I_0} = \sum_{i=1}^{n} \frac{f_i}{exp(V_{q,i}N[Q])} \tag{1.50}$$

Dynamic Quenching:

$$\frac{I}{I_0} = \frac{\tau}{\tau_0} = \sum_{i=1}^{n} \frac{f_i}{1 + k_{q,i}\tau_{0,i}[Q]} \tag{1.51}$$

Combined Static and Dynamic Quenching

$$\frac{I}{I_0} = \sum_{i=1}^{n} \frac{f_i}{1 + k_{q,i}\tau_{0,i}[Q](exp(V_{q,i}N[Q]))} \tag{1.52}$$

where N is Avogadro's number, $k_{q,i}$ is the quenching rate for the i^{th} component,f_i is the fractional contribution of the i^{th} component, [Q] is the quencher concentration,τ_i is the lifetime of the i^{th} fluorescent component in the absence of quenching species, I/I_0 is the ratio of steady state intensity at various quencher concentrations to the intensity in the absence of the quencher, and $V_{q,i}$ is the volume of the sphere of action where static quenching can occur.

1.4 Temperature based Fluorometry of complex materials

1.4.1 Low temperature studies on PAH's

Fluorescence emission is sensitive to temperature changes and is generally enhanced by lowering the temperature [146]. At room temperature the absorption and fluorescence spectra of most molecules in liquid phases are broad and featureless. The emission spectra can undergo a dramatic change if cooled to cryogenic temperatures. When aromatic solutes are dissolved in n-alkane solvents and then rapidly frozen to 77K or lower temperatures (for example liquid Helium) , highly resolved spectra may be obtained showing detail of vibronic transitions. This is known as the Shpol'skii effect which has received a wide attention since its development in the early 50's [147, 148]. The reason for the fine structure is that at low temperature, a rigid polycrystalline matrix is formed where the solute molecules are held in strictly oriented sites. For Schpol'skii behaviour, the n-alkane solvent used to dissolve the solute must be specifically matched, i.e., the length of the n-alkane must be of the same molecular dimension as the solute molecule so that the solute molecules occupy a small number of crystallographic sites (ideally just one) in the solvent lattice. The degree of complexity and unique nature of the resulting luminescence spectrum depends upon this match. Figure 1.38 shows an example of the enhancement in resolution that is obtained for the PAH benz[a]anthracene at 15 K.

In solid matrices, fluorescence quenching is less efficient than in solution due to the reduction in collisional effects. Thus, very high selectivity and low limits of detection may be achieved using the Schpol'skii method. Being able to work with very low concentration levels can also lead to a minimisation of energy transfer effects. Such procedures have been applied extensively to the analysis of PAH's in complex samples [148, 149]. In [149], the Shpol'skii method combined with HPLC has performed favourably in comparison to GC/Mass spectroscopy in the task of separation of isomers of five ring PAH's such as methylphenanthrene. LC separation has been combined with Shpol'skii spectrometry to determine methylbenzo[a]pyrene isomers in coal tar extracts [150]. The Schpol'skii effect has also been applied in

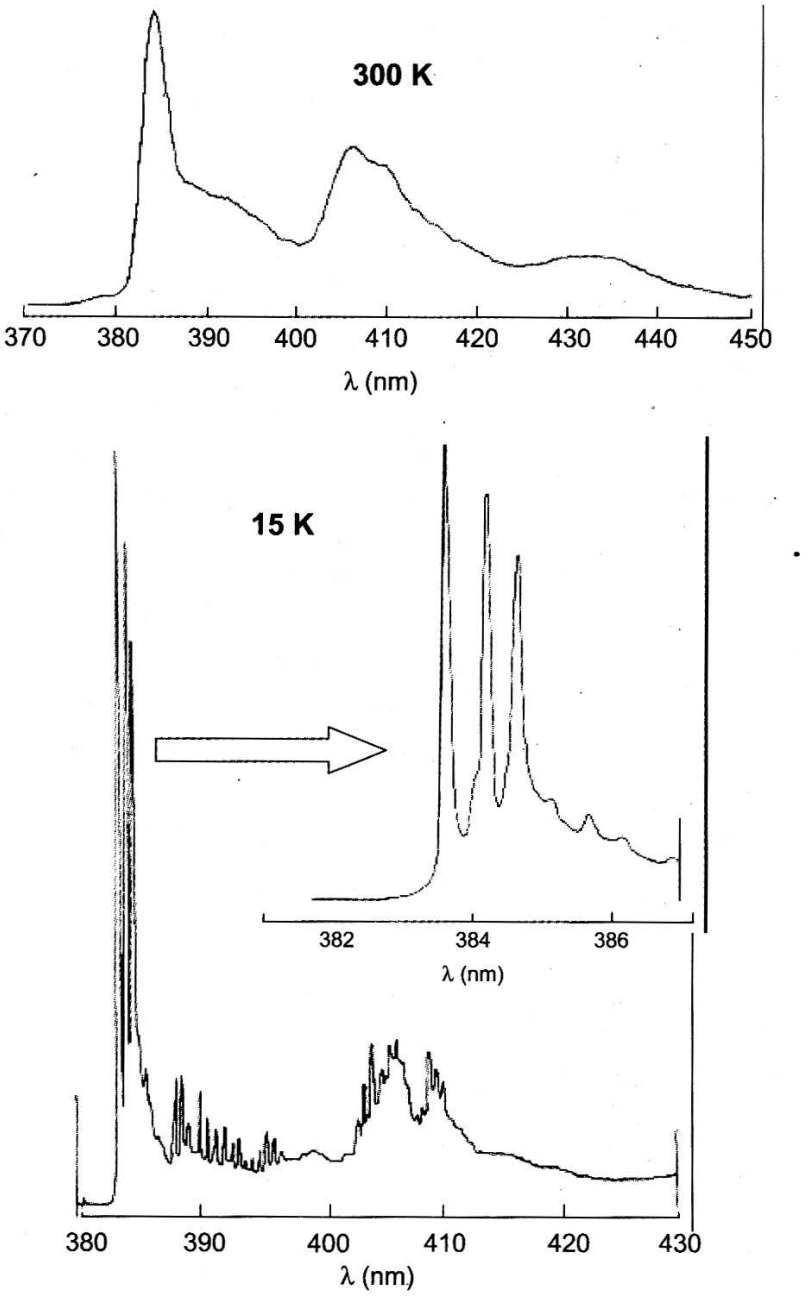

Figure 1.38: *Fluorescence spectrum of benz[a]anthracene in n-heptane liquid solution at* $300K$ *(top) and in n-heptane frozen solution at* $15K$ *(bottom). The concentration was* $2 \times 10^{-5}M$ *and the excitation wavelength was* 329.2 *nm. Reproduced from [38].*

environmental monitoring where 15 soil pollutants were effectively screened and also to synchronous fluorescence spectrometry where simultaneous analysis of PAH's has been reported [151]. Selective and sensitive as the Shpol'skii methods are, there are some drawbacks:

1. The technique is time-consuming and requires the use of cryogenics.

2. A high degree of expertise and experience on the part of the analyst is required.

Low-temperature fluorometric measurements have been combined with time resolved methods to achieve even higher selectivity in mixture analysis [152, 153]. More recently, the resolution of spectra of a mixture of PAH's was enhanced by lowering the temperature to that of liquid helium (4.2K) and coupling the spectral data with fluorescence lifetime data in the form of a wavelength-decay time matrix [154]. The authors suggest that the method could be used as an efficient method to analyse PAH's in HPLC fractions of heavily contaminated water samples.

For mixtures such as crude or refined petroleum oils, containing a multitude of PAHs, the situation becomes somewhat more complex due to the effects of quenching and energy transfer. Early studies on low temperature luminescence spectra of crude oils showed an enhancement of the fluorescence and phosphorescence spectra in various solvents at 77K compared to room temperature [155–157], and a preliminary assessment of the technique for fuel oil identification by correlating spectral enhancements with oil type was made. Recently, work on the luminescent spectra of diluted petrol in Hexane at 77 K has shown that a quantitative forensic method for trace hydrocarbon determination is possible [158].

1.4.2 High temperature studies

In comparison to the studies of PAH's at low temperatures, a greater number of studies into the high temperature effects (in any temperature range) of petroleum based materials such as kerogens, crude oils or coal have been performed [159–164]. Possibly the most thorough treatment of the temperature effects on crude oils to date is given in [160]. Here, the steady state analysis of the temperature effects on eight crude oils has been investigated. Some of the emission spectra from this work are shown in Figure 1.39.

The authors found that the fluorescence intensity decreased with increasing temperatures over 300K and conversely increased with decreasing temperature effects below circa 300K. The changes in intensity could be modeled by a simple Arrhenius

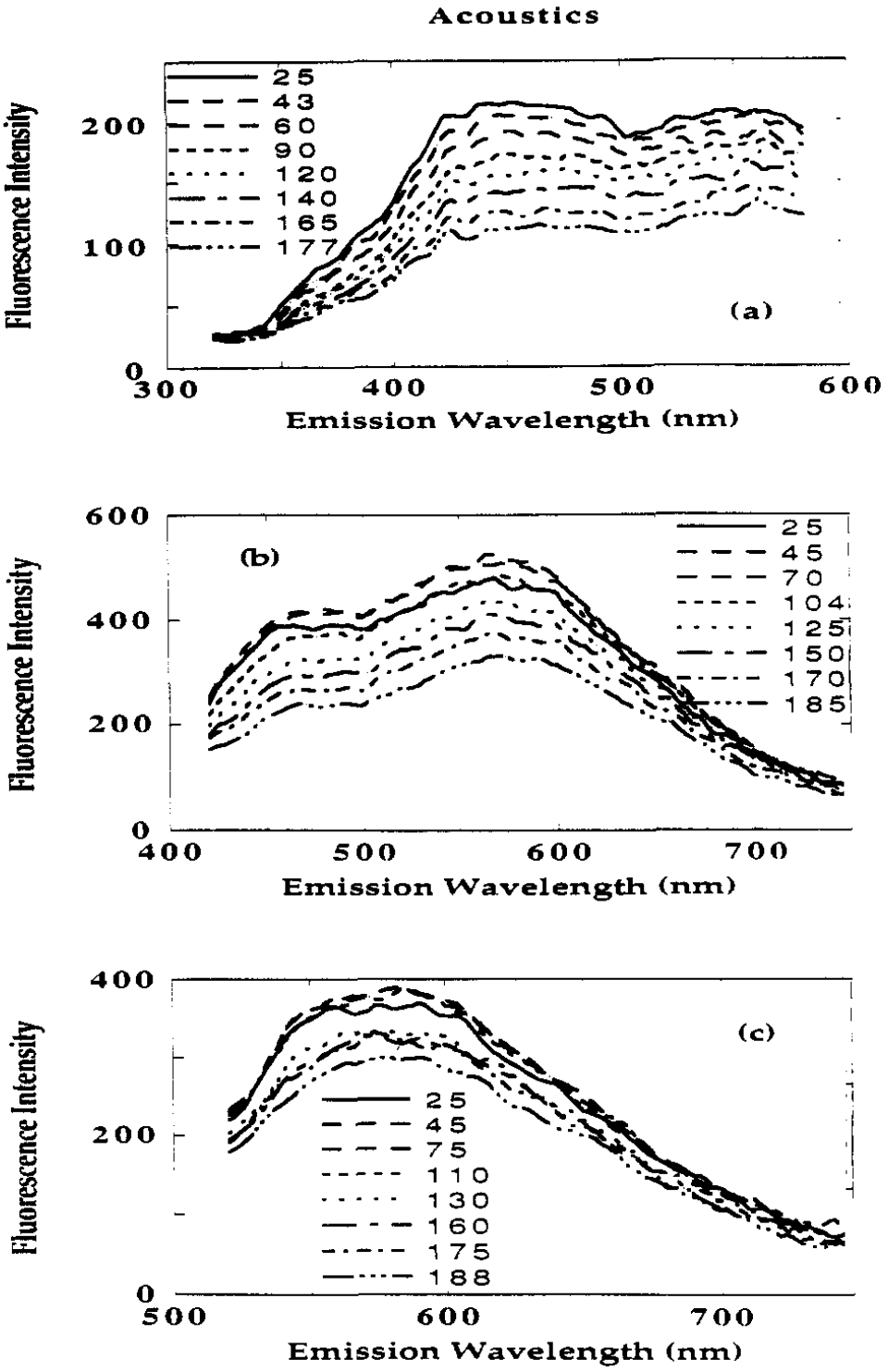

Figure 1.39: *Fluorescence spectra of a medium API gravity crude oil, measured for a series of temperatures from* 298 *to* 463K*: (a) excitation wavelength* 300 *nm; (b) excitation wavelength* 400 *nm; (c) excitation wavelength* 500 *nm. For long wavelength excitation (b and c), the fluorescence increases as the temperature is raised above* 298K *(but less than* 373K*) and then decreases when* $T >$ 373K*. Reproduced from [160].*

model. Also the authors postulated that the spectral profile of the oils seemed to be independent of temperature, indicating that the individual fluorophores that are present in the oils have similar temperature characteristics.

The fluorescence of cracking products of organic matter at elevated temperatures and pressures has been investigated as a means to quantify oil generation from source rocks. The technique uses a diamond anvil cell in conjunction with fluorescence emission spectral analysis to monitor organic matter at elevated temperatures [162, 163]. More recently, attempts were made to characterise the kerogens of oil-prone source rocks by monitoring their fluorescence intensity as a function of organic species, time and temperature [164]. The oils that were generated from kerogens at elevated temperatures and pressures in the diamond anvil cell (DAC) could be termed as 'live oils' and thus comparisons could be made to fluid inclusion studies [165] (see section 1.6). A progressive blue shift in the wavelength of maximum fluorescence intensity along with a general increase in intensity was found as the kerogens undergo thermal maturation.

1.5 Crude oil photophysics

To follow on from the photophysical discussion in section 1.2.3, the following generalised description of competing photophysical pathways of light activation and deactivation for the fluorophores in crude oil can be given.

	Process	**Total Rate**
$A + h\nu \longrightarrow A^*$	Light Absorption	$\sum k_{abs}[A][h\nu]$
$A^* \longrightarrow A + h\nu^{'}$	Fluorescence Emission	$\sum k_F[A^*]$
$A^* \longrightarrow A + \triangle$	Internal Conversion	$\sum k_{IC}[A^*]$
$A^* \longrightarrow T^*$	Intersystem crossing	$\sum k_{ISC}[A^*]$
$A^* + E \longrightarrow E^* + A$	Energy Transfer	$\sum k_{ET}[A^*]$
$E^* \longrightarrow E + \triangle$	Non-radiative energy transfer	
$E^* + A \longrightarrow E + A + h\nu^{''}$	Radiative energy transfer	
$A^* + Q \longrightarrow A + Q + \triangle$	Dynamic/Collisional quenching	$\sum k_C[Q][A^*]$
$A^* + Q \longrightarrow A^*Q$	Molecular Complex Formation	$\sum k_M[Q]$
$A^* + Q \longrightarrow A^*Q$	Sphere Of Action	$\sum k_S[Q]exp[Q]$

where A is a fluorophore, E is an interacting fluorescent/non-fluorescent species, T is a triplet state, h is Planck's constant, ν is the light frequency, $\triangle$ is heat, $*$ represents the excited electronic state and Q is a quencher. Internal conversion can provide a non-radiative pathway back to the ground state with the excess energy dissipated in the form of heat. Intersystem crossing to a triplet state provides another non-radiative pathway from the excited state. If a molecule E has an excited state E^* lower than A^* then energy transfer can occur. Quenching is the non-radiative deactivation of an excited molecule, A^* by a quencher, Q, the excited state energy eventually becoming dissipated as heat energy and the molecule A^* is restored unchanged to it's ground state A. Static quenching effects provide another non-radiative pathway for the excited fluorophore in the form of complex formation or the action of a quencher within a certain volume or sphere of action. The overall rate constants are the summations of the individual decay rates for all components involved in that particular pathway, i.e., the $\sum k_F$ rate represents the total

fluorescence from all components in the oil.

With the exception of radiative energy transfer, the sum of the non-radiative processes occurring after excitation can be termed as k_{NR}:

$$\begin{aligned}\sum k_{NR} &= \sum k_{IC}[A^*] + \sum k_{ISC}[A^*] \\ &+ \sum k_{ET}[A^*] + \sum k_C[Q] \\ &+ \sum k_M[Q] + \sum k_S[C]exp[C]\end{aligned}$$

Then, if k_T is the rate constant given by the reciprocal of the measured fluorescence lifetime, then the relationships between the rates can be given as:

$$\frac{1}{\tau_{_T}} = \sum k_T = \sum k_F + \sum k_{NR} \tag{1.53}$$

The intrinsic lifetime τ_0, which corresponds to the lifetime of the sample in the absence of non-radiative decay processes, can be defined as the reciprocal of $\sum k_F$.

1.6 Applications of crude oil fluorescence

Hydrocarbon Fluid Inclusion Analysis

Hydrocarbon Fluid Inclusions (HCFI) are very small (usually submicron to 50$\mu\, m$ in diameter) pockets of hydrocarbon fluids trapped in minerals such as quartz, feldspar and calcite. HCFI can be trapped during mineral crystallization within microfractures of sediments during the process of diagenesis [105]. The minerals can form 'overgrowths' over the trapped hydrocarbon during this phase. An example of a HCFI hosted in sandstone is given in Figures 1.40 and 1.41. Host rocks are typically sedimentary such as sandstone but can also be of igneous origin. Information about HCFI is important for understanding petroleum systems in reservoirs because they contain oils that were present at the time of inclusion trapping. The trapping process occurs during petroleum migration and reservoir evolution and fluid inclusions can be used as calibration points for modeling these processes [166]. Petroleum reservoirs are often charged by oil that has been expelled from different source rocks at varying

stages of thermal maturation, and thus oil inclusions can aid in the elucidation of complicated charge histories.

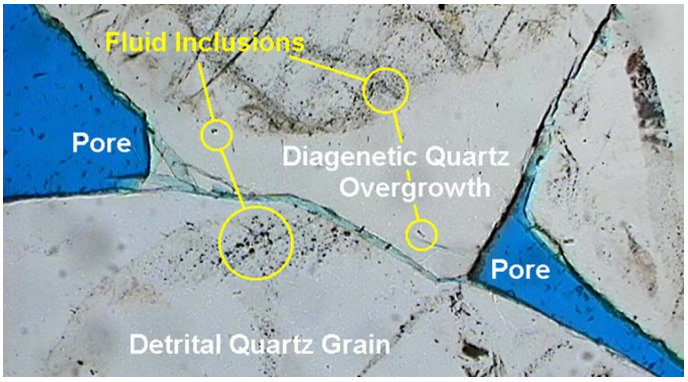

Figure 1.40: *A thin section of sandstone, illustrating detrital (denoting movement in the geological sense) quartz grains, quartz overgrowths and residual porosity. Fluid inclusion techniques focus on the small fluid encapsulations within the rock (circled areas). These may lie along healed micro-fractures within detrital grains or be contained within diagenetic cements. Reproduced from [167].*

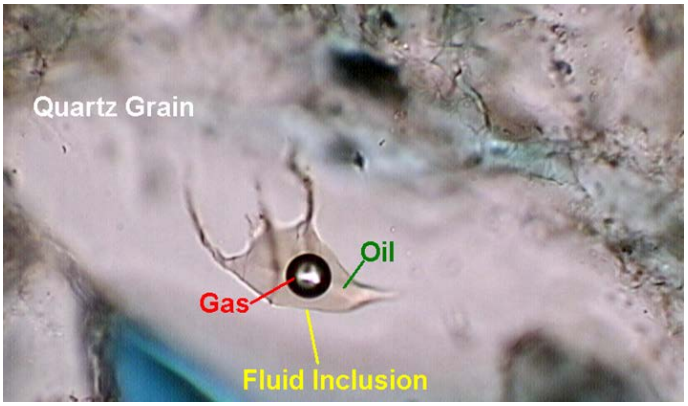

Figure 1.41: *At high magnification individual fluid inclusions can be identified. In this case, a single large oil inclusion contains a liquid petroleum phase and a methane rich gas bubble. HCFI represent pore fluids which have been successfully sampled at reservoir conditions and brought to the surface without fractionation or removal of volatiles. Reproduced from [167].*

Most reservoir studies using inclusion and crude oil geochemistry indicate that HCFI oils mainly represent oil from a first charge of petroleum and consequently the inclusion oil is protected from secondary alteration processes such as biodegradation, water washing or other post-emplacement processes that may affect their geochemical composition [168].

Analysis of HCFI gives the possibility of studying fluid and temperature-pressure profiles at the early stages of basin development [169]. The precise determination of the temperature-pressure conditions of entrapment of the fluid inclusion can be performed using *microthermometry* but this requires knowledge of the pressure-volume-temperature (PVT) properties that are derived using the chemical composition of the fluids.

To obtain compositional information for PVT modeling, destructive analytical methods have traditionally been used. Typically rock samples are crushed and extracting the fluids trapped in inclusions are extracted for chromatographic analysis [166]. There are two main problems with destructive HCFI methods:

1. It is possible to mix fluids from multiple HCFI populations or generations.

2. Analysis can be contaminated by residues of the present-day hydrocarbon fluid adsorbed on the mineral surface.

It has been possible to perform high energy laser ablation on single fluid inclusions and analyse the extracted hydrocarbons by GC-Mass Spectrometry [170]. However, the very low quantities of oil typically contained in HCFI (from ~ 10 μg to 10 ng) restricts analysis with gas chromatography and/or mass spectroscopy to rather large inclusions or groups of inclusions.

Spectroscopic techniques provide an alternative to destructive methods for HCFI analysis and the associated problems described above. In practice, oil inclusions[†] are detected using microscope-based techniques, either by visual identification [105] or by observing the emitted fluorescence [109, 166, 171]. Other spectroscopic techniques used for HCFI analysis include infrared absorption [172] and Raman [173] and a number of reviews have outlined the scope of research into fluorescence based methods for HCFI analysis [103, 166, 174].

The emitted fluorescence colour of HCFI has been used to estimate compositions, API gravities, sources, and maturities of HCFI [68, 109, 171, 175]. As indicated by Bodnar [176], in general, green and blue colours indicate light oils of high API gravity; inclusions with more mature oils of low API gravity tend to have

[†] For spectroscopic work, doubly-polished wafers of approximately 100 to 300 μm thick are cut from the rock sample.

yellow to red fluorescence colours. For example, the blue fluorescence of a 50 μm inclusion from the Cave-in-rock mining district in Illinois, USA is shown in Figure 1.42 indicating a light mature crude oil is contained within the sample.

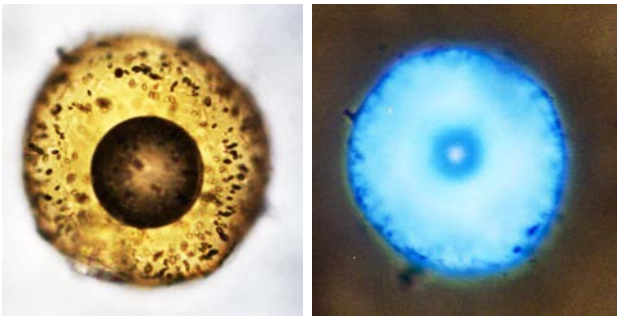

(a) (b)

Figure 1.42: *(a) Whitelight and (b) epifluorescence at* 366 *nm excitation images of a* 50 μm HCFI *from the Cave-in-rock mining district in Illinois, USA. The blue fluorescence indicates a light mature oil.*

However, the use of visually-determined fluorescence colour in spectroscopic measurements is inherently prone to misinterpretation and is not quantitative [103, 174]. Also the visual distinction between different groups of HCFI present in the same sample is very difficult.

More advanced methods have been used to exploit the fluorescent nature of HCFI. Synchronous excitation - emission spectra of single HCFI have been recorded using an epifluorescence microscope coupled to a steady state spectrophotometer [169, 177]. However, the same drawbacks in steady state fluorescence studies occurs for HCFI as for bulk crude oils such as the influence of sample geometry, opacity and turbidity on fluorescence intensity. In the case of HCFI, fluorescence originating from the host material can also affect the emission intensity. Photobleaching of the sample under steady-state intensities can also be a problem. To avoid these issues, time-resolved methods have been applied to the analysis of HCFI [131, 171, 178]. In [131], lifetime-wavelength plots were constructed for a series of HCFI and compared to bulk oil data. A similar lifetime-wavelength trend was found for the crude oils and the HCFI samples. More recently, lifetime-wavelength plots were used to distinguish subtle changes in the chemical composition of the trapped oil and hence differentiate between different populations of inclusions [178].

However, some problems have been highlighted with these methods. The longest fluorescence lifetime found for the HCFI analysed was found to be significantly longer than for lifetimes observed for light mature crude oils indicating that a significant dilution effect arises from the light hydrocarbons still present in the inclusion oils. Also, inclusions are thought to be usually trapped during the process of primary or secondary migration of oil from the source rock and are not affected by thermal processes such as biodegradation. In comparison, crude oils have undergone such processes over time. Yet conversely, results from Diamond Anvil Cell (DAC) studies indicate that inclusions with blue fluorescence cannot be trapped without alteration from the source material [165]. Because the light hydrocarbon fractions still present in the included oils will give a much longer fluorescence lifetime than for bulk dead oils, a conversion factor is necessary if there are any correlations to be made. As yet the conversion between HCFI and bulk oils in terms of lifetime has still to be made.

1.7 Thesis goal

This introduction has brought together concepts and background information on the nature and spectroscopic analysis of crude petroleum oils. Fluorescence based techniques have been used for many years in the analysis of crude oils. Despite the underlying complex nature of crude oil fluorescence and also the wide chemical variation found in nature, they display remarkable consistencies in behaviour as shown by their emission spectra and lifetime measurements. There is a strong link between the fluorescence lifetime and physico-chemical properties of crude oils. However, there is still no widely accepted quantitative technique to determine chemical or physical properties from time-resolved parameters. Time resolved measurements vary across laboratories and various fitting models are used leading to a difficulty in lifetime comparisons. Also, little progress has been made into probing the nature of photophysical transitions in crude oils, leaving large gaps in our understanding.

With this in mind, the goals of this thesis are as follows:

Develop a method to determine crude oil average lifetimes by FD with particular attention to the fitting models used and the determination of correct average lifetimes.

To understand crude oil photophysics in more detail by analysing the effects dilution and temperature on crude oil fluorescence lifetimes.

To compare the lifetimes from bulk crude oils with those from HCFI with the aim of developing a model to determine HCFI composition.

Chapter 2

Materials and Methods

2.1 Samples

Two batches (of 24 and 10 samples respectively) of crude oils were tested which had a wide chemical variance and were sourced from diverse geographical locations and rock types [131]. The physical and chemical properties of these oils have previously been published in detail [131, 132] and are reproduced in Tables 2.1, 2.3 and 2.2. The 34 crude oil samples were provided by the Petroleum Geochemistry Division of Fugro Robertson, Llandudno, North Wales.

2.1.1 Batch 1 Oils

These 24 oils originated from seven different types of source rock and 13 different geographical locations worldwide. This resulted in a very diverse sample set, as illustrated in Table 2.1, which gives the bulk physical and chemical properties of the oils using a variety of standard methods*. Table 2.2 gives the fractionation data for the oils and there are two discrete groups of samples. The first four oils (198/199/201/207) were analyzed by column chromatography after removal of the volatile hydrocarbon fraction by topping, and therefore the sample loss recorded during the analysis are all relatively small ($2.0 - 6.4\%$). The topping loss was obtained by measuring the weight loss after heating the oil at 60°C for one hour. The remaining oils were analyzed by medium pressure liquid chromatography (MPLC) without topping, resulting in higher column losses. The alkane, aromatic, and polar

* All chemical analysis was performed by Fugro Robertson in-house.

concentrations of the oils obtained from column chromatographic fractionation do not sum to 100% because of losses due to either evaporation of very light hydrocarbons or non-elution of heavy components (i.e. asphaltenes etc remaining on the column) of the oil. Column losses varied from 8.1 to 84%, with the lighter API gravity oils having the higher losses. Therefore, an alternative method for presenting the chemical compositional data is to normalize the alkane, aromatic, and polar concentrations to provide a corrected concentration. The corrected concentration is calculated by dividing the measured concentration of the component by the sum of the measured polar, alkane, and aromatic concentrations. Because oils 198, 199, 201, and 207 were analysed differently to the remaining 20 oils in Batch 1, they were excluded from correlations to physical properties and gross chemical composition.

2.1.2 Batch 2 oils

These oil samples originated from various different locations across the Middle East. The crude oils were analyzed by column chromatography after removal of the volatile hydrocarbon fraction by topping[†]. The compositional data were normalized to obtain corrected concentrations. The fractionation data and physical properties for these oils are given in Table 2.3.

[†] As for Batch 1 oils, all chemical analysis was performed in-house by Fugro Robertson.

Table 2.1: *Physical properties of Batch* 1 *oils. The oils originated from 13 different locations in the following geographical regions: Europe(EU), Middle East (ME1-ME4), Asia(A1-A3), South America(SA1,SA2). Data supplied by the Petroleum Geochemistry Division of Fugro Robertson.*

Oil	Origin	Source Rock Type	Source Age	Maturity	Appearance	API°	H_20[%]
198	EU	Marine Clastic, Type II kerogen	Jurassic	Middle Mature	Black,mobile	31.5	
199	EU	Marine Clastic, Type II kerogen	Jurassic	Middle Mature	Black,mobile	30.4	
201	EU	Marine Clastic, Type II kerogen	Jurassic	Middle Mature	Black,mobile	29.8	
207	EU	Marine Clastic, Type II kerogen	Jurassic	Middle Mature	Black,mobile	38.0	
7032	ME1	Marine Carbonate, Type II kerogen	Cretaceaous	Early mature, non-degraded	Black, mod. viscosity, slow mobility	19.1	0.1
7033	ME1	Marine Carbonate, Type II kerogen	Cretaceaous	Early mature, minor degradation	Black, mod. viscosity, slow mobility	12.8	4.6
7058	A3	Marine Clastic, Type III/II kerogen	Tertiary	Middle mature	Dark brown/black,mobile	40.1	0.1
7062	ME4	Marine Algal	Pre-Cambrian	Middle mature	Black,mobile	36.0	0.1
7086	NA1	Marine Anoxic, Type II kerogen		Middle mature, non-degraded	Dark brown/black,mobile	39.5	0.1
7090	NA2	Marine Clastic, Type II kerogen		Middle mature, minor degradation	Dark brown/black,mobile	36.8	0.1
7093	ME2	Marine Clastic, Type II kerogen		Middle mature, non-degraded	Black,mobile	30.9	0.1
7098	NA2			Late mature	Pale yellow,mobile	44.6	0.1
7130	A1	Lacustrine	Tertiary	Early mature, degraded	Black, slow mobility	15.6	
7169	SA1	Marine Clastic, Type II kerogen	Cretaceous	Extensively degraded	Black, slow mobility	21.6	
7186	A2	Marine Clastic, Type III kerogen	Tertiary	Early mature, minor degradation	Dark brown/black, immobile	34.3	
7187	A2	Marine Clastic, Type III kerogen	Tertiary	Early mature, minor degradation	Dark brown/black, immobile	29.4	
7188	A1	Lacustrine	Tertiary	Extensively degraded	Black, immobile	13.3	
7193	SA1	Marine Clastic, Type II kerogen	Cretaceous	Middle Mature	Black, mobile	36.0	
7197	SA1	Marine Clastic, Type II kerogen	Cretaceous	Middle Mature	Black, mobile	45.1	
7321					Black, Immobile	14.1	
7324	NA3	Marine Clastic, Type II kerogen	Cretaceous	Middle Mature	Black, mobile	32.3	10
7632	SA2	Lacustrine	Jurassic?	Early-middle mature	Black, moderately viscous, mobile	32.7	0.1
7633	SA2	Lacustrine high Wax Oil	Jurassic?	Middle mature	Dark brown/black, immobile	24.8	0.1
7703	ME3	Marine Carbonate	Jurassic	Late mature	Yellow, mobile	50.6	0.1

Table 2.2: *Fractionation Data for Batch* 1 *oils. Data supplied by the Petroleum Geochemistry Division of Fugro Robertson.*

		Chromatography				Normalised				
Oil	Asphaltene[%]	Alkane[%]	Aromatic[%]	Polar[%]	Loss[%]	Alkane[%]	Aromatic[%]	Polar[%]	Wax[%]	S[%]
198	0.1	58.00	28.80	11.20	2.00	59.18	29.39	11.43		0.41
199	0.03	54.60	28.50	10.50	6.40	58.33	30.45	11.22		0.43
201	0.06	55.20	29.10	10.50	5.20	58.23	30.70	11.08		0.49
207	0.30	63.10	23.70	10.20	3.00	65.05	24.43	10.52		0.13
7032	17.5	30.58	26.52	22.17	20.72	38.57	33.46	27.97	3.9	5.38
7033	16.2	19.35	25.55	26.32	28.77	27.17	35.87	36.96	1.7	5.51
7058	0.04	34.08	18.15	3.45	44.32	61.20	32.60	6.19	3.57	0.96
7062	10.8	32.28	23.33	17.21	27.18	44.32	32.04	23.64	4.06	1.74
7086	0.5	40.16	3.87	7.65	48.32	77.71	7.50	14.79	0.9	0.59
7090	1.1	53.14	4.74	10.50	31.62	77.71	6.93	15.36	0.98	0.26
7093	3.5	33.86	19.35	11.47	35.32	52.35	29.91	17.74	1.89	0.36
7098	7.5	42.18	4.61	0.70	52.51	88.82	9.70	1.48	0.95	0.04
7130	0.05	43.57	17.47	24.56	14.40	50.90	20.41	28.69	2.1	0.35
7169	1.4	44.71	18.53	20.31	16.44	53.51	22.18	24.31	4.3	0.5
7186	0.1	46.39	12.32	2.61	38.68	75.65	20.10	4.25	1.3	0.09
7187	0.8	52.20	23.90	4.39	19.51	64.85	29.70	5.46	8.3	0.1
7188	1.1	32.40	19.33	40.17	8.10	35.25	21.03	43.71	17.6	0.44
7193	1.7	50.73	12.37	4.89	32.02	74.62	18.20	7.19	1.6	0.17
7197	0.4	38.84	6.59	1.93	52.64	82.01	13.92	4.07	4.6	0.10
7321		62.61	9.06	5.30	23.03	81.34	11.76	6.89		
7324	1.0	42.87	13.95	6.57	36.60	67.62	22.01	10.37	0.6	0.32
7632	1.5	43.78	2.70	12.24	41.29	74.56	4.59	20.85	5.1	0.11
7633	0.7	67.00	2.93	3.73	26.34	90.96	3.97	5.07	13	0.05
7703	0	12.83	1.79	1.58	83.81	79.22	11.04	9.74	1.3	0.49

Table 2.3: *Fractionation Data and physical properties for the Batch 2 crude oils. Data supplied by the Petroleum Geochemistry Division of Fugro Robertson.*

		Chromatography				Normalised					
Oil	Asphaltene[%]	Alkane[%]	Aromatic[%]	Polar[%]	Loss[%]	Alkane[%]	Aromatic[%]	Polar[%]	API°	S[%]	Reservoir Interval
ME-1	3.4	58.8	28.5	8.2	4.5	61.6	29.8	8.6	32.7	1.63	Cretaceous
ME-2	4.2	57.2	28.1	7.4	7.3	61.7	30.3	8.0	28.9	1.43	Cretaceous
ME-3	3.0	60.7	29.6	7.4	2.3	62.1	30.3	7.6	30.8	1.67	Cretaceous
ME-4	0.9	66.5	20.7	6.3	6.5	71.1	22.1	6.7	39.2	0.92	Cretaceous
ME-5	0.1	75.5	14.9	3.5	6.1	80.4	15.9	3.7	44.1	0.60	Cretaceous
ME-6	0.1	68.8	17.8	3.6	9.8	76.3	19.7	4.0	39.6	0.58	Jurassic
ME-7	0	69.7	14.5	2.3	13.5	80.6	16.8	2.7	42.1	0.83	Jurassic
ME-8	0.04	62.2	17.1	1.5	19.2	77.0	21.2	1.9	44.2	1.13	Jurassic
ME-9	0	67.0	10.0	2.0	21.0	84.8	12.7	2.5	47.8	1.80	Jurassic
ME-10	8.9	48.0	38.8	6.9	6.3	51.2	41.4	7.4	24.7	2.67	Cretaceous

2.2 Frequency Domain(FD) measurements

2.2.1 FD Instrumentation

2.2.1.1 Hardware

The phase and modulation data were obtained using an Alba Fluorescence Lifetime Imaging (FLIM) system (ISS Inc, Champaign, Illinois, USA) based on an upright Olympus BX51 microscope fitted with a modulated (10 to 200 MHz) 405 nm laser diode excitation source (Figures 2.1 and 2.2). The experimental setup enabled the simultaneous recording of phase and modulation data at two narrow wavelength ranges defined by emission bandpass filters.

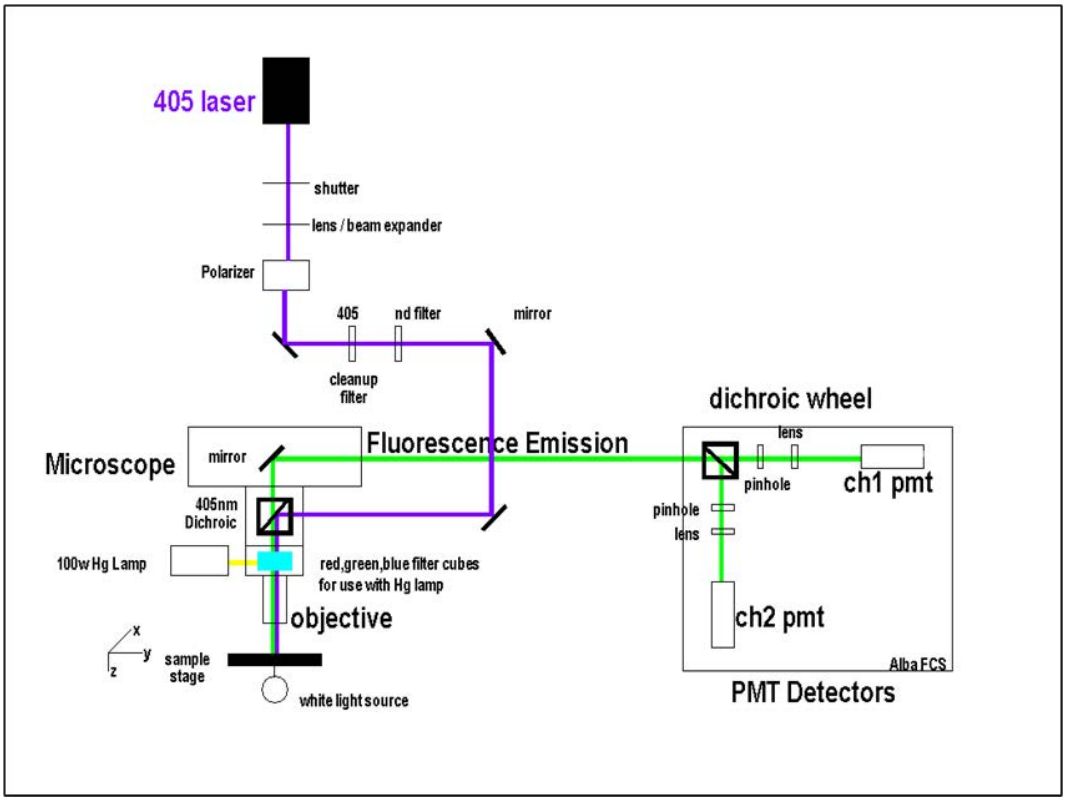

Figure 2.1: *Schematic of the frequency domain lifetime imaging system. The microscope is an upright Olympus BX-1 with* 50×0.5 *NA air objective. Two photomultiplier tubes record the fluorescence intensity after passing through a set of bandpass filters fitted on the dichroic wheel that is housed in the detector unit.*

Figure 2.2: *ISS Alba system. A: Detector unit. B: Synchronisation unit. C: RF amplifier. D: Dual frequency generator. E: dichroic mirror (separates excitation and emission light). F: filter turret. G: Widefield light source (Hg lamp). H: XY scanning stage and XYZ piezo electric stage. I: controller for XY scanning stage.*

The Alba FD instrument is principally designed for confocal fluorescence imaging, fluorescence lifetime imaging(FLIM) and FCS[‡] experiments. The schematic (Figure 2.1) shows the dual channel operation of the instrument, and the pinholes in front of the detectors enable confocal operation. A piezo-electric motorised stage (Nano-LP100, Mad City Labs Inc.) was incorporated that allows $100\mu\ m$ travel in X,Y,Z directions. This allows imaging in different planes, collection of Z-stacks and generation of 3-D images. The step size was controlled by computer and was capable of a 5 nm resolution.

Each detector incorporated a pinhole array; with each array containing nine pinholes of different sizes. The sizes of the available pinholes were 12.5,17,25,35,50,70,100,141 and 1000 μm with tolerances within 5%. The positioning tolerance on each pinhole

[‡] In Fluorescence Correlation Spectroscopy (FCS) the temporal fluctuations of fluorescence intensity can be used to determine physical or chemical parameters such as diffusion coefficients, flow rates, chemical kinetic rate constants and molecular weights [36].

was within $\pm 5\ \mu m$. Instrument control was performed using Vista control software (Version 3.5 Build 66).

2.2.1.2 FD Electronics

A dual frequency synthesizer (ISS Model A213) provided modulation frequencies in the range from 1 MHz to 300 MHz, theoretically covering a range sufficient to determine the decay times of most common fluorophores (from 0.5 to 160 ns). The principle behind the operation of the two synthesisers is as follows. One synthesizer modulated the diode light source (by superimposing the master frequency onto the diode current input) at a frequency f, which is called the master frequency. The second synthesizer modulated the gain of the light detectors (PMTs) at a frequency $f + \triangle f$ (called the slave); the frequency $\triangle f$, called the 'cross-correlation frequency' which is of the order of 1 KHz. The master frequency signal was then filtered from the cross-correlation frequency $\triangle f$ to reveal only the low frequency cross-correlation signal, which contained all the same demodulation and phase angle shift information as the fluorescence emission. The Radio Frequency amplifier (LA5) then provided amplification of the $\triangle f$ signal from the PMTs. A reference signal of 10 MHz was provided by the master frequency synthesizer that modulates the laser diode. A synchronisation unit used this reference signal to provide synchronisation between the two synthesisers and the other components of the system.

2.2.1.3 Excitation light source and beam shaping optics

The modulated excitation was provided by a 405 nm diode laser and the light intensity was controlled by a polarizer. A 405/40 nm clean up filter was used to reduce spurious emission and ND filters of varying transmission characteristics were used to further reduce the intensity if necessary. A series of beam steering mirrors passed the excitation light through a side aperture into the upright microscope (Olympus BX51). The excitation light was then reflected by a 405 nm dichroic mirror to the microscope objective (a long working distance Olympus LMPlan 50×0.5 numerical aperture objective was most commonly used). The fluorescence emission was collected through the same objective and passed through the 405 nm dichroic mirror, a 405 nm 'stopline' filter (Semrock thin film notch filter NF02-405S-25) and a 415

nm long pass filter. This setup minimised the scattered laser light present in the fluorescence emission. A standard mirror then directed the emission light into the detection unit (A in Figure 2.2).

2.2.1.4 Detection system

For all samples, the fluorescence emission was split into two channels (CH1 and CH2). A dichroic filter and bandpass filters were then used to select the emission range. Two multialkali (Na-K-Sb-Cs) photomultiplier tubes (Model R928 by Hamamatsu) were used to detect the fluorescence emission. This type of PMT gave good sensitivity between the $185 - 900$ nm range as shown in the spectral response curve (Figure 2.3).

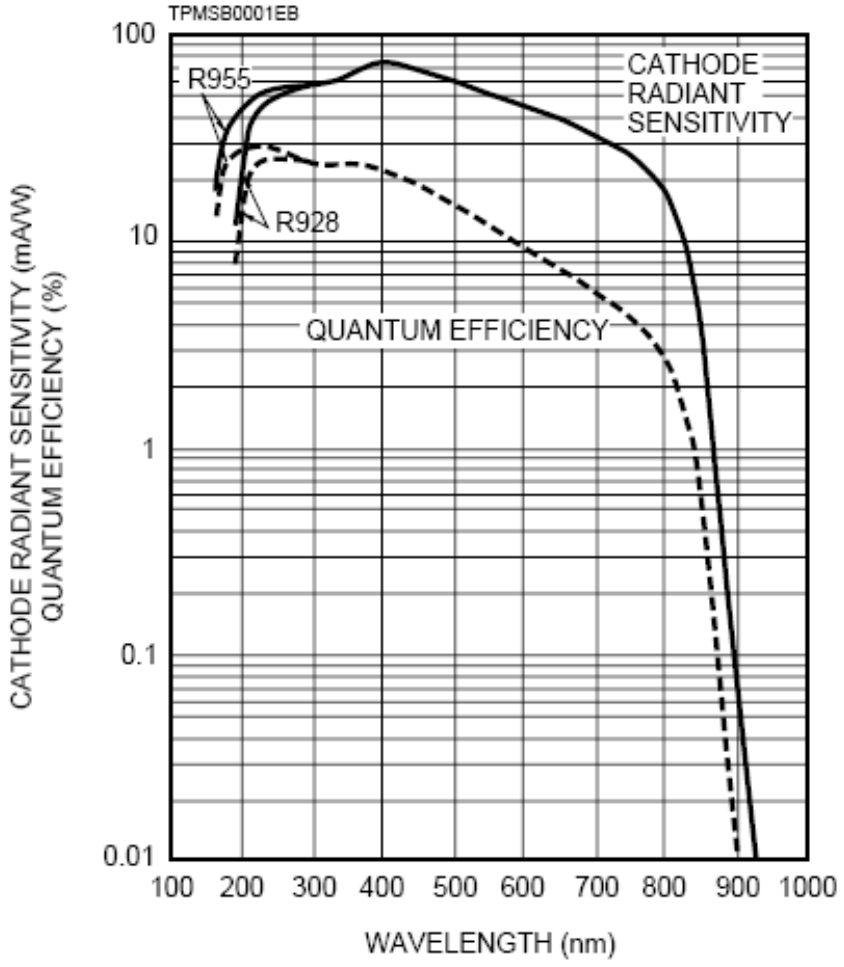

Figure 2.3: *Spectral response for the R928 PMT used in the Alba detection unit. Reproduced from [179].*

The dichroic mirror and filters were housed in a series of four filter cubes (Nikon Diaphot 18 mm), designed to cover most of the emission spectrum of crude oils. Each cube contained a dichroic mirror and two filters covering the transmitted and reflected bands.

Table 2.4: *Filter cube wavelength ranges for each channel (CH1 and 2) in the dichroic cube.*

Cube	Dichroic Mirror(nm)	CH1(nm)	CH2(nm)
1	495	542-582	426-477
2	505	573-613	465-500
3	562	600-650	480-520
4	570	575-650	510-560

All cubes, mirrors and filters were provided by AHF analysentechnik AG [180]. The emission wavelength ranges of each cube are given in Table 2.4 and the normalised transmission characteristics of each of the filter cubes are shown in Figures 2.4 and 2.5. The transmission characteristics of the dichroic mirrors and filters were measured by UV-VIS (Shimadzu UV-1601) and the transmission of light through the Alba system was measured by a compact CCD based fibre optic spectrometer (Ocean Optics USB 2000 and associated software). For the transmission characteristic of Cube 1, as shown in Figure 2.4 (top), the shorter wavelength band is cut at 426 nm due to the presence of the long pass filter in the optical system. For the rest of the transmission characteristic plots in Figures 2.4 and 2.5, the full band pass as specified by the filter UV-VIS spectra is observed by the USB2000 spectrometer with no clipping. There is a difference in measured intensity levels due to the manual placement of the USB2000 spectrometer in the Alba detector system optical path.

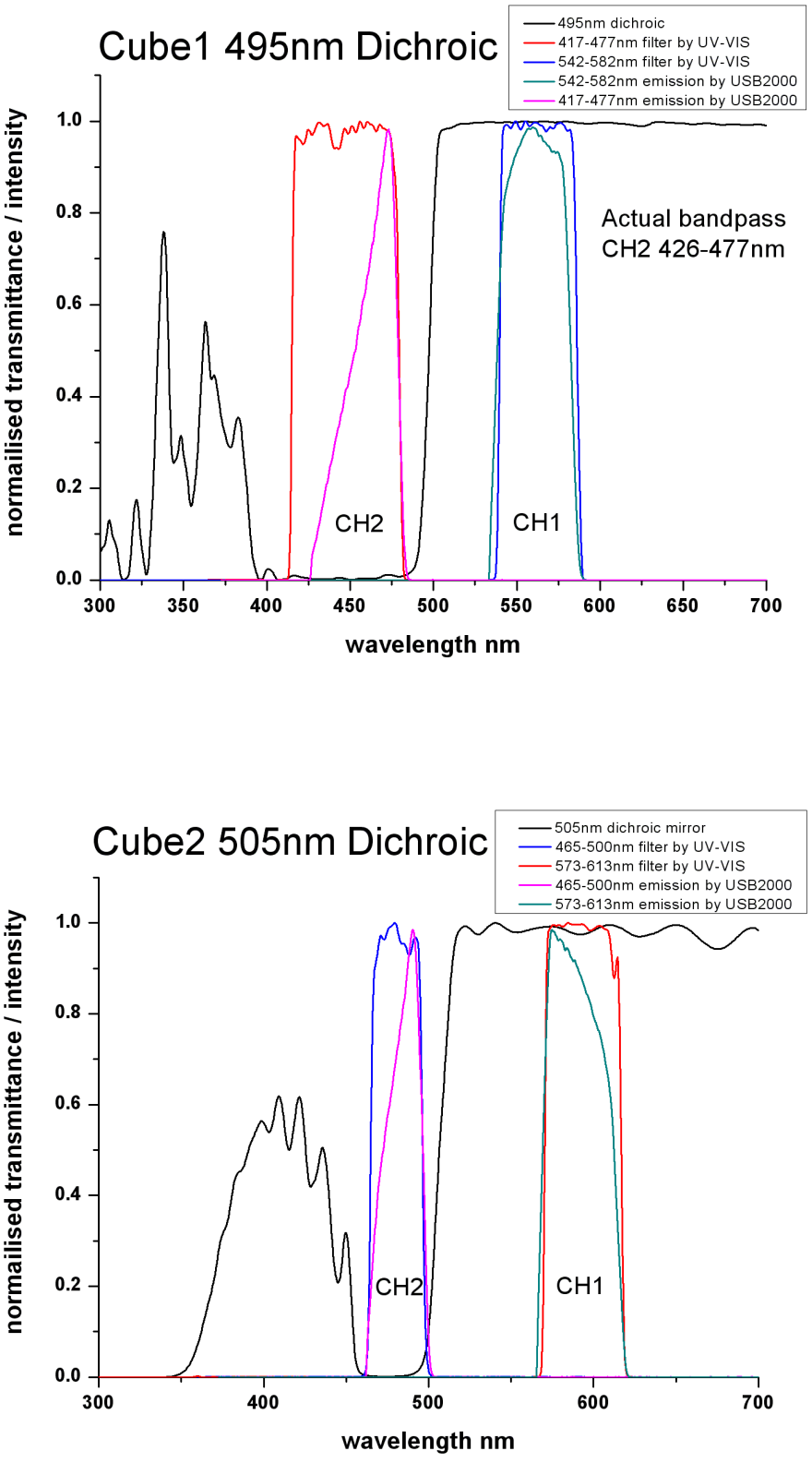

Figure 2.4: *Transmission characteristics for Cubes 1 and 2.*

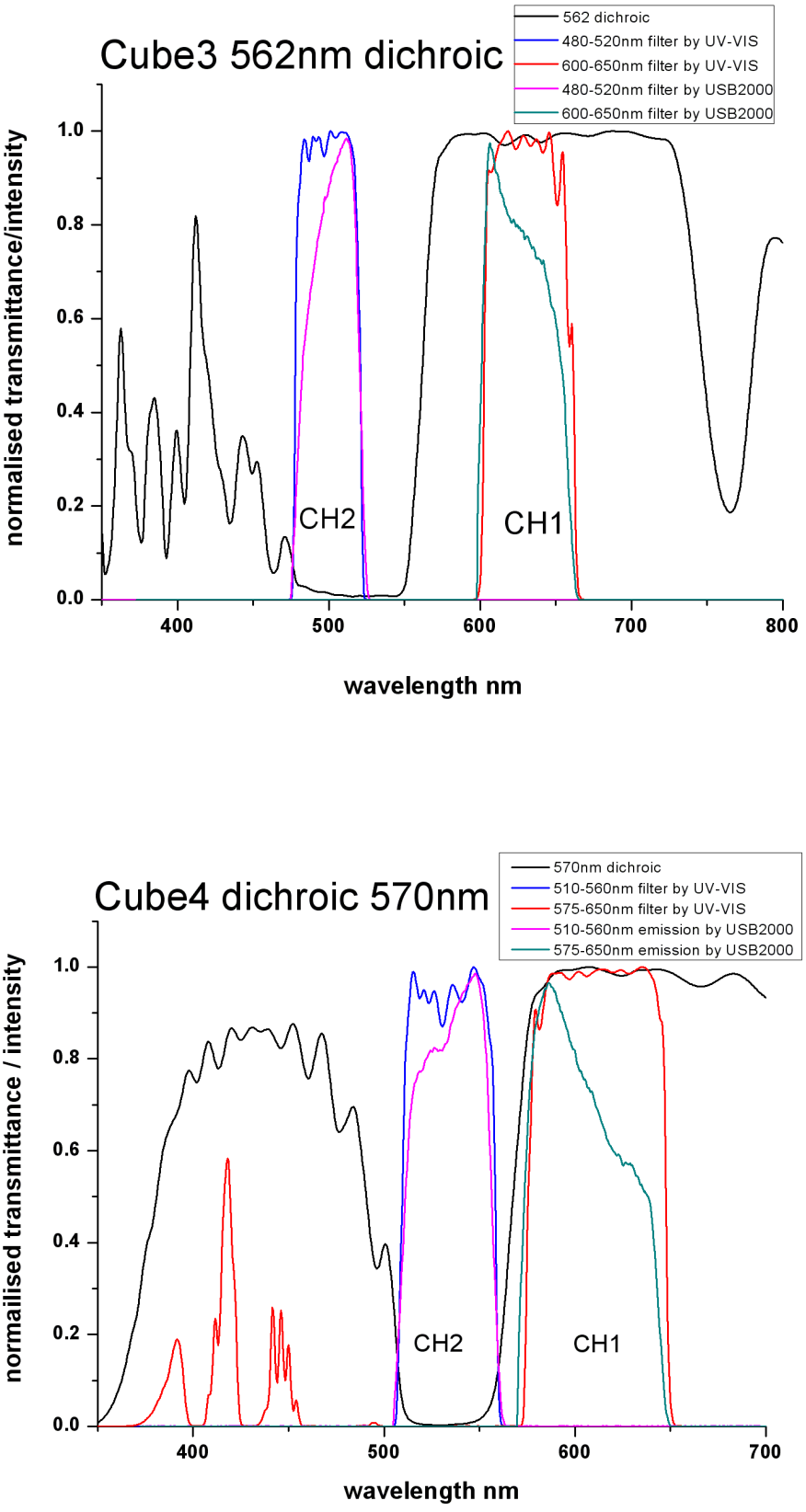

Figure 2.5: *Transmission characteristics for Cubes 3 and 4.*

Figure 2.6 shows visible light (Halogen) transmission through the Alba optical system. The red trace shows the spectrum without any filter cubes where the light is passed through the Alba optical system and to a Ocean Optics USB2000 spectrofluorimeter instead of the detector unit. In comparison the black trace shows the spectrum of the same light source recorded directly by the USB2000 spectrometer, i.e. not transmitting through any of the Alba system optics. The presence of stray light can be seen in the red trace but the main object is to show that close to the full wavelength range is passed through the Alba system. Also shown is the sensitivity curve for the CCD sensor that is housed in the USB2000 unit (Figure 2.7). The unit is more sensitive to emission at shorter wavelengths below 450 nm. However 50% sensitivity is achieved up to 700 nm which covers the emission spectrum of crude oils.

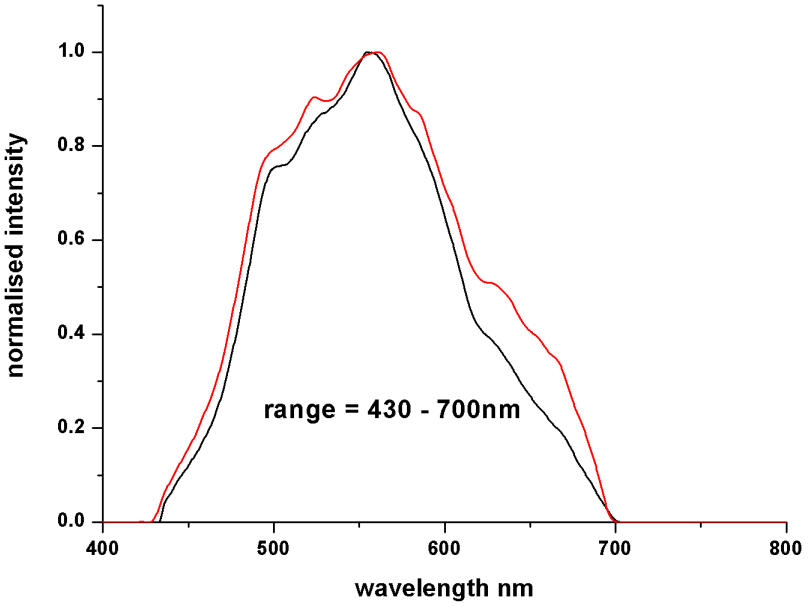

Figure 2.6: *White light source (100 W Halogen U-LH100) with no filter cubes present (red trace). Overlaid is the spectrum directly recorded from the white light source (black line). Measurement by USB2000 spectrometer.*

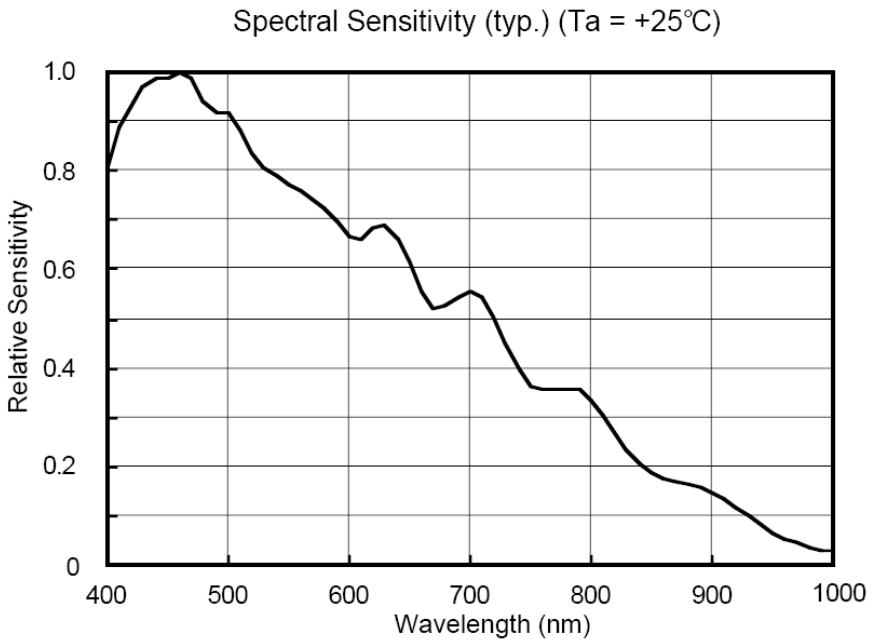

Figure 2.7: *Sensitivity curve for Sony 2048 pixel CCD linear sensor housed in the USB2000 spectrometer. Reproduced from [181].*

2.2.1.5 Data Acquisition and Analysis

Data acquisition and analysis were performed using Vista control software (Version 3.5 Build 66). Phase and modulation values at a series of modulation frequencies were first measured for a reference fluorophore of known lifetime. Subsequently, phase and demodulation values were measured for the sample at the same range of modulation frequencies and under the same optical conditions. The Vista software package was capable of determining fluorescence lifetimes using a range of models, i.e., discrete exponential, Gaussian and Lorentzian lifetime distributions). To evaluate how close the model fit the data acquired with the instrument, a Marquardt-Levenberg algorithm[§] was utilised for the minimisation of the reduced chi-squared function (Equation 1.37) that compares the selected model with the experimental data.

[§] A common optimisation algorithm for non-linear least-squares minimisation calculations [182].

2.2.2 Reference Standards

Reference standards of known fluorescence lifetime have to be used to provide phase and modulation data at each modulation frequency which are subsequently used to determine the lifetime of the sample under test. The lifetime of the reference standard should be in the same lifetime range as the sample but choice of standard is also dependent on the following criteria:

- Must be capable of excitation at 405 nm.
- Have a well defined single lifetime in the range $1 - 10$ ns (as most crude oils have lifetimes in this range).
- High fluorescence quantum yield.
- A large emission wavelength range.
- Soluble in common low volatility laboratory solvents.
- High photostability.

With this in mind, a search was made for fluorophores that fulfilled this criteria. The following fluorophores were chosen for evaluation as suitable reference standards: 1) 8-hydroxypyrene-1,3,6-trisulphonic acid trisodium salt HPTS, 2) N-(3-sulfopropyl) acridinium salt (SPA), 3) RhodamineB, 4) Acridone, 5) Coumarin 6, 6) Coumarin 30, 7) Coumarin 314 and 8) Lucifer Yellow CH.

The main objective was to find a set of fluorophores that had fluorescence emission covering the full range of wavelengths as defined by Tables 2.4. In this way the lifetime of crude oils could be determined accurately in discrete wavelength ranges (~ 40 nm steps). The photophysical data for each of the fluorophores above is given in Appendix A where the emission characteristics and the lifetimes were validated for both FD and TCSPC measurements.

An investigation was also made into how each fluorophore behaved over a range of modulation frequencies; the object being to find the optimum range of measurement frequencies for each reference fluorophore. This was achieved by comparing the apparent phase and modulation based lifetimes (calculated from the phase and modulation equations given in Chapter 1) over a range of modulation frequencies.

The variation of phase and modulation based lifeimes for four of the fluorophores tested in are given in Figures 2.8 and 2.9. In Figure 2.8, the modulation based lifetime values are fairly consistent from approximately 10 to 200 MHz. Phase measurements appear to be more sensitive with increasing variation in lifetime as the modulation frequency increases. Below 10 MHz, a large distortion from the expected lifetime is found which is greater for the modulation based values. Low modulation frequencies result in very small phase shifts and very low demodulation ratios for this fluorophore, and the measurements are at the limits of the instrument resolution. This leads to wide and random variations in the calculated lifetimes. In the case of Coumarin 30, the lifetime values decrease. A similar situation is shown in Figure 2.9 but for Rhodamine B there is very close agreement in phase and lifetime values above approximately 60 MHz. This fluorophore has a short lifetime of $\sim 1.7\ ns$ (see Appendix A for details and references) and thus has a better response at higher modulation frequencies. Above 200 MHz, it was found that instability in the generation of high frequencies (a hardware artefact) led to a large fluctuation in the phase measurements. The plot for Lucifer Yellow in Figure 2.8 shows a large distortion in the phase based lifetime values. Generally the phase and modulation lifetimes compared favorably when modulation frequencies between 30 and 110 MHz were used. To be able to measure the crude oils with longer lifetimes, the range was extended from 10 to 110 and hence this frequency range was used for all subsequent oil analysis. Most crude oils were found to have lifetimes in the 1-10 ns range so based on the criteria outlined above and the information for each fluorophore given in Appendix A, the fluorophores described in Table 2.5 were chosen as reference standards.

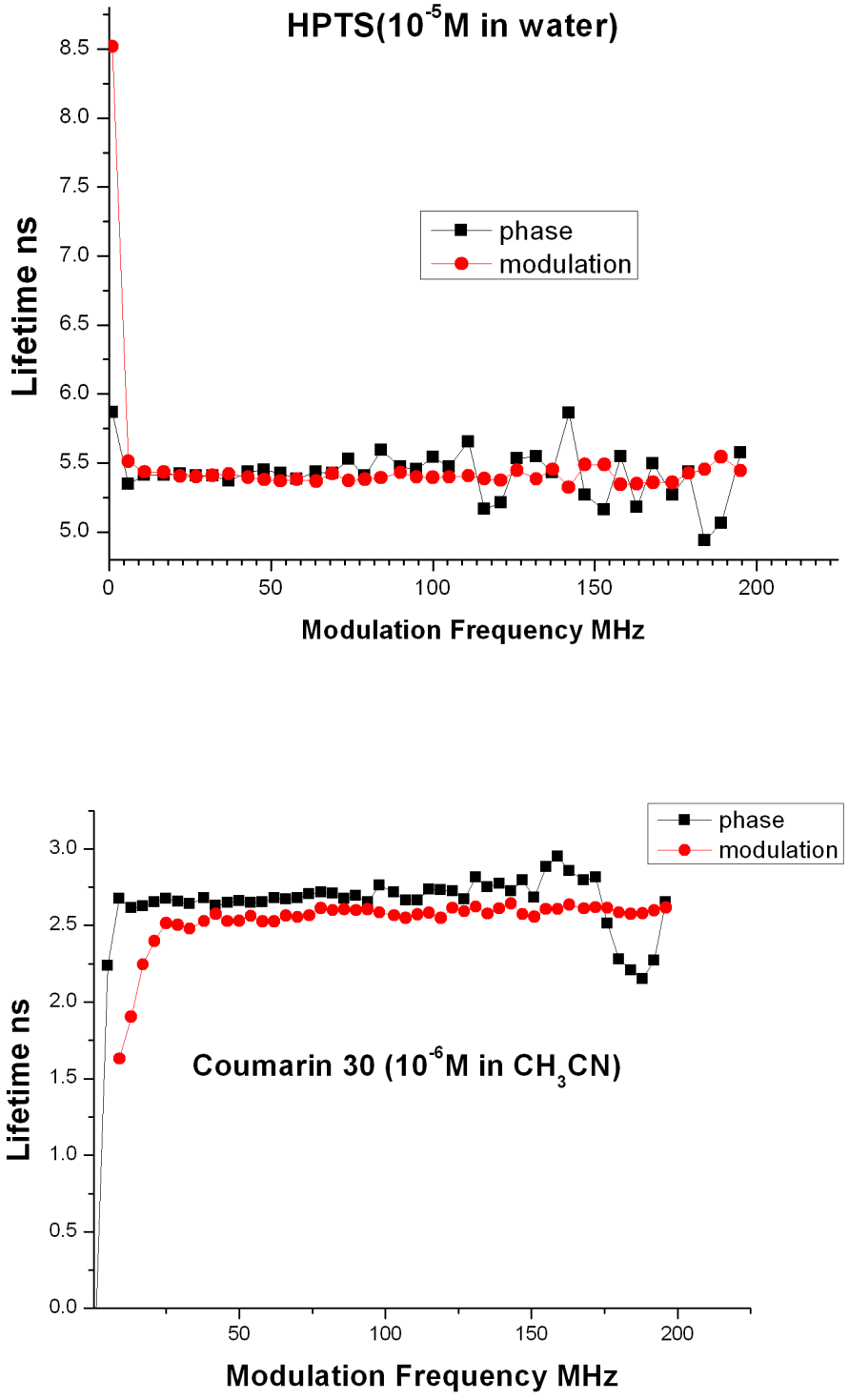

Figure 2.8: *Lifetimes calculated by phase and modulation for HPTS (5.4 ns) and Coumarin 30 (2.6 ns).*

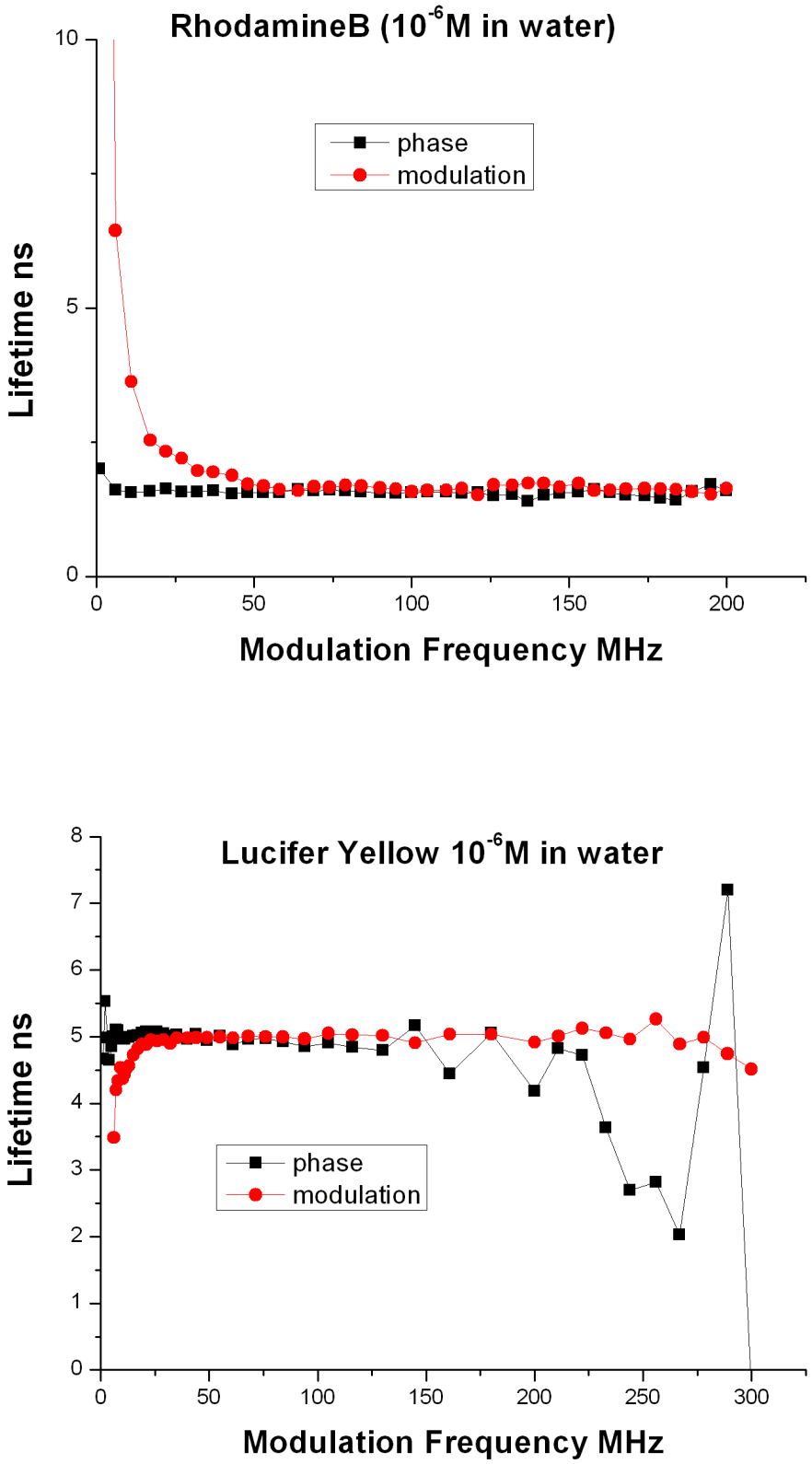

Figure 2.9: *Lifetimes calculated by phase and modulation for RhodamineB (1.7 ns) and Lucifer Yellow (5.1 ns). The large distortion of the lifetime based phase measurements above* 200 MHz *for Lucifer Yellow was found to be due to an instability in the frequency synthesiser hardware.*

Table 2.5: *Filter cube ranges and their associated reference standards. References for lifetime values can be found in Appendix A.*

Cube	Reference Standard	Lifetime(ns)
1	Coumarin30	2.6
2	HPTS	5.4
3	Lucifer Yellow	5.1
4	Lucifer Yellow	5.1

The overall steady-state emission profiles and the corresponding FD phase modulation responses are shown in Figures 2.10 and 2.11 respectively. The reference standards cover a range from 450 to 700 nm, which covers most of the spectral emission of crude oils. In Figure 2.11, the experimental values overlay simulated values generated single lifetimes of 2.6 and 5.4 ns. For clarity, the simulated data are represented by a black line. Very close agreement between the experimental and simulated values except for the phase values at higher modulation frequencies. The experimental data at these higher modulation frequencies may skew the fitting leading to inaccurate lifetime values. More accurate values for lifetime will be generated using modulation frequencies in the region around the crossing point of the phase and modulation plots.

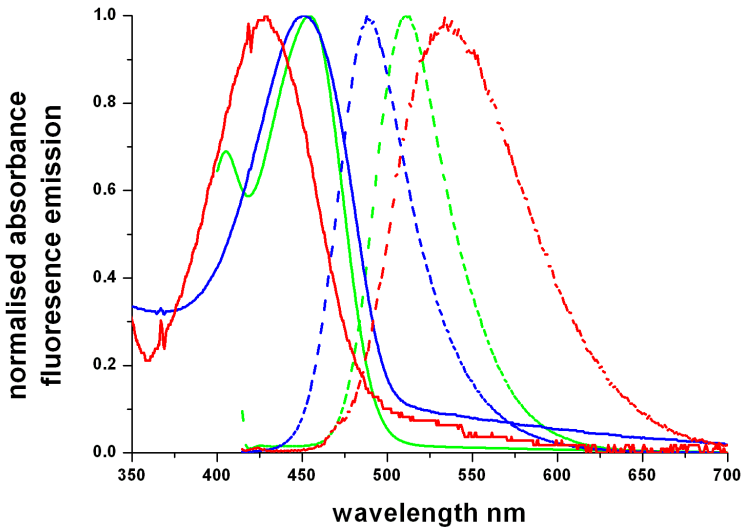

Figure 2.10: *Absorbance (solid limes) and steady state emission (dotted lines) spectra for three fluorophores used as references for the crude oil samples. The emission covers a broad range and all three are excited at 405 nm. Red: Lucifer Yellow, Blue: Coumain30 and Green:* HPTS. *All spectra taken using 10 mm pathlength quartz cuvettes. For absorption spectra, the reference cuvette contained the appropriate solvent.*

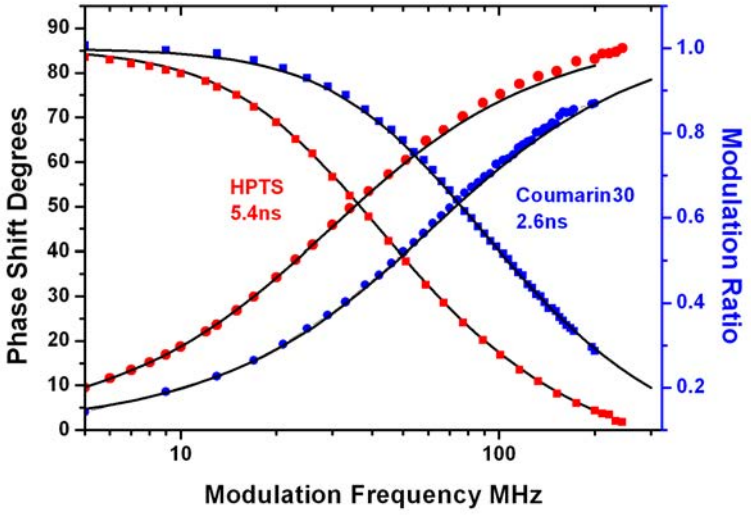

Figure 2.11: *Phase modulation plots for Coumarin30 and* HPTS. *Lucifer Yellow has been omitted for clarity due to its closeness of lifetime to* HPTS. *The black lines indicate the simulated values and the coloured data points are the experimental values.*

2.2.3 Validation of FD instrumentation

It was necessary to validate the FD system by a series of steps designed to rigourously test and determine the optimum working conditions. This was done by the following experiments:

- Resolution of a mixture of fluorophores.
- Checking the linearity of the FD system over a range of lifetimes by application of Stern-Volmer analysis.

2.2.3.1 Resolution of a mixture of fluorophores

The objective here was to investigate if the FD system could satisfactorily resolve a mixture of two different fluorescent species. To check this, it was necessary to determine the fractional contributions of each fluorophore and compare this to the results obtained by TCSPC measurements. Rhodamine B and Acridone were chosen as the two fluorophores with lifetimes of 1.7 and 14.9 ns respectively. A 1:1 mix of Rhodamine B and Acridone (10^{-6} M for both in water) was prepared, and placed into a 10 mm pathlength quartz cuvette. UV absorption spectra of the individual components (both show a very weak absorbance at 405 nm) and the 1:1 mixture was obtained (Figure 2.12). Similarly the steady-state fluorescence spectra of both components and the mixture was obtained. The fluorescence spectra were normalised by dividing the spectra by the value of absorbance at 405 nm. Then regression analysis is performed on the intensity values in the form:

$$Spectra_{mix} = x * Spectra_{Acridone} + y * Spectra_{RhodamineB} \tag{2.1}$$

where the dependent values were the Rhodamine B, Acridone mixture data and the independent values were the individual Rhodamine B and Acridone data.

Figure 2.13 shows the steady state fluorescence spectra and the simulated curve obtained using the fractions above. There is close agreement between the simulated curve (green symbols) and the experimental values for the mixture.

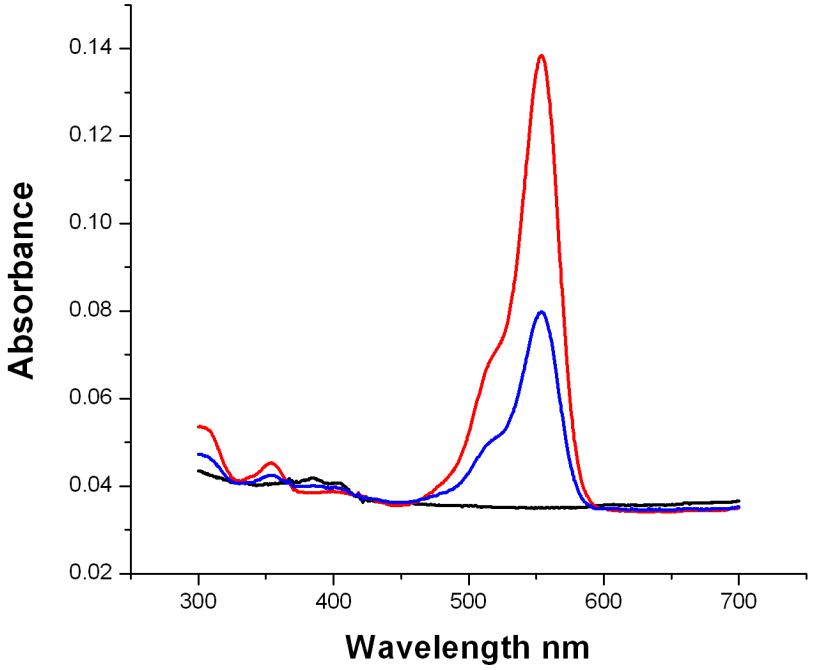

Figure 2.12: *Absorption spectra for Rhodamine B* 10^{-6} *M (red), Acridone* 10^{-6} *M (black) (and a 1:1 mixture of both (blue). The absorbance and emission spectra for Acridone is given in Appendix A.*

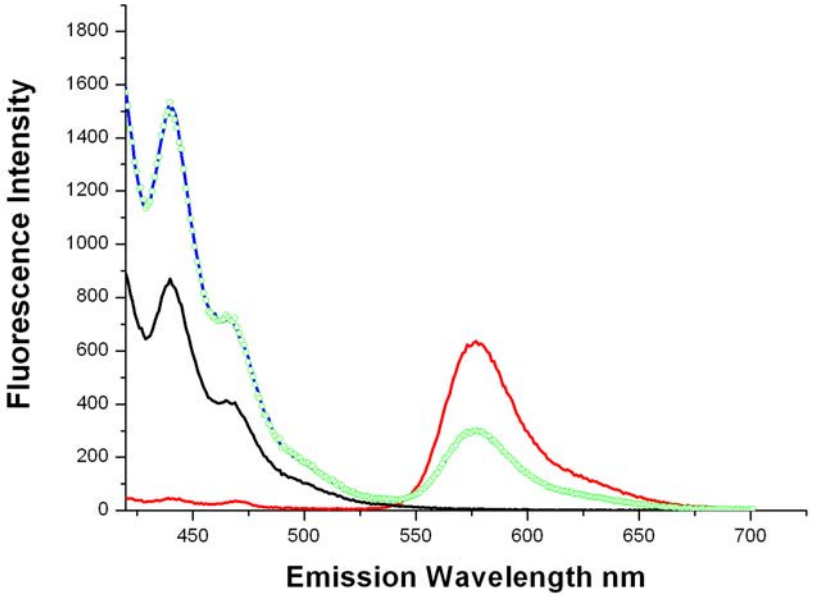

Figure 2.13: *Steady state emission spectra for Rhodamine B* 10^{-6} *M (red), Acridone* 10^{-6} *M (black) and a 1:1 mixture of both (blue).The simulated emission spectrum is given by the green symbols showing a close overlay on the experimental emission spectrum. Spectra were collected using a Cary Eclipse spectrometer.*

Time resolved analysis was then performed in both the time domain and the frequency domain. In the Frequency Domain, the mixture was run under the following conditions:

Reference standard: HPTS (10^{-5}M), Medium: front surface cuvette (1 mm), Objective: 50× air (0.5 NA), Modulation Frequencies: 1 to 200 MHz, PMT voltage: 70%, Starting DC value: approx 4500. Full emission spectrum recorded.

For TD measurements the conditions were: Medium: front surface cuvette (1 mm), Rep frequency: 10 MHz, Time Delay: 48 ns, Intensity: 70%, Slit width: 0.5 mm, Zero Cross: 20 mV, Level: −100 mV, Discriminator: 80 mV, Resolution: −35 ps, Offset: 0 ns, Scatter for IRF: LUDOX.

For Rhodamine B, lifetimes were measured at an emission wavelength of 580 nm. For Acridone, the emission wavelength for measurement was 440 nm. The fitting based on both the phase and modulation data is shown in Figure 2.14. Two discrete decay components described the data with a χ^2_ν value of 0.036.

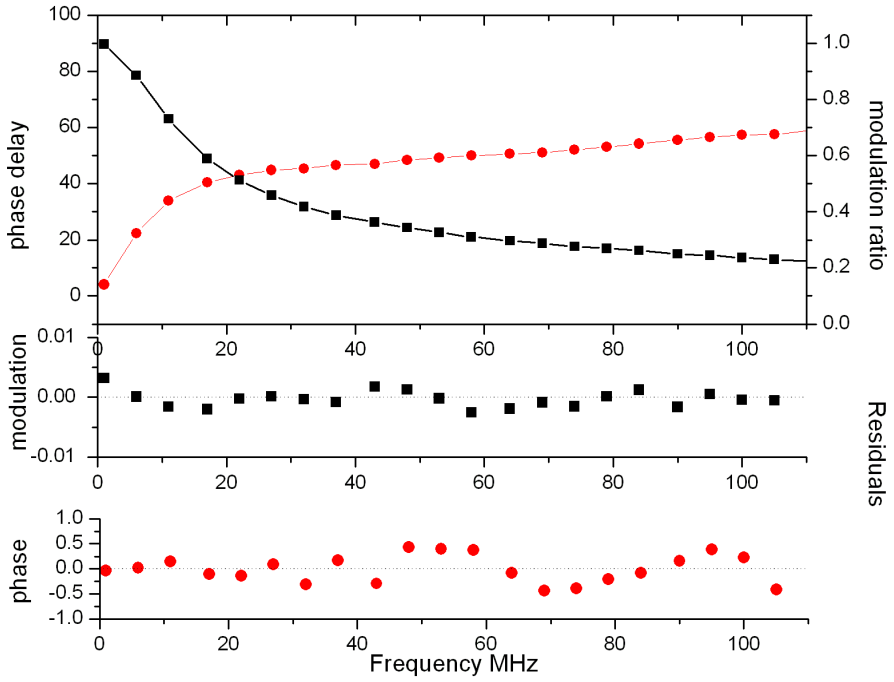

Figure 2.14: *Phase modulation response for a 1:1 mixture of RhodamineB and Acridone. Reference standard* HPTS $10^{-5}M$ *in phosphate buffer. Fitting is adequately described by two decay terms.* $\chi^2_\nu = 0.036$.

Comparison can be made between the fractional contributions of each component obtained by both the spectral and time resolved methods and this is shown in Table 2.6. There is close agreement between the TD and FD lifetimes for each component but there is a difference of $> 10\%$ in the fractional contributions. This variation importantly lead to a ns difference between the intensity based average lifetimes for TD and FD. While the FD analysis adequately resolved the two fluorophores and in terms of lifetimes, the TD method was in closer agreement with the spectral calculation leading to a more accurate determination of the average lifetime.

Table 2.6: *Fractional contributions and Lifetimes from Spectral,* TD *and* FD *measurements. Intensity based average lifetimes were calculated for the mixture values.*

Fluorophore	Spectra(%)	TD(%)	FD(%)	FD Lifetimes(ns)	TD Lifetimes(ns)
Acridone	79.1	76.4	67.6	14.6	14.4
RhodamineB	20.9	23.6	32.4	1.55	1.6
Mixture				11.5	10.28

2.2.3.2 Linearity of lifetime measurements

In order to investigate the response of the FD system from short to long lifetimes, Stern-Volmer analysis was performed using Acridone (10^{-3} M in water) that was quenched by Potassium Iodide. The same solutions were tested on the TCSPC system for comparative purposes. Acridone in water exhibits a single exponential decay time of 14.9 ns (air saturated), which has been verified on both the FD and TD instruments and is agreement with the literature values [183]. It is quenched readily by KI and the mechanism is predominantly collisional (efficiency 0.8) [36].

Solutions containing varying concentrations of KI were made up according to Table 2.7. All solutions were prepared at room temperature and in air saturated solvent. KCl was added to maintain a constant ionic strength. 1 ml of 4×10^{-3} M $Na_2S_2O_3$ solution was added to each sample as an anti-oxidant for KI and prevent liberation of free iodine. Sample 1 contained 1 ml KCl, 1 ml 10^{-3} M Acridone and 2 ml H_2O. Sample 2 contained 1 ml KCl, 1 ml KI, 1 ml of 10^{-3}M Acridone and 1 ml of 4×10^{-3} M $Na_2S_2O_3$. Samples 3-12 contained the same matrix as sample 2. Stern-Volmer plots were constructed by plotting $\tau_0/\tau - 1$ versus KI concentration where τ_0 is the unquenched lifetime for Acridone. The calculated lifetime values are

given in Table 2.7 and the Stern-Volmer plot is given in Figure 2.15. The TCSPC system was not able to provide an adequate fit for the short lifetime of sample 12 and this value was omitted. As shown by Figure 2.15, a linear response was found over the concentration range sampled for both FD and TD experiments demonstrating that dynamic quenching is the principal quenching mechanism. The Stern-volmer plots show a close match for the region of low quencher concentration. At higher quencher concentrations, the plots diverge, yet linearity over the concentration range is maintained (the FD plot linear fit shows a correlation coefficient of 0.999). The TCSPC lifetimes are consistently longer than the FD lifetimes except for lowest quencher concentrations. At low quencher concentrations, the results from both the TD and FD methods follow very similar behaviour. At lower fluorophore concentrations, the difference between the two recording methods is exaggerated, i.e. up to 13% difference in the lifetime as shown in Table 2.7).

Table 2.7: *Linearity check of* TD *system: Quenching data for Stern-Volmer analysis. Difference between the TD and FD data is given in the last column.*

Sample	[KCl]M	[KI]M	FD Lifetime(ns)	TD Lifetime(ns)	Diff (%)
1	1.1	0	14.8	14.64	-1.1
2	1.06	0.04	7.91	7.91	0
3	1.04	0.06	6.27	6.48	3.2
4	1.02	0.08	5.30	5.40	1.8
5	1.0	0.1	4.44	4.61	3.7
6	0.95	0.15	3.36	3.49	3.7
7	0.9	0.2	2.51	2.71	7.4
8	0.8	0.3	1.87	1.96	4.6
9	0.6	0.5	1.22	1.28	4.7
10	0.5	0.6	1.03	1.05	1.9
11	0.4	0.7	0.85	0.98	13.3
12	0.3	0.8	0.78	-	-

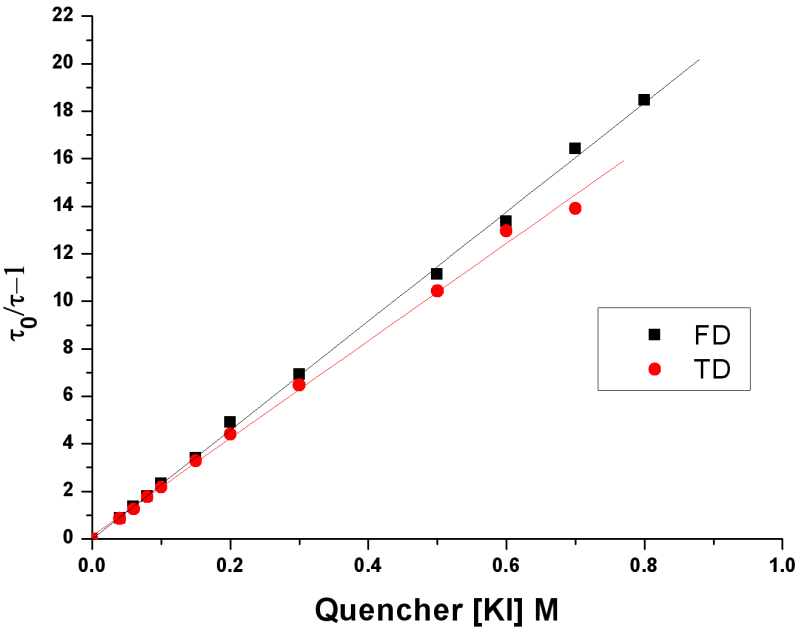

Figure 2.15: *Stern-Volmer plots based on the quenching of Acridone by potassium iodide. TD plot* $r^2 = 0.997$*, FD plot* $r^2 = 0.999$*.*

2.2.4 Crude oil lifetime measurements

The general procedure to calculate crude oil lifetimes was as follows:

For analysis of the bulk crude oils, the system was operated in non-confocal mode (for higher throughput) as lifetime imaging was not performed. First, the appropriate reference standard was chosen and the intensity of the fluorescence signal at the detector was optimised using the software controlled alignment of the detection system optics and PMT. Optimisation was performed for both channels. The system was then calibrated in terms of phase and modulation for the reference standard using the known lifetime as input which had previously been determined by TCSPC measurement. Either Coumarin 30 or Lucifer Yellow standards were then used to verify the calibration by determining the phase and modulation response compared to the calibrated system between 10 and 110 MHz. The quality of fit as judged by the proximity of the calculated lifetime (±0.1 ns) and the goodness of fit (χ^2_ν) value for a single exponential model. If this was satisfactory, the neat, non-degassed crude oils were placed directly into a 1 mm path length quartz cuvette and then placed

perpendicular to the excitation beam on the sample stage. All measurements were made in triplicate at room temperature ($20 - 22\,^{\circ}$C). Average lifetime repeatability was generally 0.1 ns. For each filter cube used subsequently, this optimisation and recording process was repeated.

2.2.4.1 Cleaning of quartz cells used for crude oil analysis

After use, the quartz cells were flushed with 1,1,1 Trichloroethane until all traces of the oils were removed, acetone washed, and then stored in dilute nitric acid overnight. Subsequently, the quartz cells were washed in distilled water and oven dried at 70°C.

2.2.5 Estimation of the uncertainty of FD lifetimes of crude oils

Due to the large number of different emitting fluorophores at every emission wavelength the calculation of a fluorescence lifetime value is not a trivial task. The phase and modulation measurements were fit to either a discrete multi-exponential decay or with multiple decay term Gaussian and Lorentzian distribution models. In most cases 2 or 3 individual decay times were required for all model types to achieve a satisfactory fit. A single decay distribution model could also be used to calculate the fluorescence lifetime. For all cases the intensity based average lifetime ($\overline{\tau}$) was reported.

The goodness of the model is judged on the minimisation of the value of χ^2_ν and also on the number of decay terms used [36, 56]. To determine the confidence limits on the average lifetimes reported, it is necessary to prepare a χ^2_ν surface plot, or Support Plane Analysis [36, 184]. This plots the value of $\chi^2_\nu/\chi^2_{\nu min}$ versus the average lifetime obtained and the F_χ statistic (appropriate for ρ and ν degrees of freedom of the measurement method) is then used to determine the confidence interval.

$$F_\chi = \frac{\chi^2_\nu(par)}{\chi^2_\nu(min)} = 1 + \frac{\rho}{\nu} F(\rho, \nu, P) \tag{2.2}$$

where, $\chi^2_\nu(par)$ is the value of χ^2_ν with a fixed parameter value, $\chi^2_\nu(min)$ is the minimum value of χ^2_ν, ρ is the number of parameters, and $F(\rho, \nu, P)$ is the F statistic

with ρ parameters and ν degrees of freedom with a probability of P. The F statistic values needed to calculate F_χ are described in Lakowicz [36]. For the analysis of crude oils, a value of P=0.32 was used, representing one standard deviation (1σ). This value of P gives an indication that the probability of F_χ is due to random errors in the data. If $P > 0.32$ then there is less than 32% chance that the parameter value is consistent with the data. When $P < 0.32$ then there is 68% chance that the parameter is consistent with the data.

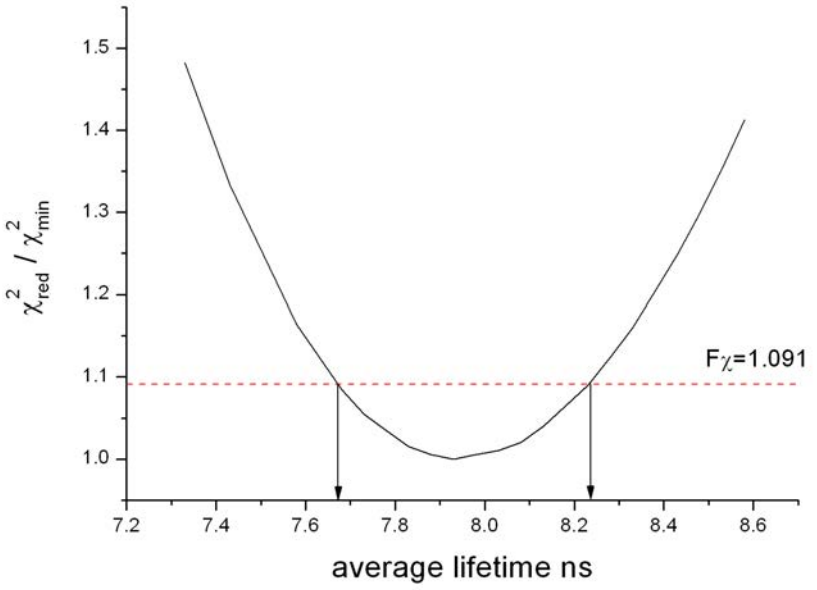

Figure 2.16: *Surface plot for the fluorescence lifetime fitting of oil* 7633 *(542-582 nm emission data) based on a three decay term discrete exponential model. The F_χ line cuts the parabola giving a value for the confidence interval. In this case the interval is* ± 0.57 *ns.*

When dealing with complex decays and average lifetime values, the most facile means of generating a plot of $\chi^2_\nu/\chi^2_\nu(min)$ versus the average lifetime is to systematically change the longest lifetime component only. The line of F_χ is superimposed on the support plane plot which cuts the parabola at a minimum and maximum level, giving a value for the average lifetime confidence interval (Figure 2.16). In practice, when studying complex systems like crude oils [116, 126, 129–132], small changes in this long lifetime have the greatest impact on the average lifetime and χ^2_ν values. As more lifetime terms are included in the fit model, a larger confidence

interval range is obtained. Also the choice of model has an effect on the confidence interval as shown by Figure 2.17.

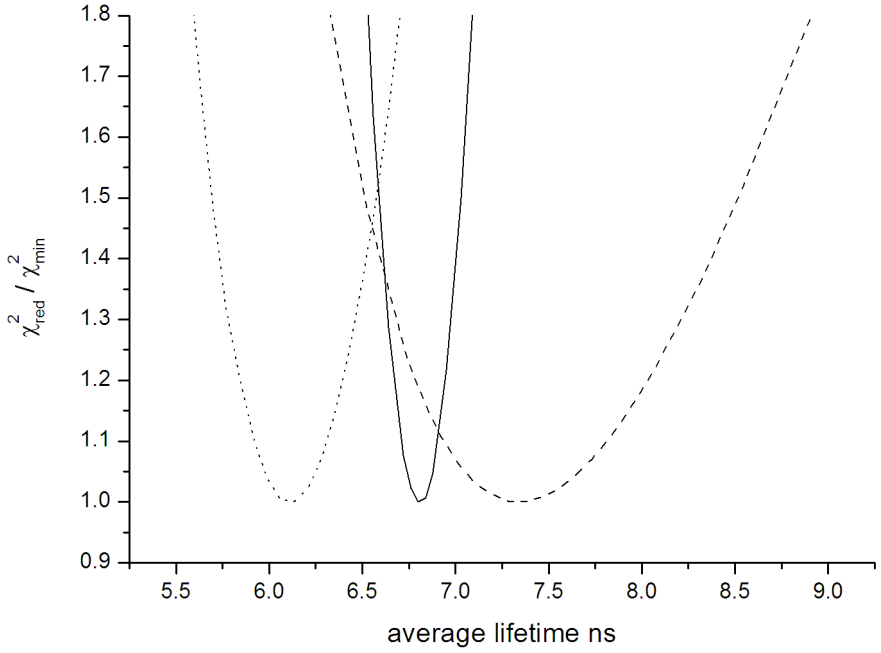

Figure 2.17: *Surface plot for the fluorescence lifetime fitting of oil* 7703 *(542-582 nm emission data) used to calculate the confidence interval in the average lifetime for the three fitting models: Multiple Discrete (dashed line), Single Lorentzian (dotted line), and Single Gaussian (line). The broader curve of the discrete model case indicates a much less precise determination of lifetime than for the narrower intervals determined for the single decay time distribution models.*

The response of the χ^2_ν surface to change in the average lifetime is generally much broader for the multiple decay term discrete model than for the single decay term Gaussian or Lorentzian distribution models.

The procedure outlined above was carried out in triplicate for each oil and the mean values of average lifetime and confidence intervals are reported.

2.3 Temperature based Lifetime Experiment - Neat Crude Oils

2.3.1 Instrumentation

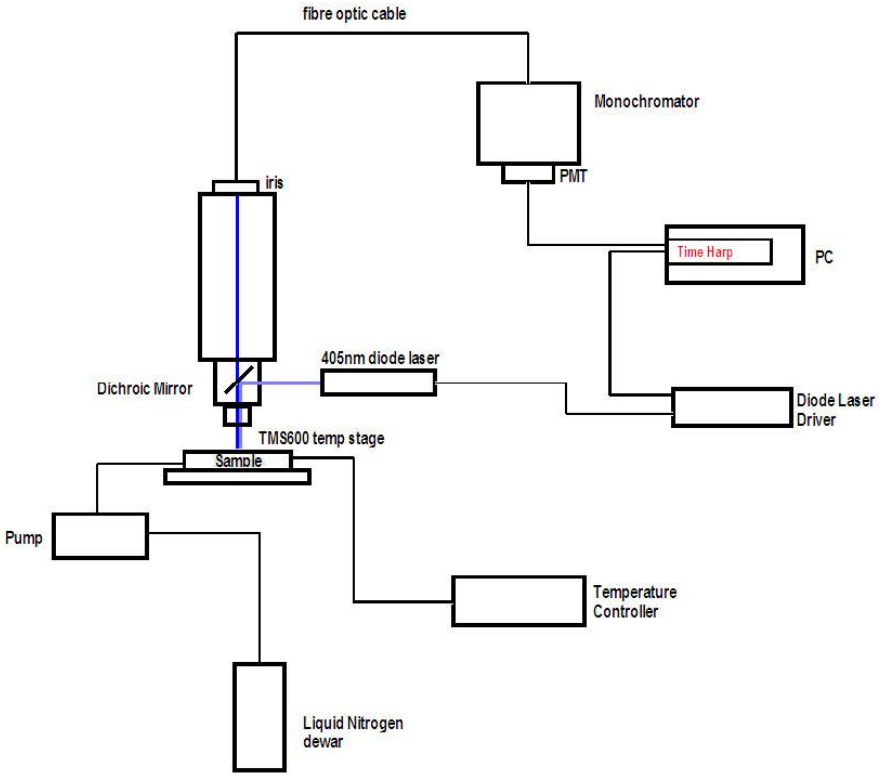

Figure 2.18: *Apparatus used for the determination of the average lifetime of neat crude oils as a function of temperature*

For the low temperature lifetime measurement of neat crude oils, a TCSPC based system coupled to a cooling stage, was assembled in house (Figure 2.18).

A liquid nitrogen cooled Linkam Heating Freezing stage (TMS600) was used to cool the samples. A pump passed the liquid nitrogen from a Dewar flask to the stage which was monitored by the controller unit. This unit was capable of maintaining

the temperature to a stability of approximately 0.1 °C. For calibration of the temperature stage, which was performed on a bi-monthly basis, the phase transition points (homogenisation temperature) for two synthetic fluid inclusion standards (H_2O and CO_2) were used [185]. The water inclusion standard gave calibration for the −110 to 20 °C range, having a homogenisation temperature of −56.6 °C. The CO_2 inclusion gave calibration for the −50 to 400°C range, with a homogenisation temperature of 390 °C. The homogenisation temperatures of the fluid inclusions were determined by observation of the homogenisation event through the microscope eyepiece.

The microscope (Olympus BX51) had the internal illuminator lenses removed so that the excitation light passed directly to the dichroic mirror. This minimised the loss of excitation light by reflection. The excitation light was focussed through a standard 10× objective (Olympus MPLAN 0.25 NA) onto the sample within the cooling stage. The resultant fluorescence emission was passed back through the dichroic mirror which incorporated a 405 nm stop-line filter and a 410 nm long-pass filter to minimise scattered excitation light from entering the detection system. The emission passed through an outlet in the head of the microscope which was fitted with an iris which was also capable of adding ND filters for IRF measurements. The system was connected to the monochromator (model 9030, Sciencetech) by fibre optic cable (Ocean Optics QP1000-2-UV/VIS). Control of the signal intensity to the PMT detector (model H5783, Hamamatsu) was achieved using the iris on the microscope head and the input/output slits on the monochromator. The start/stop cycles for excitation/emission were controlled by the TCSPC (Time Harp 100, Picoquant) electronics card on a pc using the associated software (Fluotime version 1.2, Picoquant). The output trigger signal from the laser driver was connected directly to the TCSPC board without incorporation of a delay line.

2.3.2 Method

For validation of the system, a solution (10^{-5}M in 0.2M phosphate buffer) of HPTS was used as a standard. All measurements were made at room temperature using un-degassed samples. The lifetime of the standard was also determined by a second TCSPC system (Picoquant Fluotime 200, Fluofit version 4.1) and this solution was used to determine the accuracy of the temperature based lifetime system. The

IRF of the system was obtained by removing the 405 nm stop-line and 410 nm long-pass filters from the optical path, setting the monochromator to 405 nm and recording the excitation light scattered by the stage widow. Before measurement of the IRF, the mirrors aligning the output from the laser and the input into the microscope (not shown in Figure 2.18) were adjusted to give a maximum count rate. For all lifetime measurements, $10,000$ counts in the peak channel were collected. The fluorescence decays of the Batch 1 oils (not including the topped oils) were measured at discrete emission wavelengths at 10 nm intervals between 430 and 540 nm covering the maximum fluorescence emission from the oil. The oils were subjected to temperatures ranging from -140 °C to 25 °C. For each temperature run, a drop of neat un-degassed oil was placed onto a quartz dish and sealed within the stage chamber. The oil sample was allowed to equilibrate for 20 minutes at each temperature with the excitation light switched off. The excitation light was then applied to the sample for one minute, before data acquisition. Deconvolution of the fluorescence decays from the IRF and lifetime analysis was performed using the Fluofit software. Repeatability of the average lifetime was tested at 273 and 213 K for oils 7090 and 7032 respectively and shown in Tables 2.8 and 2.9. Over 12 runs, the standard deviation on the lifetime values is low (0.03 and 0.06 ns) showing high precision. Support Plane Analysis yields the confidence interval which is taken as the error in the reported lifetime values. Longer average lifetimes typically have greater associated error intervals.

Table 2.8: *Reproducibility test for oil 7090 at 273 K. Emission recorded at 480 nm. Mean lifetime is 4.48 ns, standard deviation: 0.03 ns, mean error: 0.57 ns.*

Run	Average Lifetime	Error
1	4.52	±0.60
2	4.48	±0.60
3	4.47	±0.65
4	4.47	±0.59
5	4.46	±0.52
6	4.49	±0.57
7	4.45	±0.61
8	4.46	±0.52
9	4.55	±0.56
10	4.49	±0.54
11	4.46	±0.48
12	4.47	±0.52

Table 2.9: *Reproducibility test for oil 7032 at 213 K. Emission recorded at 480 nm. Mean lifetime is 1.30 ns, standard deviation: 0.06 ns, mean error: 0.11 ns.*

Run	Average Lifetime	Error
1	1.22	±0.10
2	1.35	±0.11
3	1.22	±0.11
4	1.28	±0.11
5	1.34	±0.13
6	1.37	±0.13
7	1.37	±0.13
8	1.21	±0.11
9	1.30	±0.12
10	1.26	±0.10
11	1.29	±0.11
12	1.30	±0.12

2.4 Temperature based Lifetime Experiment - Lifetime decays of dilute crude oils

2.4.1 Instrumentation

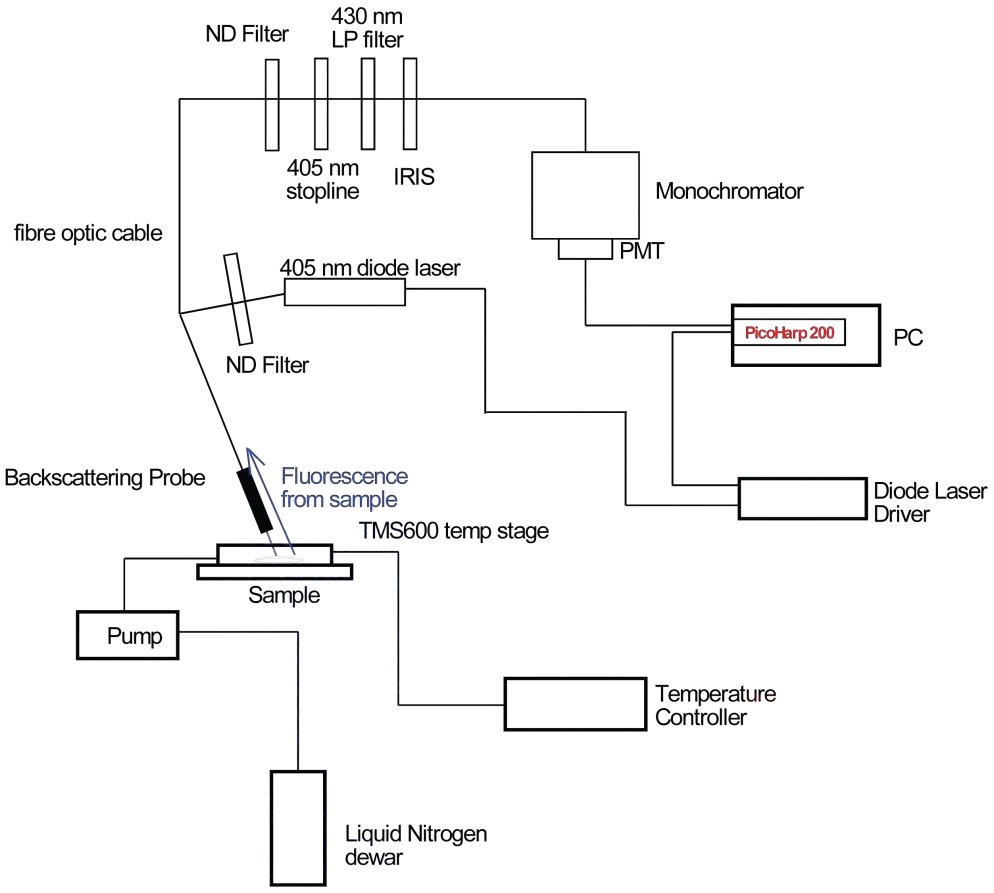

Figure 2.19: *Apparatus used for the determination of the average lifetime and spectra of dilute crude oils as a function of temperature.*

For the dilute oil samples the TCSPC system was modified to incorporate a fibre optic probe (Ocean Optics R400 – 7-UV/VIS) instead of the microscope based arrangement (Figure 2.19). The probe was used to excite the sample and collect the resultant fluorescence, giving enhanced flexibility of arrangement and positioning. The probe was capable of recording the fluorescence through the stage window and also from sample vials. The intensity of the excitation and emission light were modified appropriately using ND filters. A Picoquant Sepia laser driver controlled the excitation coupled with a PicoHarp 300 TCSPC module (version 2.2 Picoquant).

Fluorescence spectra were determined using the same probe connected to a USB2000 (Ocean Optics) spectrophotometer via fibre optic cable (Ocean Optics QP1000-2-UV/VIS).

2.4.2 Dilutions

A subset of the neat crude oil samples (Batch 1 oils) were selected for dilution/temperature analysis. For this, a 3 : 2 (volume:volume) solvent mixture of Methylcyclohexane (MeCH) and Methyl cyclopentane (MeCP) [186] was used. This solvent mix forms a clear glass at liquid nitrogen temperatures. The spectroscopic grade solvents were obtained from Sigma-Aldrich and used without further purification. The neat crude oil samples were mixed with the solvent on a mass-volume basis to obtain the following dilutions: 1:10, 1:50, 1:100, 1:500 and 1:5000.

2.4.3 Method

For dilute oils, oxygen quenching becomes a significant issue as can be seen in Figure 2.20, where 5 minutes bubbling with nitrogen (oxygen free) resulted in a dramatic 60% increase in lifetime. Further bubbling (up to one hour was measured) with nitrogen did not increase the lifetime further. To diminish the quenching effect of oxygen on diluted crude oils, it was necessary to remove oxygen from the diluted oil samples. On initial dilution, the crude oil samples were shaken to ensure thorough mixing and then deoxygenated by purging with oxygen-free nitrogen for 15 minutes. A low flow rate was maintained to minimise solvent and/or sample evaporation and the fluorescence lifetime was measured every 5 minutes. On completion of the degassing step, the sample vials were moved to an 'Atmos' atmospheric bag (Aldrich) filled with nitrogen. While maintaining a positive flow of nitrogen the sample was transferred by syringe to a quartz dish, covered with a quartz lid and sealed with PTFE and laboratory film. This was then transferred to the temperature stage (which was maintained at 288K with a positive flow of nitrogen) and the fluorescence lifetime was recorded and compared to the value recorded during deoxygenation. If the lifetime recorded after transfer was the same as during deoxygenation, the transfer was successful and fluorescence decays were recorded for

a series of wavelengths at 20 nm intervals covering the main emission band of the oil and temperatures were recorded at 20 °C intervals from room temperature($\sim$ 20 °C) down to −180 °C. Lifetime analysis was performed as for the neat crude oils.

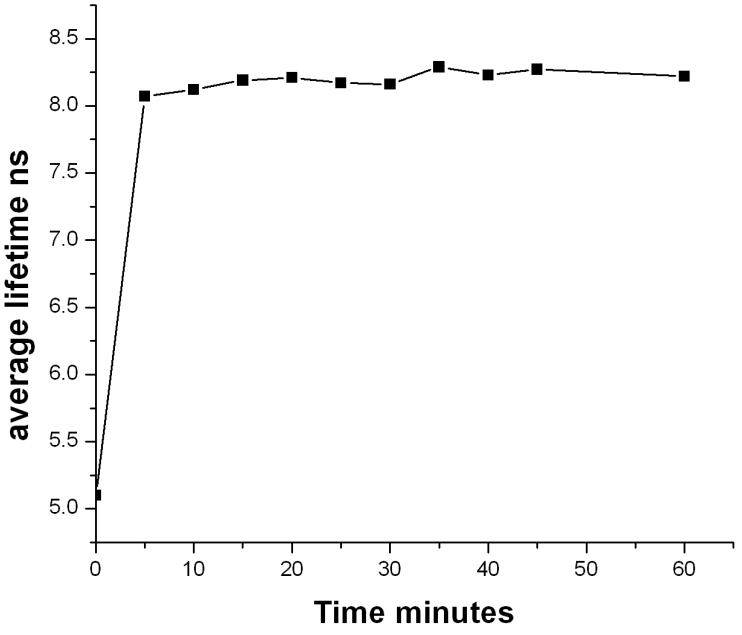

Figure 2.20: *Deoxygenation (by purging with N_2) of Oil 7058 diluted 1:50 in MeCH/MeCP over one hour.*

2.4.4 Validation Tests

Figure 2.21 shows that for three separate samples at the same dilution of light oil 7197, the deoxygenation procedure yields similar lifetime values within the recording and fitting error range (±0.2 ns). In this case, the lifetime unquenched by O_2 is obtained after only 5 minutes of nitrogen purging. The figure shows that though the procedure to obtain deoxygenated samples can be difficult, good repeatability in the measured average lifetime can be obtained.

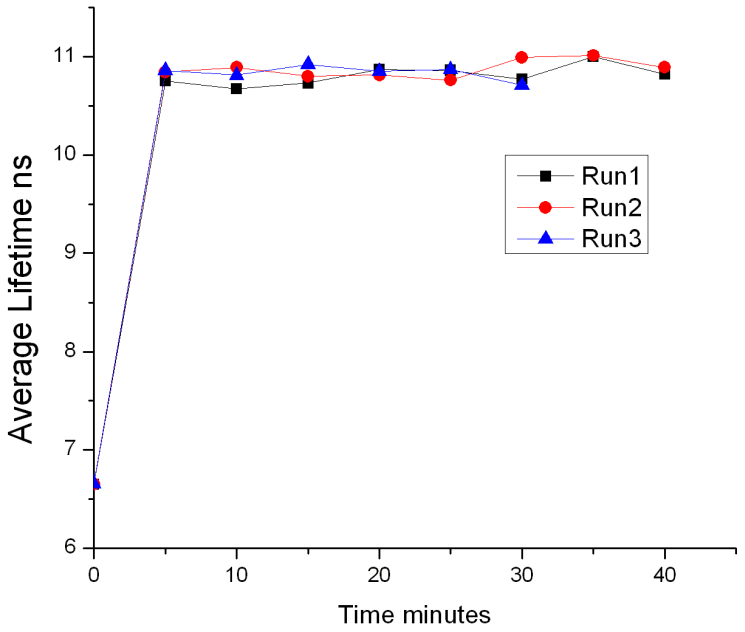

Figure 2.21: *Deoxygenation of Oil 7197 diluted 1:50 in MeCH/MeCP, procedure run 3 times.*

One of the critical steps in the method was the transfer from the atmospheric bag to the cooling stage. Much consideration has been made to eliminate the ingress of oxygen back into the diluted samples, i.e. sealing the quartz crucible in PTFE and Parafilm before removal from the atmospheric bag and maintaining the cooling stage with a positive nitrogen flow. However it was necessary to see the effect of oxygen ingress into two test solutions; a heavy and light oil. For these test dilutions, the degassing step was performed as usual and subsequent to 15 minutes bubbling with nitrogen, the vial cap was removed and the lifetime was monitored. After this, the sample was shaken while exposed to air to estimate oxygen ingress back into the sample. Figure 2.22 shows that it takes approximately 3 to 4 minutes of exposure to air before a significant effect on the lifetime is observed. For the heavy oil, this lifetime change is less pronounced as there are many other quenching mechanisms occurring and the contribution of O_2 quenching is small. Because re-oxygenation is slower for heavy oils, the procedure of transfer from vial to temperature stage is less prone to oxygen ingress problems.

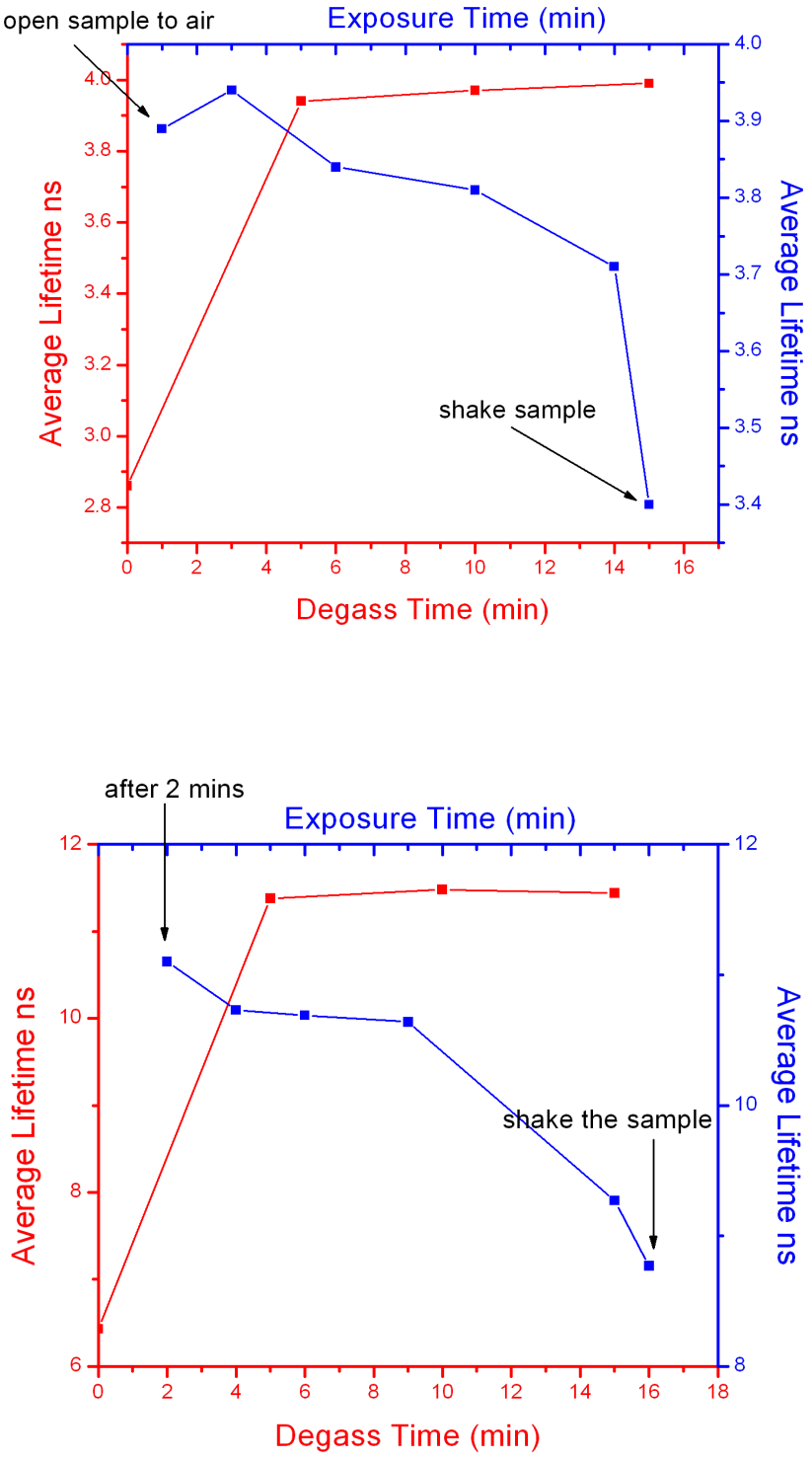

Figure 2.22: *Monitoring the effect of re-aeration on two representative oil samples : heavy oil* 7033 *(top) and light oil* 7197 *(bottom). The heavy oil is less affected by oxygen ingress with a noticeable change in lifetime occurring after* 3 *minutes. Shaking at* 15 *minutes still affects the lifetime, For the light oil, oxygen ingress affects the lifetime immediately and progressively quenches the lifetime. Shaking the sample at* 16 *minutes did not affect the lifetime considerably.*

2.5 Determination of lifetimes of oil within HCFI

The method described for the analysis of crude oils can also be applied to the measurement of HCFI. A number of HCFI were evaluated in terms of lifetimes and confocal lifetime images were obtained, using the upright confocal microscope and FD instrumentation (with the same optical configuration as for the bulk oils). Before any confocal measurements were made it was vital to check the optical alignment of the system. To test the alignment of the system, lifetime imaging was performed on 20 μm fluorescent beads. All imaging was performed using the 405 nm laser diode for excitation. First the CMOS camera was used to check the laser spot was centered on the sample. Beam expansion (software controlled) was adjusted as appropriate. The system was calibrated with the standard HPTS, no filter cubes were used for the emission and a confocal pinhole size of 141 μm was chosen.

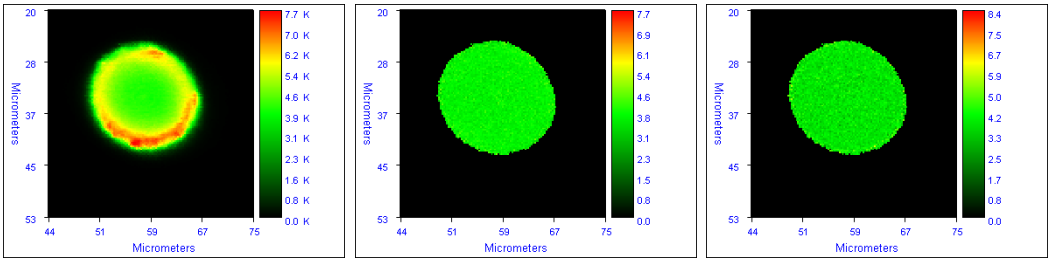

(a) Intensity (b) Phase (c) Modulation

Figure 2.23: *FLIM images of Fluorescent beads*

The images in Figure 2.23 represent the intensity, phase and modulation lifetime images for a single bead. Careful manipulation of the optical components and alignment of the emission and pinhole was performed. This gave a image of the bead as a spherical object of diameter in the region of 20 μm which was in accordance with the manufacturers specifications.

When the alignment was satisfactory, the general procedure for HCFI measurement was performed as outlined below:

1. The optical components were in the same arrangement as for bulk oil lifetime determination. The intensity of the laser source was controlled using either the polarizer or an ND filter placed in the optical path.

2. Using the on-board CMOS camera, the system was aligned so that the centre of the image displayed in a lifetime image mapped directly to the laser spot. This was achieved by monitoring the spot using the on-board CMOS camera.

3. Either the full emission spectrum where no filter cubes were in the emission light path or selected emission ranges (using cubes 1 to 4) could be selected. Also the confocal pinhole size was selected. From this point the emission range conditions and the chosen pinhole size were not altered until a new run was performed.

4. A standard fluorophore (in a 1 mm pathlength quartz cuvette) was placed normal to the objective and the laser switched on. Optimisation of the pinhole and lens alignment was performed using the software to produce the maximum signal intensity at the PMT's.

5. The residence time (exposure per pixel) and the number of frequencies to sample at were set and a calibration was performed using a known fluorescence standard. The phase and modulation values are stored by the software for each modulation frequency sampled.

6. The HCFI samples were placed normal to the excitation light and the inclusions within the wafers were isolated first under bright field illumination and then the fluorescence intensity from the inclusion of interest was optimised (i.e. so that the frequency of maximum signal intensity was kept below a system threshold, by varying the laser power and the PMT gain.

7. Using the same residence time and conditions outlined above either a single point in the sample was measured at a range of modulation frequencies or a scan was made over the sample to obtain a FLIM image. In the case of the FLIM lifetime maps, the step size (controlling the XY step conditions of the scanning stage) and the image resolution could also be set.

Chapter 3

Lifetime study on crude oils by the FD method

This chapter describes the lifetime results obtained from FD analysis, the principle findings of which have been published [112]. Expanding on the published data, lifetime trends are evaluated and comparisons to TCSPC and correlations to bulk SARA data are made.

3.1 Raw data - phase modulation plots

The phase-modulation plots for Batch 1 crude oils at different emission wavelengths are shown in Figures 3.1 to 3.3. The oils are separated into classifications of light, medium and heavy defined by their API gravity values (Light API > 40, Medium API $20-40$, Heavy API < 20). The position of where the phase and modulation plots cross (termed the cross-over point) gives an indication of the optimal frequency to be used. The cross-over point is the frequency at which the phase and demodulation are $\sim 50\%$, and where the maximum change in phase and demodulation occurs. For a single exponential decay, flurophores of short lifetime would have a cross-over point at high modulation frequencies and conversely for long lifetime decays, the cross-over point would occur at low modulation frequencies. For the crude oils, as the emission range is increased, the cross-over point of phase and modulation data shifts to lower modulation frequencies indicating an increase in lifetime. The range of frequencies between phase and modulation cross-over points is also shown (vertical

lines) and it can be seen that the range decreases for the light and medium oils as the emission wavelength is increased. This shows that the lifetimes of the individual oils tend to converge at longer emission wavelengths. The light oils show the least convergence of lifetime, some (e.g. 7098) hardly changing in lifetime as shown by the minimal change in crossing point frequency (black symbols in Figure 3.1. Oil 7058 on the other hand, shows a large change in lifetime from the 426-477 nm band to the 465-500 nm band due to the higher ($> 20\%$) fraction of heavy aromatic components.

For some of the oils (e.g. oil 7090 of the medium oils), measurement was performed from 10 to 110 MHz following the instrumental considerations as described in Chapter 2. For all other oils a larger frequency range up to 200 MHz was used. Though the extra frequency measurements were not ultimately used for fitting purposes, the data is included here to illustrate the full phase modulation response of the oil. Light and medium crude oils generally give reliable data for this modulation frequency range, but for the heavy crude oils the situation is different. Heavy oils have short fluorescence lifetimes (tending to 1 ns or less) due to quenching effects, and have cross-over points at frequencies greater than 200 MHz. They were found to exhibit noisy phase modulation responses because of weak fluorescence emission, leading to low signal to noise ratios. As shown in Figure 3.3, the noise in the phase and modulation data is significant over 175 MHz. The FLIM system is only capable of generating accurate modulation frequencies up to $\sim$ 150 MHz and thus the phase and modulation data for heavy oils therefore do not span a wide enough range; leading to relatively poor data fitting. For some heavy oils in the sample set with lifetimes of less than 0.5 ns, the generation of phase and modulation data in the cross-over point range was beyond the 300 MHz range of the instrument. It would be possible to obtain better quality data with a system capable of higher modulation frequencies (up to 1 GHz).

Figure 3.4 shows the phase modulation plots for the Batch 2 oils, following similar behaviour to the Batch 1 oils. The cross-over point range also reduces as the emission wavelength increases. As there was a mix of light, medium and heavy oils in this set, the range excludes the heaviest oil for ease of interpretation. The topped oils are shown as a separate set in Figure 3.5. The physical properties of these oils are very similar and thus the phase modulation plots give a shorter spread of modulation

frequencies at the cross over point . Similar to the other oil sets, the longer emission wavelengths give the shortest range in crossing frequencies as shown on the plots.

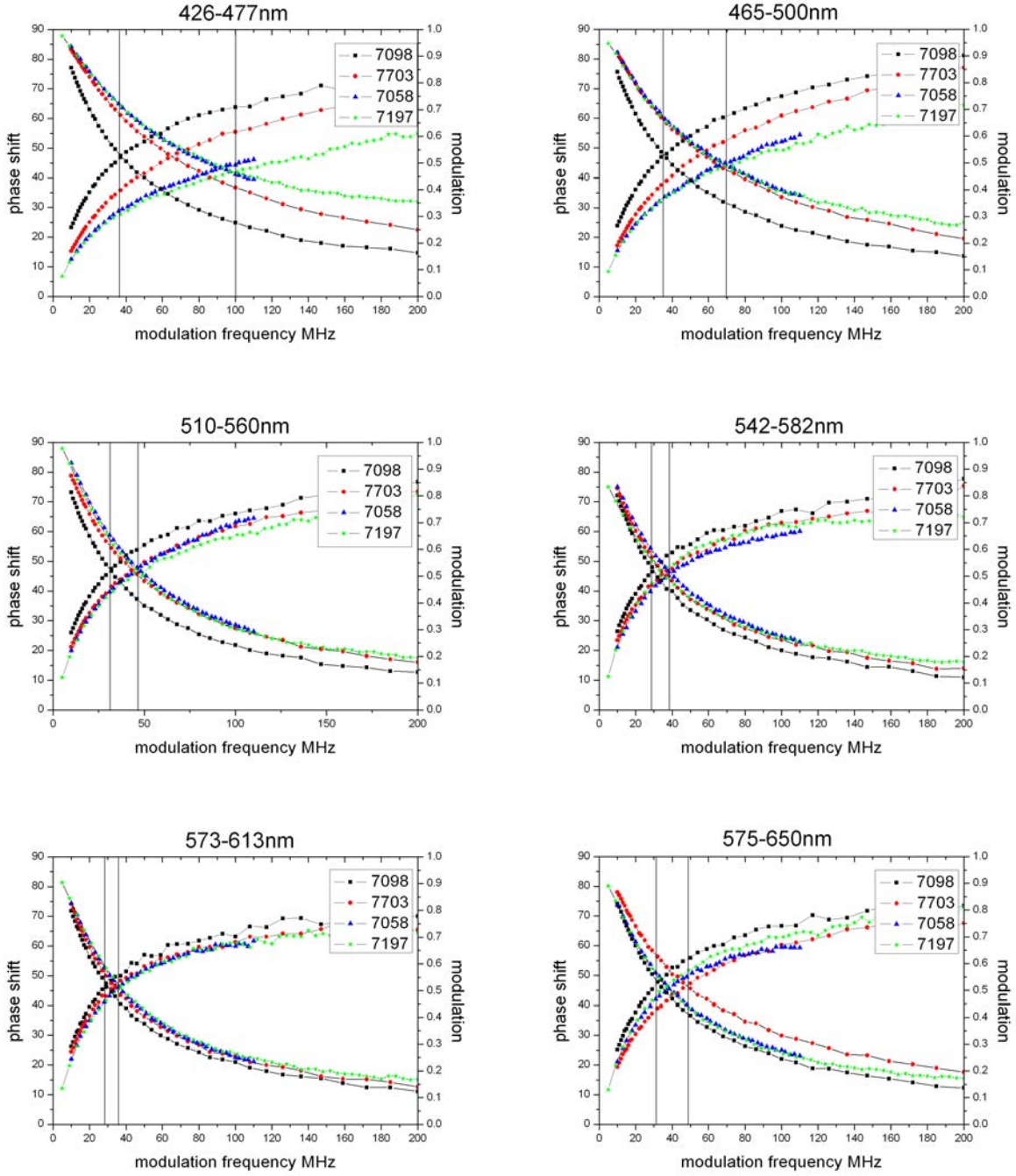

Figure 3.1: *Phase and modulation responses for light or high API gravity (> 40) crude oils from Batch 1 over the 426–650 nm emission range. As the emission wavelength is increased the position where the phase and modulation plots diverge (or the cross-over point) shifts to lower modulation frequencies. The vertical boundary lines indicate the wavelength range where the cross-over points occur. This range also decreases with longer wavelengths.*

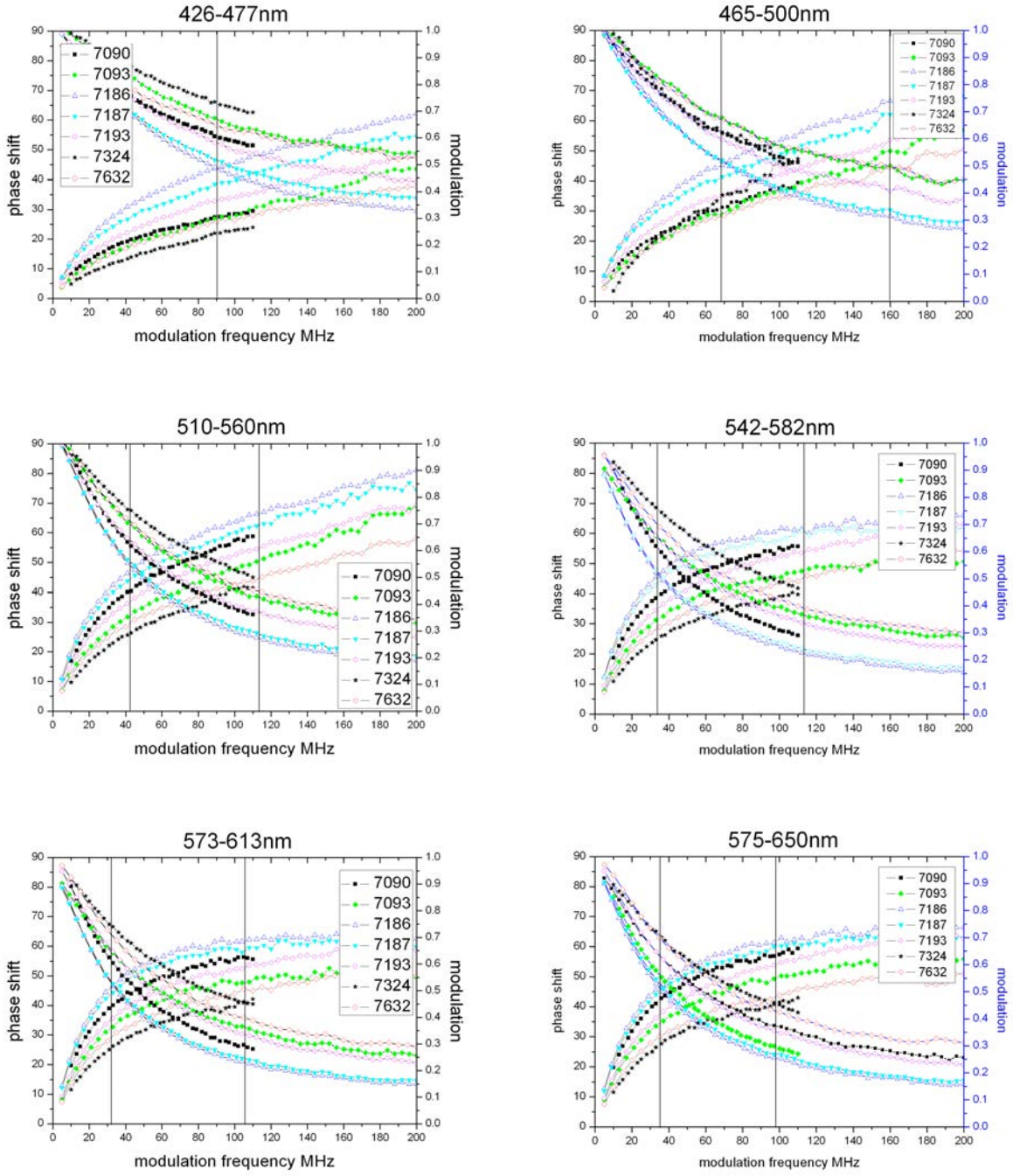

Figure 3.2: *Phase and modulation responses for medium or mid-range* API *gravity (*20-40*) Batch* 1 *crude oils over the* 426–650 *nm emission range. The vertical boundary lines indicate the wavelength range where the cross-over points occur.*

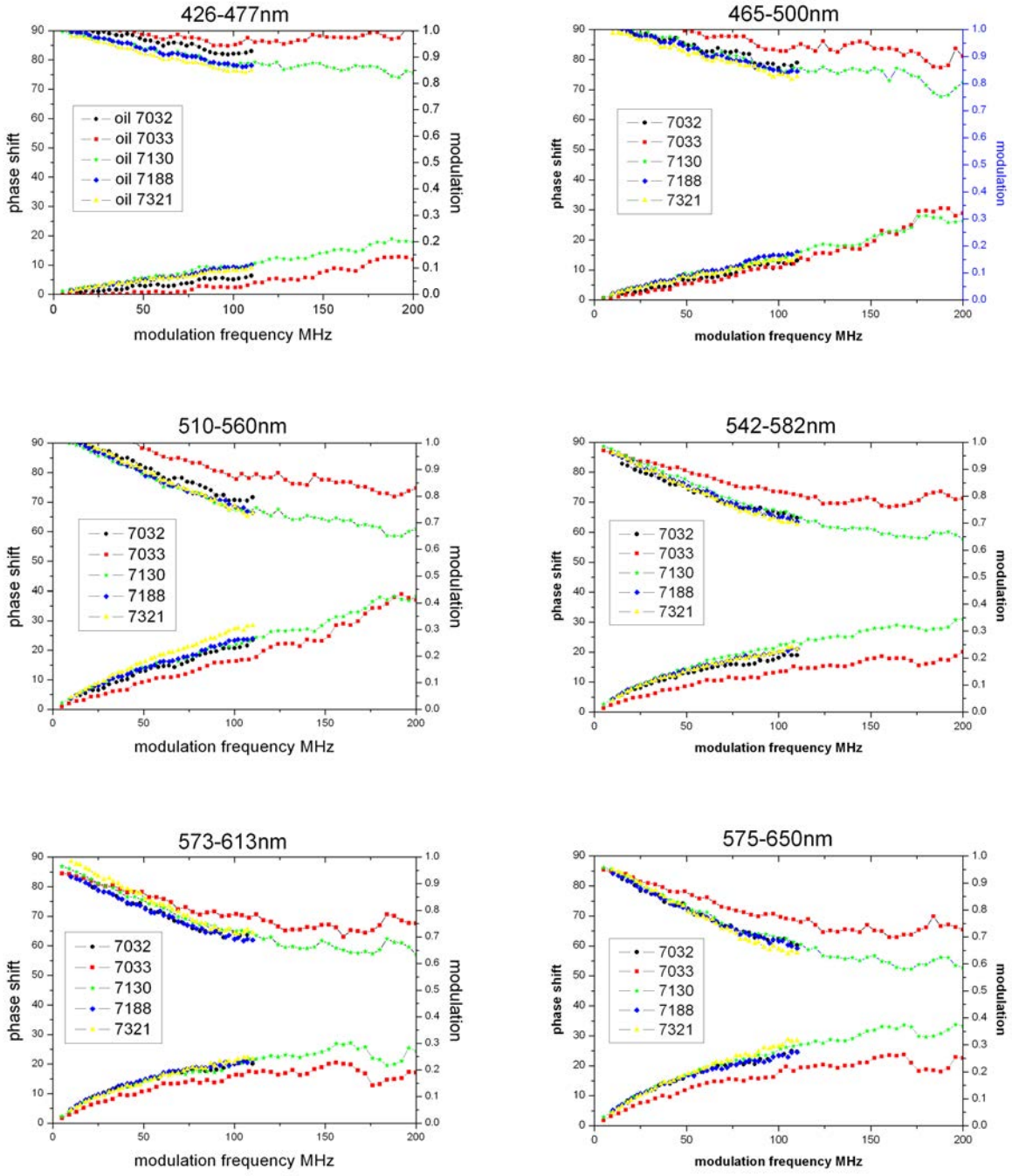

Figure 3.3: *Phase and modulation responses for heavy or low* API *gravity (*< 20*) Batch* 1 *crude oils over the* 426–650 *nm emission range.*

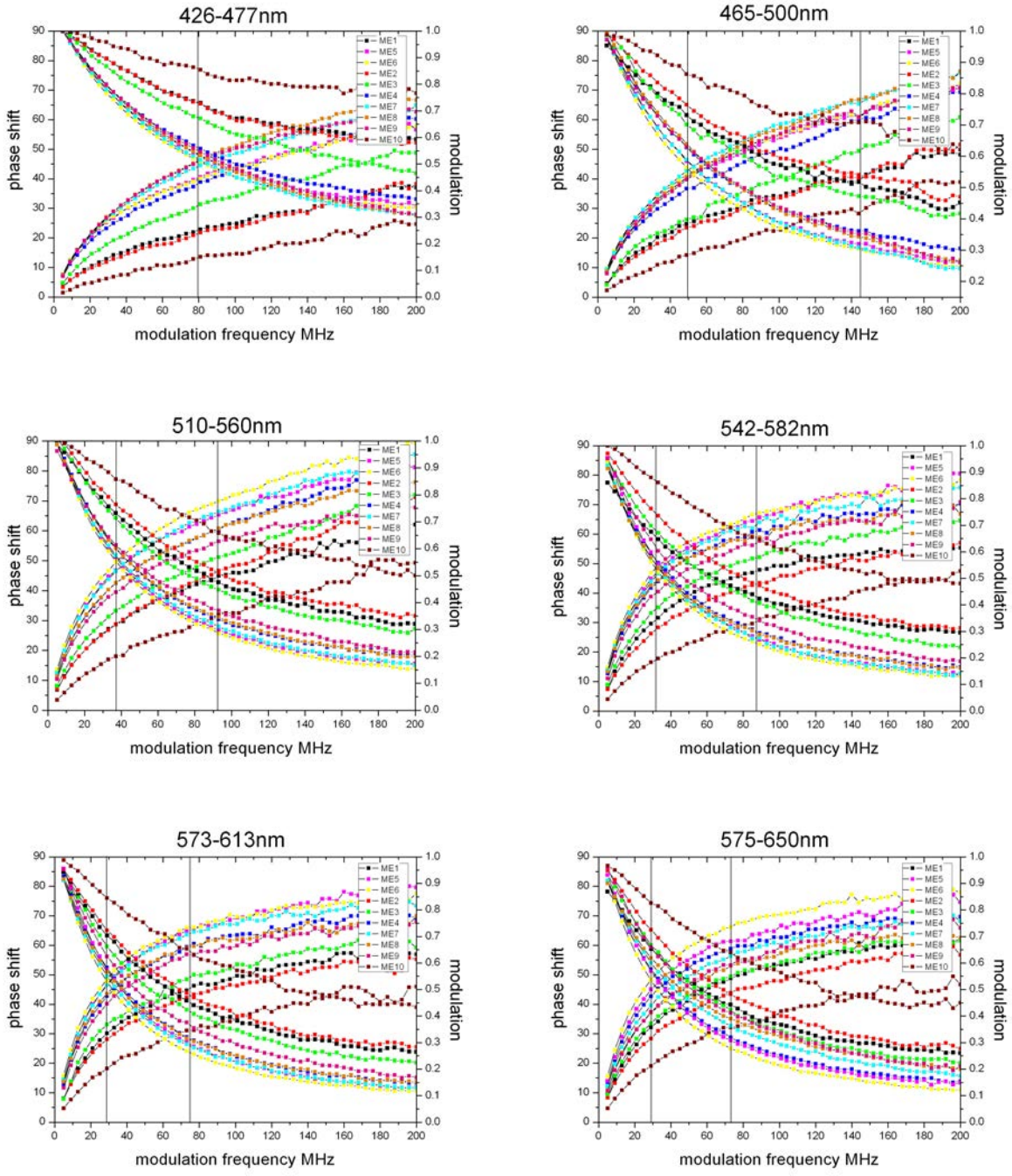

Figure 3.4: *Phase and modulation responses for Batch 2 crude oils over the 426–650 nm emission range. The crude oils shown have API gravity values from 24.7 to 47.8.*

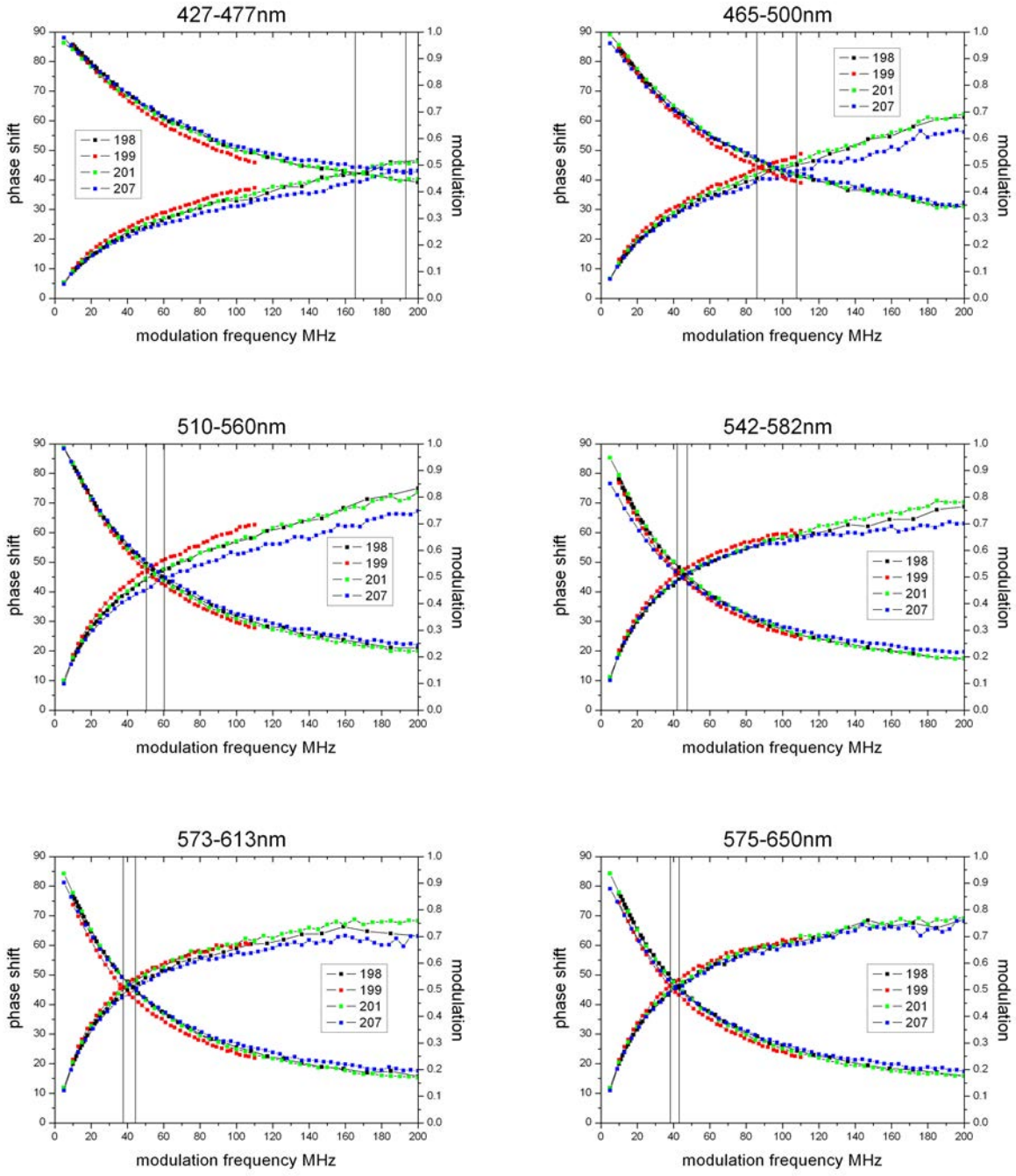

Figure 3.5: *Phase and modulation responses for the four topped crude oils over the* 426–650 *nm emission range. The crude oils shown have API gravity values from 29.8 to 38.0.*

3.2 Calculation of lifetimes from phase modulation data

In previous work from the Nanoscale Biophotonics Laboratory [116, 126, 129–132] a multiple discrete exponential model was used to calculate average lifetimes of crude oils from TCSPC data. Decays were fit with two or three lifetime terms and while this model is not an accurate representation of the emitting species (crude oils have a multitude of emitting components), it had utility in the determination of an average lifetime. This was used to describe general trends in the photophysics of crude oils. Part of the reason for undertaking this study was to evaluate the different distribution methods available for calculating FD based lifetime calculations that may be more applicable to heterogeneous samples such as crude oils.

There are a number of criteria that must be taken into account when deciding on the correct lifetime that is determined from a fitting procedure. Determination of the correct number of decay terms has a direct influence on the average lifetime value; the goal being to determine an average lifetime with the minimum number of decay terms (to avoid overfitting of the data). For the average lifetimes generated in this chapter the following criteria for choice of decay terms was:

- Minimisation of χ^2 values
- a minimum of 40 modulation frequencies are used for fitting
- The stability of the fit - no artificially short lifetime components
- Consistency with replicate experiments

The first criterion is illustrated by showing an example of the output from the fitting (using the Vista software package) of phase modulation plots (Figures 3.6 to 3.8). The black curve indicates the model data and the residuals are given in the lower part of each figure. Typically for crude oil data, the phase values show greater deviation from the model at higher modulation frequencies, which is illustrated by the greater spread of residuals. In this example, two exponential decay terms give a reasonable fit but the residuals are clearly more randomly spread around the zero line for the three decay term case. The spread of residuals are described

mathematically by the χ^2 values as determined by the Vista software package. In practice, introduction of an extra decay term into a fit must reduce the χ^2 by a minimum of 20%. In this case of Figure 3.8, the χ^2 value indicates the correct number of decay terms. Note also the increase in lifetime value from fitting one to three decay terms (an increase in 100%).

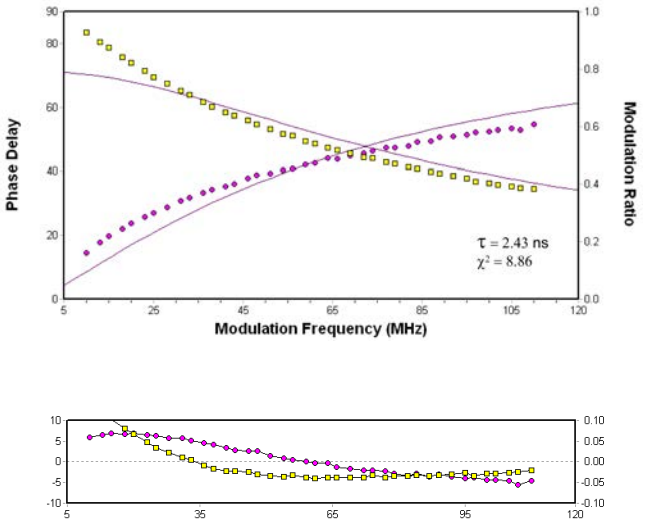

Figure 3.6: *Fit plots for phase (circles) and modulation (squares) data using a* ***single*** *discrete lifetime model. The residuals determined for this model are given below. Data from the measurement of oil 7186,* $\lambda_{ex} = 405nm$, $\lambda_{em} = 465 - 500nm$.

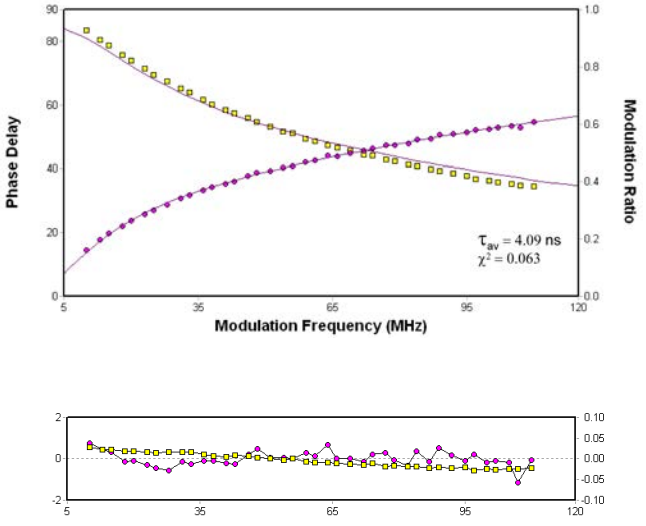

Figure 3.7: *Fit plots for phase (circles) and modulation (squares) data using a* ***two decay term*** *discrete lifetime model. The residuals determined for this model are given below. Data from the measurement of oil 7186,* $\lambda_{ex} = 405nm$, $\lambda_{em} = 465 - 500nm$.

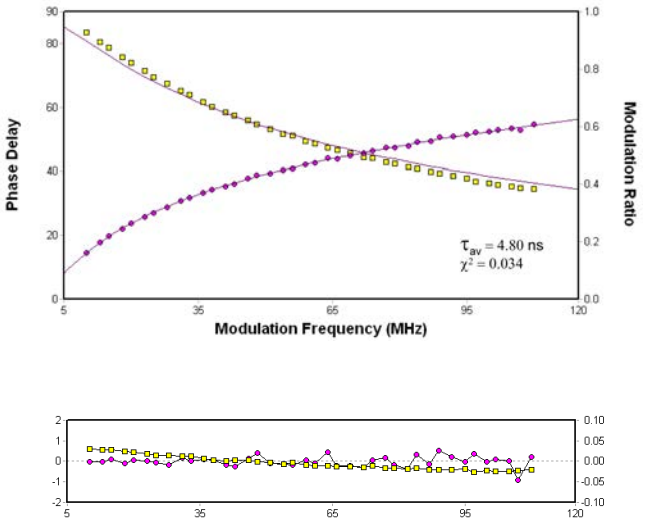

Figure 3.8: *Fit plots for phase (circles) and modulation (squares) data using a* ***three decay term*** *discrete lifetime model. The residuals determined for this model are given below. Data from the measurement of oil 7186,* $\lambda_{ex} = 405nm$*,* $\lambda_{em} = 465 - 500nm$*.*

There are often cases where there is an ambiguity over whether two are three decays terms should be used to determine the correct average lifetime. To illustrate this, the influence of varying the number of frequencies used in the fitting process is shown in Table 3.1.

Table 3.1: *Variation of average lifetime,* χ^2 *and Confidence Interval (CI) values with number of frequencies sampled for oil* 7186 465-500 *nm emission band. DNF: Did Not Fit. NC: Not calculated.* χ^2 *are not reduced values.*

Number frequencies	Decay terms	Average Lifetime	χ^2	CI
3	2	3.84	0.00043	0.06
5	2	3.72	0.087	0.15
10	2	3.97	0.065	0.11
20	2	4.00	0.063	0.08
30	2	4.04	0.074	0.08
40	2	4.08	0.071	0.07
3	3	DNF	NC	NC
5	3	DNF	NC	NC
10	3	DNF	NC	NC
20	3	7.06	0.041	0.97
30	3	5.33	0.044	0.25
40	3	4.82	0.036	0.14

It can be seen in Table 3.1 that it is possible to fit the data using only three modulation frequencies and two decay terms. The average lifetime value obtained is

a function of the number of sampled frequencies and the number of decay terms used. The goodness of fit is shown by the χ^2 values and it can be seen that an artificially low χ^2 value is achieved with 3 frequencies and two decay terms. Between 20 to 40 frequencies, the 2 decay term fit gives the lowest χ^2 and confidence interval values. The situation is different for the three decay term fits where for three, five and ten modulation frequencies, the χ^2 value could not be minimised. For 20 modulation frequencies, a high average lifetime is obtained but with a large confidence interval. Fitting using 40 modulation frequencies gives and lower average lifetime value and the narrowest confidence interval.

The question now is which fitting situation gives the most accurate representation of the crude oil average lifetime - 2 or 3 decay terms? At first glance at Table 3.1, it seems there three decay terms gives the best fit and if the decision was solely based on the χ^2 value then the three decay term model (4.80 ns) would be chosen. If the decision was based on using a simpler two decay term model (i.e. fewer parameters mean fewer sources of error), then a value of 4.04 ns would be chosen for the average lifetime. Unfortunately, for the analysis of crude oil phase and modulation data, it often happens that there may be a number of models that produce χ^2 values within an acceptable value and it is difficult to reject based on χ^2 alone. Local minima can sometimes be found by the minimization algorithm particularly when three decay terms are used involving six independent fitting parameters. Thus the χ^2 value must be used with caution and can not be used solely as an indication of the most accurate fit.

Table 3.2: *Average lifetimes for oil* 7186 *calculated from TCSPC decay curves recorded at a bandwidth of 470-490 nm along with the associated* χ^2_ν *and Confidence Interval (CI) values.*

Decay terms	Average Lifetime	χ^2_ν	CI
1	3.88	17.09	0.08
2	4.76	2.96	0.2
3	5.00	1.04	0.5

Comparison with TCSPC (Table 3.2) results show that a three decay terms gives the best χ^2_ν value and given that the error associated with fitting (by Support Plane

analysis) of this TCSPC data is ±0.5 ns, the true lifetime lies between 4.75 and 5.25 ns. Based on comparison to the TCSPC result, the 40 frequency, three decay term model would be chosen. Overall, using the results shown in Table 3.1, and the experience drawn from numerous fitting calculations performed on the other oils tested, phase and demodulation data were fitted using 40 sampled frequencies.

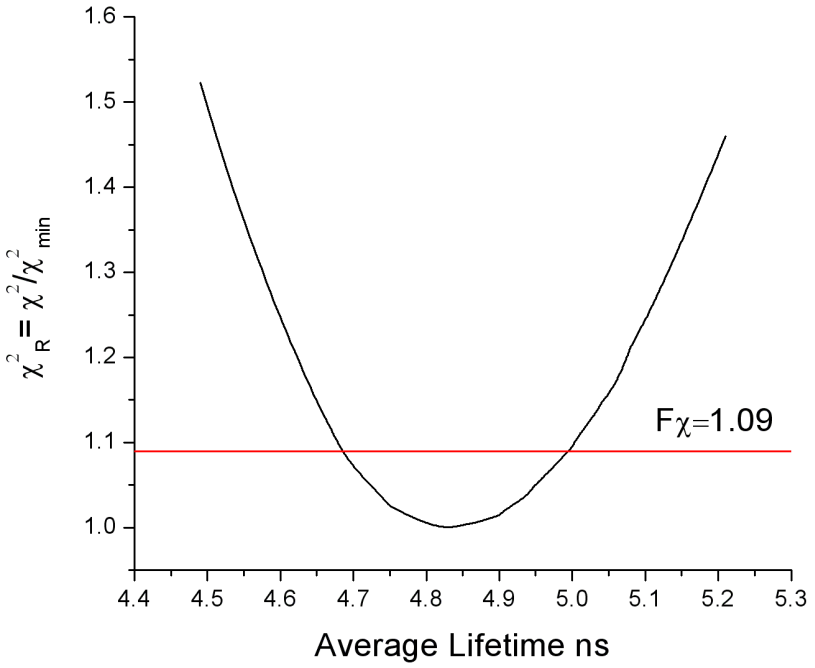

Figure 3.9: *Confidence Interval of FD average lifetime for oil* 7186 *recorded at* 465-500 *nm.*

Figure 3.9 shows an example of a surface plane analysis to generate the average lifetime confidence interval. The calculation of confidence interval goes as follows. The number of data points was 40, and three decay terms were used (thus number of parameters $p = 6$. The degrees of freedom $\nu = 2 \times no\ of\ points - p - 1 = 73$. $F_\chi = 1 + p/\nu(F_{stat}) = 1 + 6/73(1.19)$ where the F_{stat} value is extracted from Lakowicz [36]. This gives an F_χ value of 1.09. The confidence interval is obtained by extrapolation from the intersection points to the x-axis, giving an interval of ±0.15 ns. This procedure is followed for all confidence intervals (including distribution models) reported herein. This gives a value for the average lifetime of 4.82 ± 0.15 ns for three decay terms which is in close agreement with the TCSPC result.

The final criterion used was comparison of fitting results from three replicate measurements. The fitting model was selected if the fit model applied for at least two of the three runs. The preceding discussion has highlighted that when fitting phase and modulation data, it is necessary to perform a series of steps before deciding on the average lifetime value.

To reiterate, the steps involved are:

1. Compare χ^2 values between a 2 and 3 decay term model.
2. Ensure local minima are not found by the minimization algorithm, particularly for three decay term models
3. Ensure there are no artificially low lifetime components.
4. Compare chosen model across three separate experiments - does the model apply for each or at worst two out of three experiments?

The steps outlined above can be used to determine the correct average FD lifetime for a particular fitting model and its associated confidence interval. The drawback is that the process for generating confidence intervals is manual and laborious to perform.

As discussed previously, the discrete exponential decay model assumes that all fluorophores of the sample decay to two or three unique decay rates. This hypothesis may be very improbable for the heterogeneous mix of fluorophores that is encountered in crude oils and so the complex decay behaviour may then be defined by a distribution of lifetimes. Using the steps indicated above, phase and modulation data can be fitted to either single or multiple lifetime distributions. As one would expect the Lorentzian distribution gives a narrower distribution of lifetimes when compared to the Gaussian fit leading in most cases of a reduction in average lifetime values. In some cases the Gaussian and Lorentzian models incorporate a very narrow peak. This indicates a peak width that is too narrow to display, effectively a discrete component. For fitting to single distributions, a small fraction discrete component must be added to achieve adequate χ^2 values. A comparison between the discrete lifetime fitting and a lifetime distribution for three representative oils are shown in Figures 3.10 to Figure 3.12. In these plots the five different methods for

determination of a lifetime value are displayed, i.e., Discrete exponential (top left), Multiple Gaussian decay (middle left), Multiple Lorentzian decay (Bottom left), Single Lorentzian decay (top right) and Single Gaussian decay (bottom right). In Figure 3.10, heavy oil 7188 can be fit to two decay terms for the three models giving similar average lifetime values of ~ 0.7 ns. A single decay term Lorentzian fit gives an asymmetric distribution of lifetimes with respect to the center of the distribution (0.33 ns) and the fit is poor as indicated by the χ^2 value. In the Gaussian case, the distribution can not be resolved using a single distribution alone and it is necessary to add a long lifetime discrete component of small fractional contribution to obtain a lifetime value. In Figure 3.11, the average lifetime obtained is also similar for each of the multi-modal fits. The distributions are symmetric around a center lifetime value. A similar set of lifetime distributions is encountered for light oil 7098 in Figure 3.12.

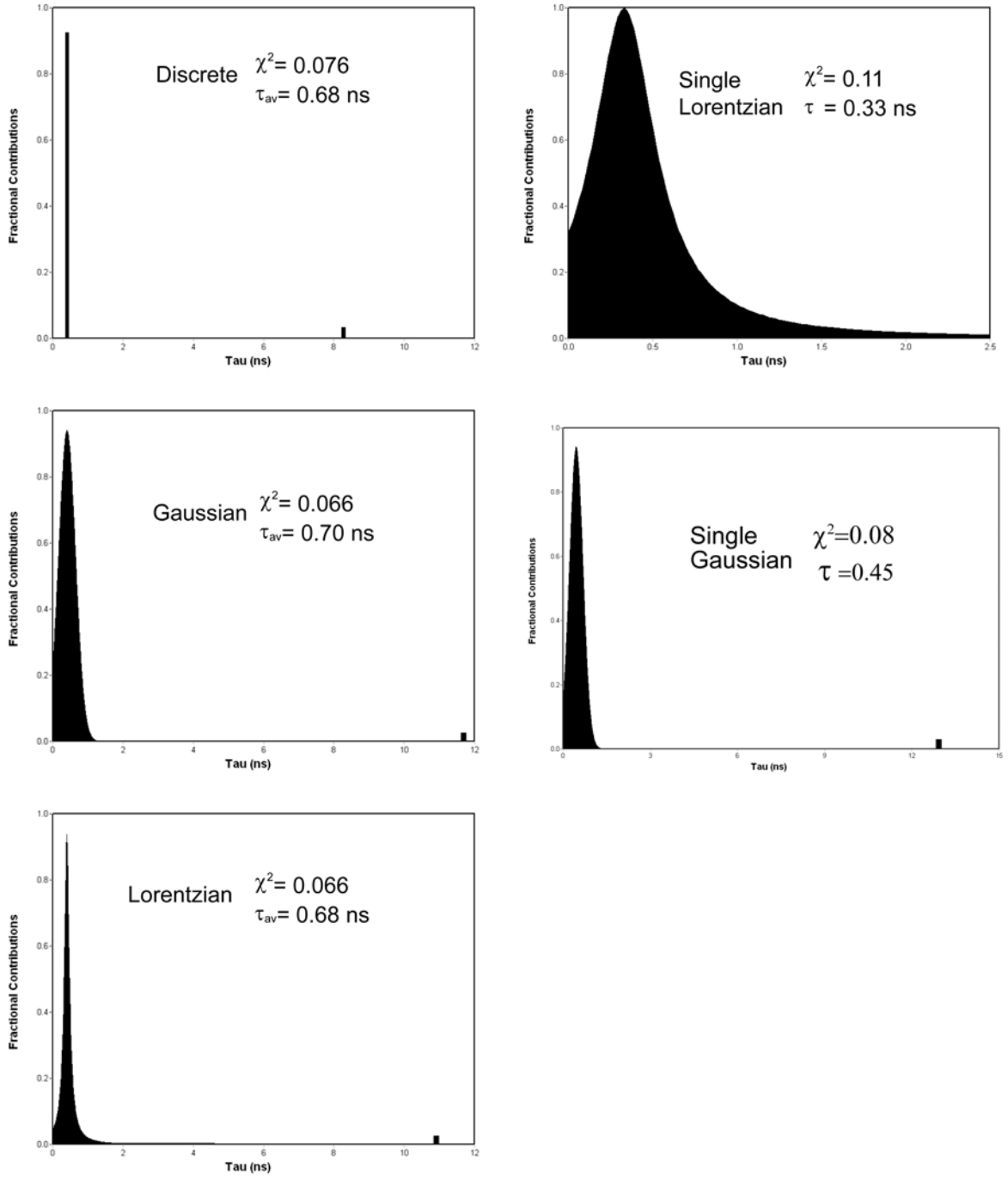

Figure 3.10: *Fitting results for low API gravity oil 7188, 465-500 nm emission band. Single bars in the distribution fitting indicate components that have widths that are too narrow to display, in effect these are similar to discrete components. The single Gaussian distribution needs an extra 'fake' lifetime to generate adequate fitting.*

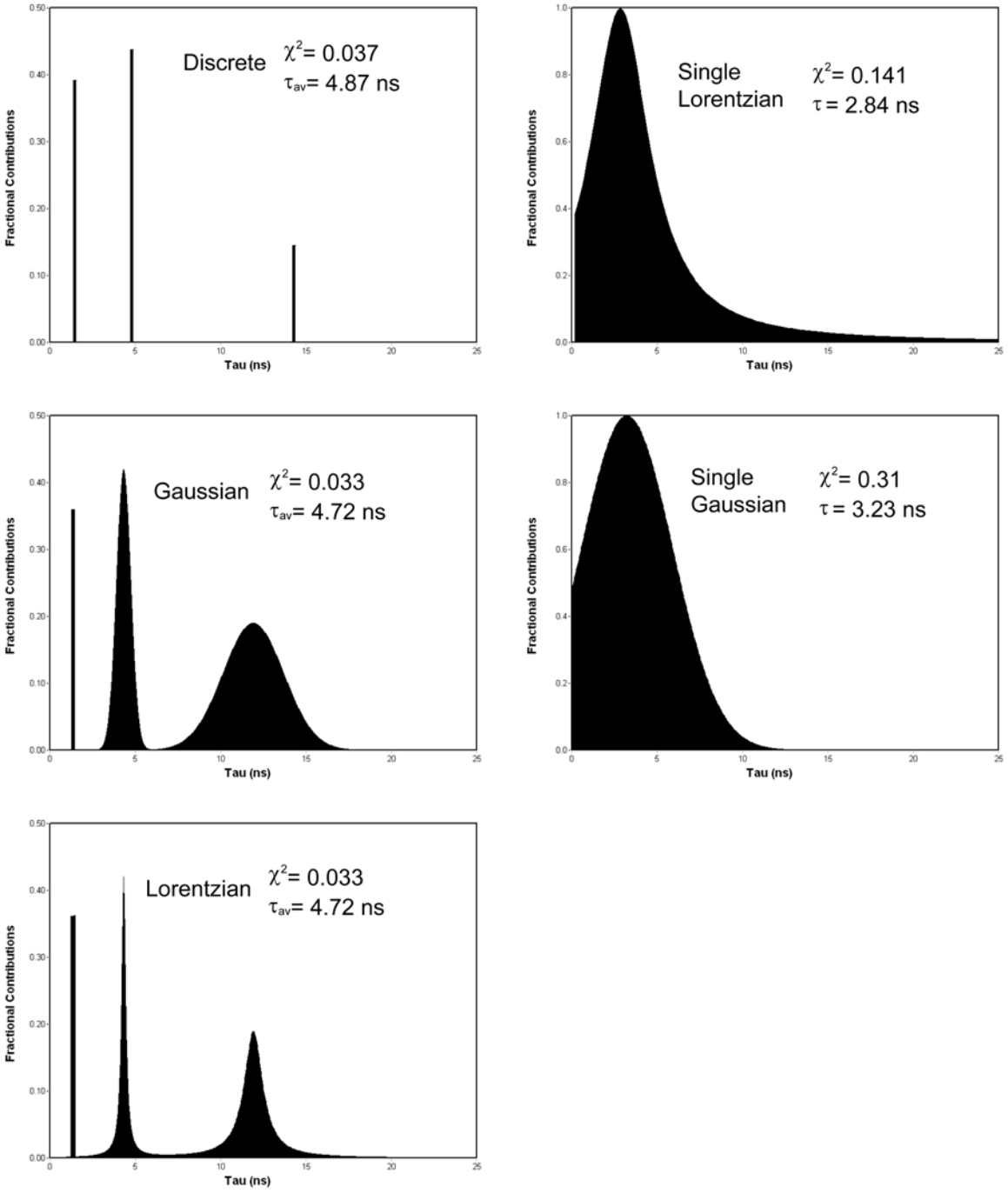

Figure 3.11: *Fitting results for medium API gravity oil 7186, 465-500 nm emission band. Single bars in the distribution fitting indicate components that have widths that are too narrow to display, in effect these are similar to discrete components.*

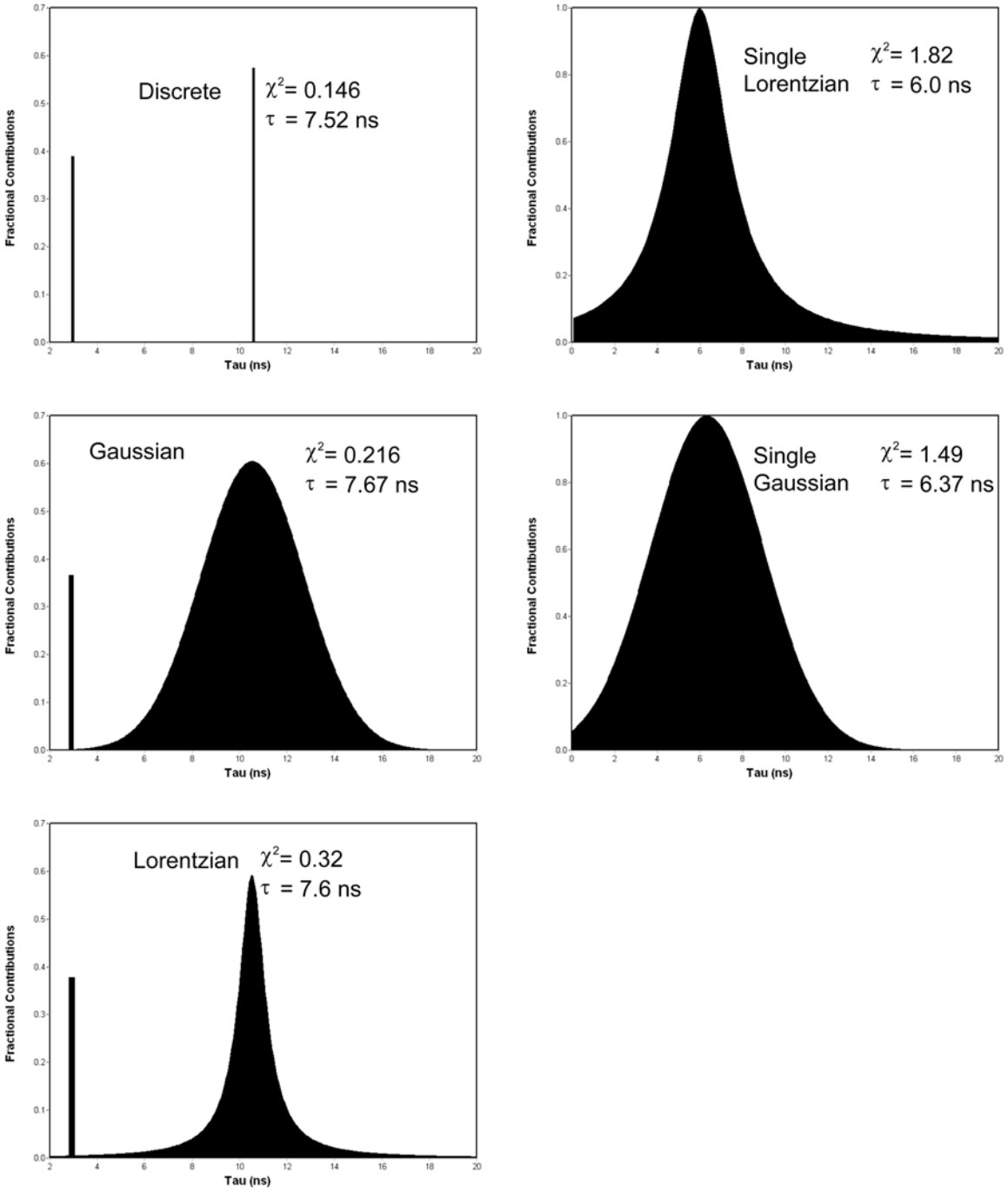

Figure 3.12: *Fitting results for high API gravity oil 7098, 465-500 nm emission band. Single bars in the distribution fitting indicate components that have widths that are too narrow to display, in effect these are similar to discrete components.*

3.3 Fitting of Phase Modulation data

Tables 3.3 to 3.6 gives listings of the average lifetimes and fitting parameters for Batch 1 and Batch 2 crude oils at an emission wavelength range of 465-500 and 542-584 nm*. A minimum of 40 modulation frequencies were used to fit the phase and modulation data and hence calculate lifetime values. The lifetime values and fitting data shown in the tables are the average values obtained from three replicate experiments. The data for the 465-500 nm emission band is included to make comparisons with the average lifetimes recorded by TCSPC under similar conditions (See Section 3.4). The confidence intervals for the TCSPC average lifetimes were calculated using support plane analysis as performed for the FD data. As lifetime comparisons are being made in this chapter, the topped oils have been removed from the Batch 1 set. Batch 2 make up the other set of oils. All crude oil phase and modulation data could be fit to the models selected: Multiple discrete, Multiple Lorentzian, Multiple Gaussian, Single Lorentzian and Single Gaussian. The single distribution lifetimes reported here are the lifetime at the center of the calculated distribution. Some gaps do occur in Table 3.3 when fitting is not possible. This occurs in some cases (7033 and 7032) for short lifetime oils where the non-linear least squares minimization algorithm does not converge. The range indicates the spread of lifetime values calculated using the various models. A small range indicates close agreement and one could say that the lifetime value is accurate. A larger range indicates a larger degree of uncertainty in the average lifetime value.

Also shown is the range between the multiple decay term models showing the relative difference in the average lifetime. Generally a short range between multiple decay term models is found, indicating consistency across the results and thus more confidence in the average lifetime result. Where a large range exists, there is inconsistency across the models leading to a reduced confidence in that result.

For all oils, the single decay term Gaussian and Lorentzian distributions yield lifetime values that are considerably shorter than the multiple decay term models. The associated error on this lifetime is very low compared to the confidence intervals calculated based on the multiple decay term models. However, the χ^2 values are quite

* Some of the results given in Tables 3.3 to 3.6 do not match those published [112]. Since the publication of this paper, the fitting protocol was improved leading to changes in some of the lifetime values.

high compared to the multiple decay term models. The confidence intervals reported are dependent on the average lifetime; i.e., there is a greater uncertainty associated with the average lifetime for lighter oils which reduces as the lifetime reduces. The greater uncertainty is introduced by the long lifetime component that is used in the fitting of a multiple decay model. This uncertainty is exacerbated if the long lifetime component has a greater fractional contribution. For the TD data in Tables 3.5 and 3.3, a lower confidence interval is found ($\sim$ 0.1 ns for the Batch 1 set of oils and $\sim$ 0.2 ns for the Batch 2 set of oils) which agrees with comparative studies between FD and TD lifetimes [187, 188]. There are also differences between the oil batches. For the Batch 1 oils, the multiple decay term models yield longer lifetimes, but with shorter confidence intervals and better fits. For the Batch 2 oils, single Lorentzian distributions give the best fits based on the χ^2 and confidence interval values. The origin of this distinction between data sets is not clear.

Table 3.3: *Average lifetime and single decay distribution lifetimes (all in ns) calculated for the* 465-500 *nm emission band (empty cells indicate unable to fit) of the Batch 1 oils. The left hand number in brackets indicates the number of individual decay times used to achieve an accurate fit. The right hand bold number in brackets is the* χ^2 *value from the fit. The lifetimes and* χ^2 *values reported are the averages of fitting results from three separate runs. The range gives the difference in lifetime between the shortest and longest multi-exponential model results.*

Oil	API	Gauss.(Single)	Gauss.(multiple)	Lorentz.(single)	Lorentz.(multiple)	Discrete(multiple)	Range	TD
7703	50.6	4.21 ± 0.05(**1.75**)	(2)5.26 ± 0.30(**0.27**)	3.98 ± 0.04(**1.87**)	(2)5.27 ± 0.30(**0.27**)	(2)5.24 ± 0.70(**0.31**)	0.03	5.86 ± 0.16
7197	45.1	3.11 ± 0.03(**1.68**)	(3)5.37 ± 0.63(**0.32**)	2.73 ± 0.03(**1.74**)	(3)5.33 ± 1.07(**0.32**)	(3)5.33 ± 0.55(**0.19**)	0.04	5.32 ± 0.14
7098	44.6	6.35 ± 0.08(**1.67**)	(2)7.52 ± 0.26(**0.31**)	5.98 ± 0.06(**2.03**)	(2)7.52 ± 0.30(**0.31**)	(2)7.50 ± 0.20(**0.21**)	0.02	8.55 ± 0.08
7058	40.1	3.13 ± 0.07(**0.48**)	(3)5.49 ± 0.16(**0.05**)	2.90 ± 0.05(**0.24**)	(3)4.93 ± 0.13(**0.03**)	(3)5.00 ± 0.10(**0.03**)	0.49	5.45 ± 0.08
7086	39.5	0.94 ± 0.40(**0.41**)	(3)4.81 ± 0.19(**0.08**)	1.71 ± 0.07(**0.18**)	(3)4.38 ± 0.21(**0.04**)	(3)4.04 ± 0.11(**0.04**)	0.77	4.85 ± 0.06
7090	36.8	3.58 ± 0.20(**0.04**)	(3)3.39 ± 0.15(**0.07**)	3.39 ± 0.10(**0.06**)	(3)3.23 ± 0.11(**0.06**)	(3)3.27 ± 0.12(**0.07**)	0.16	3.52 ± 0.07
7193	36.0	2.03 ± 0.02(**2.38**)	(3)4.05 ± 1.06(**0.29**)	1.80 ± 0.01(**1.84**)	(3)4.26 ± 0.22(**0.27**)	(3)4.17 ± 0.10(**0.28**)	0.21	5.11 ± 0.03
7062	36	0.74 ± 0.4(**0.13**)	(2)1.43 ± 0.13(**0.14**)	0.89 ± 0.05(**0.11**)	(2)1.48 ± 0.12(**0.13**)	(2)1.57 ± 0.09(**0.13**)	0.14	1.58 ± 0.08
7186	34.3	3.22 ± 0.04(**0.32**)	(3)4.89 ± 0.15(**0.04**)	2.83 ± 0.09(**0.06**)	(3)4.82 ± 0.13(**0.03**)	(3)4.80 ± 0.14(**0.04**)	0.09	5.03 ± 0.14
7632	32.7	0.74 ± 0.40(**0.26**)	(2)2.19 ± 0.14(**0.08**)	0.81 ± 0.10(**0.11**)	(2)2.38 ± 0.09(**0.06**)	(2)2.40 ± 0.09(**0.11**)	0.21	2.58 ± 0.07
7324	32.3	0.78 ± 0.20(**0.19**)	(2)1.88 ± 0.13(**0.08**)	0.80 ± 0.06(**0.10**)	(2)1.86 ± 0.07(**0.06**)	(2)1.90 ± 0.07(**0.06**)	0.04	2.08 ± 0.11
7093	30.9	$1.27 \pm 0.0.9$(**0.10**)	(2)2.70 ± 0.30(**0.55**)	1.14 ± 0.05(**0.10**)	(2)2.70 ± 0.32(**0.63**)	(2)2.70 ± 0.28(**0.64**)	0.0	2.90 ± 0.07
7187	29.4	1.55 ± 0.30(**0.28**)	(3)4.86 ± 0.27(**0.09**)	2.01 ± 0.07(**0.10**)	(3)4.89 ± 0.10(**0.05**)	(3)4.87 ± 0.13(**0.03**)	0.03	5.20 ± 0.15
7633	24.8	3.55 ± 0.06(**2.49**)	(2)7.04 ± 1.42(**2.76**)	3.62 ± 0.09(**2.35**)	(2)7.04 ± 1.43(**2.73**)	(2)7.02 ± 1.43(**2.82**)	0.02	6.27 ± 0.22
7169	21.6	0.81 ± 0.06(**0.07**)	(2)1.16 ± 0.15(**0.07**)	0.77 ± 0.02(**0.07**)	(2)1.18 ± 0.10(**0.08**)	(2)1.14 ± 0.07(**0.10**)	0.04	1.39 ± 0.03
7032	19.1	0.53 ± 0.90(**0.18**)	–	0.34 ± 0.01(**0.15**)	–	(1)0.52 ± 0.40(**0.18**)	0	0.33 ± 0.1
7130	15.6	0.52 ± 0.01(**0.09**)	(1)0.42 ± 0.004(**0.52**)	0.34 ± 0.10(**0.10**)	(1)0.42 ± 0.01(**0.52**)	(2)0.66 ± 0.22(**0.56**)	0.24	1.25 ± 0.04
7321	14.1	0.44 ± 0.20(**0.08**)	(2)0.90 ± 0.21(**0.06**)	0.17 ± 0.10(**0.1**)	(2)0.93 ± 0.31(**0.06**)	(2)0.86 ± 0.07(**0.07**)	0.07	1.04 ± 0.04
7188	13.3	0.45 ± 0.04(**0.08**)	(2)0.79 ± 0.16(**0.06**)	0.32 ± 0.06(**0.11**)	(2)0.69 ± 0.13(**0.08**)	(2)0.68 ± 0.07(**0.08**)	0.11	0.84 ± 0.08
7033	12.8	–	–	0.41 ± 0.04(**3.16**)	–	(1)0.41 ± 0.004(**2.68**)	0	–

Table 3.4: *Average lifetime and single decay distribution lifetimes (all in ns) calculated for the* 542-582 *nm emission band (empty cells indicate unable to fit) of the Batch 1 oils. The left hand number in brackets indicates the number of individual decay times used to achieve an accurate fit. The right hand bold number in brackets is the* χ^2 *value from the fit. The lifetimes and* χ^2 *values reported are the averages of fitting results from three separate runs. The range gives the difference in lifetime between the shortest and longest multi-exponential model results.*

Oil	API	Gauss. (Single)	Gauss. (multiple)	Lorentz. (single)	Lorentz. (multiple)	Discrete (multiple)	Range
7703	50.6	6.47 ± 0.07(**0.69**)	(3)7.56 ± 0.50(**0.18**)	5.64 ± 0.06(**0.23**)	(3)7.73 ± 0.50(**0.56**)	(3)7.81 ± 0.45(**0.54**)	0.25
7197	45.1	6.37 ± 0.08(**0.69**)	(2)6.84 ± 0.27(**0.72**)	5.45 ± 0.07(**0.91**)	(3)6.80 ± 0.27(**0.21**)	(3)6.82 ± 0.27(**0.20**)	0.04
7098	44.6	7.89 ± 0.10(**0.73**)	(3)10.02 ± 1.26(**0.65**)	7.11 ± 0.08(**0.83**)	(3)9.25 ± 0.96(**0.44**)	(3)10.83 ± 0.86(**0.87**)	0.34
7058	40.1	5.65 ± 0.06(**0.08**)	(3)7.14 ± 0.14(**0.06**)	4.90 ± 0.05(**0.13**)	(3)7.09 ± 0.14(**0.02**)	(3)6.90 ± 0.13(**0.02**)	0.24
7086	39.5	4.64 ± 0.08(**0.06**)	(3)5.97 ± 0.17(**0.05**)	4.05 ± 0.05(**0.11**)	(3)5.89 ± 0.18(**0.05**)	(3)6.04 ± 0.17(**0.03**)	0.15
7090	36.8	3.49 ± 0.40(**0.04**)	(3)5.86 ± 0.10(**0.05**)	3.94 ± 0.05(**0.06**)	(3)5.88 ± 0.21(**0.05**)	(3)5.93 ± 0.13(**0.04**)	0.07
7193	36.0	3.50 ± 0.04(**0.31**)	(3)5.59 ± 0.31(**0.11**)	3.00 ± 0.03(**0.14**)	(3)5.31 ± 0.17(**0.08**)	(3)5.39 ± 0.17(**0.07**)	0.28
7062	36	1.09 ± 0.30(**0.11**)	(2)2.37 ± 0.18(**0.10**)	0.65 ± 0.30(**0.07**)	(2)2.39 ± 0.07(**0.10**)	(2)2.35 ± 0.16(**0.06**)	0.04
7186	34.3	6.53 ± 0.08(**0.13**)	(2)7.27 ± 0.16(**0.18**)	5.71 ± 0.06(**0.18**)	(2)6.66 ± 0.20(**0.25**)	(3)7.16 ± 0.29(**0.09**)	0.61
7632	32.7	0.75 ± 0.50(**0.07**)	(3)3.72 ± 0.30(**0.05**)	1.77 ± 0.50(**0.06**)	(3)3.70 ± 0.40(**0.05**)	(3)3.83 ± 0.07(**0.05**)	0.13
7324	32.3	0.91 ± 0.40(**0.05**)	(3)3.29 ± 0.08(**0.03**)	1.40 ± 0.09(**0.05**)	(3)3.28 ± 0.05(**0.02**)	(3)3.29 ± 0.08(**0.02**)	0.01
7093	30.9	2.92 ± 0.10(**0.07**)	(2)3.74 ± 0.10(**0.27**)	2.55 ± 0.20(**0.05**)	(2)3.55 ± 0.11(**0.31**)	(2)3.50 ± 0.14(**0.79**)	0.24
7187	29.4	6.09 ± 0.10(**0.09**)	(3)6.65 ± 0.12(**0.09**)	5.51 ± 0.90(**0.09**)	(3)6.55 ± 0.23(**0.10**)	(3)6.53 ± 0.11(**0.10**)	0.12
7633	24.8	7.86 ± 0.10(**0.25**)	(3)8.93 ± 0.40(**0.31**)	7.08 ± 0.10(**0.25**)	(3)8.90 ± 0.29(**0.27**)	(3)8.89 ± 0.56(**0.28**)	0.04
7169	21.6	0.77 ± 0.30(**0.06**)	(3)1.99 ± 0.05(**0.02**)	0.32 ± 0.90(**0.03**)	(3)2.01 ± 0.06(**0.02**)	(3)2.00 ± 0.07(**0.02**)	0.02
7032	19.1	0.80 ± 0.20(**0.09**)	(2)0.98 ± 0.33(**0.08**)	0.72 ± 0.06(**0.07**)	(2)0.98 ± 0.33(**0.08**)	(2)0.98 ± 0.64(**0.08**)	0
7130	15.6	0.73 ± 0.20(**0.04**)	(2)1.07 ± 0.07(**0.08**)	0.36 ± 0.10(**0.043**)	(2)1.07 ± 0.05(**0.08**)	(2)1.07 ± 0.05(**0.09**)	0.03
7321	14.1	0.72 ± 0.10(**0.05**)	(2)1.15 ± 0.03(**0.04**)	0.95 ± 0.10(**0.03**)	(2)1.15 ± 0.03(**0.04**)	(2)1.15 ± 0.03(**0.04**)	0
7188	13.3	0.76 ± 0.20(**0.04**)	(3)1.35 ± 0.04(**0.02**)	0.30 ± 0.10(**0.03**)	(3)1.35 ± 0.05(**0.02**)	(3)1.35 ± 0.05(**0.02**)	0
7033	12.8	0.38 ± 0.10(**0.28**)	(2)0.56 ± 0.05(**0.35**)	0.28 ± 0.06(**0.27**)	(2)0.55 ± 0.05(**0.31**)	(2)0.55 ± 0.04(**0.33**)	0.01

Table 3.5: *Average lifetime and single decay distribution lifetimes (all in ns) calculated for the* 465-500 *nm emission band of the Batch 2 oils. The left hand number in brackets indicates the number of individual decay times used to achieve an accurate fit. The right hand bold number in brackets is the* χ^2 *value from the fit. The lifetimes and* χ^2 *values reported are the averages of fitting results from three separate runs. The range gives the difference in lifetime between the shortest and longest multi-exponential model results.*

Oil	API	Gauss. (Single)	Gauss. (multiple)	Lorentz. (single)	Lorentz (multiple)	Discrete (multiple)	Range	TD
ME9	47.8	3.13 ± 0.04(**1.32**)	(3)4.79 ± 0.9(**0.25**)	2.98 ± 0.03(**1.33**)	(3)4.83 ± 0.85(**0.25**)	(3)4.84 ± 0.80(**0.21**)	0.05	4.79 ± 0.26
ME8	44.2	3.05 ± 0.04(**0.33**)	(2)5.07 ± 0.88(**0.97**)	2.97 ± 0.03(**0.21**)	(2)5.02 ± 0.87(**0.97**)	(2)5.08 ± 0.78(**0.90**)	0.06	5.66 ± 0.19
ME5	44.1	3.28 ± 0.05(**0.38**)	(2)4.81 ± 0.32(**0.42**)	3.07 ± 0.03(**0.30**)	(2)4.82 ± 0.33(**0.41**)	(2)4.81 ± 0.33(**0.41**)	0.01	5.59 ± 0.15
ME7	42.1	3.40 ± 0.05(**0.35**)	(2)5.26 ± 0.57(**0.64**)	3.28 ± 0.04(**0.23**)	(2)5.26 ± 0.57(**0.73**)	(2)5.25 ± 0.58(**0.63**)	0.01	5.72 ± 0.13
ME6	39.6	3.44 ± 0.05(**0.35**)	(2)5.22 ± 0.35(**0.41**)	3.23 ± 0.04(**0.16**)	(2)5.19 ± 0.39(**0.52**)	(2)5.16 ± 0.23(**0.40**)	0.06	5.95 ± 0.17
ME4	39.2	2.65 ± 0.04(**0.36**)	(2)4.54 ± 0.49(**0.82**)	2.53 ± 0.03(**0.24**)	(2)4.54 ± 0.5(**0.82**)	(2)4.56 ± 0.51(**0.83**)	0.02	5.30 ± 0.18
ME1	32.7	1.03 ± 0.09(**0.13**)	(2)2.33 ± 0.14(**0.35**)	1.12 ± 0.03(**0.08**)	(2)2.33 ± 0.18(**0.36**)	(2)2.30 ± 0.14(**0.37**)	0.03	2.75 ± 0.14
ME3	30.8	1.74 ± 0.02(**0.64**)	(2)3.10 ± 0.34(**0.65**)	1.63 ± 0.01(**0.43**)	(2)3.06 ± 0.34(**0.56**)	(2)3.06 ± 0.33(**0.55**)	0.04	3.74 ± 0.12
ME2	28.9	1.29 ± 0.01(**0.19**)	(2)2.29 ± 0.20(**0.46**)	1.14 ± 0.01(**0.09**)	(2)2.29 ± 0.20(**0.46**)	(2)2.27 ± 0.20(**0.45**)	0.02	2.71 ± 0.15
ME10	24.7	0.68 ± 0.1(**0.10**)	(2)1.20 ± 0.17(**0.38**)	0.63 ± 0.04(**0.07**)	(2)1.2 ± 0.17(**0.36**)	(2)1.20 ± 0.16(**0.35**)	0	1.15 ± 0.20

Table 3.6: *Average lifetime and single decay distribution lifetimes (all in ns) calculated for the* 542-582 *nm emission band of the Batch 2 oils. The left hand number in brackets indicates the number of individual decay times used to achieve an accurate fit. The right hand bold number in brackets is the* χ^2 *value from the fit. The lifetimes and* χ^2 *values reported are the averages of fitting results from three separate runs. The range gives the difference in lifetime between the shortest and longest multi-exponential model results.*

Oil	API	Gauss. (Single)	Gauss. (multiple)	Lorentz. (single)	Lorentz. (multiple)	Discrete (multiple)	Range
ME9	47.8	5.19 ± 0.07(**0.17**)	(3)6.46 ± 0.32(**0.24**)	4.54 ± 0.08(**0.55**)	(3)6.46 ± 0.31(**0.22**)	(3)6.45 ± 0.44(**0.37**)	0.01
ME8	44.2	6.24 ± 0.10(**0.58**)	(3)7.72 ± 0.53(**0.40**)	5.46 ± 0.07(**0.49**)	(3)7.61 ± 0.53(**0.35**)	(3)7.67 ± 0.53(**0.41**)	0.11
ME5	44.1	6.74 ± 0.10(**0.31**)	(2)7.42 ± 0.65(**0.85**)	6.22 ± 0.1(**0.30**)	(2)7.42 ± 0.62(**0.85**)	(2)7.40 ± 0.66(**0.87**)	0.02
ME7	42.1	6.84 ± 0.10(**0.27**)	(2)7.41 ± 0.16(**0.37**)	6.19 ± 0.09(**0.20**)	(2)7.28 ± 0.64(**1.00**)	(2)6.67 ± 0.33(**0.70**)	0.74
ME6	39.6	7.47 ± 0.1(**0.23**)	(2)7.56 ± 0.33(**0.42**)	6.89 ± 0.10(**0.21**)	(2)7.68 ± 0.25(**0.43**)	(2)7.49 ± 0.33(**0.43**)	0.19
ME4	39.2	6.01 ± 0.10(**0.49**)	(3)7.43 ± 0.49(**0.24**)	5.41 ± 0.07(**0.36**)	(3)7.25 ± 0.47(**0.30**)	(3)7.44 ± 0.51(**0.30**)	0.19
ME1	32.7	3.11 ± 0.05(**0.13**)	(3)4.33 ± 0.11(**0.08**)	2.70 ± 0.03(**0.17**)	(3)4.33 ± 0.11(**0.08**)	(3)4.33 ± 0.12(**0.09**)	0
ME3	30.8	3.79 ± 0.04(**0.29**)	(2)4.54 ± 0.20(**0.13**)	3.28 ± 0.03(**0.19**)	(2)3.75 ± 0.07(**0.18**)	(3)4.91 ± 0.23(**0.19**)	1.16
ME2	28.9	1.79 ± 0.10(**0.26**)	(3)3.90 ± 0.13(**0.10**)	1.73 ± 0.05(**0.16**)	(3)3.90 ± 0.15(**0.12**)	(3)3.80 ± 0.12(**0.09**)	0.10
ME10	24.7	0.93 ± 0.20(**0.11**)	(2)2.13 ± 0.11(**0.42**)	0.60 ± 0.10(**0.08**)	(2)1.96 ± 0.15(**0.18**)	(2)1.98 ± 0.10(**0.23**)	0.17

Analysis of the fitting results in Tables 3.3 to 3.6 shows that the FD lifetimes (regardless of fit model) follow expected trends for crude oils, i.e., a curved response with emission wavelength, heavy oils have short lifetimes and light oils have longer lifetimes. These characteristics are shown in Figure 3.13. Heavy oils contain greater proportions of polar and asphaltic compounds and so are affected by energy transfer and fluorescence quenching ultimately leading to shorter lifetimes. Lighter oils have higher alkane content and fewer polar molecules which give rise to longer lifetimes due to reduced energy transfer and quenching effects.

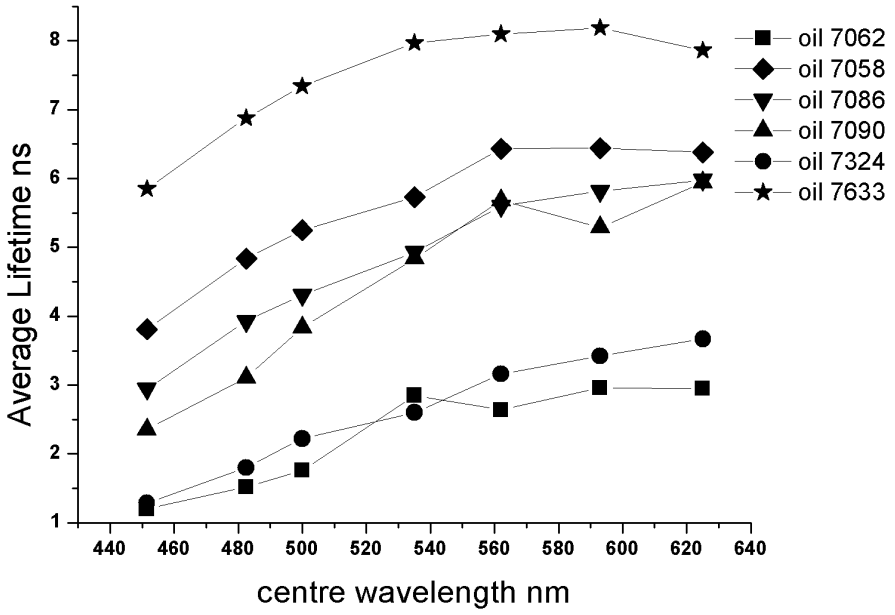

Figure 3.13: *Average lifetimes (discrete model) for some selected medium density crude oils. A general increase in lifetime is observed with increasing emission wavelength. A similar trend occurs with heavy and light crude oils. The data used to construct this graph is given in Appendix B.*

As discussed in Chapter 1, the value of average lifetime calculated at a specific emission range depends on the interplay between energy transfer and quenching effects. At each wavelength range, the emission from a different population of fluorophores is collected. Each fluorophore population will have different rates of energy transfer and quenching which changes the average lifetime value. At short emission wavelengths, energy transfer is the dominant process which gradually reduces as the emission wavelength increases. At longer wavelengths the lifetime decreases due to

increased amounts of collisional quenching and higher rates of internal conversion processes [124, 126].

3.4 Comparison of average lifetimes determined by FD and TD methods

For simple systems containing a single fluorophore, the two measurement methods, FD and TD should give the same lifetimes. The TD method provides an absolute measurement of lifetime and has been found to give lifetimes with shorter confidence intervals [187]. In comparison, the FD method calculates the lifetime based on phase and modulation values relative to those obtained for a standard of known lifetime. In practical terms, data collection times for each method are comparable, although the shorter acquisition times for single frequency phase and modulation measurements is a distinct advantage for rapid imaging or sensing applications. The greater sensitivity of TCSPC is an advantage with weakly emitting heavy crude oils. However, the majority of oils are strongly fluorescent and are therefore suited to FD analysis. The most significant difference between the two methods was fitting of the data to extract average lifetimes which were found to be faster for FD than for TCSPC although the evaluation of the lifetime error was similar in both cases. To determine which FD model gives the correct average lifetime, it was necessary to compare the results from the FD models with TD values. The TD decay curves were obtained by recording at a center wavelength of 480 nm (approximately 16 nm bandpass). The calculated TD lifetimes were compared to FD lifetimes determined from phase and demodulation data recorded at 465 to 500 nm emission. The TCSPC measurements covered $\sim$ 472 to 488 nm, while in the FD system the emission covered 465 to $\sim$ 500 nm.

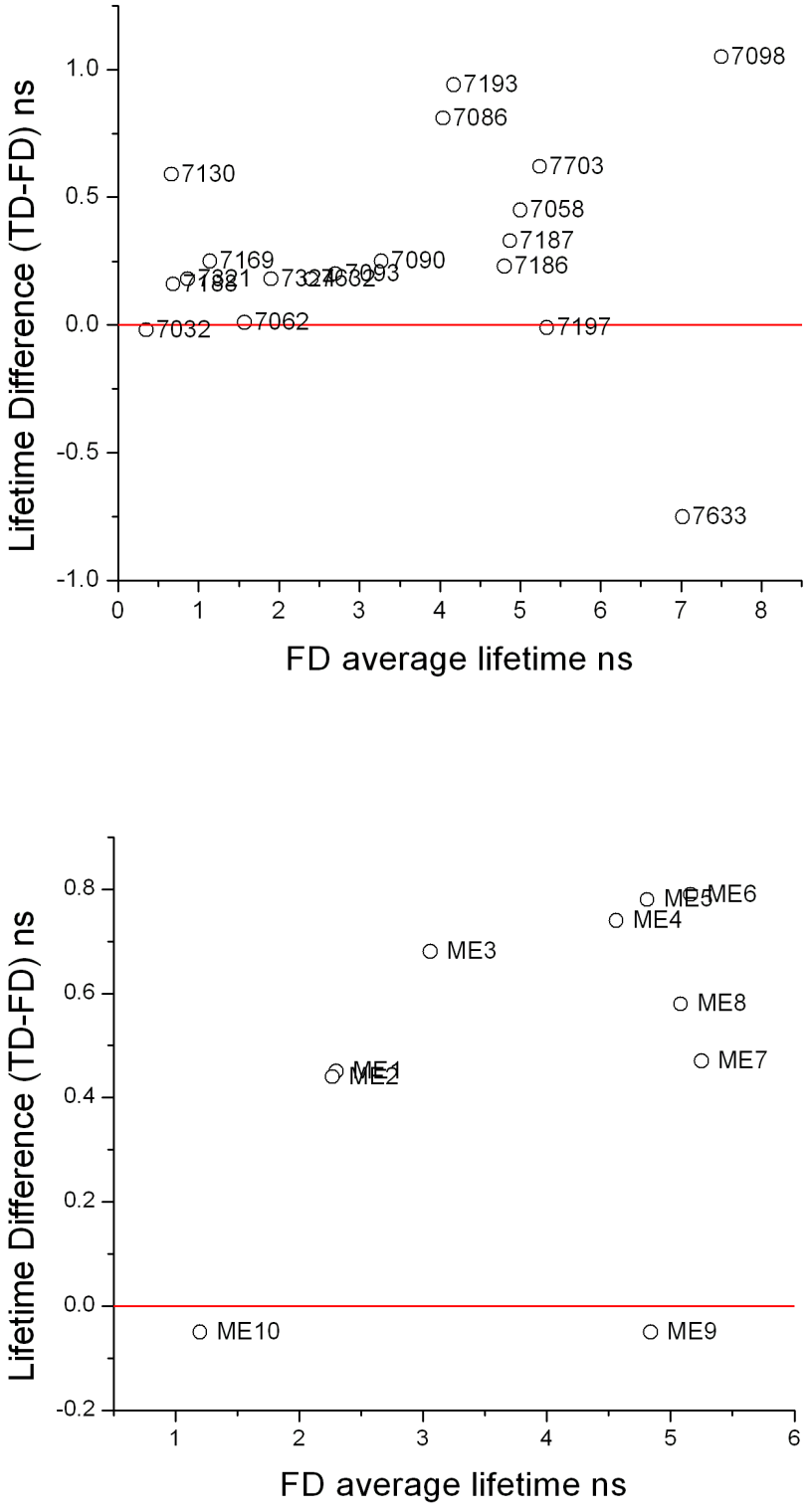

Figure 3.14: *Plot of the average lifetimes determined by Frequency Domain (*FD*) method and the difference with the* TD *average lifetimes determined using* TC-SPC*. Both lifetimes calculated using discrete average lifetime model. Data recorded at a centre wavelength of* 480 *nm using* 405 *nm excitation. Top: Batch 1 oils; Bottom: Batch 2 oils. Positive lifetime differences indicate the oils whose TD average lifetimes are longer than the FD measured average lifetimes.*

Figure 3.14 shows the difference between TD and FD lifetimes (calculated using the discrete decay term model) across the oils sampled. Values close to the zero line show oils for which the two methods give similar lifetimes[†]. For most oils, the TD values are greater than the FD values. A notable exception is for oil 7633 where the TD lifetime is shorter than the FD lifetime (The physical reasons for the different characteristics of this oil are examined in a later section). However, Table 3.3 shows that the phase modulation data for this oil is poorly fitted leading to a large error in the average lifetime value. The lighter oils with a large uncertainty in the calculated lifetime also show the greatest difference compared to the TD results. A similar situation can be seen for the ME oils (Figure 3.14 bottom part) where most TD lifetime values are longer that the FD values.

Figures 3.15 and 3.16 show correlation plots for each oil set where values on the line through the origin indicate close matches to the TD average lifetimes. For the Batch 1 and 2 oils, the distribution models do not give any improvement when based on the correlation coefficients. When the confidence intervals and goodness of fit are included into the discussion on Batch 1 oils, the discrete model out-performs the distribution models (Tables 3.3 to 3.6). In contrast, for Batch 2 oils, the Lorentzian model out-performs the others as discussed previously. However, modeling the phase and demodulation by discrete lifetimes was in practice the simplest fitting to perform and also was found to be quicker, having distinct advantages in lifetime imaging. While, all phase and modulation data could be fitted to a multiple decay term model, it is possible that overfitting the data can occur leading to incorrect evaluations of the lifetime.

[†] The data shown in the top part of Figure 3.14 do not match those published [112]. Since the publication of this paper, the fitting protocol was improved leading to changes in some of the lifetime values.

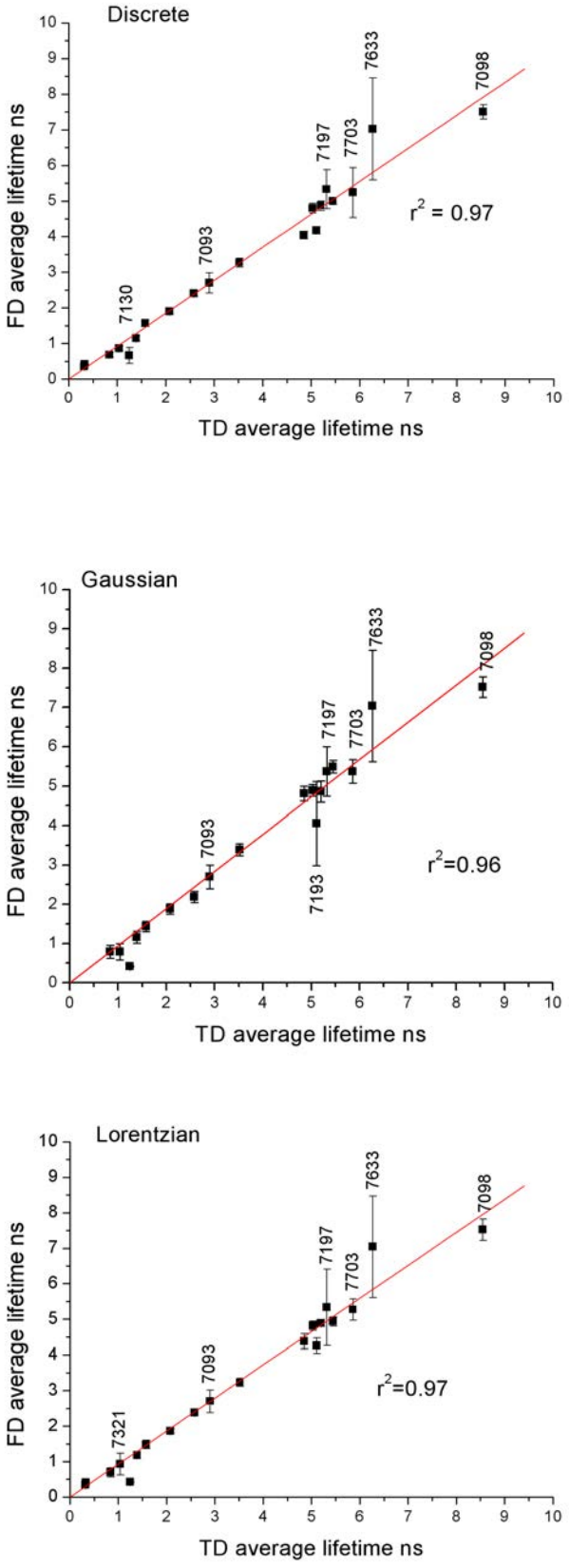

Figure 3.15: *Plot of TD versus FD lifetimes for the three models (multiple decay terms) tested on Batch 1 oils. Error bars are shown for the FD lifetimes. Plots correspond to data presented in Table 3.3 ($\lambda_{em} = 465 - 500$ nm).*

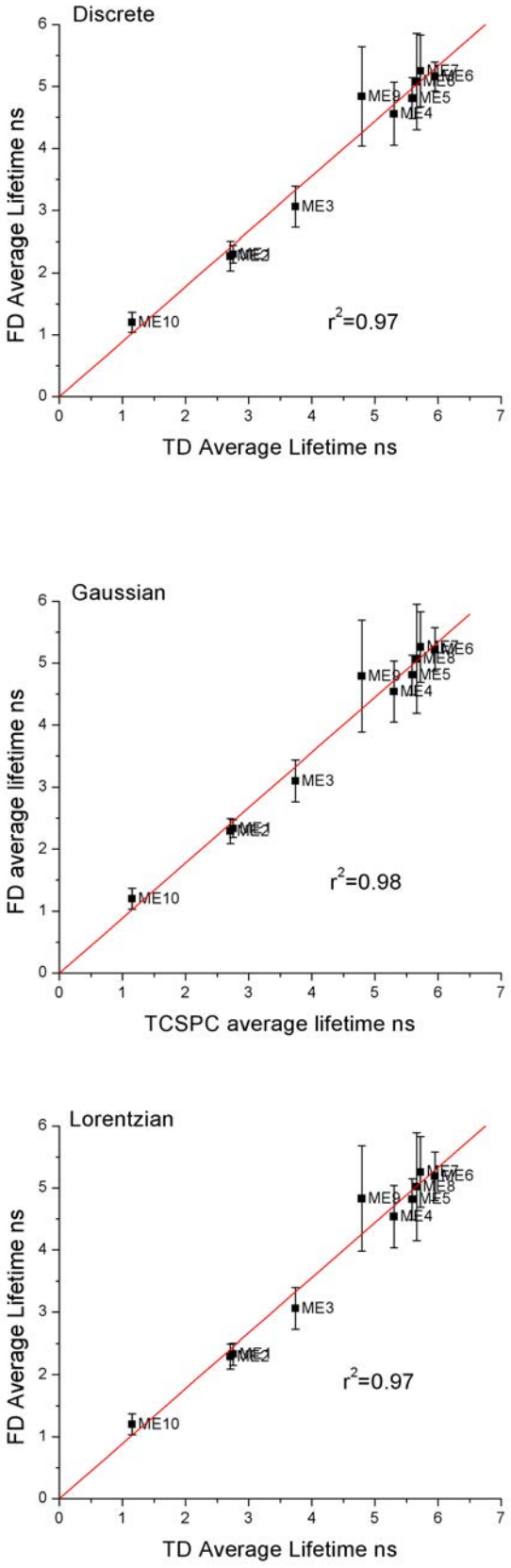

Figure 3.16: *Plot of TD versus FD lifetimes for the three models (multiple decay terms) tested on Batch 2 oils. Error bars are shown for the FD lifetimes. Plots correspond to data presented in Table 3.5 ($\lambda_{em} = 465 - 500nm$).*

3.5 Single Lifetime distributions

When a multiple decay model is fit to phase and modulation data, a reduction in the χ^2 values generally indicates a better fit. Yet the addition of subsequent terms in the model may actually result in overfitting and lead to longer lifetimes. For crude oils, one does not expect that a limited number of discrete decay terms will realistically describe the decay and an alternative is to fit the phase and modulation data to a single Lorentzian or Gaussian distribution. Continuous distribution functions such as the Gaussian and Lorentzian distributions are defined by the center of the distribution and the full width at half maximum or FWHM. For a Lorentzian distribution, the curve is characterised by a narrow peak with a large spread in the limits on either side of the centre lifetime [47]. This function can be solved analytically giving a value for the FWHM. In contrast the Gaussian distribution gives a broader peak with a shorter spread of the limits at either side of the center lifetime. This function must be solved by numerical integration and the width of the distribution is given by twice the standard deviation. In this work, the distribution widths quoted equate to the spread of lifetimes at half the maximum of the distribution (FWHM). The variation of the width of the distribution of the lightest and heaviest oil in both samples sets are shown from Figures 3.17 to 3.24[‡]. The Lorentzian fits show narrow distributions with contributions from a longer range of lifetimes than the Gaussian function. In contrast the Gaussian distribution gives a broader distribution but over a range of shorter lifetimes. In some cases, a discrete component of longer lifetime has been added to improve the fitting. This has the effect of forcing a more symmetric distribution giving a value for the distribution width. For the purposes of this discussion the addition of this discrete term does not have any physical significance. The addition of discrete components to distributions in this manner have been used in the study of tryptophan conformations in Human Serum Albumin [189, 190].

When fitting distributions using this method, the utmost care must be taken to ensure that the model is robust and can be applied to phase and demodulation data from all replicate experiments. The reason for this is that single distributions are prone to local minima that can produce incorrect lifetimes and distribution widths.

[‡] Note that these figures represent the lifetime distribution from a single fitting rather than the average of three fittings as reported in Tables 3.5 and 3.4.

The addition of a discrete component of small contribution also is used for fitting the data of heavy oils with short lifetimes, e.g., ME10 and 7130. This second component is generally characterised by its low fractional contribution in the order of $5-10\%$ of the total contribution. In the case of oil 7130, it was not possible to obtain lifetime or FWHM data as indicated by DNF in the 426-477 nm band plot in Figure 3.20. For the light oils 7703 and ME9, a discrete term of higher fractional contribution (30%) is required when fitting the data from the 426-477 nm band (Figures 3.17 top left and 3.21 top left).

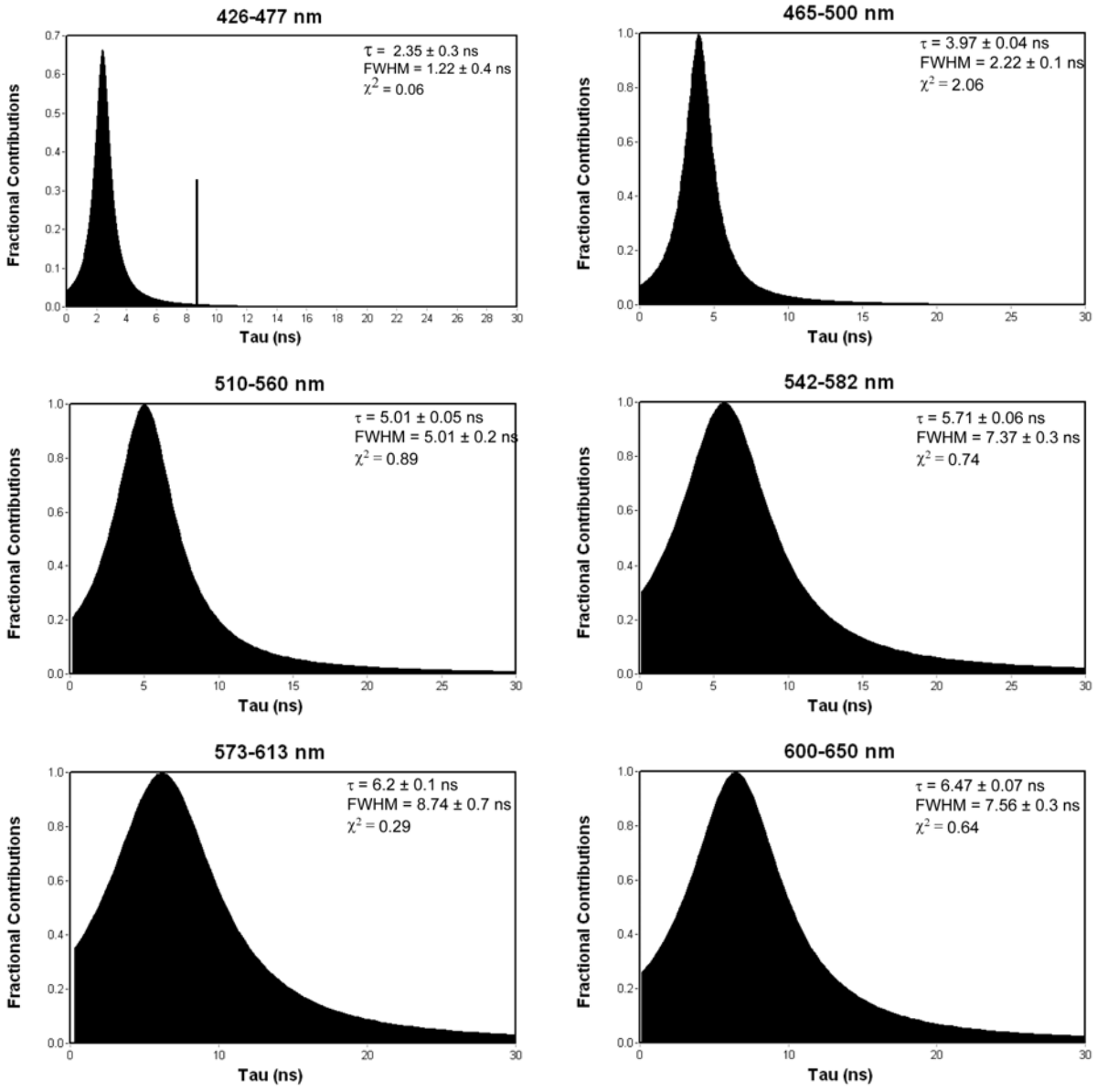

Figure 3.17: *Lorentzian distributions for light oil 7703 (API 50.6) over the emission range studied (centre wavelengths of the emission bandpass are plotted).*

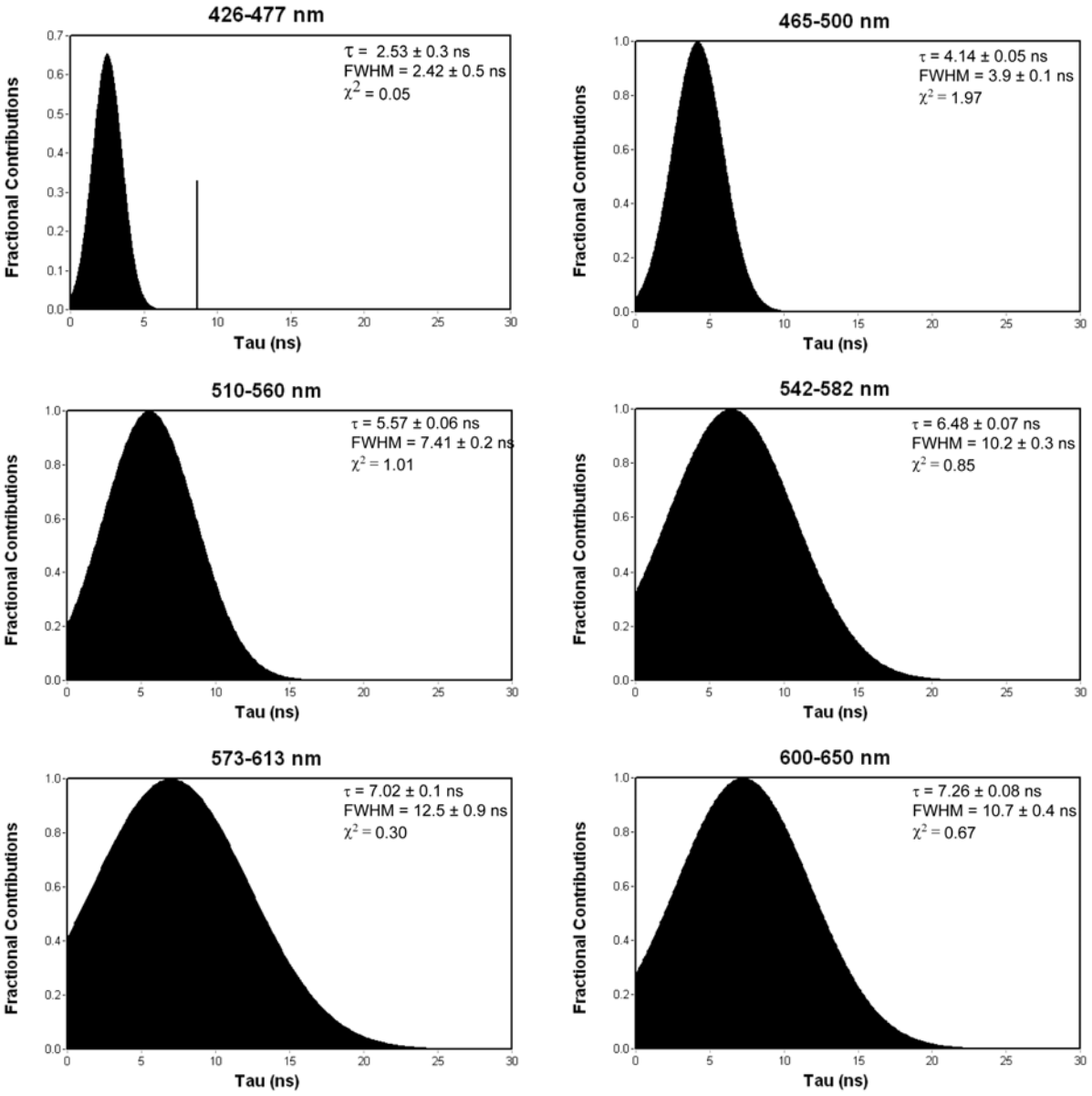

Figure 3.18: *Gaussian distributions for light oil 7703 (API 50.6) in Batch 1, over the experimental emission range(centre wavelengths of the emission bandpass are plotted).*

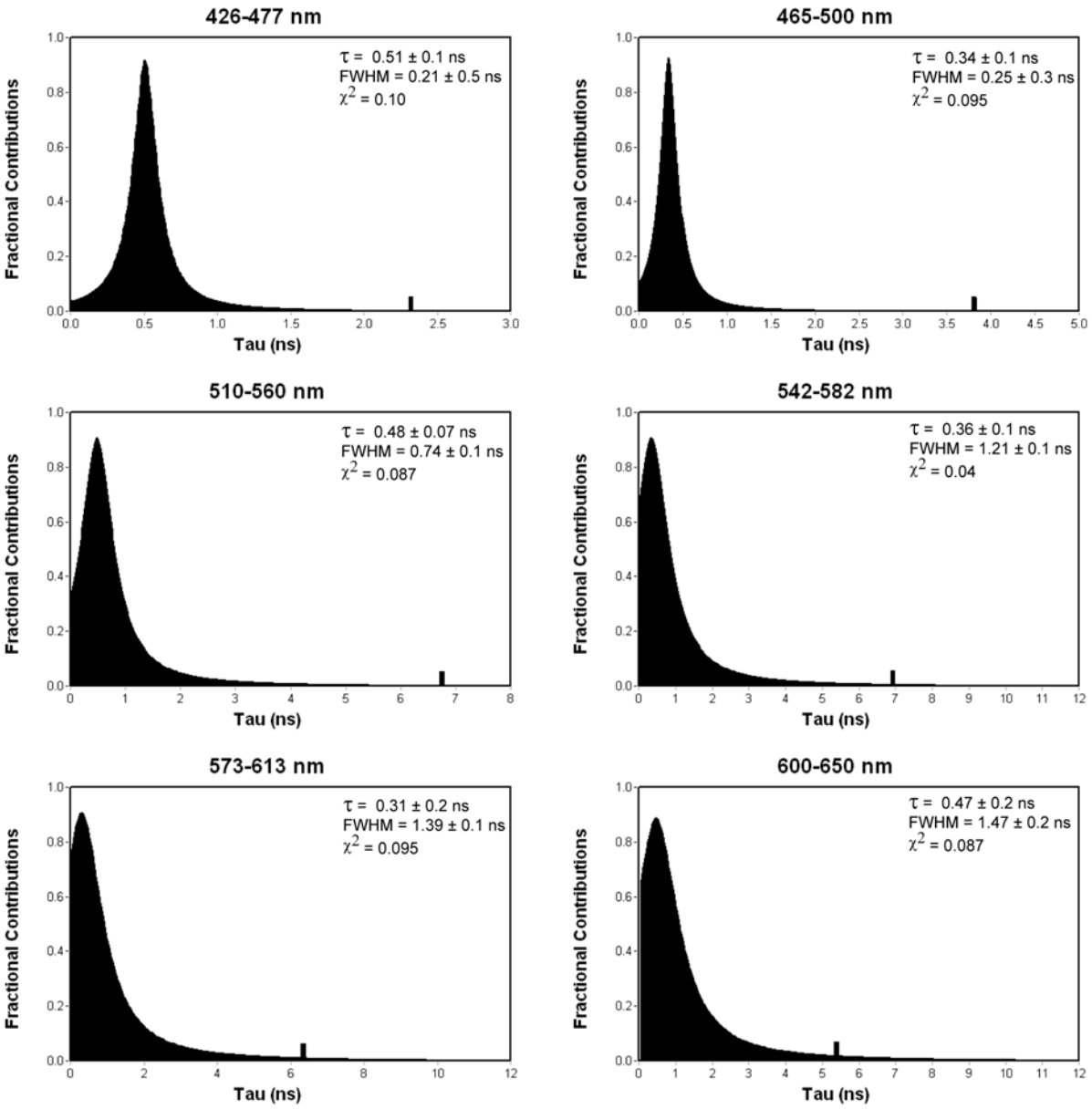

Figure 3.19: *Lorentzian distributions for heavy oil 7130 (API 15.6) over the emission range studied (centre wavelengths of the emission bandpass are plotted).*

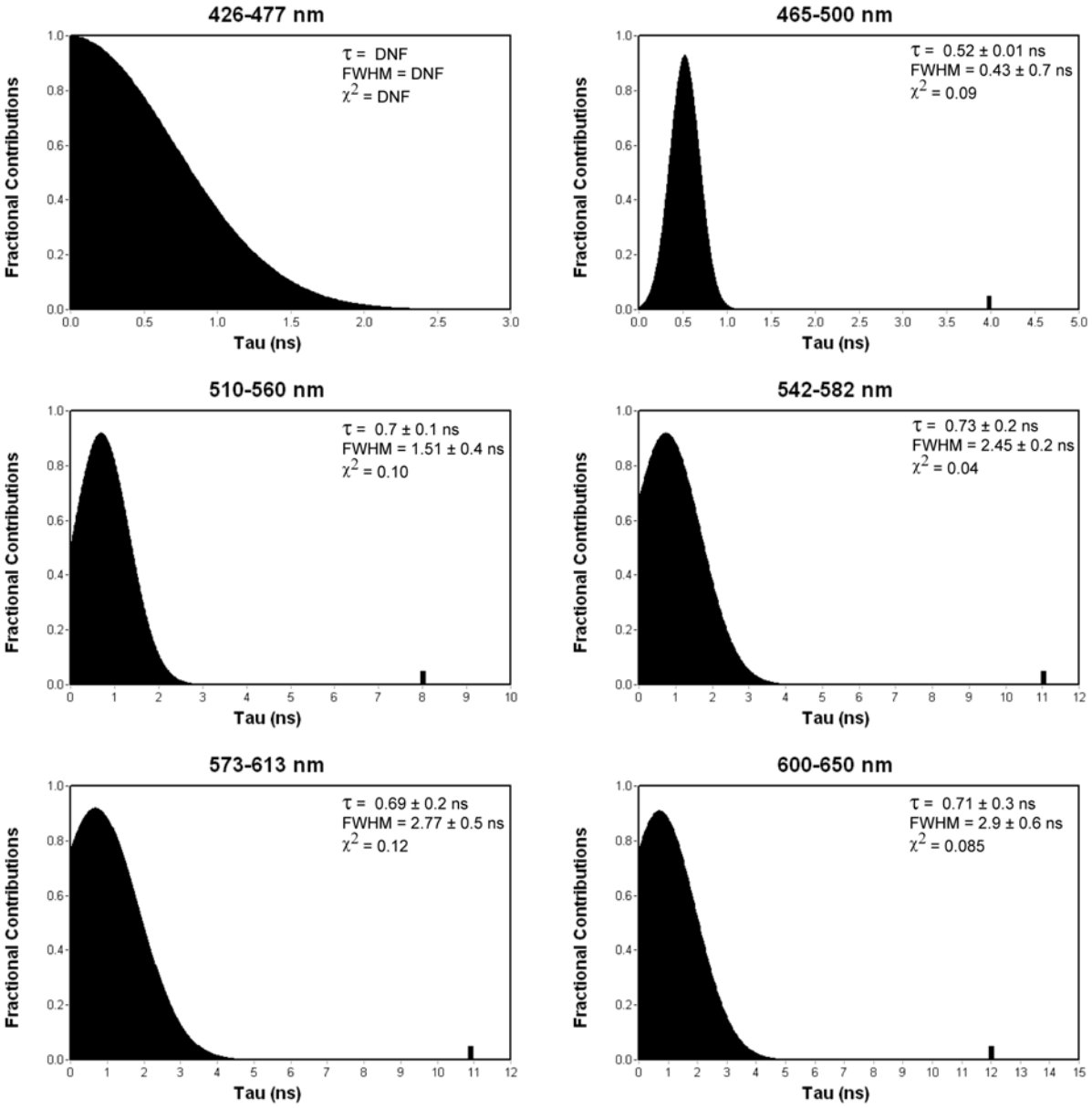

Figure 3.20: *Guassian distributions for heavy oil 7130 (API 15.6) over the emission range studied (centre wavelengths of the emission bandpass are plotted). DNF = Did Not Fit.*

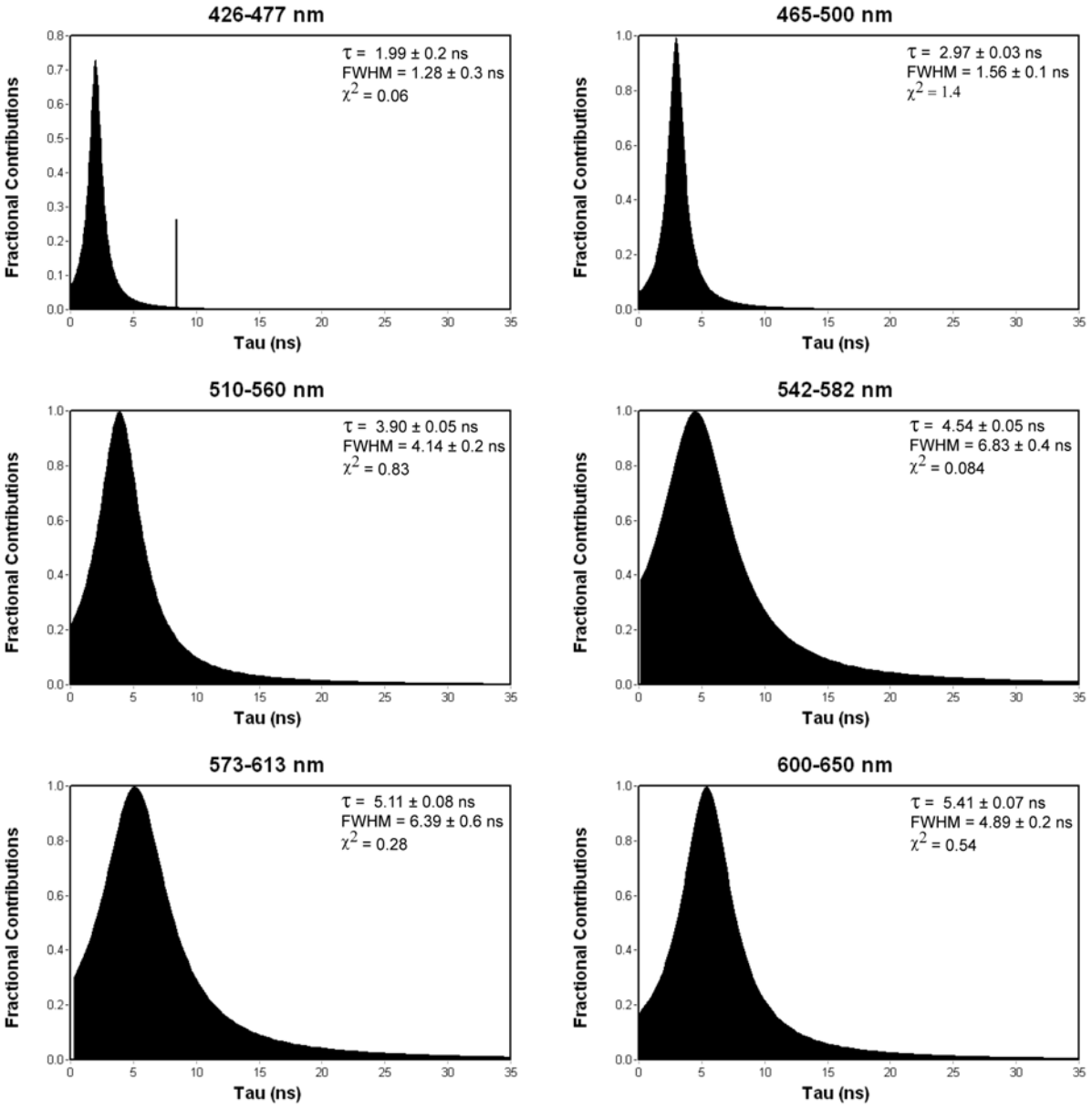

Figure 3.21: *Lorentzian distributions for heavy oil ME9 (API 47.8) over the emission range studied (centre wavelengths of the emission bandpass are plotted).*

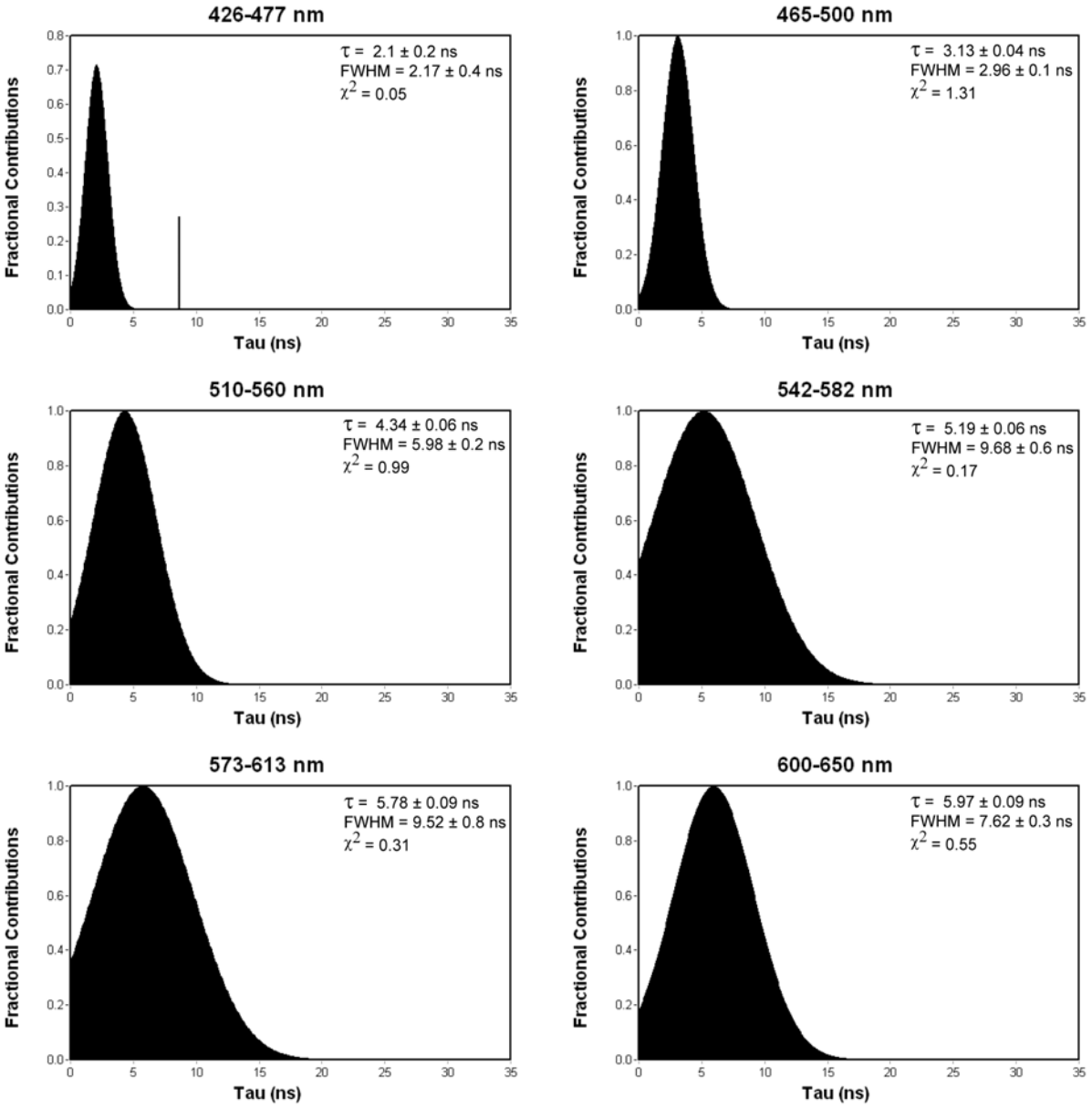

Figure 3.22: *Gaussian distributions for light oil ME9 (API 47.8) over the emission range studied (centre wavelengths of the emission bandpass are plotted).*

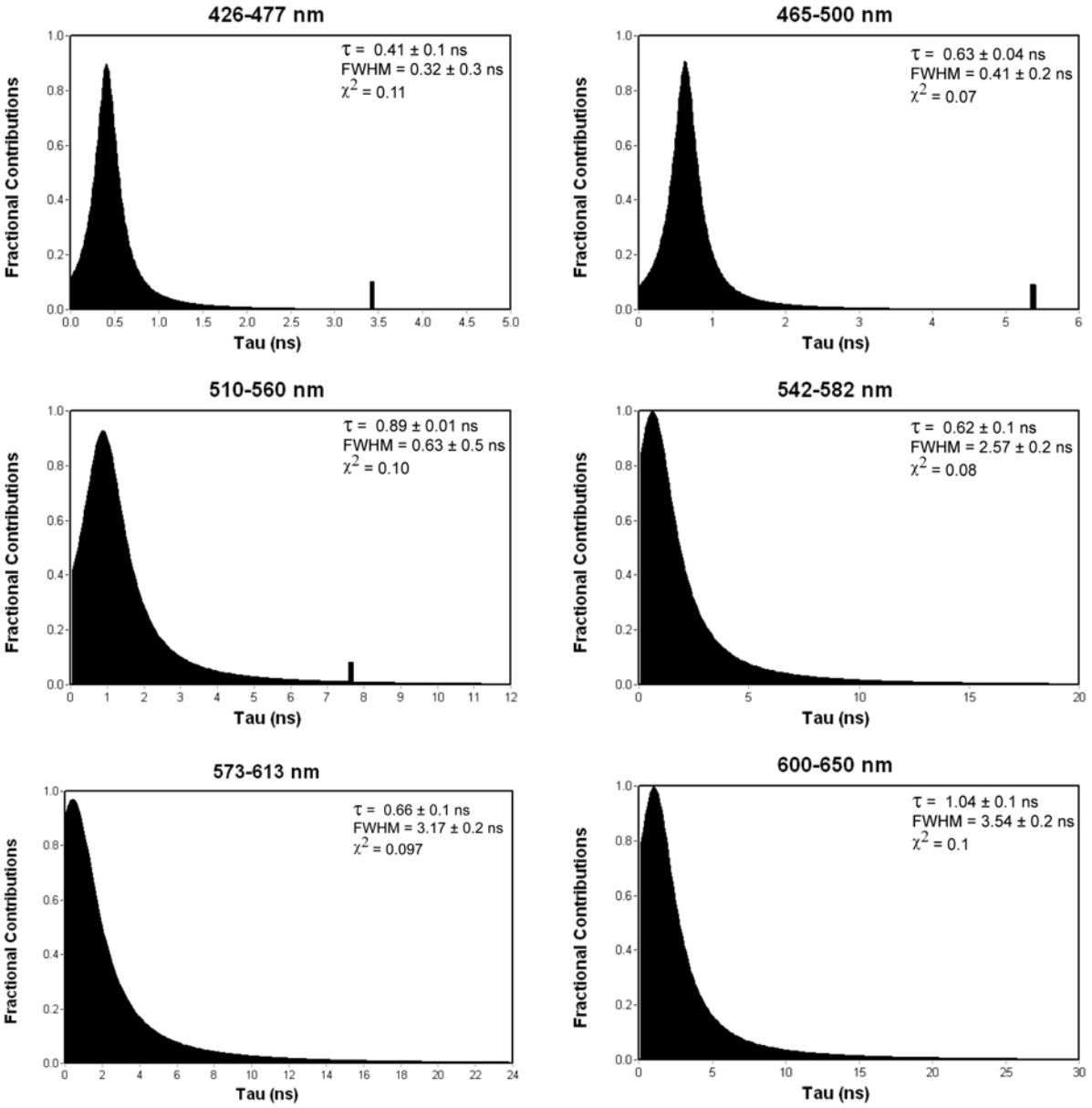

Figure 3.23: *Lorentzian distributions for the heaviest oil ME10 (API 24.7) in the Batch 2 oils, calculated from phase and modulation data measured over the full emission range (centre wavelengths of the emission bandpass are plotted).*

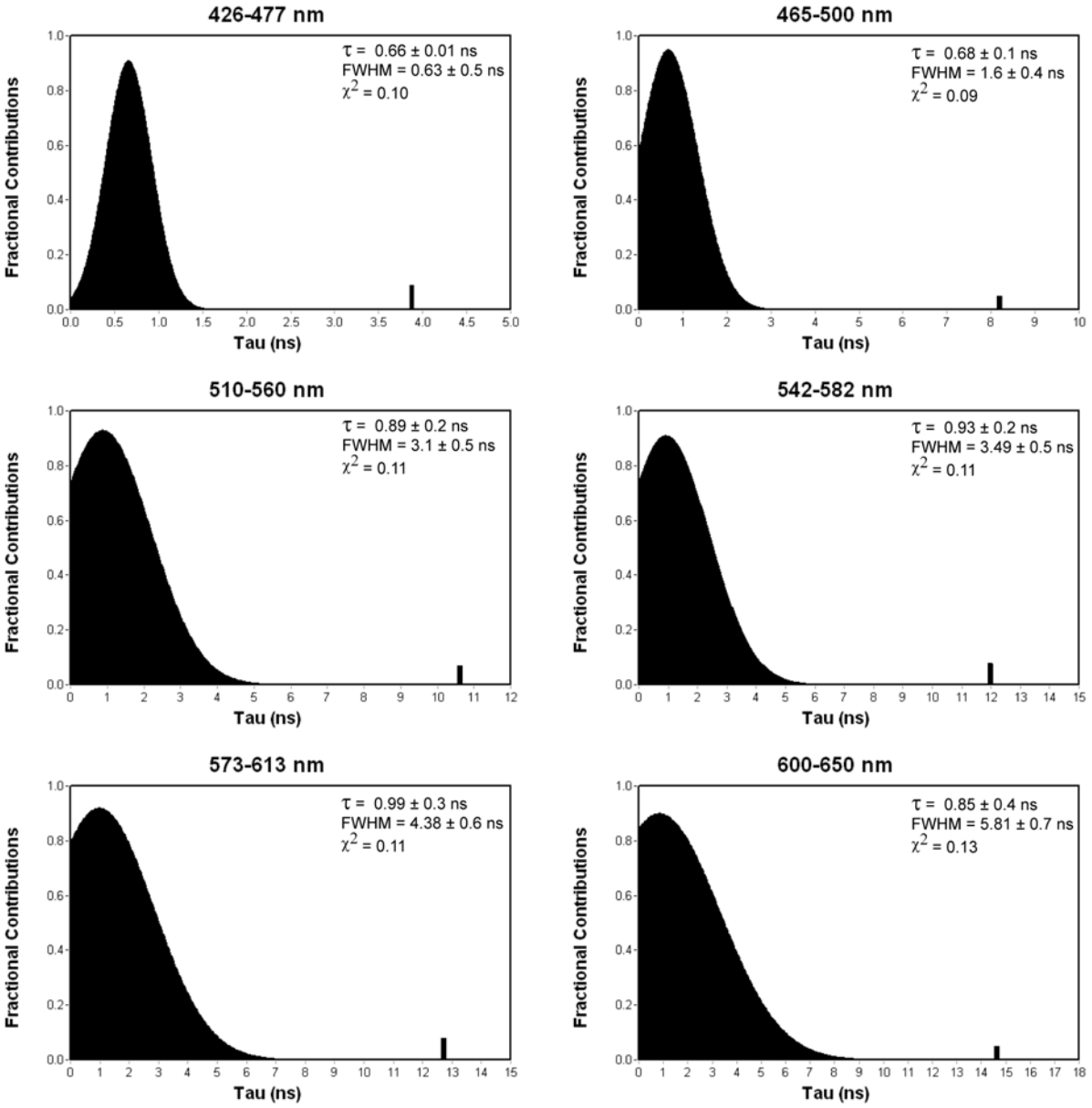

Figure 3.24: *Gaussian distributions for the heaviest oil ME10 (API 24.7) in the Batch 2 oils, calculated from phase and modulation data measured over the full emission range (centre wavelengths of the emission bandpass are plotted).*

The most important feature of the lifetime-distribution analysis is that the center lifetime of the distribution and the distribution width increases with emission wavelength for both models (Gaussian and Lorentzian). Similar observations have been found with average lifetime versus emission wavelength plots which have been discussed earlier in Section 3.3. Figures 3.25 and 3.26 show the variation of the center lifetime and FWHM as a function of emission wavelength. Since the FD data was recorded at an emission band pass rather than a specific wavelength, the

center of the wavelength range sampled is plotted for each measurement. As the emission wavelength increases, the activity of different fluorophore populations are shown by the changes in center lifetime and the width of distribution. At shorter wavelengths the emission largely occurs from smaller aromatics with relatively large HOMO-LUMO band gaps where energy transfer is the dominant mechanism. The center lifetime and distribution width vary with emission wavelength in a manner similar to the curved response that has been discussed for average lifetime values. A balance point between energy transfer and quenching processes is shown where the FWHM values reach a plateau. As the emission wavelength increases further (beyond 600 nm), collisional quenching becomes the dominant mechanism of larger aromatics emitting in this band leading to a reduction in lifetime (not shown). A reduction in FWHM follows from this lifetime change.

Tables 3.7 and 3.8 compare the values of distribution width across all the oils in both batches, calculated from data obtained for the 542-582 nm emission band. The distribution widths presented are the average results from fitting of a single decay distribution model (including the long dummy lifetime) to the phase and modulation data. High API gravity oils yield the widest distributions and in contrast heavy oils show a narrow range of lifetimes. If the distribution is taken as an indication of amount of fluorophores emitting at the 542-582 nm emission band, then this would indicate that there light oils have a greater population of emitting fluorophores than for heavy oils. In heavy oils more quenching and energy transfer leads to less fluorophores actually emitting. Oil 7633 stands out as having a wide distribution for both Gaussian and Lorentzian models, despite having an API gravity of 24. This API value almost classifies it as a heavy oil, yet a long lifetime and a large distribution width are found. Looking at the chemical properties in Chapter 2, this oil has a high wax content and contains a low concentration of heavy aromatic molecules. The wax acts to dilute the oil, which leads to longer lifetimes. Less heavy aromatics mean that energy transfer and quenching effects are reduced which also leads to a longer lifetime. Due to the same reasons, a greater population of emitting fluorophores yield a larger distribution width.

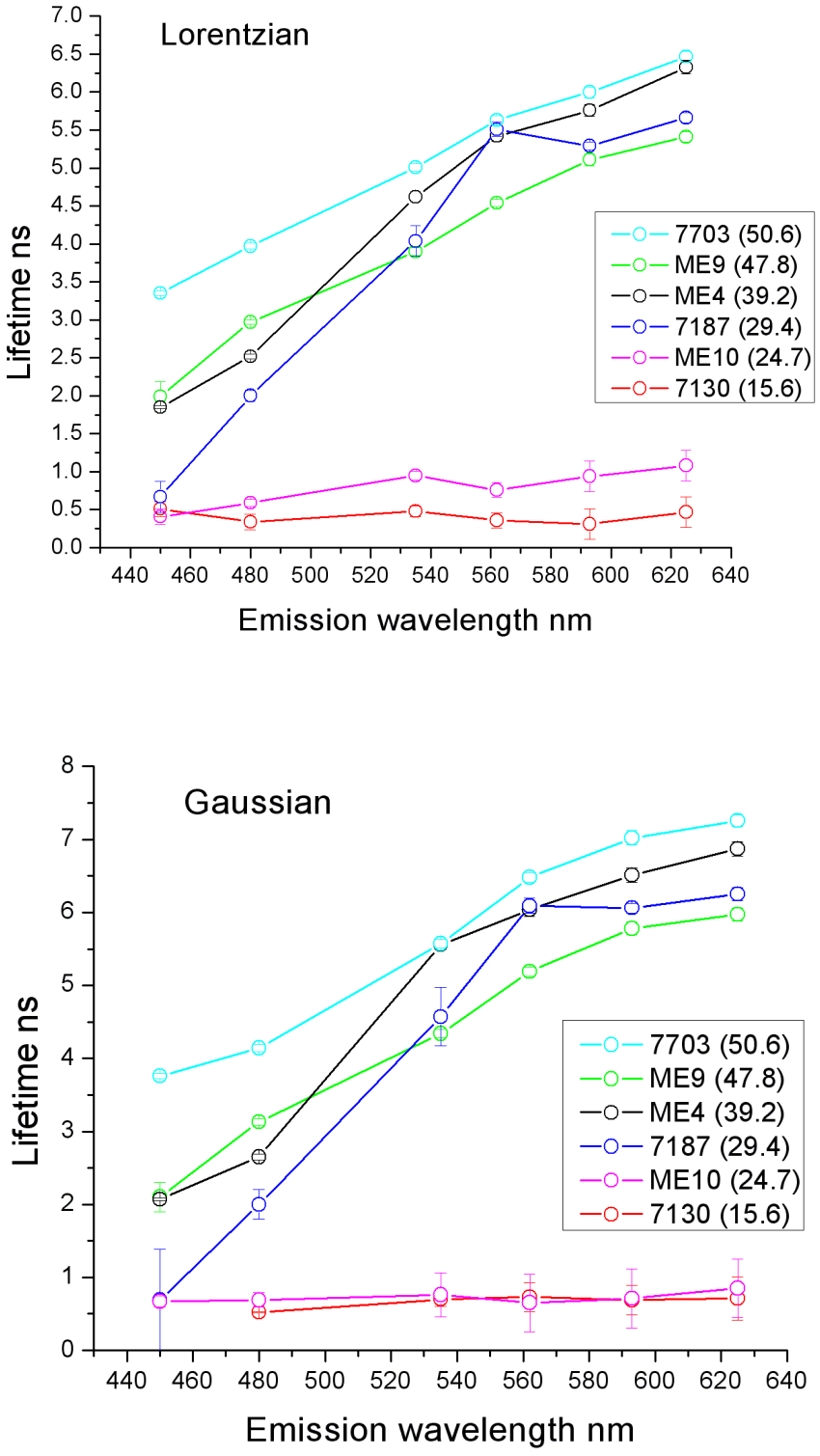

Figure 3.25: *Lifetimes calculated from single distributions for selected oils. API gravities are given in brackets. Error bars on the lifetime are also shown. Oils ME10 and 7130 are poorly fitted and lifetimes omitted at longer wavelengths could not be calculated.*

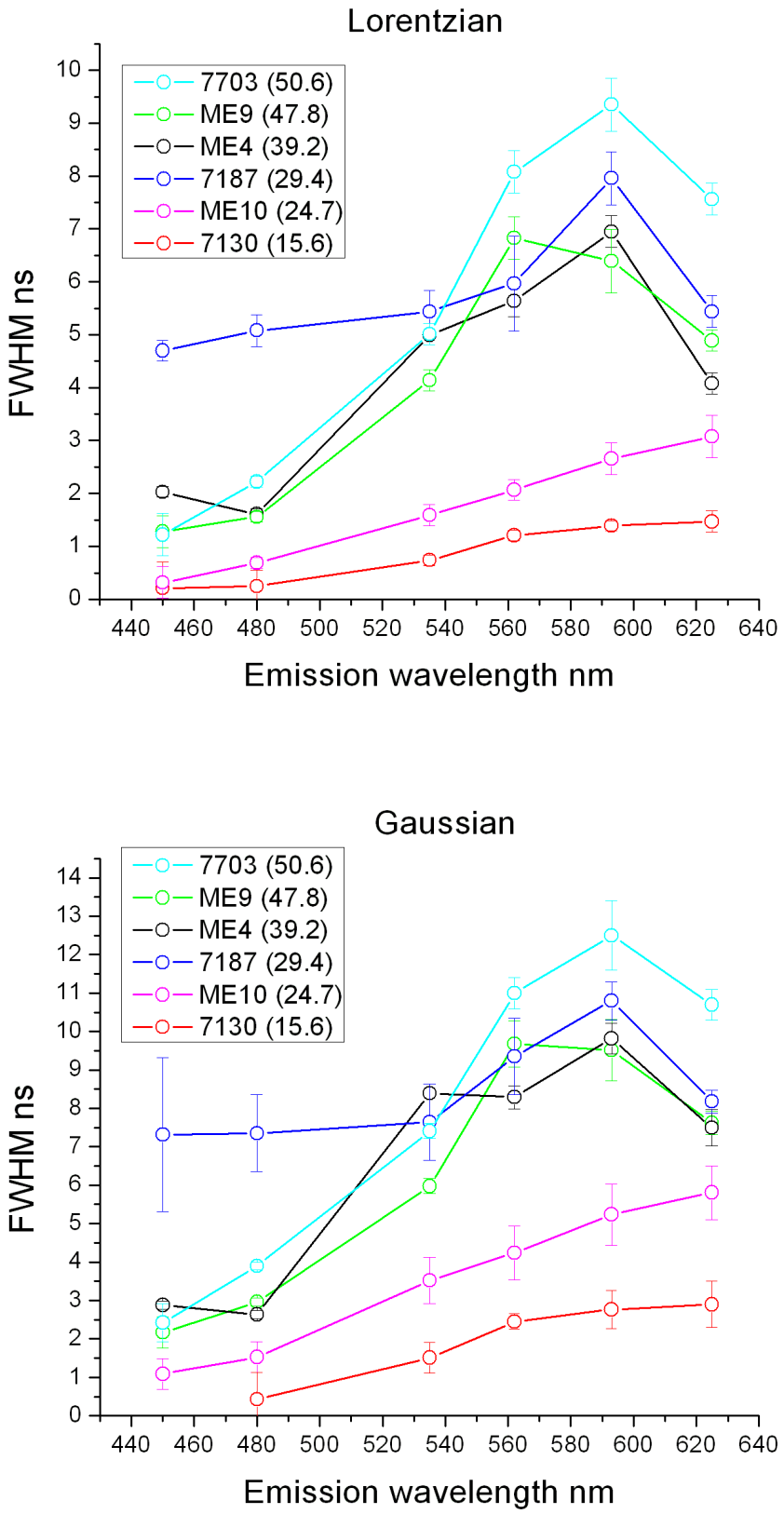

Figure 3.26: *FWHM calculated from single distributions for selected oils. API gravities are given in brackets. Error bars on the lifetime are also shown. The width for oil ME10 could not be calculated due to poor fitting.*

Table 3.7: *Full width half maximum values (in nanoseconds) for Batch* 1 *oils. Single decay term Gaussian and Lorentzian distributions calculated from data recorded at the* 542-582 *nm emission band (the data presented is an average of three experiments). The error in the distribution width is given in brackets.*

Oil	API	Gaussian	Lorentzian
7703	50.6	11.0 ± 0.40	8.08 ± 0.40
7197	45.1	13.1 ± 0.55	9.78 ± 0.47
7098	44.6	10.91 ± 0.57	7.61 ± 0.57
7058	40.1	11.43 ± 0.60	8.45 ± 0.48
7086	39.9	10.38 ± 0.66	7.43 ± 0.45
7090	36.8	11.9 ± 1.0	7.55 ± 0.40
7193	36.0	8.14 ± 0.39	5.89 ± 0.28
7062	36.0	5.10 ± 1	3.10 ± 0.4
7186	34.3	9.16 ± 1.0	5.93 ± 0.90
7632	32.7	10.54 ± 0.3	5.64 ± 0.6
7324	32.3	7.5 ± 0.7	4.50 ± 0.2
7093	30.9	8.51 ± 0.5	5.67 ± 0.3
7187	29.4	9.35 ± 1.0	5.97 ± 0.90
7633	24.8	12.1 ± 0.5	8.28 ± 0.9
7169	21.6	3.97 ± 0.7	2.52 ± 0.3
7032	19.1	2.15 ± 0.5	1.06 ± 0.1
7130	15.6	2.45 ± 0.2	1.21 ± 0.1
7321	14.1	1.96 ± 0.4	0.95 ± 0.1
7188	13.3	2.49 ± 0.5	1.32 ± 0.1
7033	12.8	1.34 ± 0.2	0.79 ± 0.1

Table 3.8: *Full width half maximum values (in nanoseconds) for Batch 2 oils. Single decay term Gaussian and Lorentzian distributions were calculated from data recorded at the 542-582 nm emission band. The error on distribution width is given in brackets.*

Oil	API	Gaussian	Lorentzian
ME9	47.8	9.68 ± 0.6	6.83 ± 0.4
ME8	44.2	10.70 ± 0.4	7.90 ± 0.4
ME5	44.1	7.59 ± 0.4	4.51 ± 0.3
ME7	42.1	8.81 ± 0.4	5.76 ± 0.4
ME6	39.6	8.35 ± 0.4	4.87 ± 0.2
ME4	39.2	8.29 ± 0.3	5.64 ± 0.3
ME1	32.7	7.86 ± 0.4	5.54 ± 0.3
ME3	30.8	6.48 ± 0.3	5.15 ± 0.2
ME2	28.9	6.64 ± 0.5	4.12 ± 0.2
ME10	24.7	3.49 ± 0.5	2.57 ± 0.2

The next step is to analyse the variation of the single distribution lifetimes and widths with the physical and chemical properties of the oils.

3.6 Correlations between Photophysical parameters and Crude Oil Chemical Data

Part of the original objective of this work was to develop a quantitative model for analysing crude oils. Since the fluorescence of crude oils is strongly influenced by chemical composition, it follows that correlations between lifetime/distribution width and chemical properties should be investigated. The data from the individual batches of crude oils must be treated separately as the SARA bulk chemical data for each batch comes from a different testing regime. The topped oils (Figure 3.5) were also removed due to fact that these oils were heated to remove the volatile fraction. Previous studies [131] have showed that there was a positive linear correlation between intensity based average fluorescence lifetime and API gravity but with a high degree of scatter. Average lifetimes determined by the FD method also follow

a linear trend with API gravity as shown in Figure 3.27 where the TD lifetimes are generally longer than the FD lifetimes. For both oil batches there is a similar degree of scatter. A similar set of plots are obtained using data recorded from the full emission wavelength range (i.e. 426-477 nm, 465-500 nm, 510-560 nm, 542-582 nm, 573-613 nm and 575-650 nm). However, it has been shown earlier that the largest distribution of lifetimes is found in the 542-582 nm range. In addition, it was determined that the TCSPC average lifetimes recorded in the 540 nm emission range also gave the best correlations (in terms of r^2 values) to the bulk oil composition parameters[131]. Taking these points into account, all further analysis is made using data from the 542-582 nm emission wavelength range.

Figure 3.28 shows a poor relationship between average lifetime from all the multiple decay models with % Alkane and Aromatic. Better fits with average lifetime have been obtained using the Corrected Alkane, Polar and Corrected Polar parameters (Figures 3.29 and 3.30 including the API gravity plot for the 542-582 nm emission wavelength range). In each of these figures, the data for the Discrete, Gaussian and Lorentzian models are overlaid in each plot. For the Polar and Corrected Polar plots, a non linear first order decay curve gives better correlation to the data than a linear fit. In all cases the fit line based on the Lorentzian model is given.

Table 3.9: *Correlation coefficients (r^2) associated with best linear fits for the Batch 1 crude oils recorded at* $542 - 582$ *nm as shown in Figures 3.29 and 3.30.*

Fitting method	Corrected Alkane	Polar	Corrected Polar	API gravity
Discrete	0.60	0.67	0.67	0.59
Gaussian	0.59	0.68	0.68	0.59
Lorentzian	0.60	0.66	0.67	0.59

The correlation coefficients (discrete model) from Figures 3.28 to 3.30 are given in Table 3.9. There is little improvement between the three multiple decay models (Discrete, Gaussian or Lorentzian). A similar table can be drawn up for the Batch 2 oils.

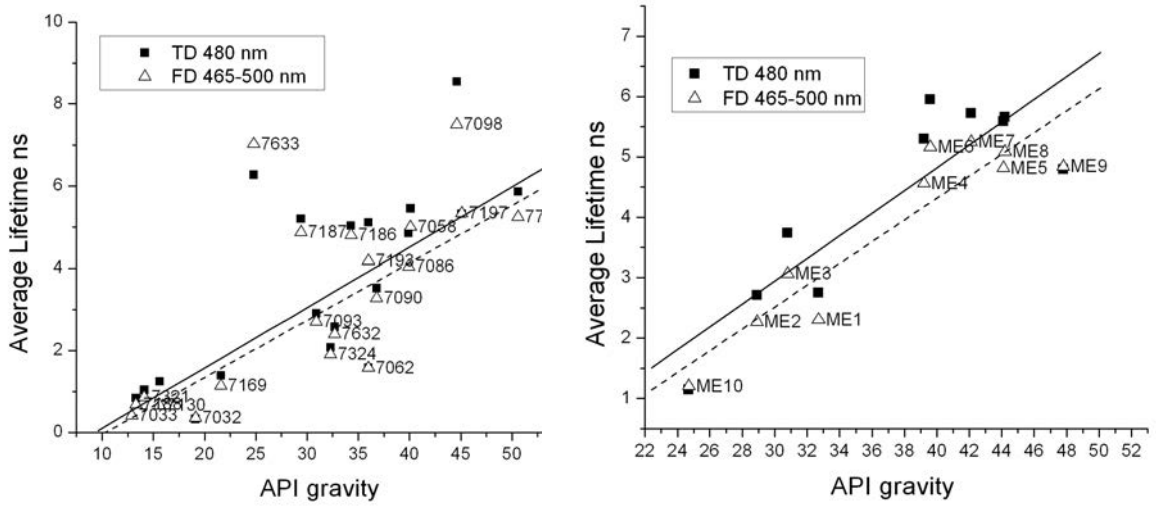

Figure 3.27: *Correlation between API gravity and TCSPC/FD average lifetimes for Batch 1 oils (left) and Batch 2 oils (right). All data was measured at an emission wavelength of* 480 *nm and average lifetimes were calculated using the discrete multiple decay model. Solid line: TD trend; Dashed line: FD trend.*

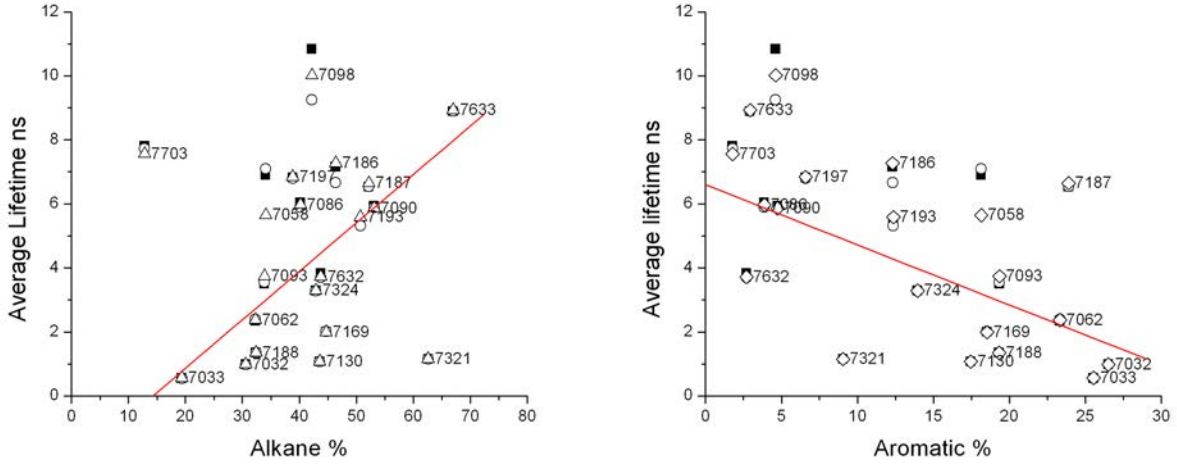

Figure 3.28: *Correlations between FD average lifetimes and gross chemical composition parameters (% Alkane and Aromatic) for* 20 *crude oils. Filled square: Discrete, Empty circle: Lorentzian, Empty diamond: Gaussian. Linear fit line to the Lorentzian data is shown (Alkane Plot* $r^2 = 0.41$*, Aromatic Plot* $r^2 = 0.39$*). Emission wavelength was* $542 - 582$ *nm*

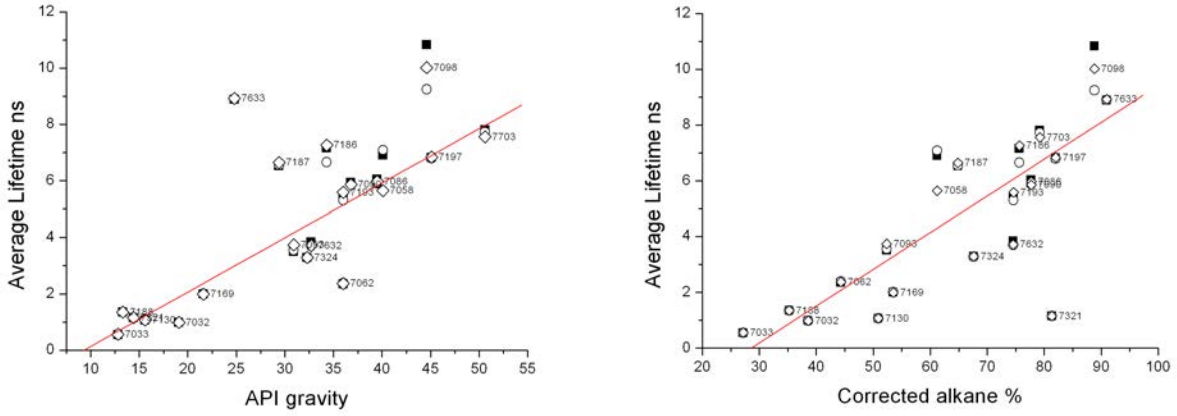

Figure 3.29: *Correlations between FD average lifetimes with corrected alkane% and API gravity for the Batch 1 crude oils. Filled square: Discrete, Empty circle: Lorentzian, Empty diamond: Gaussian. The regression lines are based on the Lorentzian average lifetimes. Emission wavelength was* $542 - 582$ *nm.*

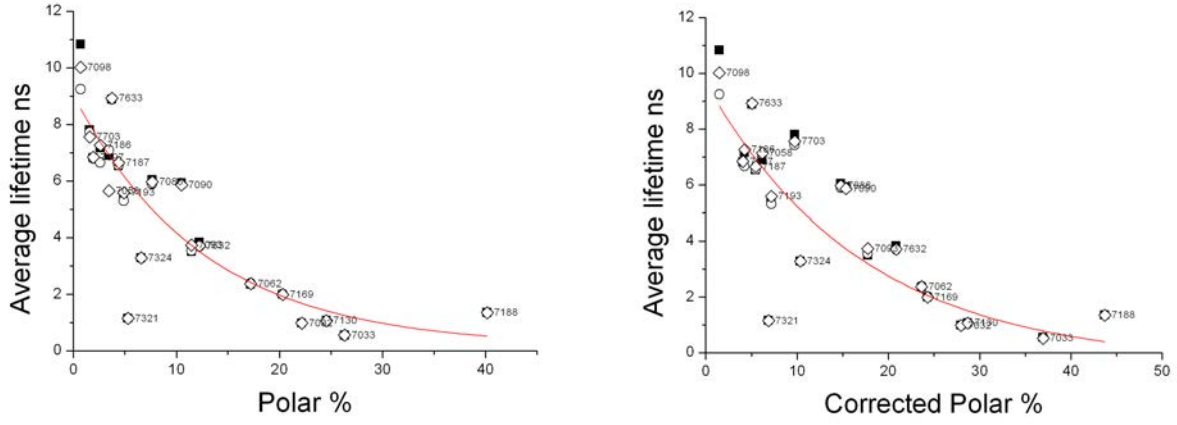

Figure 3.30: *Correlations between FD average lifetimes with % Polar and Corrected Polar% for the Batch 1 crude oils. Filled square: Discrete, Empty circle: Lorentzian, Empty diamond Gaussian. The regression lines are based on the Lorentzian model average lifetimes. Emission wavelength was* $542 - 582$ *nm.*

In Table 3.10, the correlations to the same chemical parameters and API gravity are shown for comparison with the Batch 1 oils. The accompanying plots with API gravity and Corrected Alkane are shown in Figure 3.31. The Batch 2 oils are more closely correlated to API gravity and Corrected Alkane than the Batch 1 oils but Polar and Corrected Polar plots are not as strongly correlated.

Table 3.10: *Correlation coefficients (r^2) associated with best linear fits between the chemical parameters and the FD average lifetimes for the Batch 2 crude oils. Emission recorded at 542–582 nm as shown in Figures 3.31.*

Fitting method	Corrected Alkane	Polar	Corrected Polar	API gravity
Discrete	0.75	0.49	0.52	0.77
Gaussian	0.63	0.41	0.43	0.65
Lorentzian	0.76	0.51	0.53	0.81

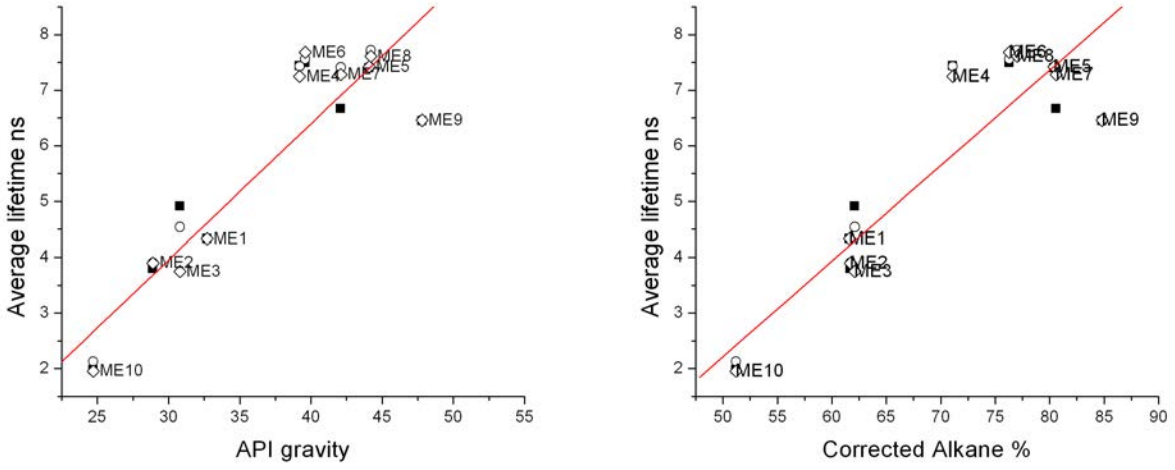

Figure 3.31: *Correlations between FD average lifetime and API gravity and % Corrected Alkane for Batch 2 crude oils. Filled square: Discrete, Empty circle: Lorentzian, Empty diamond: Gaussian. The regression lines are based on the Lorentzian model average lifetimes. Emission wavelength was* $542-582$ *nm.*

3.6.1 Correlations made with data obtained from distribution models

The center lifetime of and width of a lifetime distribution are obtained when fitting the phase and demodulation data to either a Gaussian or Lorentzian distribution model. These parameters can also be plotted against the chemical properties and API gravity. Figure 3.32 shows the trend of center lifetime with API gravity and % Polar based on both the distribution models. A linear model can be used to show the API gravity trend and an exponential model is used for the Polar plot. In both cases a high degree of scatter is found.

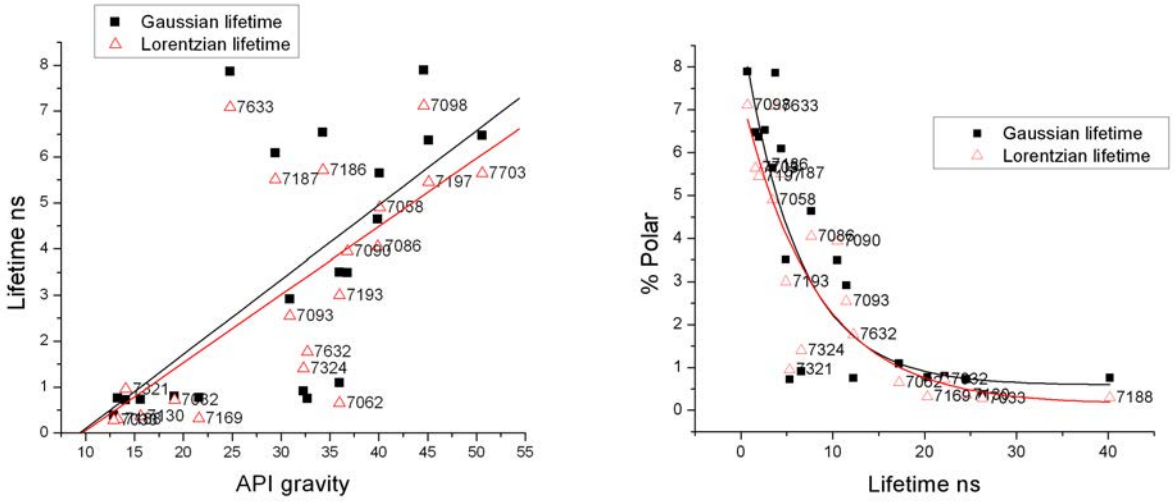

Figure 3.32: *Left figure: Correlation between API gravity and the center of a lifetime distribution for Batch 1 oils. Black line: Gaussian linear fit, Red line: Lorentzian linear fit. Right figure: Variation of center lifetime with % Polar for Batch 1 oils. A non-linear least squares fit of an exponential decay model was used to show the trend (Black: Gaussian Red: Lorentzian). For both plots an emission wavelength of* $542 - 582$ *nm was used.*

Along with the center lifetime of the distribution, the width of the distribution varies with API gravity as shown by Figures 3.33 and 3.34. For the Batch 2 oils from a similar geographical area, the degree of scatter does not reduce when compared to the plot for Batch 1 oils. The correlation coefficients from these plots are compared in Tables 3.11 and 3.12. In some cases, no discernable trend in the data was ascertained and highlighted as DNF in the table. In comparison to the correlations shown in Tables 3.9 and 3.10, there is no general improvement by using the center lifetime or

distribution width. However, the best correlation of all the models is found between the distribution width and API gravity, where r^2 is 0.86.

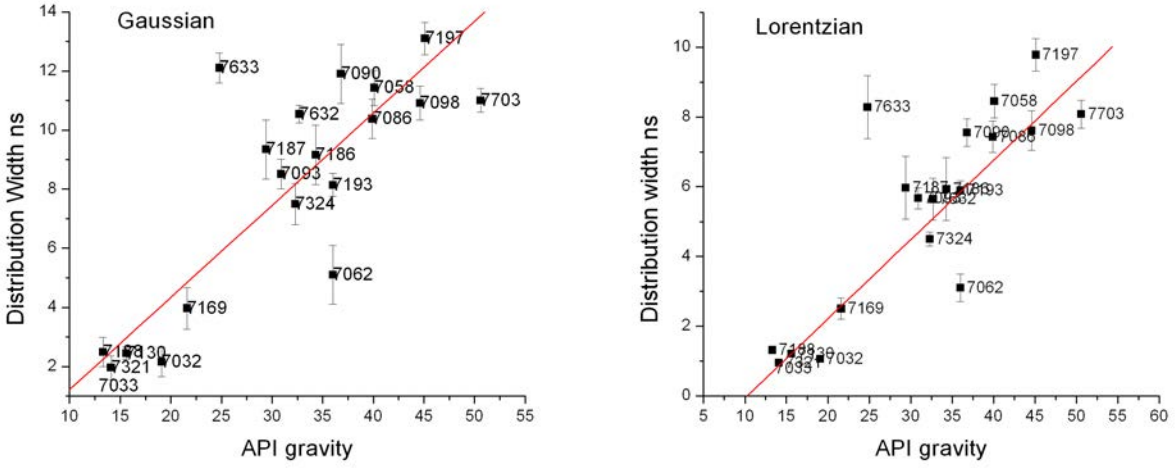

Figure 3.33: *Variation of the width of lifetime distribution with API gravity for Batch 1 oils. Left: Gaussian distribution, Right: Lorentzian distribution. Emission wavelength was* $542 - 582$ *nm. Also shown are the error bars on the width value in ns.*

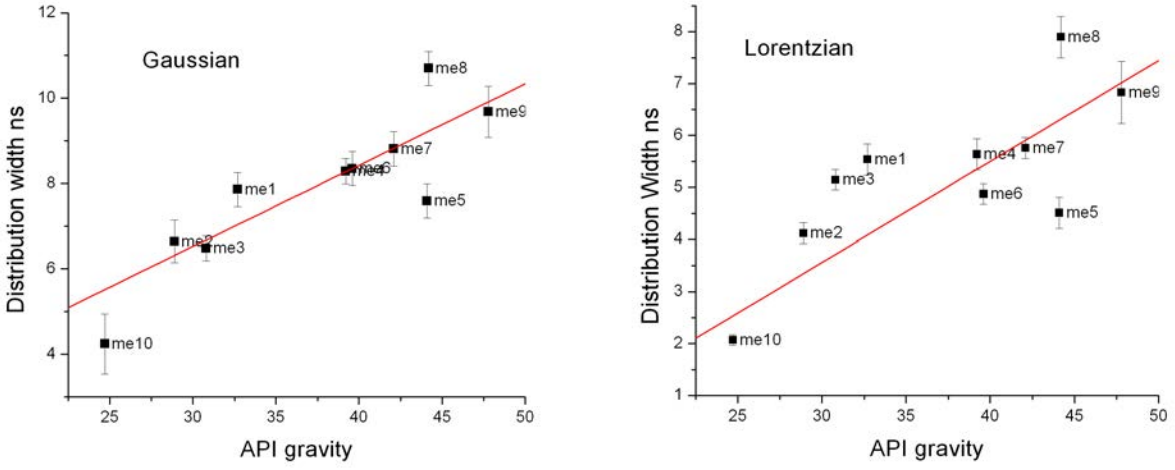

Figure 3.34: *Variation of the width of lifetime distribution with API gravity for Batch 2. Left: Gaussian distribution, Right: Lorentzian distribution. Emission wavelength was* $542 - 582$ *nm. Also shown are the error bars on the width value in ns.*

Table 3.11: *Correlation coefficients (r^2) associated with best fits of center lifetime and distribution width to gross chemical compositional parameters and API gravity for the Batch* 1 *crude oils recorded at* 542–582 *nm. DNF indicates that no discernable trend was ascertained.*

		Center Lifetime		Dist. Width	
Model Parameter	Fit	Gaussian	Lorentzian	Gaussian	Lorentzian
API	Linear	0.45	0.47	0.66	0.86
Corrected Polar	Exponential	0.68	0.70	0.52	0.54
Corrected Aromatic	Linear	DNF	DNF	DNF	DNF
Corrected Alkane	Linear	0.47	0.56	0.56	0.54
Polar	Exponential	0.75	0.76	0.59	0.63
Aromatic	Linear	DNF	DNF	0.45	0.42
Alkane	Linear	DNF	DNF	DNF	DNF

Table 3.12: *Correlation coefficients (r^2) associated with best fits of center lifetime and distribution width to gross chemical compositional parameters and API gravity for the Batch* 2 *crude oils recorded at* 542–582 *nm.*

		Center Lifetime		Dist. Width	
Model Parameter	Fit	Gaussian	Lorentzian	Gaussian	Lorentzian
API	Linear	0.63	0.72	0.69	0.75
Corrected Polar	Exponential	0.62	0.60	0.64	0.58
Corrected Aromatic	Linear	0.59	0.73	0.66	0.46
Corrected Alkane	Linear	0.64	0.75	0.68	0.46
Polar	Exponential	0.60	0.57	0.64	0.59
Aromatic	Exponential	0.59	0.72	0.72	0.5
Alkane	Linear	0.64	0.77	DNF	DNF

3.6.2 Explanation of outliers in correlation plots

The preceding correlation plots showed that most oils followed a linear trend with API gravity. Figure 3.27 shows two oils that lie outside this trend and are worth extra consideration. Both oils have high alkane content which is responsible for the long average lifetimes obtained. Yet oil 7703 has also a high alkane content but lies along the API gravity trend-line. A test that may explain these long lifetimes is the Colloidal Instability Index (CII) [28, 191][§]. This index has origins in screening crude oil SARA fractionation data for unstable oils that are prone to precipitation and deposition of the asphaltene fraction on extraction from the reservoir. The Colloidal Instability Index (CII) considers the crude oil as a colloidal solution made up of the components: Saturates, Aromatics, Resins, and Asphaltenes. The CII is defined as the ratio of the sum of the Asphaltene and Saturate fractions to the sum of the Polar and Aromatic fractions. Although a different method (ASTM D2007-93) was used to calculate the SARA fractions and develop the CII, it has been applied to the Batch 1 crude oil SARA data.

Figures 3.35 and 3.36 shows that there is a definite connection between the CII factor and the average lifetime (in this case the Discrete average lifetime). Comparisons are made to both the 465-500 and 542-582 nm emission bands showing that the CII trend follows a similar pattern at different emission wavelengths. All the low API gravity, short lifetime oils have a low CII factor, which increases as the oil API gravity increases. The main importance here is that the CII test also differentiates oils 7633, 7098 (as shown already in the API gravity plot). The low polar content can be used as a reason for longer lifetimes (less quenching) but there are many oils in Batch 1 that have similar or even less polar fractions but these oils do not show 'unstable' behaviour. For oils such as 7633 and 7098, the Asphaltene fraction may be kept out of solution as a colloid leading to less quenching and longer fluorescence lifetimes. Oil 7321 also stands out as a possible 'unstable' oil, and stands out as an outlier in the Corrected Alkane, Polar and Corrected Polar plots in Figures 3.29 and 3.30.

[§] The original purpose of this index was to provide a means to determine if a crude oil would be prone to Asphaltene precipitation. According to Asomaning, a value of 0.9 delineates high ratios from low ratios and thus enabling differentiation between oils likely to precipitate and those not likely. Oils with high CII factors are termed as 'unstable' meaning that Asphaltenes are likely to precipitate. [28, 191]

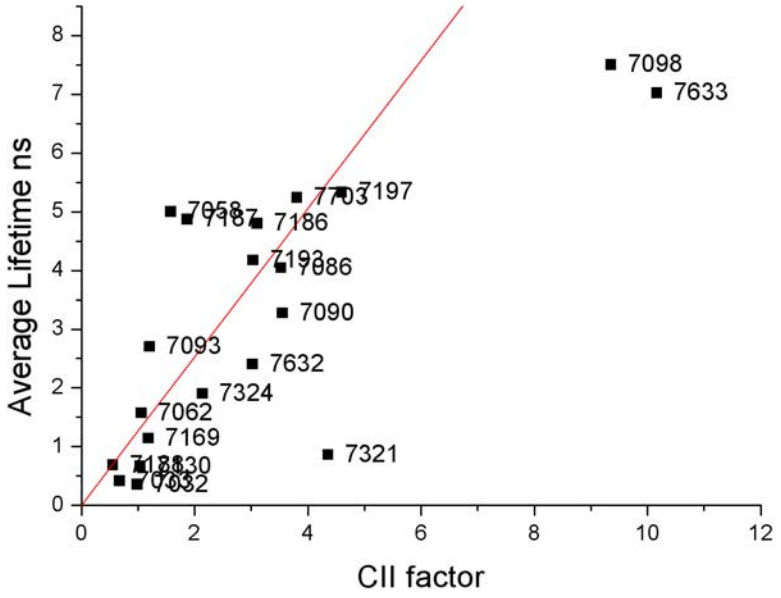

Figure 3.35: *Trend between the Colloidal Instability Index (CII) and Discrete average lifetimes (FD) calculated for Batch* 1 *oils (*465-500 *nm emission).*

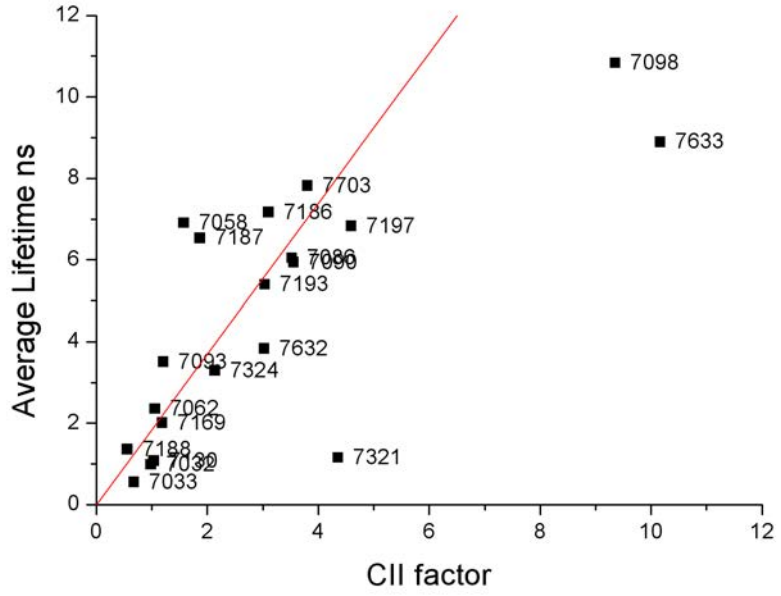

Figure 3.36: *Trend between the Colloidal Instability Index and Discrete average lifetimes (FD) calculated for Batch* 1 *oils (*542-582 *nm emission).*

3.7 Geological trends

The crude oils of Batch 1 were supplied with data about their geological source age, rock type, and trends could be shown by grouping crude oil lifetimes in terms of these geological parameters. (Tables 2.1 and 2.3). As described in Chapter 1, maturation of crude oils is considered to involve cracking, isomerization and aromatisation reactions, as well as alkylation and dealkylation of aromatic rings [7, 13]. The degree of oil maturity is based on the distribution and abundance of saturated and aromatic hydrocarbons and is defined in terms of early, middle and late maturity generally corresponding to heavy, medium and light oils [13]. Using the discrete fitting model, the FD lifetimes versus emission wavelength plots give an indication of this diversity (Figure 3.37). These plots show the lifetime-emission wavelength plots for Batch 1 oils, classified in terms of maturity. Note that oil 7321 did not have a maturity classification and was not included. In general, an older oil has longer maturation time and should have higher API gravity values and longer lifetimes. As shown in Figure 3.37, this statement is over-simplified and crude oils within a particular maturity classification are very diverse in terms of composition leading to a wide range of fluorescence lifetimes. Early maturity oils have API values from 12 to 34 with lifetime values ranging from sub nanosecond to 6 ns. The lifetime is affected by the degree of bio-degradation as shown by the oil 7169 and 7188. These oils both have middle range API values, yet lifetimes are comparable to the heaviest oils. Also oils 7187, 7632, and 7186 have API values and lifetime values that indicate middle maturity yet they are classified as early maturity oils. The main bulk of the oils fall into the middle maturity category, which spans a large API range from 24 to 45. The middle maturity grouping spans a large range of lifetimes (1-8 ns) and the lifetime-emission wavelength trends are more consistent. As stated in preceding chapters, oil 7633 stands out as an outlier - it has been designated a middle maturity oil yet the lifetime observed is higher than the rest of the middle mature oils due to the relatively high proportion of alkanes. The lightest oils 7703 and 7098 fall into the late maturity classification. Both are light oils of high mobility and since oil 7098 has less polar compounds it has longer lifetimes than oil 7703. From these plots it can be seen that lifetime-emission wavelength plots cannot be used to discriminate oils based on maturity alone.

Another way to display the lifetime emission wavelength trends is to give the lifetime trends in terms of source age starting from the youngest (tertiary - 42 million years old) to the oldest (jurassic - 61.5 million years old) ages (Figure 3.38). Note that source age information was not available for all oils and hence these oils are excluded. For the oldest oils originating in the Tertiary period, there is a distinction between low and high polar content and source rock type and bio-degradation. Oils 7186, 7187, and 7058 all come from a marine source containing Type III Kerogen, their Polar content is low ($\leq 4.4\%$), and they do not have bio-degradation. Oils 7188 and 7130 have opposing properties, containing a higher amount of polar compounds and bio-degraded. They also (perhaps incidentally) originated from a lacustrine environment. The correlation between lifetime and % Polar is clearly followed for the oils originating in the Cretaceous time period; longer lifetimes relating to low polar content. A similar pattern between lifetime and polar content is followed for the Jurassic grouping.

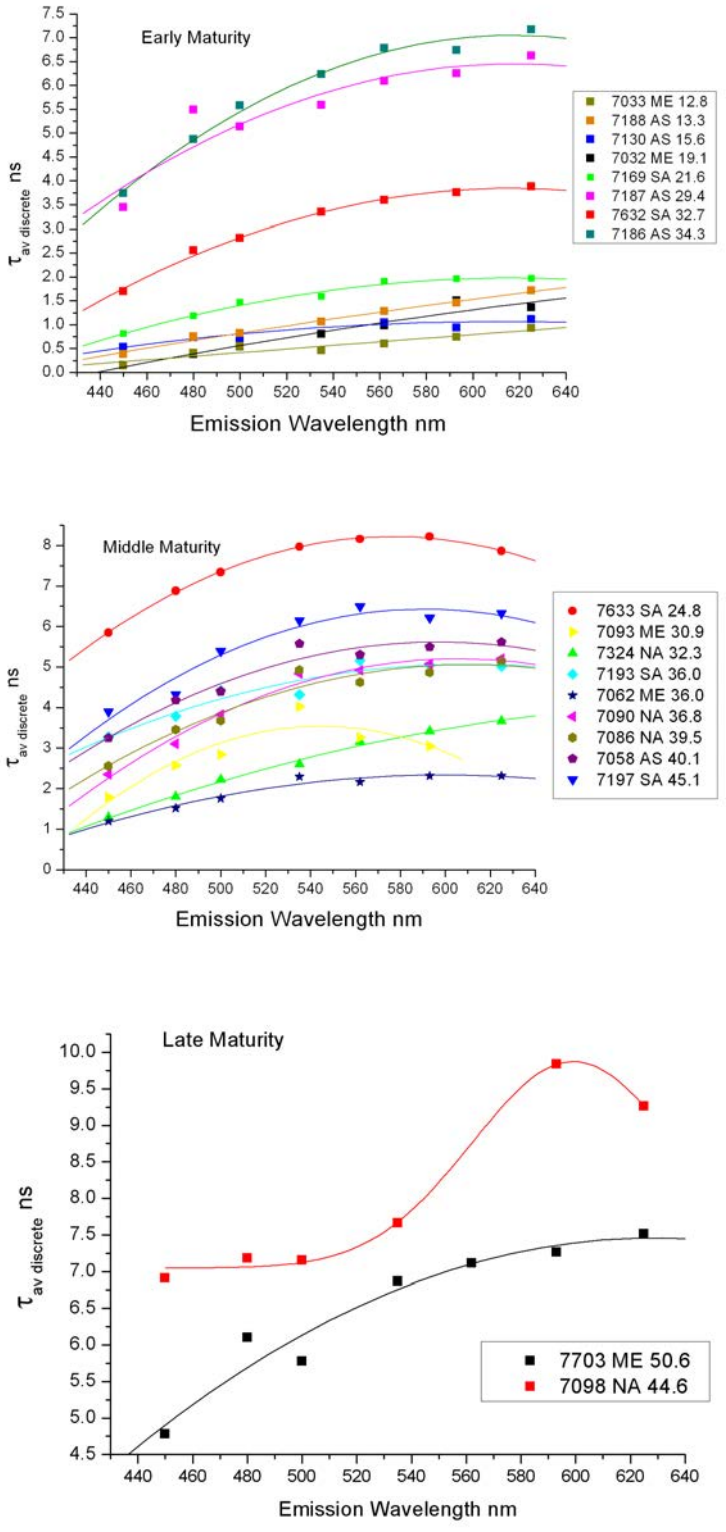

Figure 3.37: *Plots of average lifetime (using the FD discrete model) versus emission wavelength for oils grouped by maturity (as determined by Fugro Robertson). The legend gives details such as API gravity, the source age and the origin (ME: Middle east, AS: Asia, EU: Europe, NA: North America and SA: South America). Top: Early maturity; Middle: Medium maturity and Bottom: Late maturity.*

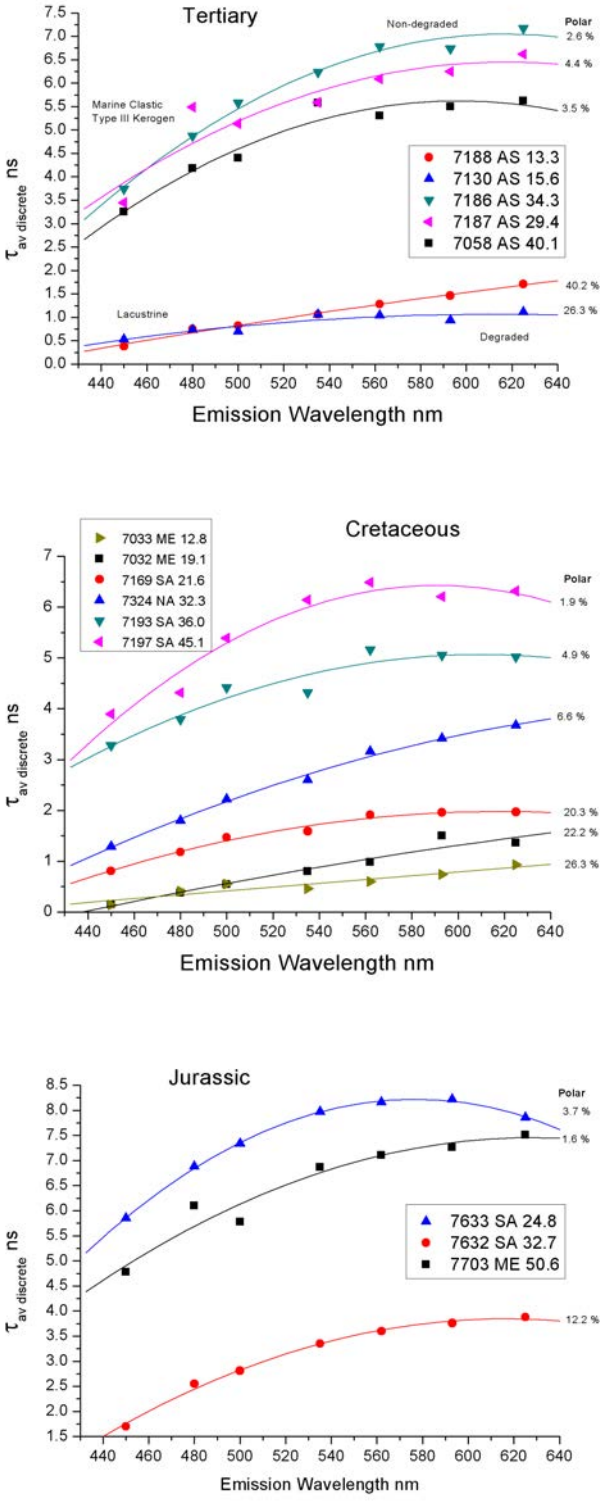

Figure 3.38: *Plots of average lifetime (using the FD discrete model) versus emission wavelength for different formation ages moving from the youngest to the oldest: Top: Tertiary, Middle: Cretaceous, Bottom: Jurassic (oldest formation age). The legend gives details such as* API *gravity and the source rock type.*

3.8 Conclusions

The value of lifetime determined by this fitting is highly dependent on the fitting model chosen. In practical terms, while collection times for both FD and TCSPC methods are comparable, the shorter acquisition times for single frequency phase and modulation measurements can be advantageous in imaging applications. Data fitting in this particular case of complex crude oils was on balance, found to be quicker for FD than for TCSPC, particularly for a model containing discrete decay terms. The TD lifetimes are found to be usually greater than those for FD. Comparisons between the three multiple decay models show that while the differences in lifetime are subtle, the discrete model outperforms the others in terms of speed of fitting and the closeness of the fit to the raw data. Yet for complex systems where one cannot resolve individual components, there can be a tendency to overfit the data. A guiding principle should be to fit the data to the simplest model possible. In the fluorescence emission of crude oils, the fitting of lifetime data should also follow this principle. During the course of the data analysis, we observed that most of the oils could be fitted to relatively simple single lifetime distributions. When quoting fluorescence lifetimes of complex fluids such as crude petroleum oils, one must specify precisely both the data acquisition method and the exact fit model.

The average lifetimes determined by the FD method vary with chemical parameters and API gravity. The large degree of scatter obtained with most of the plots is due to the large diversity of chemical composition of the oils studied. The correlation between lifetime and bulk chemical data was found to be independent of the three primary models used (Discrete, Gaussian and Lorentzian). In addition, single decay term distribution models can be used which can give values for the center lifetime of the distribution and the FWHM (or distribution width). These parameters vary with emission wavelength. The width of the distribution increase with emission wavelength and then reduces at longer wavelengths (at around 550 nm). As for the relationship between fluorescence lifetime and emission wavelength, this variation can also be attributed to the balance between energy transfer and quenching in the crude oil. The center lifetime and distribution width varies with API gravity and the best correlation is found using the Lorentzian model. Since crude oils exhibit a broad range of emitting fluorophores over a wide range of lifetimes, it follows that a

Lorentzian distribution that covers a large range of lifetime components would give a closer approximation to the true lifetime distribution.

Analysis of lifetime-emission plots in terms of source age can reduce overlap and expose correlation to polar content which may be promising for future work on HCFI (see Appendix C for details on the FD analysis of HCFI). However the sample size is small as source age data was not available for all oils and also the data from Batch 2 oils could not be included.

Chapter 4

Energy Transfer and Quenching processes in crude petroleum oils

Dilution of crude oils results in changes to the emission spectra and lifetime and by examining these changes, it is possible to study the effects of energy transfer and quenching processes. This chapter gives details of how dilution influences the effects of dilution on the fluorescence emission and lifetime of crude petroleum oils. It has long been recognized that dilution influences the physical and chemical properties of crude oils. The influence of dilution on emission spectra and fluorescence lifetime has been previously published [108, 124]. For the lifetime-dilution study [124], a two component decay model was used and the influence of dilution on the long lifetime component was discussed. Poor fits to the decay curves (χ^2 values of 2) were reported and overall a thorough treatment of the influence of dilution on the average lifetime value was not given. In this chapter, I expand on this by reporting the average lifetimes of neat and dilute crude oils and then using this data to study the effects of energy transfer and quenching. Preceding the discussion on fluorescence lifetime, the influence of dilution on emission spectra of the oils is explored. The findings in this chapter will serve as a precursor to the temperature based study in Chapter 5.

4.1 Crude oil dilutions and the influence of solvent

Each dilution was made by diluting the equivalent weight of 1 ml of oil (using the oil density values) with the appropriate volume of solvent. An example of the dilutions and conversion factors for oil 7197 is given in Table 4.1.

Table 4.1: *Dilutions and conversion factors based on Oil 7197.*

mg/L	factor	v/v	%
1.6×10^{5}	1:5	0.2	20
8×10^{4}	1:10	0.1	10
1.6×10^{4}	1:50	0.02	2
8×10^{3}	1:100	0.01	1
1.6×10^{3}	1:500	2×10^{-3}	0.2
8×10^{2}	1:1000	1×10^{-3}	0.1
160	1:5000	2×10^{-4}	0.02
80	1:10000	1×10^{-4}	0.01
16	1:50000	2×10^{-5}	0.002

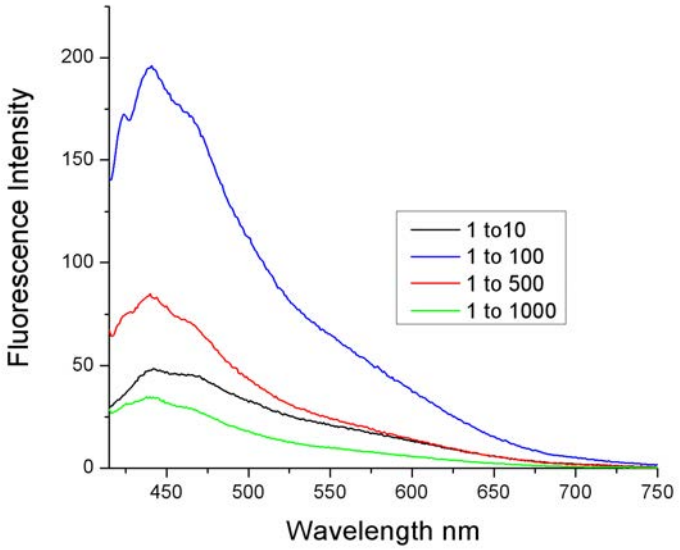

Figure 4.1: *Emission spectra (uncorrected) for the light oil* 7197 *over a range of dilutions in Toluene (non deoxygenated). An initial increase in fluorescence intensity is observed followed by a reduction at higher dilutions. Spectra recorded at* 405 *nm excitation using a Cary Eclipse spectrophotometer, with the oil held in a* 1 *mm path length quartz cell.*

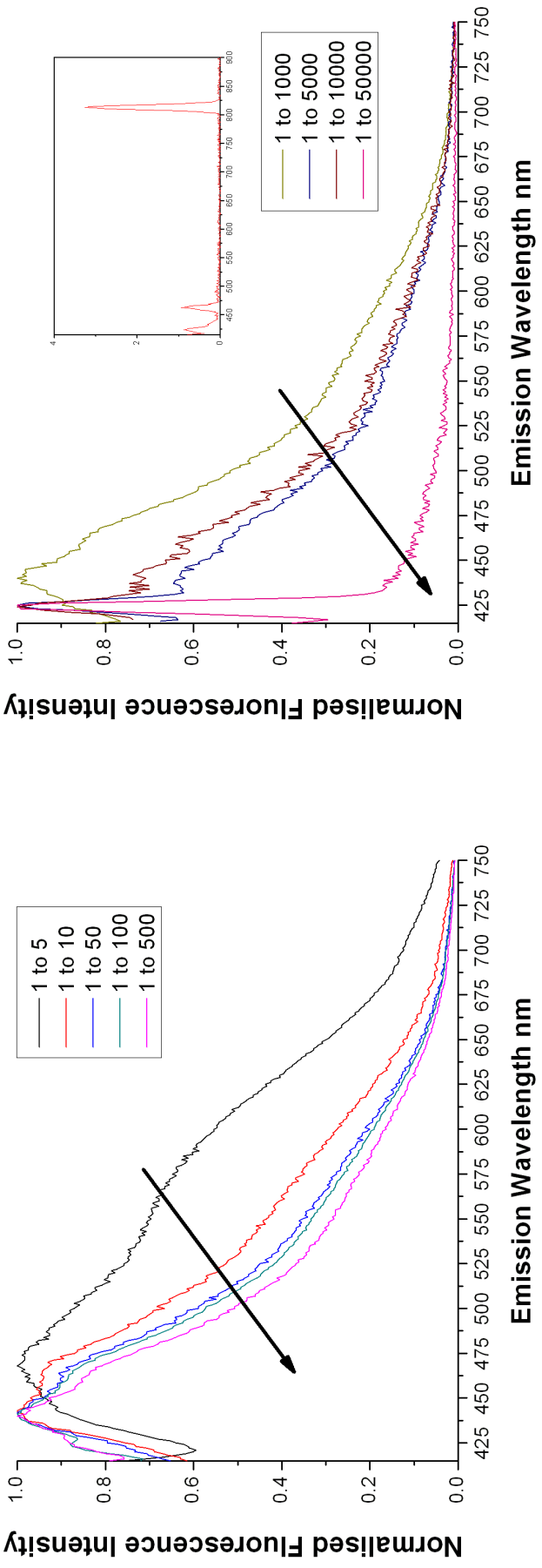

Figure 4.2: *Normalised emission spectra (uncorrected) for the light oil 7197 over a range of dilutions in non-deoxygenated toluene. The broad emission is gradually reduced as the dilution factor increases (direction of arrow). For very dilute oils Raman scattering becomes dominant over the weak fluorescence at dilutions of* $1:5000$ *and above. Inset graph shows the blank Toluene spectrum. Spectra recorded at 405 nm excitation on a Cary Eclipse spectrophotometer using a 1 mm path length quartz cell.*

Figure 4.1 shows the emission spectra for oil 7197 in Toluene. On initial dilution the fluorescence intensity is increased due to a reduction in energy transfer and quenching processes, for example, there is a $\sim 75\%$ increase in intensity from 1:10 to 1:100 dilution. Riveros *et al* [192] also found that on dilution, fluorescence intensity rises to a maximum value, and reduces at very low concentrations. At low concentrations, the reduction in intensity is simply due to the reduced amount of concentration of fluorophores.

A better way of examining the influence of dilution on energy transfer is to normalise the emission spectra to maximum intensity (Figure 4.2) [108, 193]. The emission spectrum shows an increasing blue shift in λ_{max} and decrease in emission bandwidth with increasing dilution due to a reduction in energy transfer processes. Above dilutions of 1:1000, the fluorophore concentration becomes very low, leading to a reduced fluorescence intensity and Raman scattering becomes large, relative to the emission peak. The inset graph of Figure 4.2 shows the spectrum of neat Toluene using 405 nm excitation. Filtering of the emission spectrum is adequate to remove first order Rayleigh scattering but weak C-H stretching peaks are shown occur at 423 and 464 nm. Second order Rayleigh scattering occurs at ~ 810 nm, beyond the emission range for crude oils. The choice of solvent for dilution studies of crude oils is an important consideration. The solvent should be non-fluorescent and have a reasonably low evaporation rate. We have used Hexane, Toluene and a 3:2 mixture of Methylcyclohexane and Methylcyclcopentane in these studies. The normalised spectra of two dilutions of the 'Connemara' crude oil* in non-deoxygenated toluene and hexane are compared in Figure 4.3. A large shift in the λ_{max} and reduction in FWHM for the 1:500 dilution is due to a reduction in energy transfer in the more diluted (1:500) oil. A small increase in the FWHM and an accompanying shift in the red edge of the emission spectrum for the 1:5 dilution of hexane is also found. Hexane has a lower viscosity than toluene [194, 195], thus having a higher rate constant for diffusion. Assuming that energy transfer is primarily diffusion-controlled in crude oils, then more energy transfer occurs in less viscous solvents which is shown by the red shift in the emission spectrum for hexane at high crude oil concentration. For more diluted oils, such as 1:500 as shown in Figure 4.3, energy transfer is at a

* This is a stand-alone medium oil that originated from the western approaches to Ireland (API = 35.5). This oil was considered as separate to the oils in Batches 1 and 2.

minimum and now the emission spectra overlap closely so that no distinction can be made between the two solvents.

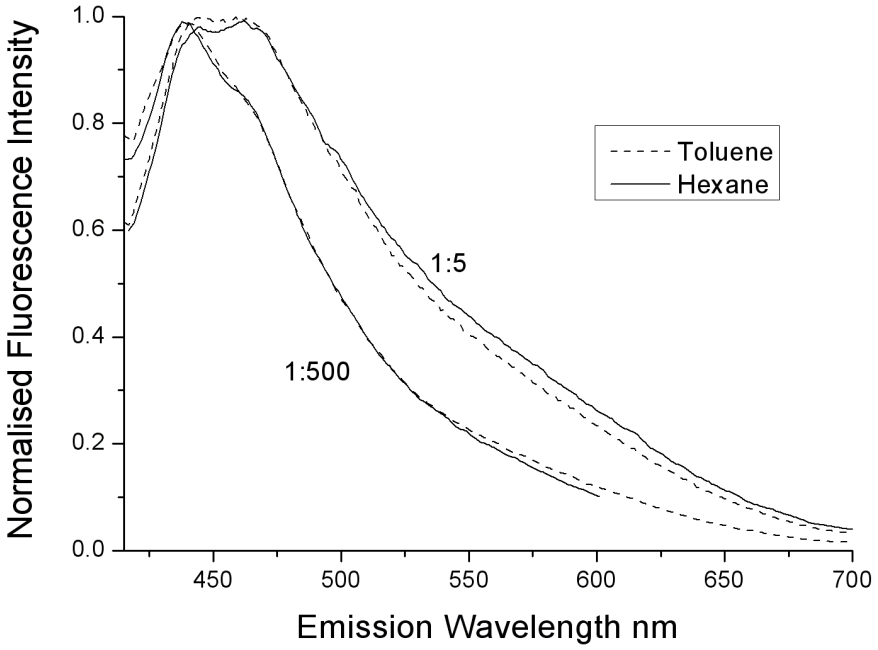

Figure 4.3: *Emission spectra (uncorrected) for Connemara crude oil at 1:5 and 1:500 dilutions in non-deoxygenated Toluene and Hexane. Spectra recorded at* 405 *nm excitation using a Cary Eclipse spectrophotometer, with the oil held in a* 1 *mm path length quartz cell.*

Removal of the highly efficient quencher, oxygen, also influences the emission spectra as shown by Figure 4.4. The increase in intensity gives a measure of the how much quenching is reduced. The top part of the figure shows the increase in fluorescence intensity as a result of deoxygenation of a 1:5 dilution of Connemara crude oil in hexane. It was found that the change in intensity is dependent on the concentration of the oil. Highly concentrated (such as the 1:5 dilution) oils show a greater change in fluorescence intensity on deoxygenation compared to lower concentrations such as 1:100 as shown in Figure 4.4. Removal of oxygen also results in an increased fluorescence lifetimes due to reduced quenching. The increase in lifetime on deoxygenation has already been discussed in Chapter 2 (Figure 2.20).

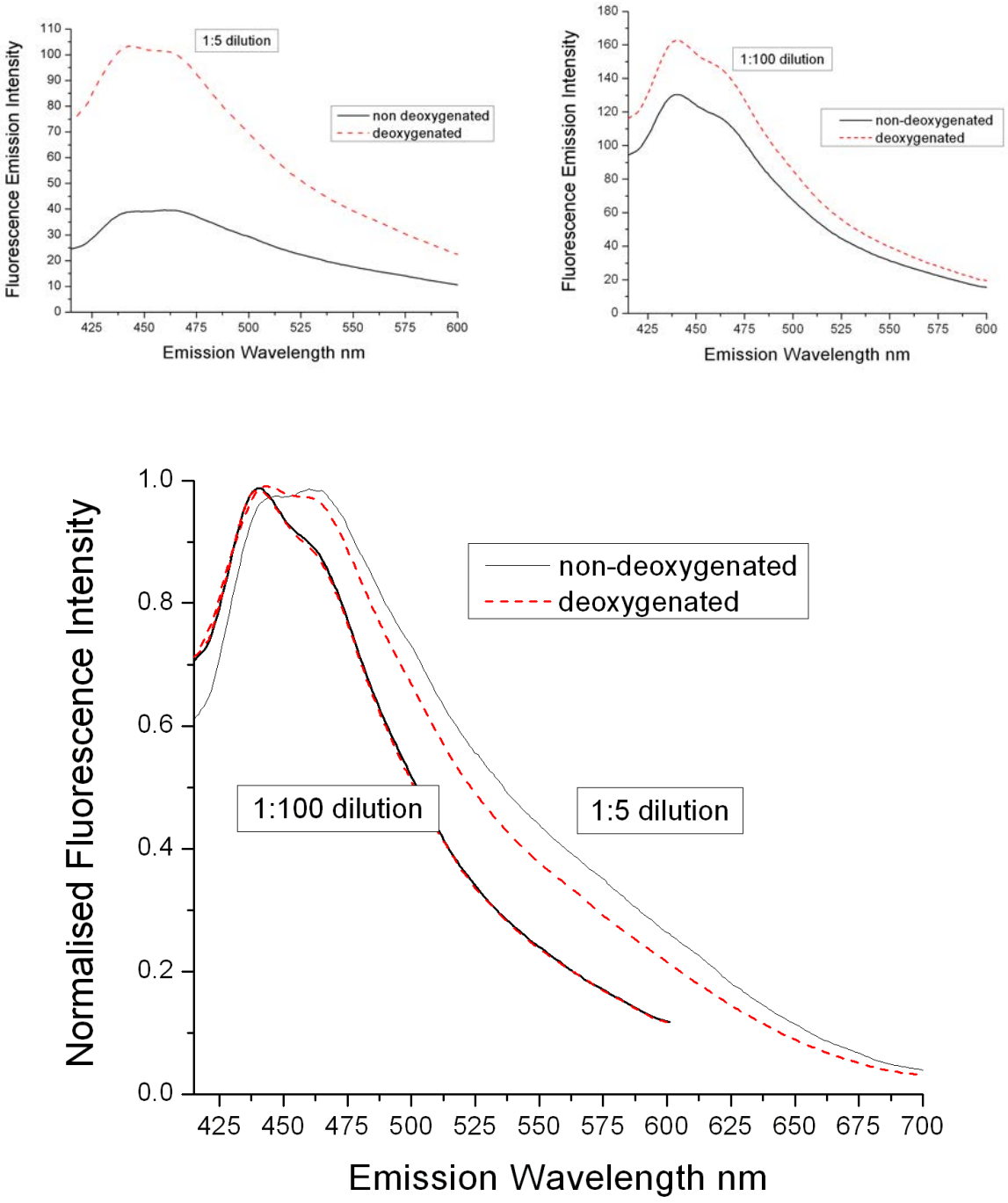

Figure 4.4: *Top: Emission spectra (uncorrected) for non de-oxygenated and deoxygenated Connemara crude oil at a 1:5 dilution. Bottom: The effect of deoxygenation for two dilutions 1:5 and 1:100 of Connemara crude oil in hexane. Spectra recorded at* 405 *nm excitation using a Cary Eclipse spectrophotometer, with the oil held in a* 1 *mm path length quartz cell.*

On dilution of crude oils, the fluorescence lifetime also increases due to a reduction in the energy transfer *and* quenching effects [124]. The relationship between energy transfer and quenching is dependent on the emission spectrum as different regions represent different populations of emitting fluorophores.

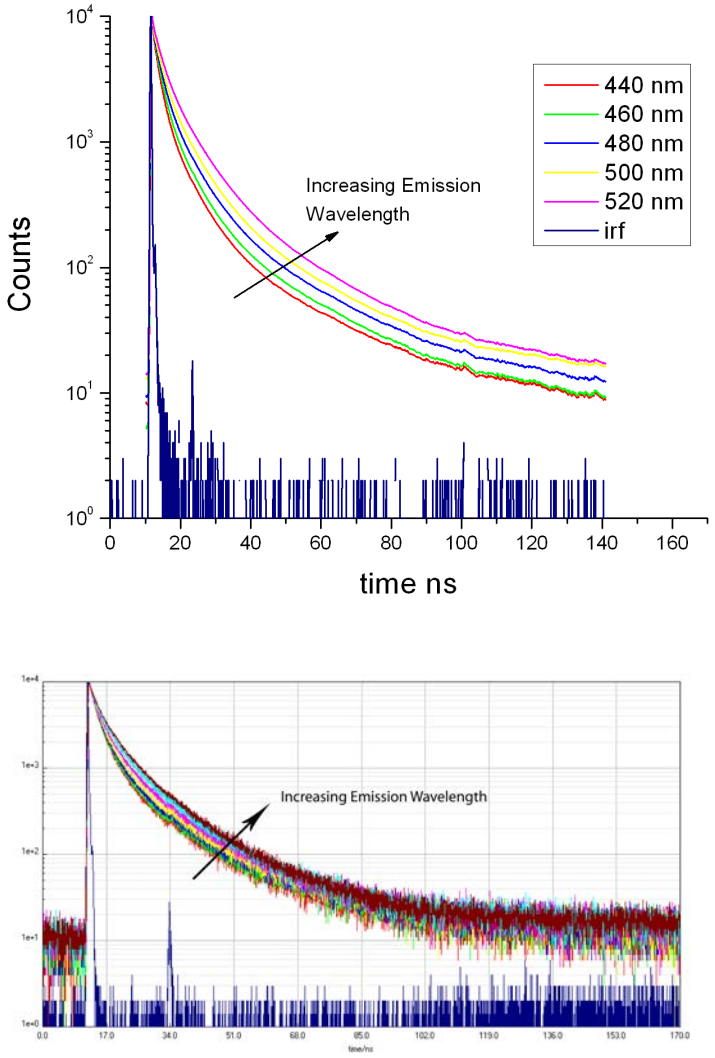

Figure 4.5: *Top: TCSPC decay curves (processed for better visualisation) for a light* neat *oil* 7058 *at different emission wavelengths, showing an increase in lifetime from 3.8 to 6.4 ns . Bottom: TCSPC decay curves for 1:100 dilution of oil* 7058 *in 3:2 MeCH:MeCP (deoxygenated) at different emission wavelengths from* 440 *nm (red trace) to* 560 *nm (brown trace) in steps of* 20 *nm where the average lifetime increases from 8.5 to 9.7 ns. At excitation wavelength of 405 nm was used for all measurements.*

Figure 4.5 shows the difference the TCSPC decay traces obtained for a light oil 7058, in neat (top) and dilute (bottom) forms. In the neat case, the average lifetime

increases from 3.6 to 6.4 ns with increasing emission wavelength. (440-520 nm). For the 1:100 dilution of the oil, average lifetimes of 8.5-9.7 ns are found between 440 and 560 nm.

The average lifetimes measured at 500 nm for the Connemara crude oil at a range of dilutions in hexane and toluene are listed in Table 4.2. Lifetime increases with increasing dilution in both solvents, but small but significant differences in the lifetime at the low (1:5 and 1:10) dilutions are found. As described above, toluene has a greater viscosity than hexane. Furthermore, oxygen solubility in toluene is less than hexane [196, 197]. The combination of higher viscosity and less dissolved oxygen leads to lower quenching rates which results in longer lifetimes. At lower concentrations (higher dilutions than 1:100), a point is reached where diluting further does not increase the lifetime (a limiting dilution) and there is no distinction between solvents.

Table 4.2: *Average lifetimes of crude oil 'Connemara' (API =35.5) diluted in non-deoxygenated Toluene and Hexane. Conditions: TCSPC decays recorded at room temperature using 405 nm excitation wavelength, 500 nm emission wavelength.*

Dilution factor	$\overline{\tau}_{Toluene}$ ns	$\overline{\tau}_{Hexane}$ ns
1:5	5.69	5.41
1:10	6.06	5.78
1:25	6.27	6.21
1:50	6.28	6.22
1:100	6.28	6.27
1:125	6.29	6.25
1:500	6.23	6.27
1:1000	6.26	6.19
1:2000	6.15	6.28
1:4000	6.21	6.26
1:5000	6.19	6.22

Table 4.3: *Average lifetimes of light crude oil 7197 diluted with Toluene and a 3:2 mixture of MeCH and MeCP (non deoxygenated). Conditions: TCSPC decays recorded at room temperature using 405 nm excitation wavelength, 500 nm emission wavelength.*

Dilution factor	$\overline{\tau}_{Toluene}$ ns	$\overline{\tau}_{MeCH:MeCP}ns$
1:10	6.50	6.56
1:50	6.73	6.68
1:100	6.71	6.66

For comparative purposes, the lifetime of oil 7197 in 3:2 MeCH:MeCP and toluene are given in Table 4.3. In this case, the light oil already has inherently less quenching and the lifetime reaches the limiting dilution at 1:50. For this light oil, no difference in lifetime is found between Toluene and the 3:2 MeCH:MeCP mixture. In general there were no significant differences in lifetimes when the oils were diluted in different non-deoxygenated solvents (Tables 4.2 and 4.3). Throughout this chapter, observations are made using emission spectra of crude oils diluted in two different solvents are given (Toluene or 3:2 MeCH:MeCP). This is justified as the lifetimes of crude oils diluted with different hydrocarbon solvents were found to be the same.

4.2 Energy Transfer and Quenching

As discussed above, the reduction in energy transfer by dilution can be shown by a blue shift in the emission spectrum. Figure 4.6 highlights how energy transfer is influenced by crude oil type. In this figure, the neat and diluted emission spectra of two representative oils (medium oil 7186 and heavy oil 7033) are shown. In the following examples, a 1:5000 dilution represents a limiting dilution in terms of where energy transfer is minimised. A blue shift of $\sim$ 8 nm between the neat and dilute spectrum is found. For heavy oils such as 7033, the emission spectrum shifts to the blue by a larger amount, in this case $\sim$ 60 nm showing that heavy oils are more heavily influenced by energy transfer effects.

A method was proposed by Downare *et al* [108] that determined the extent of energy transfer from the steady state emission spectra of dilute and neat oils which is outlined as follows. By numerically integrating the area under the normalised

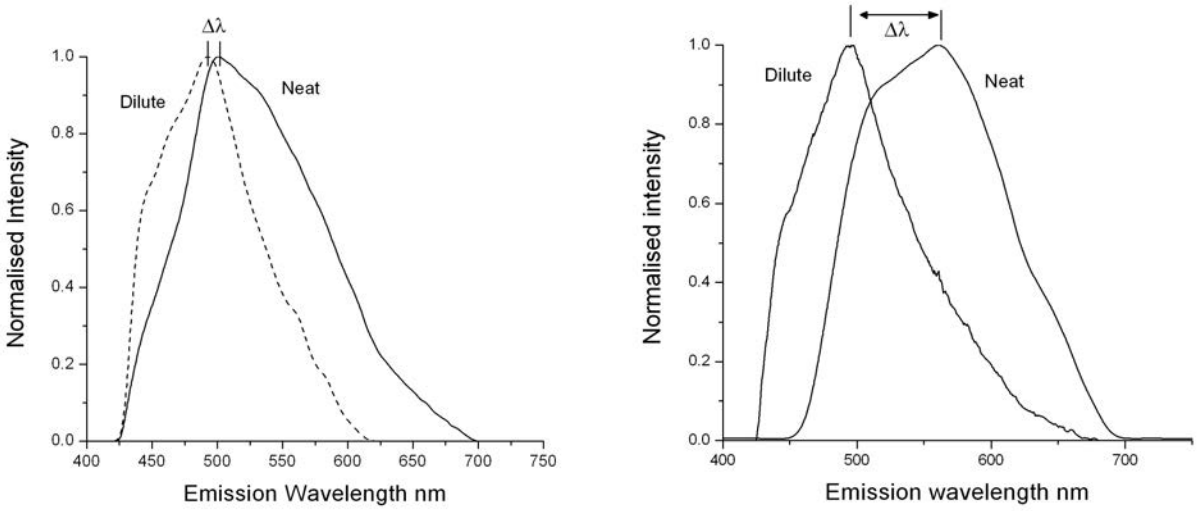

Figure 4.6: *Left: Normalised emission spectra for light oil* 7186 *from neat to dilute (1:5000) in 3:2 MeCH:MeCP. Right: Normalised emission spectra for heavy oil* 7033 *from neat to dilute (1:5000) in MeCH:MeCP (deoxygenated). A* $\sim$ 90% *change in fluorescence intensity from neat to dilute is shown. Excitation 405 nm; uncorrected spectra recorded by USB2000 spectrometer at 293K.*

emission spectra for the neat and the diluted oil, the following relationship can be used to calculate % Energy Transfer which was used to calculate the data in Table 4.4.

$$\%ET = \frac{AREA_{neat} - AREA_{5000}}{AREA_{neat}} \times 100 \tag{4.1}$$

Table 4.4: *% Energy transfer based on area of crude oil spectrum (determined using Equation 4.1. Excitation 405nm.*

Crude oil	API	λ shift (nm)	% Energy Transfer
7033	12.80	68.0	23.0
7130	20.78	65.2	20.78
7186	25.50	9.10	25.50
7197	45.1	27.56	26.14

The shift in the position of maximum wavelength indicates that the fluorescence emission from heavy oils is influenced to a greater amount by energy transfer, yet energy transfer values based on the integrated areas are not conclusive with this statement. Although the oil API varies between 12.8 and 45.1, the energy transfer

values only vary between 20.8 and 26.1 % and there is no clear trend between the two parameters. However, there are problems with this method; emission spectra can be adversely affected by steady state artifacts and also deconvolution of scattered light from the emission spectrum becomes a problem at high dilutions or where fluorescence is weak.

The proportion of energy transfer and quenching in crude oils can be determined by incorporating the fluorescence lifetime into an analogous relationship to Equation 4.1:

$$\%ET + Quenching = \frac{\tau_{5000} - \tau_{Neat}}{\tau_{5000}} \times 100 \tag{4.2}$$

where a limiting dilution of 1 : 5000 is used for all calculations. Energy transfer and quenching can be correlated with API gravity and % Polar content as shown by the plots in Figure 4.7. The difference between the results from equations 4.1 and 4.2, gives an estimation for the proportion of quenching and as expected, quenching is greatest in heavy crude oils.

Table 4.5: *Energy transfer values as determined by Equation 4.1. Energy transfer and Quenching values are determined by Equation 4.2. The Quenching value is obtained by the difference of the first two columns. All data recorded at an excitation wavelength of 405 nm and an emission wavelength of 500 nm. Missing data indicates spectra that were not obtained.*

Oil	API	Energy Transfer(%)	ET + Quenching (%)	Quenching(%)
7703	50.6		39.0	-
7197	45.1	26.14	50.6	24.46
7058	40.1		49.36	-
7062	36.0		73.6	-
7186	34.3	25.50	43.87	18.37
7187	29.4		52.1	-
7169	21.6		81.78	-
7130	15.6	20.78	90.41	69.63
7033	12.8	23.0	84	61.0
7188	13.3		89.44	-

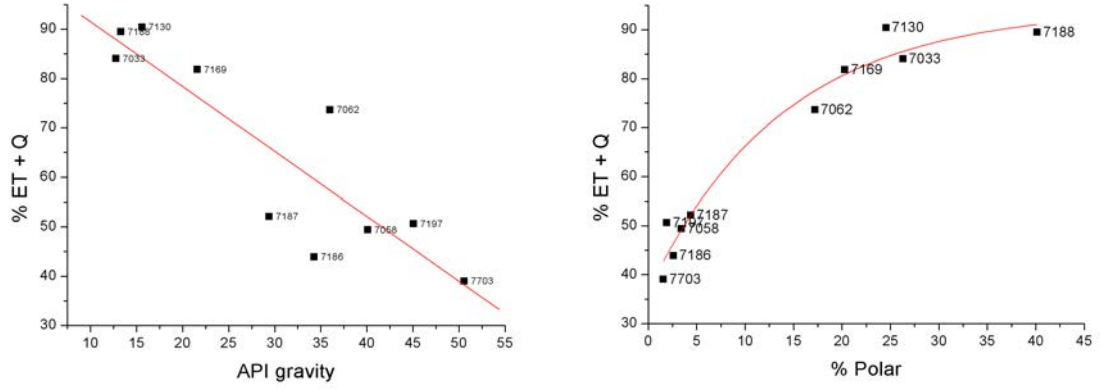

Figure 4.7: *Correlation of energy transfer and quenching with* API *gravity and* % *Polar for crude oils at* 293*K. Fluorescence data was recorded at* 500 *nm emission.*

To gain further insight into energy transfer and quenching effects, one can look at the lifetime-emission wavelength plots. The variation in average fluorescence lifetime with dilution factor at different emission wavelengths is shown for light oil 7197 in non-deoxygenated toluene in Figure 4.8.

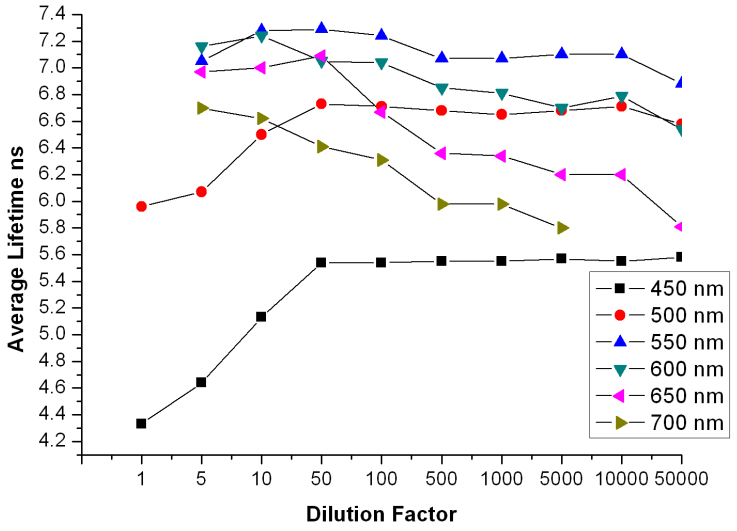

Figure 4.8: *Variation of average lifetime for the light oil* 7197 *from neat to a* 1 : 50000 *dilution with non-deoxygenated toluene at room temperature. For* 450 *and* 500 *nm emission, the lifetime increases to a plateau where no further changes in lifetime are observed. At longer wavelengths, lifetimes begin to decrease with dilution which is most prominent at the longest wavelength sampled,* 700 *nm. Lifetimes were recorded using TCSPC decays recorded at an excitation wavelength of 405 nm.*

At an excitation wavelength of 405 nm, small blue emitting molecules with large bandgaps are excited directly, and will readily undergo energy transfer to larger aromatic small bandgap molecules [124] resulting in shorter lifetimes. On dilution, the concentrations of both small and large bandgap fluorophores and quenchers are reduced which will decrease the rate of energy transfer and quenching, thereby increasing the fluorescence lifetime. For the data recorded at an emission wavelength of 450 nm in Figure 4.8, no further increases in lifetime are observed after diluting 50 times; energy transfer and quenching effects are at a minimum for this dilution. At 500 nm emission there is a small reduction in the lifetime at dilutions above 1 to 50. For emission wavelengths greater than 500 nm the reduction in lifetime with increasing dilution is more apparent, the effect of which is most prominent at the longest wavelength sampled, 700 nm. The effect of dilution on the average lifetimes versus emission wavelength trend can be examined more closely by rearranging Figure 4.8 and then compared to the lifetimes obtained in a deoxygenated solvent to give Figure 4.9. A 'curved' lifetime-wavelength dependence is obtained due to the interplay between quenching and energy transfer effects. At short emission wavelengths, small blue emitting fluorophores readily undergo energy transfer to larger red emitting fluorophores and lifetimes are shorter. This gradually reduces as the emission wavelength is increased. Above a certain wavelength or $\lambda_{\tau max}$, fluorescence is primarily originating from larger red-emitting fluorophores that have been excited by energy transfer and not by the excitation source. These large aromatic fluorophores with relatively small band gap energies are more prone to quenching leading to overall shorter lifetimes [113]. In the diluted oil, a different population of fluorophores are emitting, or more specifically, less energy transfer occurs and blue emitters are becoming more dominant or provide a greater influence on the fluorescence lifetime. This is shown by the shift in the emission wavelength of maximum lifetime ($\lambda_{\tau max}$) to shorter wavelengths on increasing dilution. The lifetime of small emitting fluorophores at short wavelengths (425-500 nm) increases on dilution as energy transfer is reduced. For longer emission wavelengths (greater than 500 nm), dilution does not act to increase the lifetime, rather the lifetime is reduced due to more quenching.

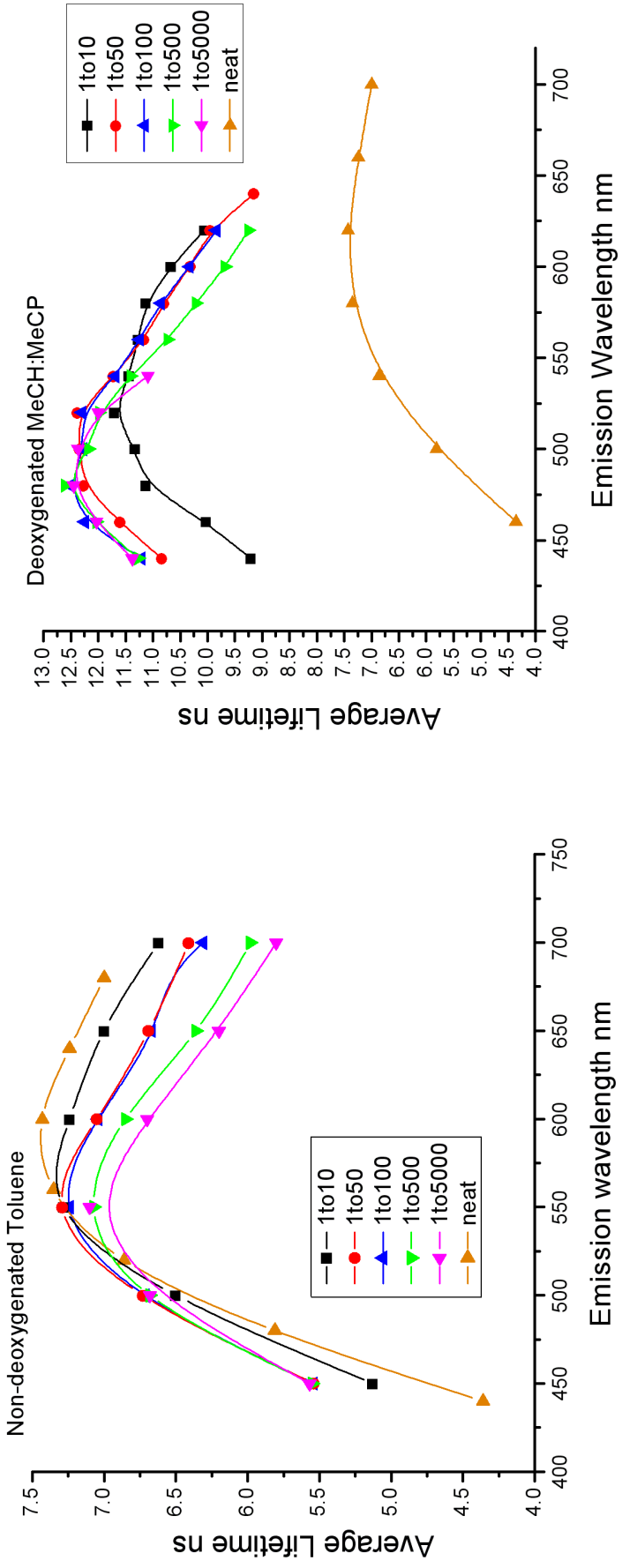

Figure 4.9: *Variation of average lifetime for the light oil 7197 from neat to a 1 : 50000 dilution at room temperature. Left: Non-deoxygenated toluene; Right: Deoxygenated MeCH:MeCP. As the dilution increases, the wavelength of maximum lifetime ($\lambda_{\tau max}$) shifts to the blue region of the emission spectrum. Lifetimes were recorded using TCSPC using an excitation wavelength of 405 nm.*

Removal of oxygen has a large effect on the fluorescence lifetime (right hand plot of Figure 4.9), increasing almost 2 fold in some cases for example the 1 to 10 dilution at 440 nm. In both non-deoxygenated and deoxygenated cases, the curved lifetime-emission wavelength dependence still occurs and the emission wavelength of maximum lifetime ($\lambda_{\tau max}$) moves to the blue region on dilution but by different amounts. A shift of 50 nm is found for the light oil 7197 in non-deoxygenated Toluene; in deoxygenated MeCH:MeCP, a greater blue shift of 120 nm is found. In the non-deoxygenated solvent, oxygen quenches blue emitting fluorophores rather than transferring energy to large red emitting fluorophores resulting in a smaller blue shift; i.e. less energy transfer occurs. In the deoxygenated case, less quenching occurs and more energy transfer leads to greater blue shifts. Thus the presence of oxygen influences quenching and energy transfer in crude oils. A similar set of average lifetime-emission wavelength curves are obtained for medium and heavy oils as shown in Figure 4.10. For both plots, deoxygenated MeCH:MeCP is used. Lifetime-emission wavelength plots give an qualitative view of how energy transfer and quenching processes occur in crude oils and it is clear that the combination of these processes results in complex photophysical behaviour. Oxygen has a large influence on this behaviour and deoxygenated average lifetimes reflects the interaction of *intrinsic* energy transfer and quenching processes within crude oils.

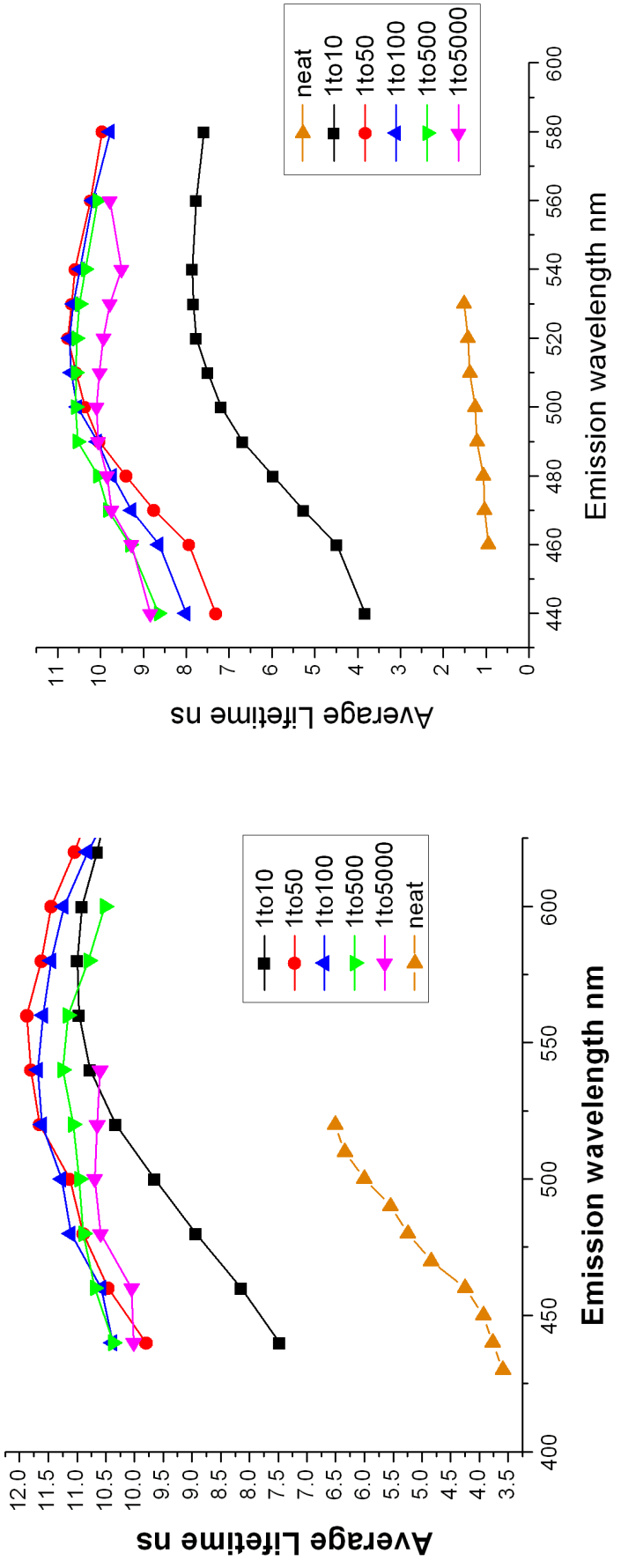

Figure 4.10: *Left: Average fluorescence lifetimes of a medium API gravity oil (7186) at various dilutions in deoxygenated MeCH:MeCP at room temperature. Right: Average fluorescence lifetimes of a heavy oil (7188) at various dilutions in deoxygenated MeCH:MeCP at room temperature. Lifetimes recorded by TCSPC, excitation wavelength 405 nm.*

4.3 Stern-Volmer Analysis

Since the amount of quenching is dependent on the type of oil, it is important to develop our understanding of the quenching mechanism. Oxygen quenching in crude oils has a large influence on the fluorescence lifetime, it must be removed and all analysis in this section involves deoxygenated solutions. For crude oils, Stern-Volmer analysis can be used to study the mechanism of quenching. In this case, rather than adding a quencher to the system as in classic Stern-Volmer analysis, the concentration of quenchers reduces as the oil is diluted thereby increasing the fluorescence lifetime up to a limiting lifetime or τ_0. In [124], a simple Stern-Volmer analysis was applied to a series of diluted crude oils. Linear plots indicated the dominance of a diffusion-based quenching mechanism at high concentrations although a detailed investigation for low concentrations was not described. It seems likely that while the mechanism of quenching may be approximated to a purely diffusion based model, an alternative approach uses a modified form of the equation to include the influence of static effects. When describing the diffusion controlled reactions between particles in solution, the rate constant can be defined using the Smoluchowski equation [36]:

$$k(t) = 4\pi RND[1 + R(\pi Dt)^{-1/2}] \tag{4.3}$$

where R is the interaction radius, i.e., the sum of the radius of the fluorophore and the quencher, N is Avogadro's number, and D is the sum of the fluorophore and quencher diffusion coefficients. This equation describes the rate constant in terms of a steady-state component and a time dependent component or transient term. The transient term arises from the influence of quenching on the decay kinetics whereby the decay is not adequately described by a sum of exponentials. For viscous materials or where quenching has a large effect on fluorescence, this transient effect becomes more important [36, 198]. A modified Stern-Volmer equation that incorporates this transient term can be given as:

$$\frac{I_0}{I} = \frac{1 + K_{sv}[Q]}{W} \tag{4.4}$$

where K_{sv} is the Stern-Volmer constant, [Q] is the quencher concentration and W is a transient term coined by Smoluchowski for describing diffusion controlled

reactions [198, 199]. Keizer [200] describes a modified Stern-Volmer equation that includes the effect of non-fluorescent complexes and dynamic quenching on the fractional intensity:

$$\frac{I_0}{I} = (1 + K_{complex}[Q])(1 + K_{sv}[Q]) \tag{4.5}$$

where $K_{complex}$ is the formation constant for non-fluorescent complex. Equating equations 4.4 and 4.5 and substituting lifetime for intensity yields:

$$\frac{\tau_0}{\tau} = \frac{1 + K_{sv}[Q]}{W(1 + K_{complex}[Q])} \tag{4.6}$$

The probability that no quencher molecules are within the sphere of action at the time of excitation is given by the expression $exp(-VN[Q])$ where VN is the static quenching constant (K_{st}) [198]. V is the volume of the sphere of action and N_A is avogadro's constant. If the transient term and non-fluorescent complex formation are represented by $exp(-VN[Q])$ then:

$$\frac{\tau_0}{\tau} = (1 + K_{sv}[Q])(exp(K_{st}[Q])) \tag{4.7}$$

This equation is of the same form of Equation 1.52 but given in terms of fluorescence lifetime instead of intensity. If we approximate Equation 1.52 so that it represents the overall response from a large mixture of fluorophores, the fraction of all fluorophores is summed to 1. The reciprocal of equation 1.52 then would give Equation 4.7. K_{sv} ($= k_q \times \tau_0$) is the Stern-Volmer constant and represents collisional quenching of fluorescence. As average lifetimes give a numerical value that represents the net summation of the excited state processes in crude oils, the parameters K_{sv} and K_{st} can be viewed as average quenching constants. For crude oils the quencher concentration can not be calculated directly and alternatively one must describe each dilution in terms of a volume ratio.

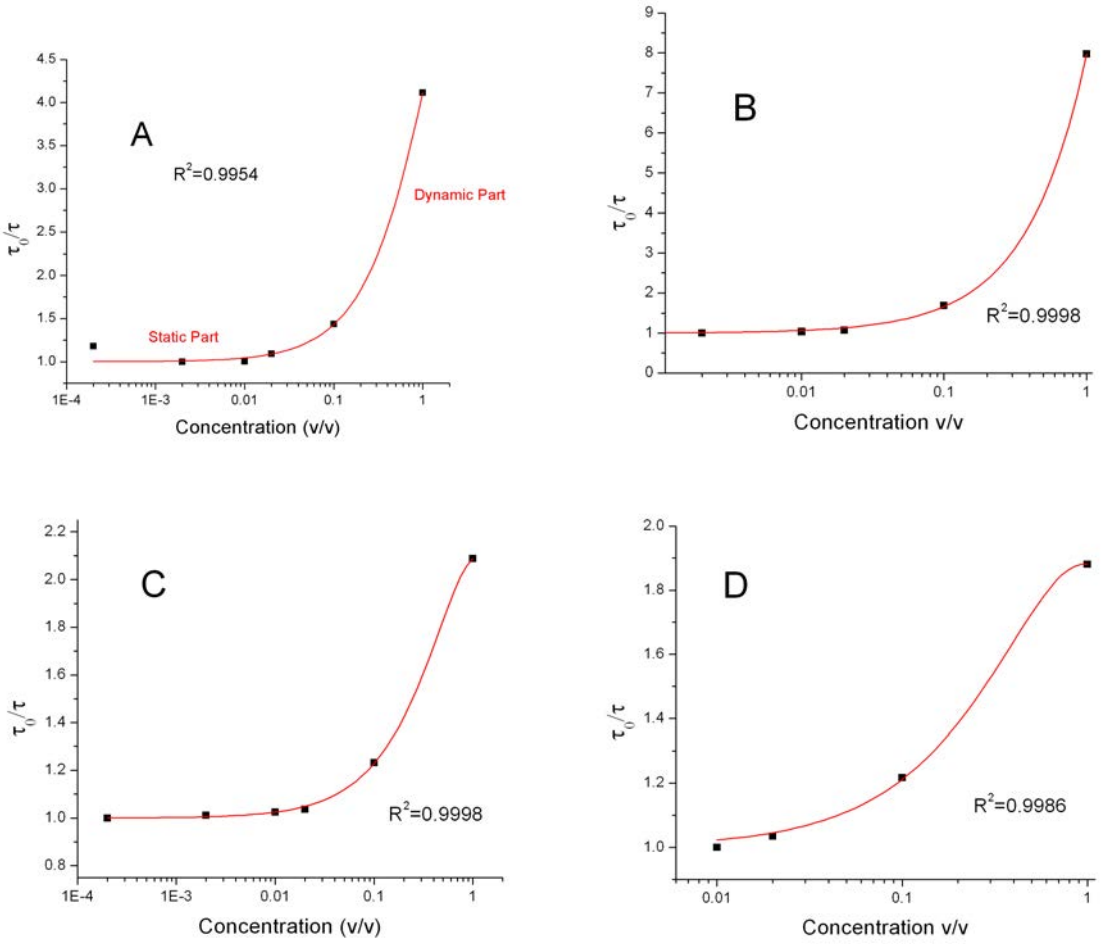

Figure 4.11: *Modified Stern-Volmer plots for a series of oils A: 7033 (API = 12.8), B: 7188 (API = 13.3), C: 7187 (API = 29.4), D: 7197 (API = 45.1). Red fit line to Equation 4.7 is shown. Dilutions using 3:2 mixture of Methylcyclohexane:Methylcyclopentane (deoxygenated). Lifetimes recorded at 500 nm and room temperature.*

Figure 4.11 shows that Equation 4.7 fits the deoxygenated fluorescence lifetime data closely where τ_0 is given by the lifetime at 1:5000 dilution. The red line shows the non-linear least squares fitting of the lifetime data to equation 4.7, giving the fitted parameters: K_{sv} and K_{st}. The curvature of the semi-log plots in Figure 4.11 are quite pronounced indicating a large influence of static effects in heavy oils particularly at low dilutions. The static and dynamic regions are shown in plot A of Figure 4.11. For the light oil 7197, a more sigmoidal shape in the Stern-Volmer plot is observed which may be due to residual oxygen quenching.

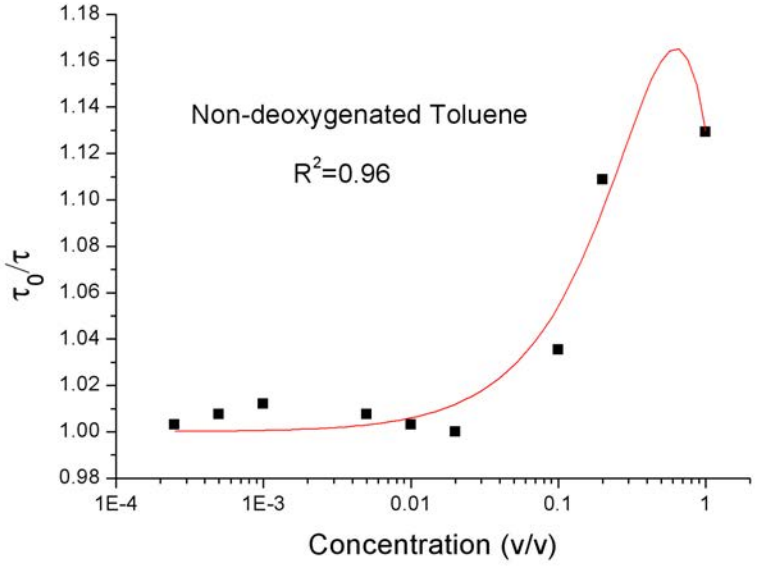

Figure 4.12: *Modified Stern-Volmer plots for light oil 7197 (API = 45.1). Dilutions using 3:2 mixture of non-deoxygenated toluene. Lifetimes recorded at 500 nm and room temperature.*

One can compare this to the modified Stern-Volmer plot for oil 7197 in non-deoxygenated toluene (Figure 4.12). The sigmoidal shape of the fitted curve is now enhanced as oxygen quenching adds to intrinsic quenching processes and the model starts to break down although K_{sv} and K_{st} values could be recovered. A table of Stern-Volmer fitting parameters for nine crude oils is given in Table 4.6. τ_0 was given by the lifetime of the 1:5000 dilution. k_q is determined by K_{sv}/τ_0. Note that because the concentration is expressed in terms of a volume ratio, the concentration term can be omitted from the value for k_q, giving units of s^{-1}. Heavy oils have a larger quenching constant, k_q than lighter oils giving a quantitative measure of the efficiency of quenching in oils; i.e. heavy oils are quenched more efficiently. This relationship compares with the data in Table 4.5 where the % quenching values vary with oil type in a similar manner. Oil 7197 has two sets of values, one set in deoxygenated MeCH:MeCP and the other in non-deoxygenated toluene, denoted by †. Note that the intrinsic lifetime is decreased by ~ 4.5 ns for the non-deoxygenated case. The Stern-Volmer parameters can still be recovered in the non-deoxygenated case. One would expected that quenching efficiency should increase and a higher value of k_q found. Rather, a lower value of k_q is found which may be attributed to

the break down of the dynamic part of the model. The static part can be modeled by Equation 4.7 and the static constant remains close to that of the deoxygenated case.

Table 4.6: *Quenching parameters from fitting of data recorded at 500 nm to the modified Stern-Volmer Equation 4.7. Dilutions were made using a 3:2 Methlycyclohexane:Methylcyclopentane mix at room temperature. Errors calculated for the collisional quenching constant are also given in brackets. † indicates oil 7197 in non-deoxygenated toluene.*

oil	API	K_{sv}	K_{st}	R^2	τ_0	$k_q \times 10^8 s^{-1}$
7033	12.8	4.81	0.35	0.9994	3.99	12.06 (3.13)
7188	13.3	6.57	0.052	0.9998	10.05	6.54 (0.15)
7130	15.6	5.58	0.48	0.9999	10.59	5.27 (0.32)
7169	21.6	3.30	0.25	0.9998	9.63	3.43 (0.41)
7187	29.4	3.17	0.69	0.9998	12.13	2.61 (0.22)
7186	34.3	2.28	0.56	0.9926	11.27	2.03 (0.44)
7062	36.0	1.48	0.44	0.9999	8.22	1.79 (0.48)
7058	40.1	2.46	0.58	0.9563	9.33	2.64 (0.08)
7197	45.1	3.10	0.78	0.9986	11.21	2.76 (0.48)
7197†	45.1	1.33	0.73	0.958	6.71	1.98 (0.18)

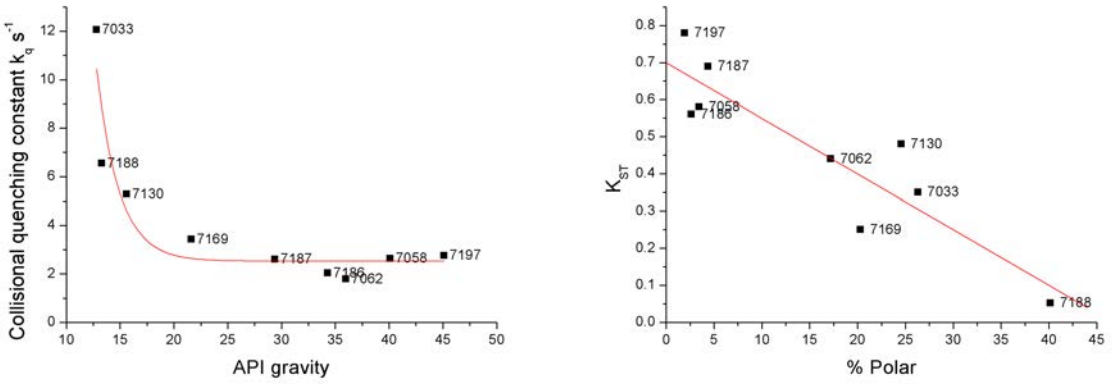

Figure 4.13: *Left: Variation of collisional quenching constant with API gravity. Right: Variation of static quenching constant with % Polar gravity. All data at room temperature.*

To reiterate the influence of oil type on quenching, the variation of collisional quenching constant and API gravity is shown the left plot of Figure 4.13. The fitting line is added to the figure to highlight the trend of decreasing collisional quenching as the oil density reduces. The static quenching constant does not show the same

variance with API gravity but does show a linear trend with % polar content as shown in the right plot of Figure 4.13.

Table 4.7: *Quenching parameters for heavy oil 7033 from fitting of data recorded at a range of emission wavelengths to the modified Stern-Volmer Equation 4.7. Dilutions were made using deoxygenated 3:2 Methlycyclohexane:Methylcyclopentane at room temperature. Errors calculated for the collisional quenching constant are also given in brackets.*

wavelength	K_{sv}	K_{st}	R^2	τ_0	$k_q \times 10^8 s^{-1}$
460	8.84	0.65	0.9939	3.48	25.4 (5.1)
480	7.27	0.72	0.9888	3.76	19.34 (4.87)
500	4.81	0.35	0.9954	3.99	12.07 (3.11)
520	3.82	0.03	0.9967	4.56	8.37 (2.76)
540	3.05	0.12	0.9997	5.10	5.98 (5.79)
560	2.88	0.18	0.9986	5.59	5.15 (1.53)
580	2.38	0.38	0.9999	5.94	4.01 (1.43)
600	2.33	0.34	0.9999	6.20	3.76 (1.37)

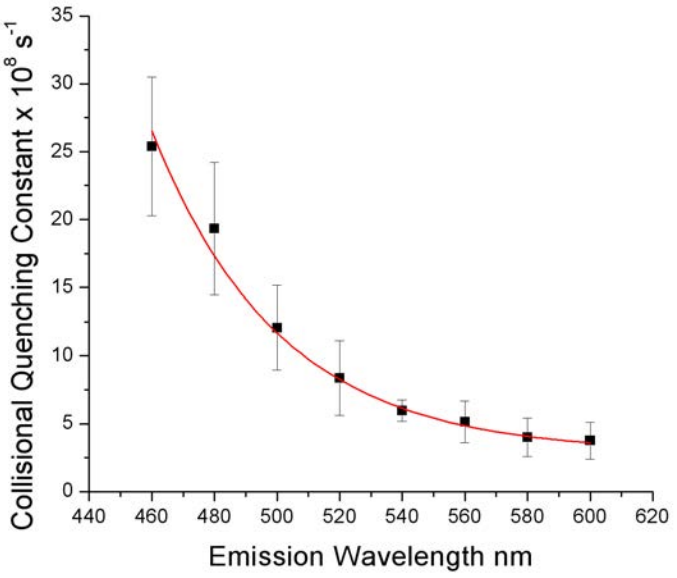

Figure 4.14: *Collisional quenching constants for heavy oil* 7033 *diluted with deoxygenated 3:2 MeCH:MeCP determined at a range of emission wavelengths. Lifetimes recorded by TCSPC, excitation wavelength 405 nm. Error bars on the quenching constants are also shown.*

The modified Stern-Volmer parameters can also be calculated at a series of emission wavelengths, an example of which is given for heavy oil 7033 in Table 4.7. The

Stern-Volmer quenching constants follow an exponential trend with emission wavelength as shown in Figure 4.14. At shorter emission wavelengths, where the lifetime values represent emission from small blue emitting fluorophores the efficiency of quenching is high. As the emission wavelength increases, the efficiency of quenching red emitting fluorophores reduces.

4.4 Conclusions

Intensity is initially increased on dilution due to less quenching. Emission spectrum shifts to the blue as energy transfer is reduced. Qualitative evaluation of energy transfer can be determined using the integrated areas of the neat and dilute emission spectra.

Lifetime increases as crude oils are diluted due to a reduction in both energy transfer and quenching. The difference between the neat and dilute average lifetimes can be used to determine a value for the extent of energy transfer and quenching. Fluorescence is quenched to a greater degree by quenching and energy transfer in heavy oils than for light oils.

Deoxygenation of crude oil solutions reduces quenching, reduces energy transfer at low dilutions. At a specific dilution, deoxygenation does not affect the spectra.

Lifetime-Emission wavelength plots can show how different populations of fluorophores interact photophysically. Similar behaviour is found for in both the neat and dilute oils, where the lifetime increases to a maximum value thereafter decreasing at longer emission wavelengths. The wavelength of max lifetime shifts to the blue on dilution. Smaller blue emitting fluorophores more heavily influence the lifetime at higher dilution showing that the population of fluorophores changes from neat to dilute. The presence of dissolved oxygen adds complexity to these plots, and they can be simplified by using data measured in the absence of oxygen.

Since the oil composition affects the rate of quenching, it follows that the mechanism of quenching needs to be understood. A modified Stern-Volmer has been applied that combines dynamic and static quenching parts, but this equation does not fit to non-deoxygenated solutions. . There are two ways to model static behaviour; either by a sphere of action or a non-fluorescent dark complex. In this

study, the former is chosen but the real scenario may include a mixture of both effects. By performing a non-linear least squares fit to the lifetime-concentration data, dynamic and static quenching constants can be calculated; dynamic quenching constants are highest for heavy crude oils, reducing as the oil density reduces. The diffusion related quenching constants also reduce exponentially with emission wavelength. At short emission wavelengths, quenching is most efficient which reduces as the emission wavelength increases. Stern-Volmer static quenching constants can be correlated with polar content but in order to quantify static quenching further, low temperature analysis must be applied.

Chapter 5

Influence of low temperature on fluorescence emission from crude oils

This chapter gives a detailed analysis of the effects of temperature on the fluorescence emission of crude petroleum oils. It is the aim of work to expand our knowledge of crude oil photophysics by investigating the effect of temperature with the fluorescence spectra and lifetimes of crude oils. The analysis of low temperature effects for neat and dilute crude oils was undertaken.

5.1 Effect of low temperature on the fluorescence emission of crude oils

It is well documented that the fluorescence intensity of aromatic hydrocarbons increases as the temperature is reduced [36, 38, 146, 201, 202]. As the temperature reduces, viscosity increases leading to a reduction of collisional quenching and hence a increase in fluorescence intensity. In Figure 5.1, the emission spectra of the neat light crude oil 7197 are given at a range of temperatures down to 77 K. From room temperature down to 113 K, the fluorescence intensity increases gradually.

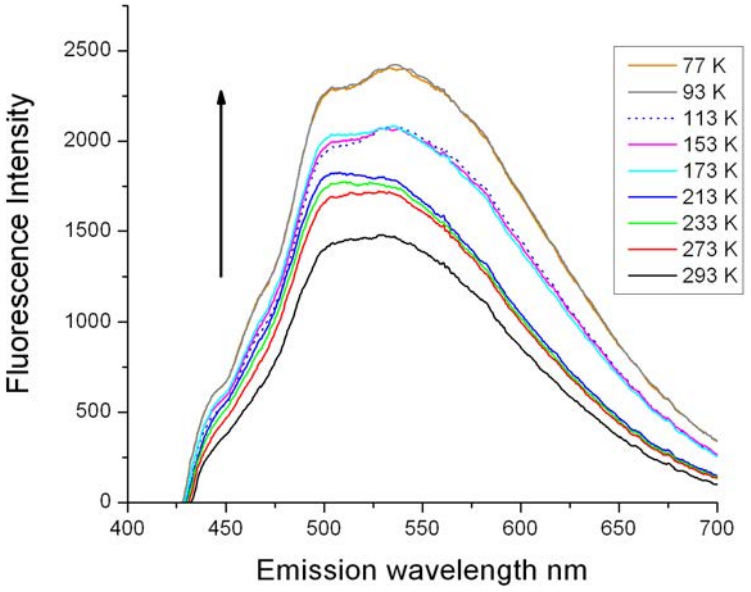

Figure 5.1: *Steady state emission spectra (uncorrected) for neat light oil* 7197 *at a range of temperatures down to 77 K. Arrow denotes the increase in emission intensity as the temperature reduces. Emission spectra recorded by USB2000 spetrophotometer. Excitation wavelength 405 nm.*

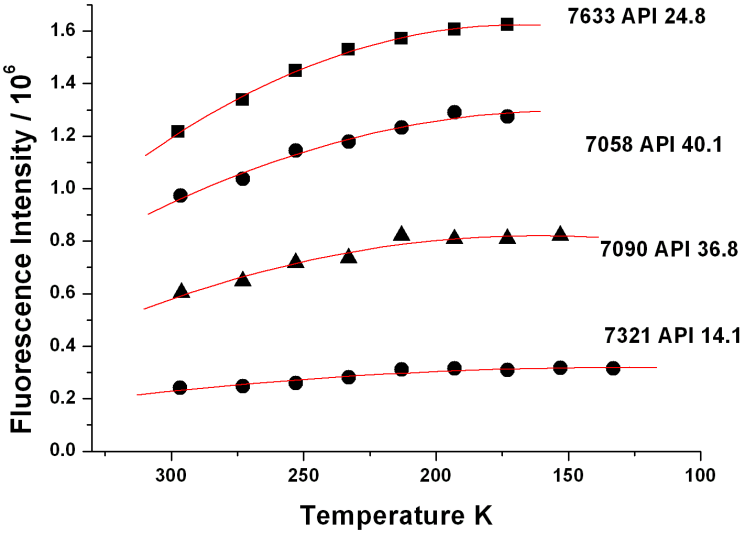

Figure 5.2: *Variation in fluorescence intensity at an emission wavelength of* 480 *nm with temperature for four typical neat crude oils. Intensity increases of* 20-25% *are obtained for the oil shown. The intensity tends to reach a plateau point where no further increase is observed, around* 200 *K.*

As the temperatures is lowered further, close to the temperature of liquid nitrogen, a further intensity increase is observed which could be due to a glass like state occurring at this extreme temperature. Direct recording of fluorescence intensity is prone to interference of steady state artifacts and alternatively time resolved intensity measurements can be recorded. Such measurements can be calculated by multiplication of the recorded counts/second by the time taken to record 10000 counts. The result of this is given in Figure 5.2 where for measurements taken at 480 nm a gradual increase in intensity is observed. Light oils show a greater relative change in intensity as the temperature is lowered $(20 - 25\%)$. Also fluorescence intensity increases with API gravity, except in the case of oil 7633 which has a low API gravity yet due to the high wax content acts a like a very light oil. The intensity of emission from heavy oils also increases with temperature although by a smaller factor. The effect of temperature on the spectra of dilute oils is examined in Figure 5.3. As discussed in the previous chapter, on dilution of crude oils (in this case $1:5000$), the effects of energy transfer and quenching at room temperature are minimised leading to a narrowing of the emission spectrum and a blue shift in λ_{max} (wavelength of highest intensity) of 70 nm. The non-polar solvent mix of MeCH and MeCP should not have an effect on the various excited states in the crude oil since there is no effective dipole moment as the solvent polarity function $\triangle$f is ~ 0)*. In Figure 5.3, the emission spectrum of neat oil 7033 does not show a significant change in the normalised emission spectra recorded at $293K$ (solid line) and $133K$ (dotted line). The reason for this is that in this neat heavy oil (containing a large proportion of quenching species) is highly viscous at room temperature. Cooling does not have a large affect on the inherent viscosity and hence quenching and energy transfer are

* In solution, polar solvent molecules surrounding a fluorophore in the ground state have dipole moments that can interact with the dipole moment of the fluorophore to yield an ordered distribution of solvent molecules around the fluorophore. Energy level differences between the ground and excited states in the fluorophore produce a change in the molecular dipole moment, which ultimately induces a rearrangement of surrounding solvent molecules. However, the Franck-Condon principle dictates that, upon excitation of a fluorophore, the molecule is excited to a higher electronic energy level in a far shorter time-frame than it takes for the fluorophore and solvent molecules to re-orient themselves within the solvent-solute interactive environment. As a result, there is a time delay between the excitation event and the re-ordering of solvent molecules around the solvated fluorophore, which generally has a much larger dipole moment in the excited state than in the ground state. This energy difference between ground and excited states can be approximated by the Lippert-Mataga equation [203]. The solvent polarity function is one of the terms of the Lippert-Mataga equation and is given by $\triangle \mathrm{f} = (\varepsilon - 1)/(2\varepsilon + 1) - (n^2 - 1)/(2n^2 + 1)$, where ε is the dielectric constant and n is the refractive index of the solvent.

not reduced at low temperatures. Dilution of a crude oil results in diluted quenchers which leads to reduced collisional quenching and energy transfer, illustrated by a blue shift in the emission spectrum in Figure 5.3. When the diluted oil is cooled down, collisional quenching is reduced as the solvent becomes more viscous but now energy transfer becomes more effective as shown by the small reverse shift to the red (2-3 nm) in the low temperature spectra.

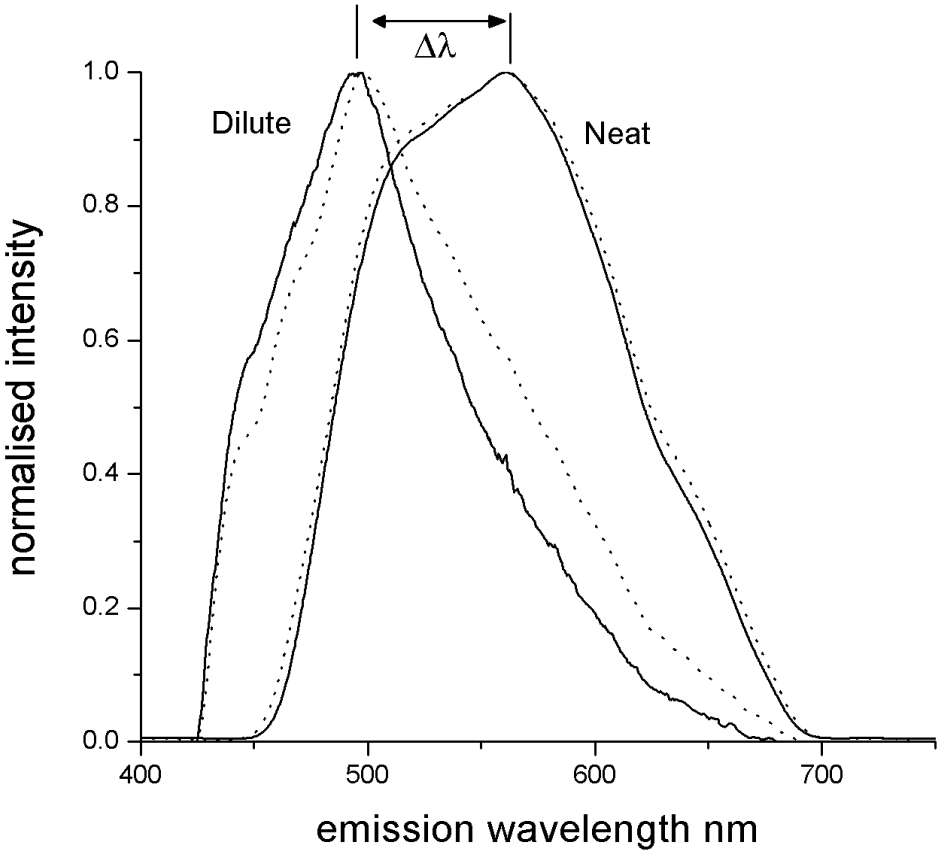

Figure 5.3: *Steady state emission spectra (uncorrected) for a heavy oil* 7033. *Each spectrum was normalised to the maximum intensity.* $293K$ *(solid line) and* $133K$ *(dotted line).*

The variation of emission spectra with temperature is shown in Figure 5.4 where normalised spectra for the heavy crude oil 7033 at a range of temperatures up to 133 K are given. An expanded view of the region of maximum intensity is given in the inset graph. An arrow indicates the red shift in the spectra as the temperature is lowered due to a small increase in energy transfer.

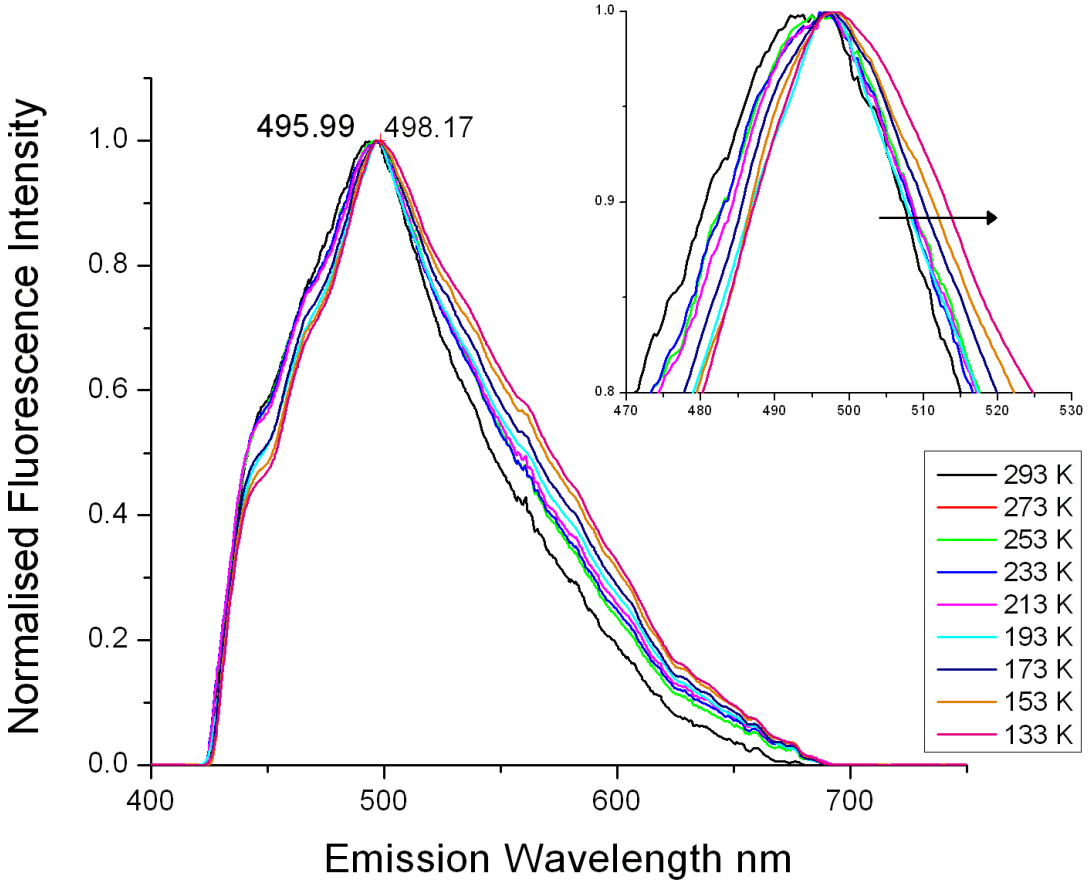

Figure 5.4: *Steady state emission spectra (uncorrected) for heavy oil* 7033 *at a range of temperatures from* 293 *to 133 K. Lowering the temperature results in red shifted emission spectra. Inset is a expanded view of the spectra. Each spectrum was normalised to the maximum intensity.*

To recap, crude oils typically contain many quenching species that cause a reduction in the fluorescence emission. As discussed in Chapter 4, this reduction in fluorescence intensity is attributed to static and dynamic quenching processes and also energy transfer. As the temperature is lowered dynamic or collisional quenching is reduced and there is a small increase in energy transfer. The effect of temperature on static quenching is unclear. Previously in Chapter 4, I used lifetime data at a range of room temperature dilutions to form modified Stern-Volmer plots which were used to model the influence of both collisional quenching and static quenching in the form of a sphere of action. To determine how low temperature influences collisional and static quenching and energy transfer effects, a similar analysis using

fluorescence lifetimes must be performed.

5.2 Low temperature lifetime analysis

Lowering the temperature of neat oils causes an increase the lifetime as shown in Figure 5.5. Lifetime increases with decreasing temperature until a point where the rate of change is small - this is the 'limiting' temperature where collisional quenching effects are at a minimum (Figure 5.6).

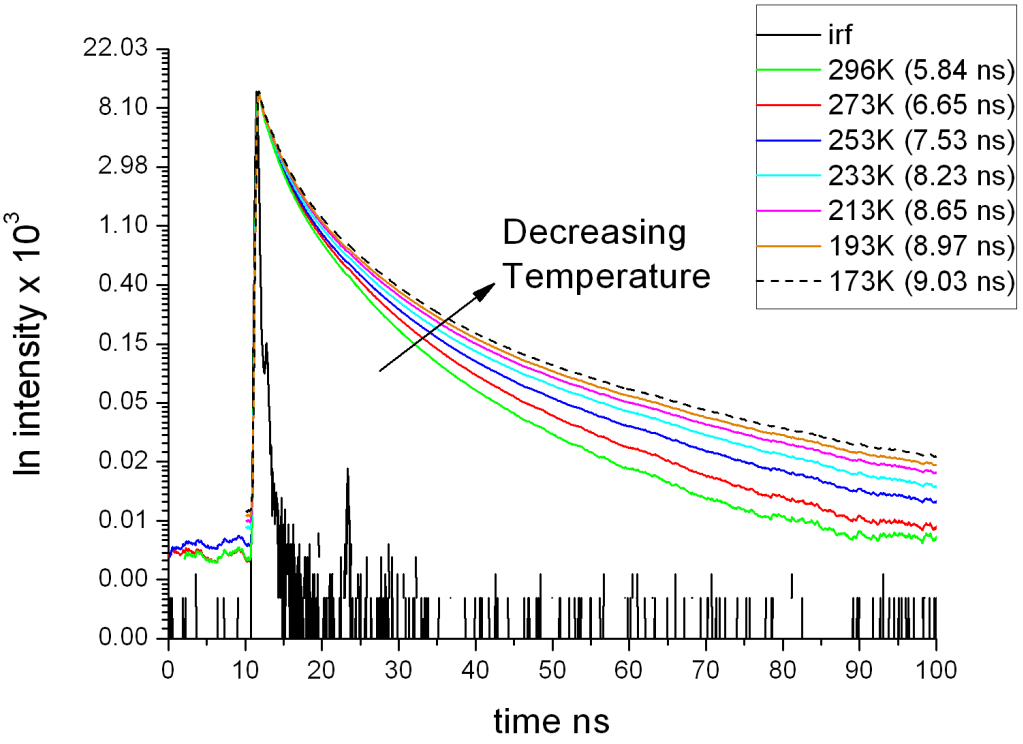

Figure 5.5: *Lifetime decays (recorded using* 405 *nm excitation and emission at* 500 *nm by TCSPC) for a neat light oil* 7058 *over a series of decreasing temperatures to* 173*K. Also shown are the average lifetimes calculated for each decay.*

In this figure, all oils irrespective of oil type or API gravity show this behaviour. For neat light oils, which tend to have a relatively low quencher concentration, a decrease in temperature causes an increase in viscosity, causing a large drop in mobility (of fluorophores and quenchers) leading to reduced dynamic quenching. For neat heavy oils, the change in lifetime is not as significant with only slight

increases observed. This is because the neat heavy crude oils have a high proportion of quenchers where quenching effects are high. For these highly viscous lowering the temperature induces a smaller change in the effective quenching rate, when compared to the lighter oils.

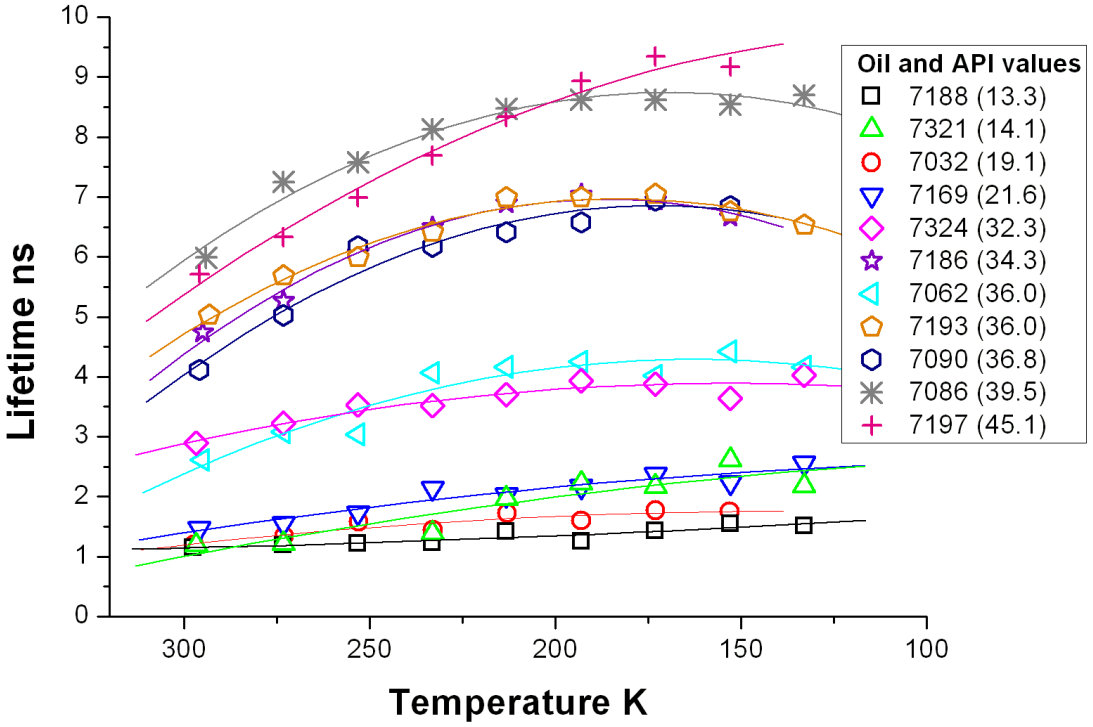

Figure 5.6: *Average lifetimes for selected crude oils (reduced for clarity) over the range of recorded temperatures. The legend shows the API gravity values for each oil. Heavy oils (low* API*) show a smaller change in lifetime with temperature than for the light oils (High* API*) but it is shown that the proportional change in lifetime varied considerably across the range of oils tested. Data recorded at* 405 *nm excitation and* 500 *nm emission using TCSPC.*

Figure 5.7 shows the effects of dilution and temperature on the lifetimes of a heavy crude oil (7033) recorded at an emission wavelength of 500 nm. In the top figure, lowering the temperature has a small influence on the lifetimes for the neat crude oil. The situation is different for the diluted oil, where collisional quenching plays a greater role leading to longer lifetimes.

The effect of dilution on the average lifetime values is shown more clearly in the bottom graph of Figure 5.7 where plots of lifetime versus dilution factor are

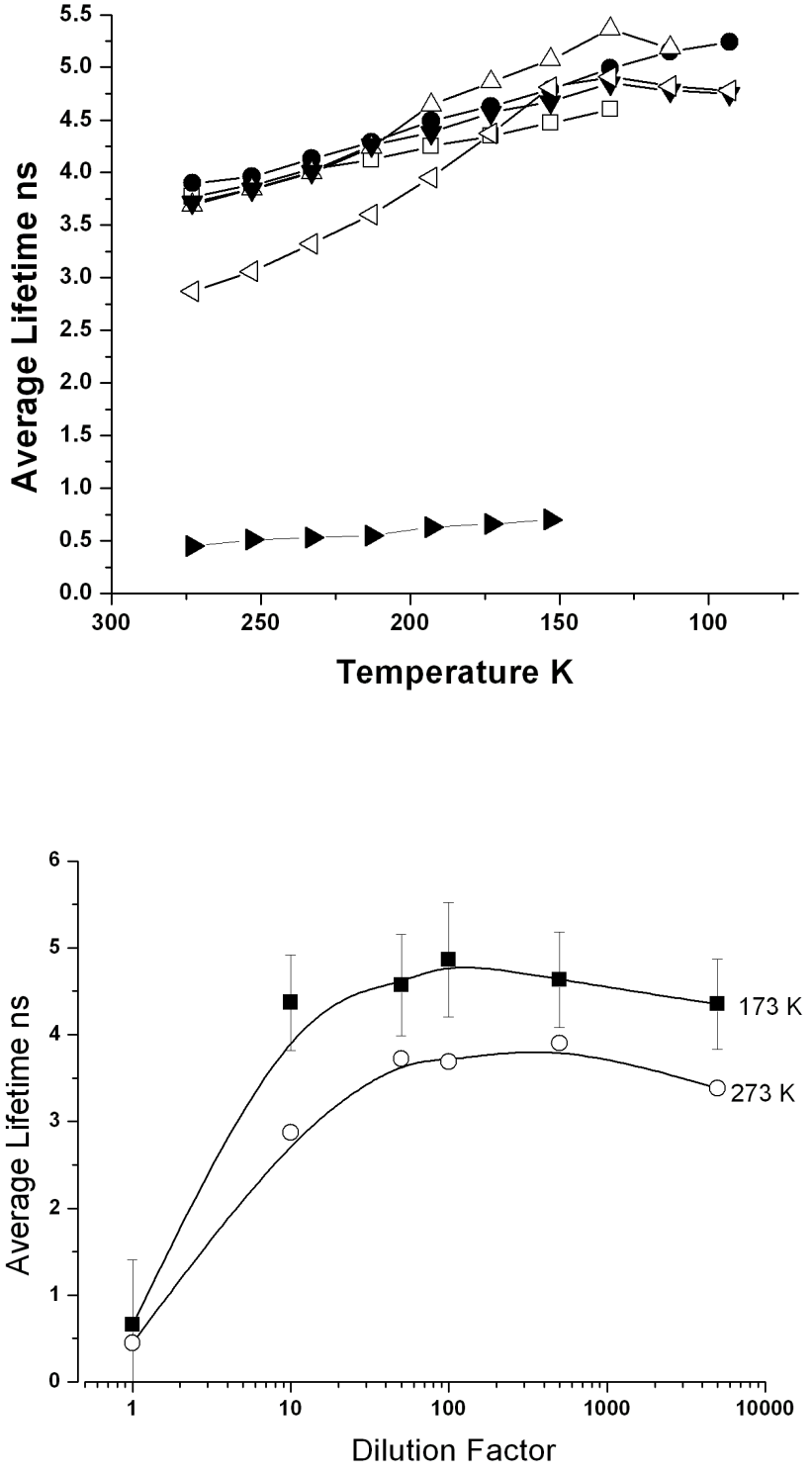

Figure 5.7: *Top: Variation of fluorescence lifetime with temperature for a series of dilutions of oil* 7033. *Dilution factors are :* ▶*: neat,* ◁ : 1 : 10, ▼ : 1 : 50, △: 1 : 100, ● : 1 : 500 , □ : 1 : 5000. *The longest lifetimes are found the lowest temperatures sampled. Bottom: Variation of average lifetime of the oil (taken at* ■ : 173K *and* ○ : 273K*) with dilution. For both graphs, data was recorded at an emission wavelength of* 500 *nm.*

displayed for a high (273 K) and low temperature (173 K). The 1 to 100 dilution gives the longest lifetimes and at subsequent higher dilutions, lifetime reductions are found. The error bars represent one standard deviation on the average lifetime and are calculated from a support-plane analysis as described in Chapter 2. The shape of the curves follow a similar trend at both temperatures and the drop in the fluorescence lifetime at higher dilutions is clear. From the findings in Chapter 4, small blue emitters are more dominant at higher dilutions. When excited at 405 nm, these fluorophores with large energy gaps readily undergo energy transfer to larger red emitting fluorophores with smaller energy gaps. These large red emitting fluorophores exhibit larger rates of internal conversion leading to shorter lifetimes as described by the Energy-Gap law. The Energy-Gap law is given as $k_{ic} = Aexp(-\alpha\Delta E)$ where k_{ic} is the rate of internal conversion, ΔE is the energy difference between the ground and excited states, α is a proportionality constant , and A is the frequency factor [204]. From the Energy-Gap law, we can see that the rate of internal conversion increases exponentially with decreasing energy gap. For neat oils, collisional quenching and energy transfer usually far outweigh internal conversion processes but in a highly diluted state, the rate of internal conversion becomes more significant which results in decreased fluorescence lifetimes (for longer wavelength emission). As further argument to this explanation, Ralston and Mullins [113] have found that the quantum yields of the fluorophores in crude oils follow the Energy-Gap law.

Expanding on this discussion, Figures 5.8 to 5.10 show data for three heavy oils (7033, 7130 and 7169) at a short and long emission wavelength , 440 nm and 600 nm, corresponding to two very different populations of fluorophores (i.e. more blue / red emitting fluorophores). For the heaviest (lowest API gravity) oil, 7033 (Figure 5.8), the lifetime-temperature curves generally follow a similar pattern except for 1:10 and 1:50 dilutions at 600 nm. For these dilutions, a decrease in lifetime is found at temperatures lower than $\sim$ 150-170 K. This may be due to enhanced energy transfer at low temperature. The inset graphs of Figure 5.8 allow examination of how temperature-dilution affects lifetime values. Similar curves are obtained at both 440 and 600 nm emission at 273 K. But at 173 K, there is a greater reduction in lifetime at 600 nm at low concentrations (dilutions greater than 1:100). Again this is may be attributed to enhanced energy transfer of the dominant blue emitting

fluorophores (at high dilutions) to more red emitting fluorophores which undergo faster internal conversion when compared to fluorescence. Ultimately these processes lead to reduced lifetime values. Figures 5.9 and 5.10 give further examples. Similarly for these oils, lifetimes at 440 nm increase with decreasing temperature. For the lifetimes calculated at 600 nm emission, a sharp reduction in lifetime is found at dilutions of 1:100 and lower.

For the three heavy oils shown here, the lifetime-dilution behaviour follows the same curved trend at low and high temperature. The interpretation of how dilution influences lifetime is difficult; in contrast temperature induced changes in lifetime seem to follow a simpler relationship. The inset graphs of Figures 5.8 to 5.10 show a similar curved Lifetime-Dilution trend at different temperatures. Figure 5.11 plots the difference between the dilute and neat lifetimes ($\Delta\tau$) with temperature. A linear change of $\Delta\tau$ with temperature is found for all dilutions. For oil 7033, the slope reduces after the limiting dilution of 1 to 100. For oil 7169, dilution based lifetime change are almost complete at 1 to 50 as shown by the almost static slope of each plot.

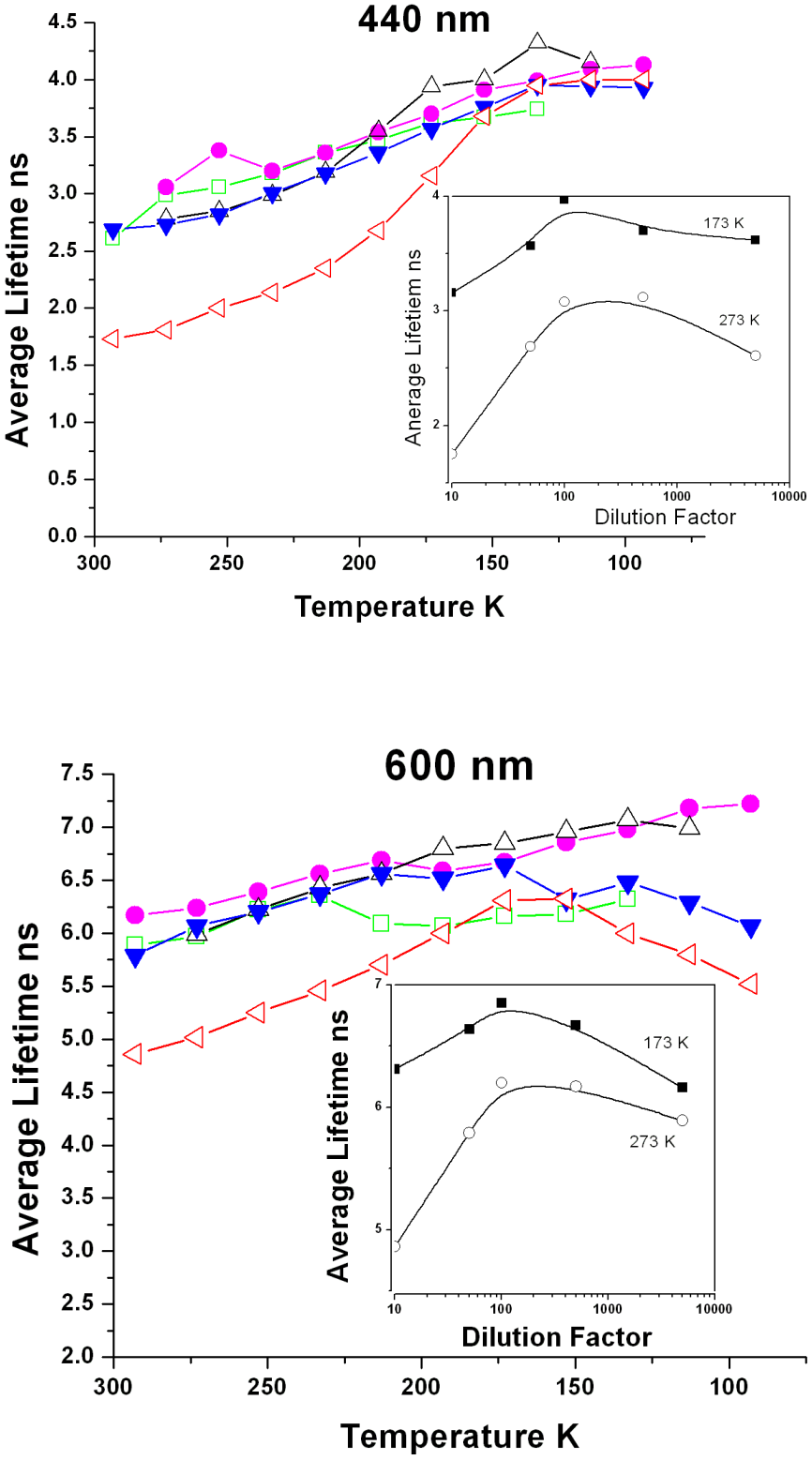

Figure 5.8: *Average lifetime - temperature / dilution response for oil* 7033 *(API 12.8) for two emission wavelength extremes. Top: 440 nm, Bottom: 600 nm. Red:* $1:10$*, Blue:* $1:50$*, Black:* $1:100$*, Magenta:* $1:500$ *and Green:* $1:5000$*. Inset graphs show the lifetime versus dilution curve at two temperatures;* ■ : $173K$ *and* ○ : $273K$*.*

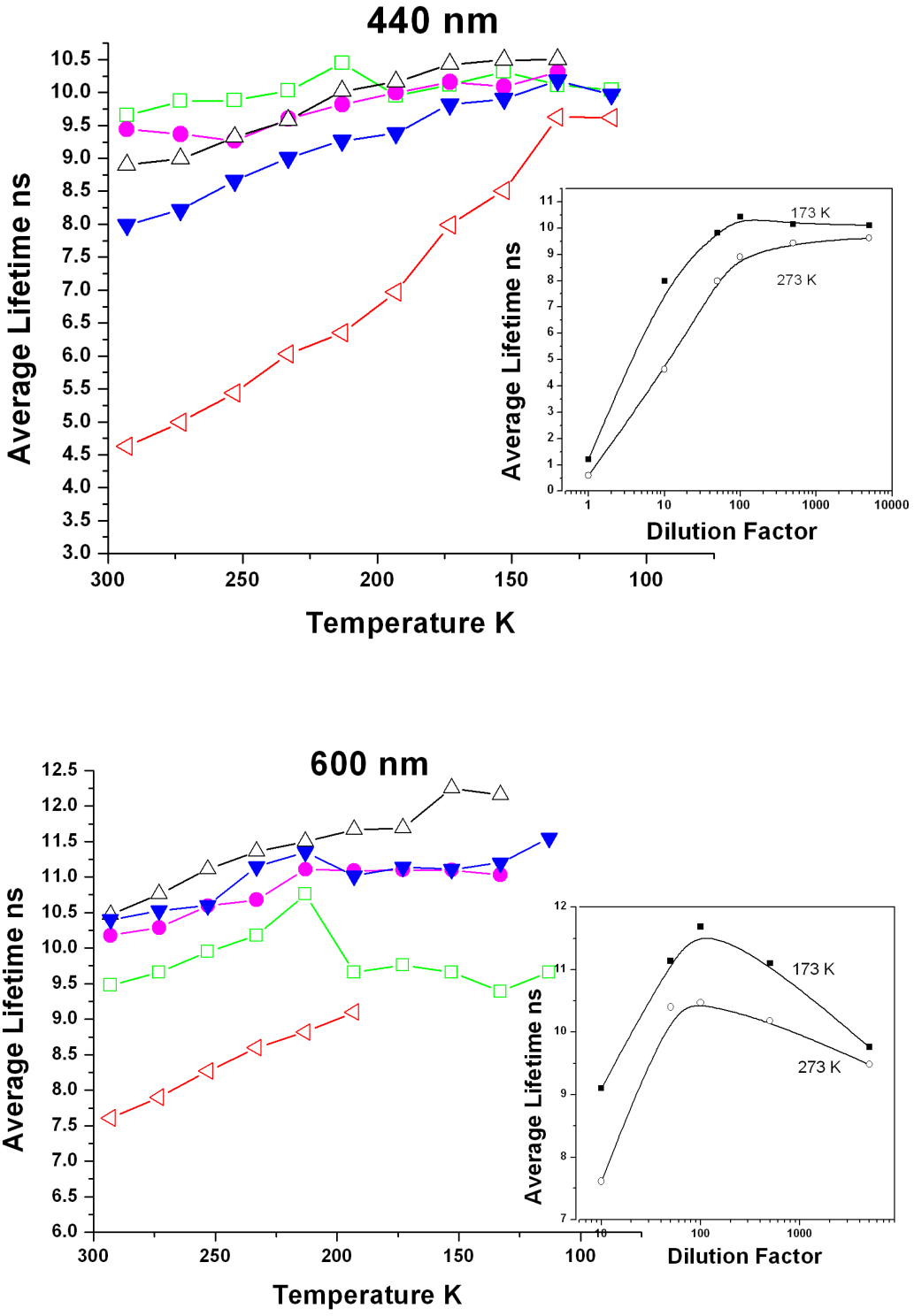

Figure 5.9: *Average lifetime - temperature / dilution response for oil* 7130 *(API 15.6) for two emission wavelength extremes. Top: 440 nm, Bottom: 600 nm. Red:* 1 : 10*, Blue:* 1 : 50*, Black:* 1 : 100*, Magenta:* 1 : 500 *and Green:* 1 : 5000*. Inset graphs show the lifetime versus dilution curve at two temperatures;* ■ : $173K$ *and* ○ : $273K$*.*

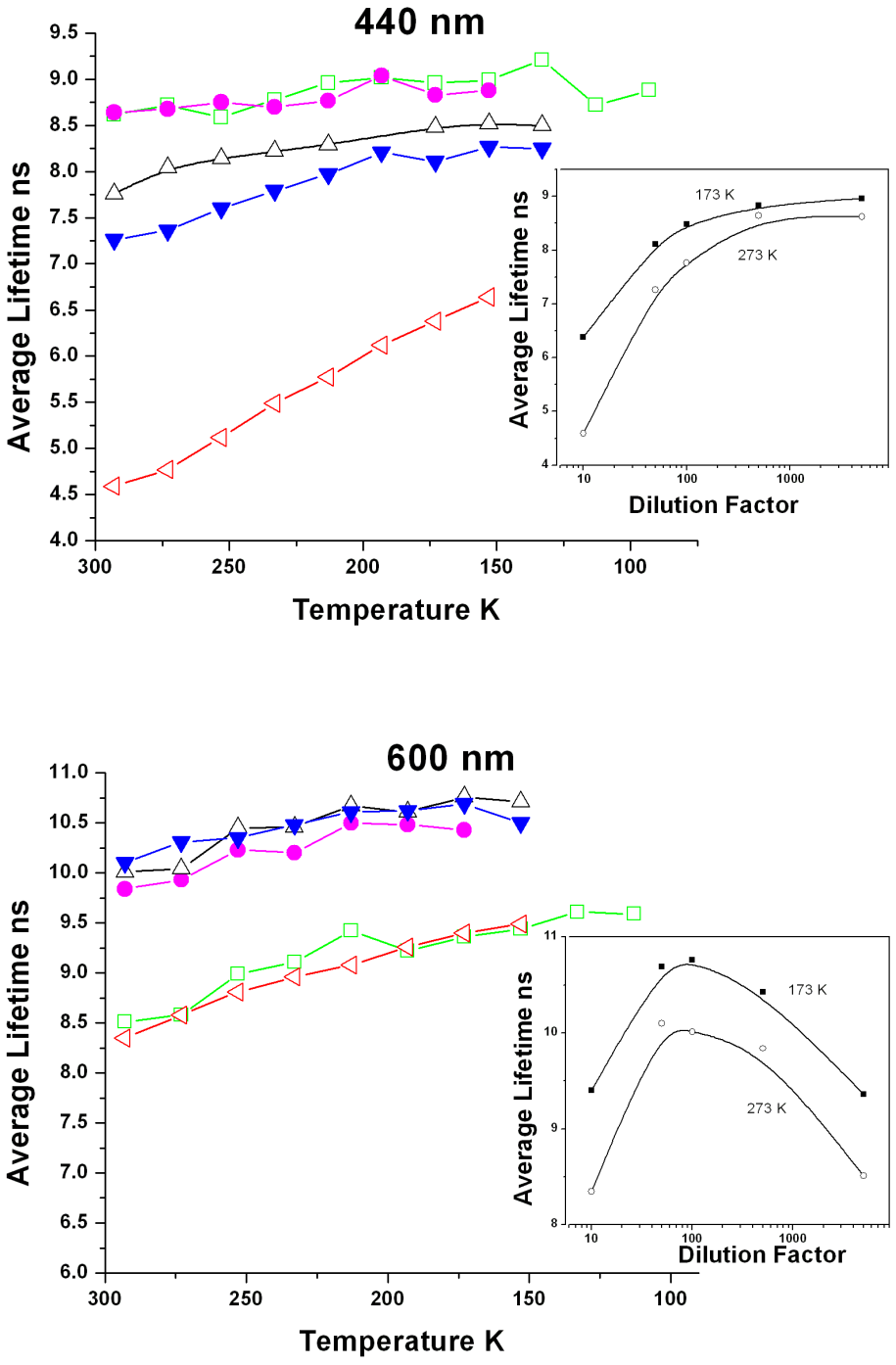

Figure 5.10: *Average lifetime - temperature / dilution response for ligher oil* 7169 *(API 21.6) for two emission wavelength extremes. Top: 440 nm, Bottom: 600 nm. Red:* 1 : 10, *Blue:* 1 : 50, *Black:* 1 : 100, *Magenta:* 1 : 500 *and Green:* 1 : 5000. *Inset graphs show the lifetime versus dilution curve at two temperatures;* ■ : $173K$ *and* ○ : $273K$.

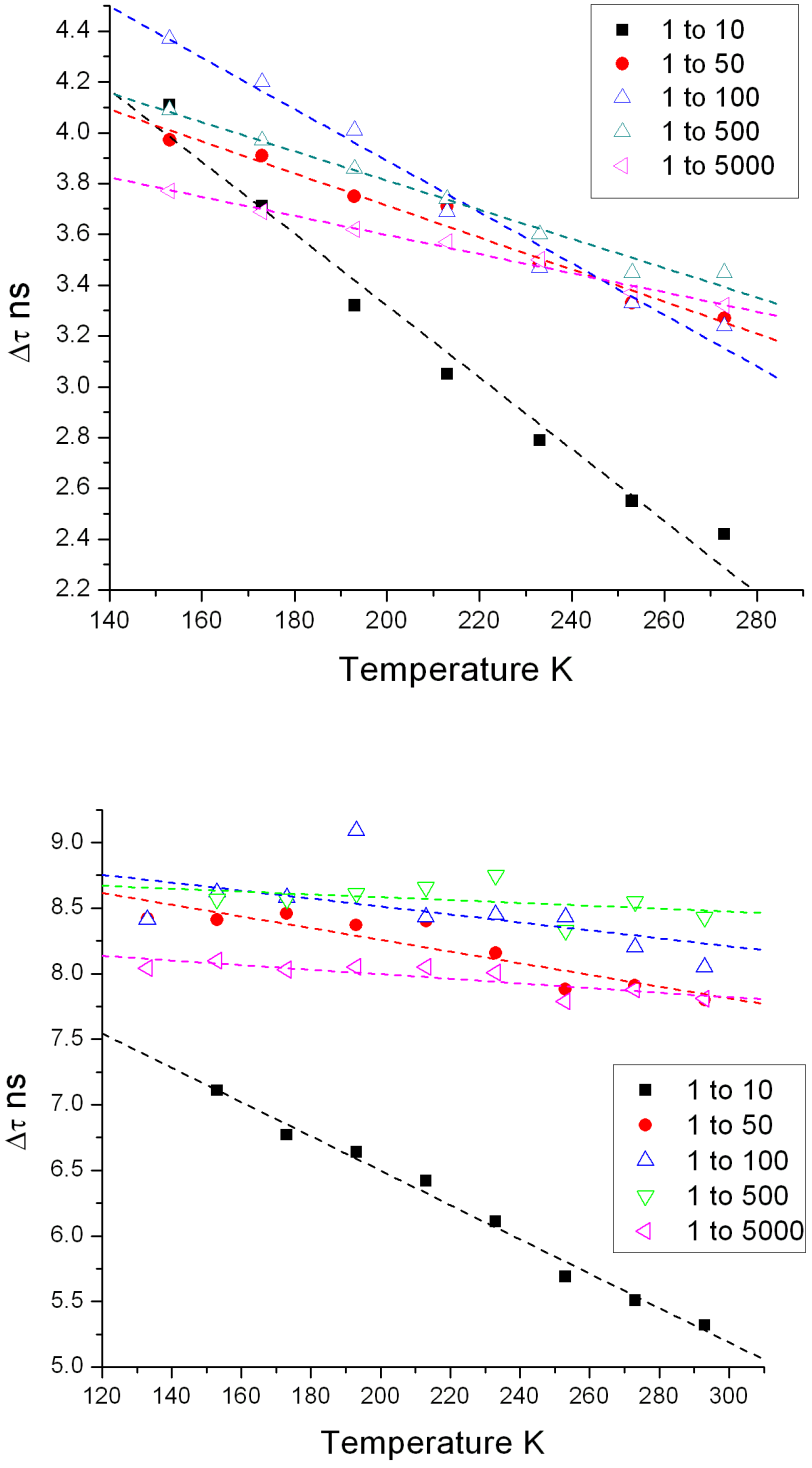

Figure 5.11: *Difference between neat and dilute lifetimes (recorded at* 500 *nm) for oil* 7033 *(Top) and* 7169 *(bottom) over the range of temperatures sampled. The neat-dilute lifetime difference increases gradually as the temperature decreases but at varying rates as shown by the slope of each plot. For oil 7169, the neat-dilute lifetime remains relatively static at higher dilutions.*

5.3 Energy Transfer and Quenching at low temperature

Using Equation 4.2, lifetime values at varying temperatures can be used to determine the percentage energy transfer and quenching and the results for 6 neat oils are given in Figure 5.12. Neat heavy oils show little change in the rate of energy transfer and quenching as the temperature is lowered. In comparison to neat light oils which are inherently less viscous, the value for % energy transfer and quenching decreases by a larger amount.

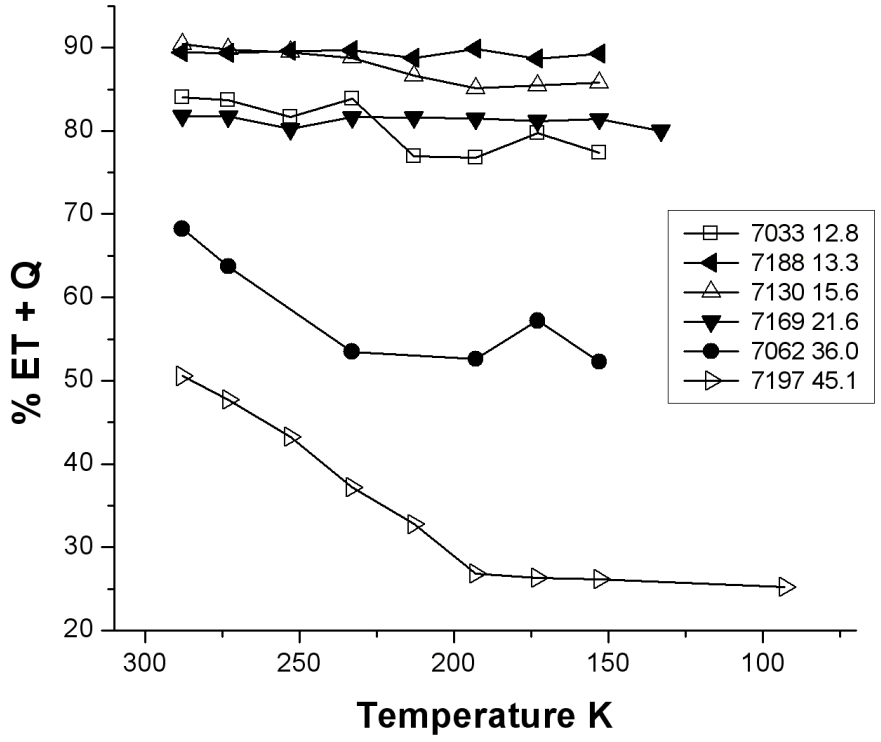

Figure 5.12: *Variation of % Energy transfer and quenching with temperature. Energy transfer and quenching values were determined using Equation 4.2. Heavy oils show a high degree of energy transfer and quenching and little change is observed with decreasing temperature (approx* $5 - 10\%$*). Lighter oils show a greater change of energy transfer and quenching with temperature. Data recorded at an emission wavelength of 500 nm.*

At lower temperatures, the percentage change in Energy Transfer and Quenching remains relatively static. It is important to compare % Energy Transfer values

calculated using the areas under the emission spectra, according to Equation 4.1. For oil 7130, no change in energy transfer is observed while for 7033 there seems to be a reduction in energy transfer with temperature. However, consideration should be made on the possibly large error on these values for energy transfer and the nature of how these values are calculated, i.e, % Energy Transfer is calculated using the difference in integrated peaks between neat and dilute cases. The large fluctuation in the values of % Energy Transfer for oil 7033 are considered to be due to symptomatic of this method using spectral areas. While analysis on lighter oils would enhance the findings presented here; the expectation is that quenching simply reduces until a solidification of the sample and after solidification, energy transfer can be deemed to remain relatively constant across the range of temperature sampled.

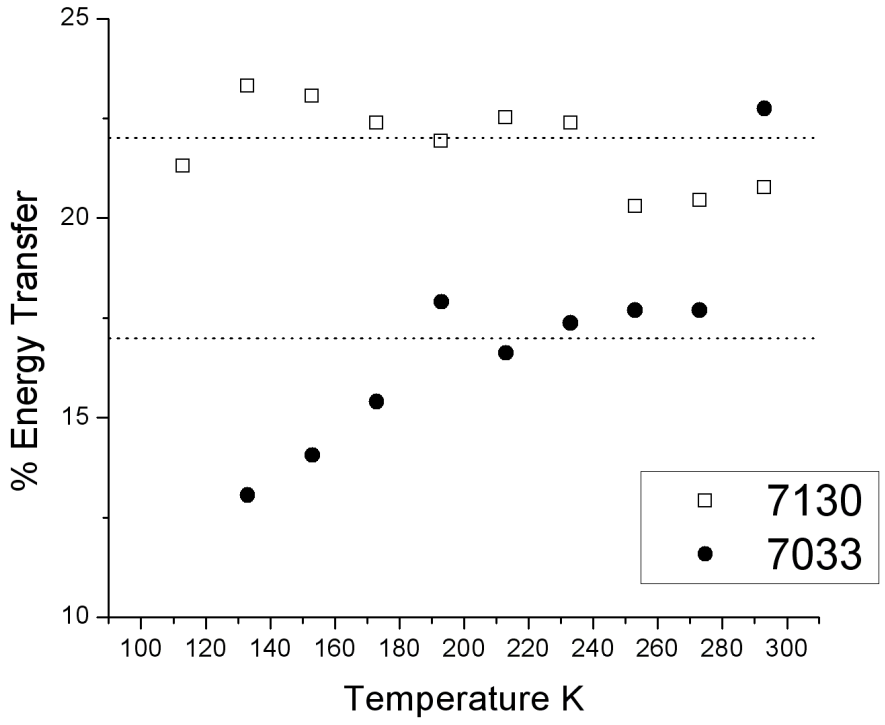

Figure 5.13: *Variation of % Energy transfer with temperature for two heavy oils, determined using Equation 4.1. Data recorded at an emission wavelength of 500 nm.*

5.4 Modeling the temperature effect on crude oil fluorescence

Few studies [201, 202, 205–210] on the determination of Arrhenius parameters for aromatic hydrocarbons have been reported in the literature and to the best of my knowledge; no studies pertain to Arrhenius behaviour of crude oils. The average lifetime versus temperature data was found to fit an Arrhenius plot, some examples of which is shown in Figure 5.14. The oils presented in this figure represent a range of API gravities, covering heavy to light neat oils. All lifetimes were recorded at 500 nm emission.

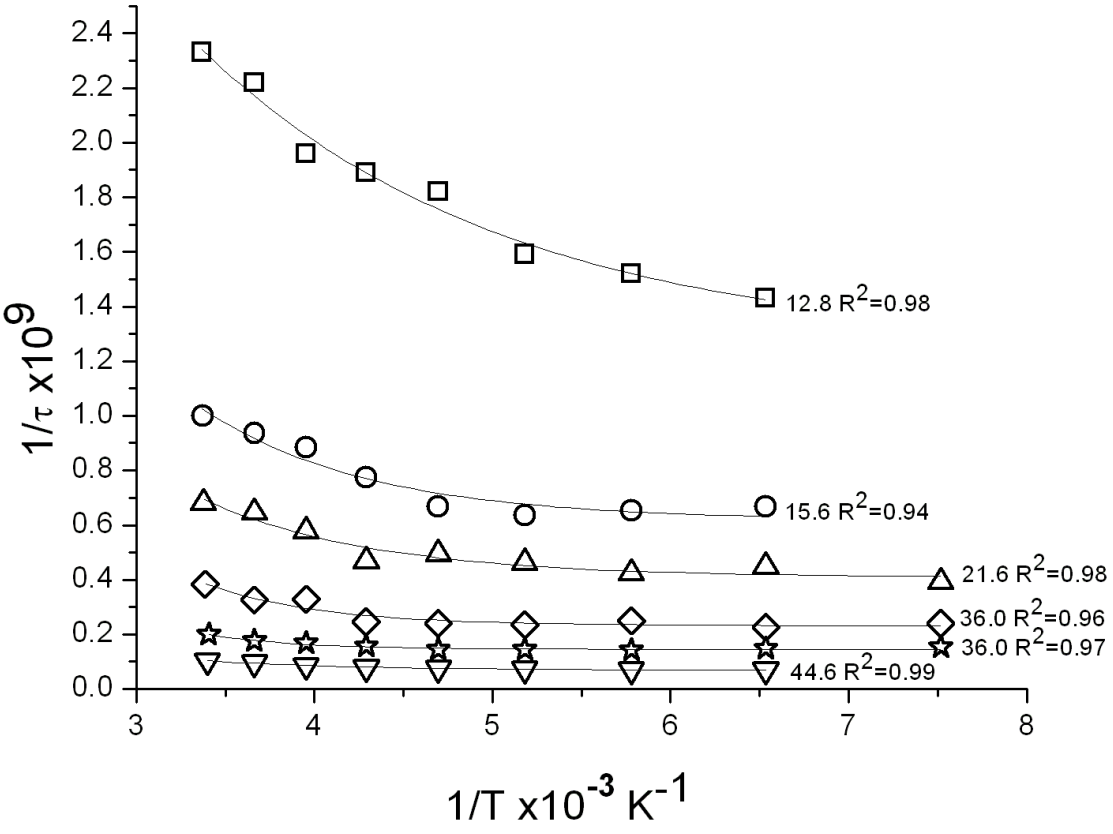

Figure 5.14: *Effect of temperature on average lifetimes (recorded at* 500 *nm emission) for* 6 *representative neat crude oils. Also shown are the* API *gravities and the correlation coefficients for the non-linear least squares fitting line to the Equation 5.1. (* □*:*7033,○*:*7130, △*:*7169, ◊*:*7062, ☆*:*7193, ▽*:*7098*).*

As discussed in the previous section, energy transfer and quenching in light oils decreases as the temperature is reduced. For heavy oils, energy transfer and transfer varies to a lesser degree. For the other non-radiative pathways in crude oils, the influence of temperature is unknown. If the non-radiative components (collisional quenching, energy transfer, internal conversion, static quenching (sphere of action quenching)) are be collectively represented by an Arrhenius type temperature dependent term then the data in Figure 5.14 can be fitted to:

$$\frac{1}{\tau} = \frac{1}{\tau_0} + A\ exp\left(\frac{-E_{NR}}{RT}\right) \tag{5.1}$$

where τ is the recorded fluorescence lifetime, τ_0 is the intrinsic lifetime, E_{NR} is the activation barrier to non-radiative decay, R is the gas constant and A is the pre-exponential factor of the temperature-dependent process (adapted from [146, 205]). As discussed in [146], this Arrhenius type equation implies that for a fluorescence decay, the rate of conversion to ground state is constructed from both non-radiative decay temperature-dependent component and temperature-independent intrinsic lifetime. Due to the heterogeneous nature of crude oils, and in this context, the activation term can be viewed as a summation of all the non-radiative processes occurring during excitation of crude oils. Non-linear least squares fitting of equation 5.1 to the data gives values for A, E_{NR} and τ_0 for each crude oil. In this context, the intrinsic lifetime (τ_0) indicates the lifetime where non-radiative processes are at a minimum. Heavy oils show a weaker temperature dependence when compared to light oils which is illustrated by the difference between oil 7033 and oil 7098 in Figure 5.14. As the crude oil is cooled, the effect of collisional quenching tends to zero, static quenching and energy transfer effects become more prominent. The fitted intrinsic lifetimes are also in good agreement with the lifetimes determined from visual inspection of the plateau point temperatures (Figure 5.6). The expansion of equation 5.1 to include extra exponential terms was also performed but this did not result in a better fit or lower correlation coefficients. Tables 5.1 to 5.3 show the recovered Arrhenius parameters and τ_0 values for three representative crude oils (light, medium, and heavy). Note that the units of activation energy of kJ per unit concentration take into account the fact that the fluorophore concentration can not be determined accurately for neat crude oils and for the purposes of this work is

left as an arbitrary concentration unit. The R^2 values indicate that reasonable fits to the Arrhenius equation were found with values of A and E_{NR} largely remaining unchanged over the emission wavelength range when the large fitting errors for these values are taken into account. This result suggests that non-radiative processes are *independent* of fluorophore composition since the emission wavelengths represent different populations of emitting fluorophores in crude oils.

Table 5.1: *Parameters recovered from the Arrhenius equation at different emission wavelengths for oil* 7032 *(*API *gravity* 19.1*). The error in the intrinsic lifetime averaged at* ± 0.2 *ns, while the error on the activation energies and pre-exponential factors is given in brackets. Correlation coefficients are given as a measure of the goodness of fit of the data to linear fitting.*

Wavelength nm	τ_0 ns	$A \times 10^{10} s^{-1}$	$E_{NR}(kJconc^{-1})^{\dagger}$	R^2
440	0.87	1.33(0.5)	6.74(1.0)	0.991
450	0.87	2.19(2.1)	7.94(2.5)	0.951
460	0.93	1.39(1.3)	6.92(2.4)	0.949
470	0.96	2.10(1.1)	8.41(1.3)	0.986
480	0.99	2.54(1.5)	9.24(1.5)	0.984
490	1.08	2.37(2.0)	9.31(2.3)	0.965
500	1.13	3.49(5.0)	10.87(3.6)	0.927
510	1.29	1.02(1.2)	8.06(3.1)	0.926
520	1.36	1.78(2.4)	9.76(3.5)	0.924
530	1.45	2.26(2.7)	10.88(3.0)	0.948

We have seen before that average lifetime versus emission wavelength are curved in nature that reflects how different populations of fluorophores interact. If the intrinsic lifetime is plotted against the emission wavelength a linear response is now obtained as shown in Figure 5.15. Now, the non-radiative processes are not reflected in the lifetime value and so a simpler picture is obtained: the short blue emitting fluorophores have short lifetimes and the larger red emitting fluorophores have longer lifetimes. A linear trend is found for the oils shown, but a greater spread is found for the light oil 7703 even though the fitting error for all oils is ~ 0.2 ns. Since all oils give reasonable fluorescence emission intensity in the 480-520 nm range, a wavelength of 500 nm was chosen for comparison of all the Batch 1 oils by their Arrhenius and intrinsic lifetime values, given in Table 5.4. The error on the Arrhenius parameters

† The units of activation energy of kJ per unit concentration take into account the fact that the fluorophore concentration can not be determined accurately for neat crude oils and for the purposes of this work is left as an arbitrary concentration unit.

Table 5.2: *Parameters recovered from the Arrhenius equation at different emission wavelengths for oil* 7062 *(*API *gravity* 36.0*). The error in the intrinsic lifetime averaged at* ±0.2 *ns, while the error in the activation energies and pre-exponential factors is given in brackets. Correlation coefficients are given as a measure of the goodness of fit of the data to linear fitting.*

Wavelength nm	τ_0 ns	$A \times 10^{11} s^{-1}$	$E_{NR}(kJconc^{-1})^{\ddagger}$	R^2
440	3.24	2.39(2.3)	15.24(2.4)	0.975
450	3.40	1.66(1.5)	14.59(2.2)	0.977
460	3.43	2.77(2.7)	16.09(2.4)	0.977
470	3.67	2.3(2.3)	16.03(2.5)	0.976
480	3.83	2.56(3.2)	16.75(3.1)	0.966
490	3.89	3.03(4.4)	17.41(3.6)	0.958
500	4.12	2.29(3.0)	16.91(3.2)	0.964
510	4.45	1.06(1.6)	15.16(3.7)	0.943
520	4.59	1.85(2.3)	16.75(3.1)	0.966
530	4.73	3.4(4.7)	18.23(3.4)	0.976

Table 5.3: *Parameters recovered from the Arrhenius equation at different emission wavelengths for oil* 7703 *(*API *gravity* 50.6*). The error in the intrinsic lifetime averaged at* ±0.2 *ns, while the error in the activation energies and pre-exponential factors is given in brackets. Correlation coefficients are given as a measure of the goodness of fit of the data to linear fitting.*

Wavelength nm	τ_0 ns	$A \times 10^{9} s^{-1}$	$E_{NR}(kJconc^{-1})^{\S}$	R^2
440	9.41	7.50(2.0)	10.46(0.7)	0.996
450	9.79	6.94(1.8)	10.44(0.6)	0.996
460	8.84	11.62(0.6)	13.07(1.3)	0.987
470	10.28	4.19(1.6)	9.43(0.9)	0.991
480	10.66	3.7(1.2)	9.41(0.8)	0.994
490	10.50	4.63(1.9)	10.26(1.0)	0.991
500	11.17	4.65(2.8)	10.38(1.5)	0.982
510	12.38	2.28(0.5)	8.63(0.6)	0.996
520	13.14	1.87(0.9)	8.27(1.2)	0.988
530	13.66	1.77(0.7)	8.19(1.09)	0.991

have been calculated by the graphing program Origin[¶].

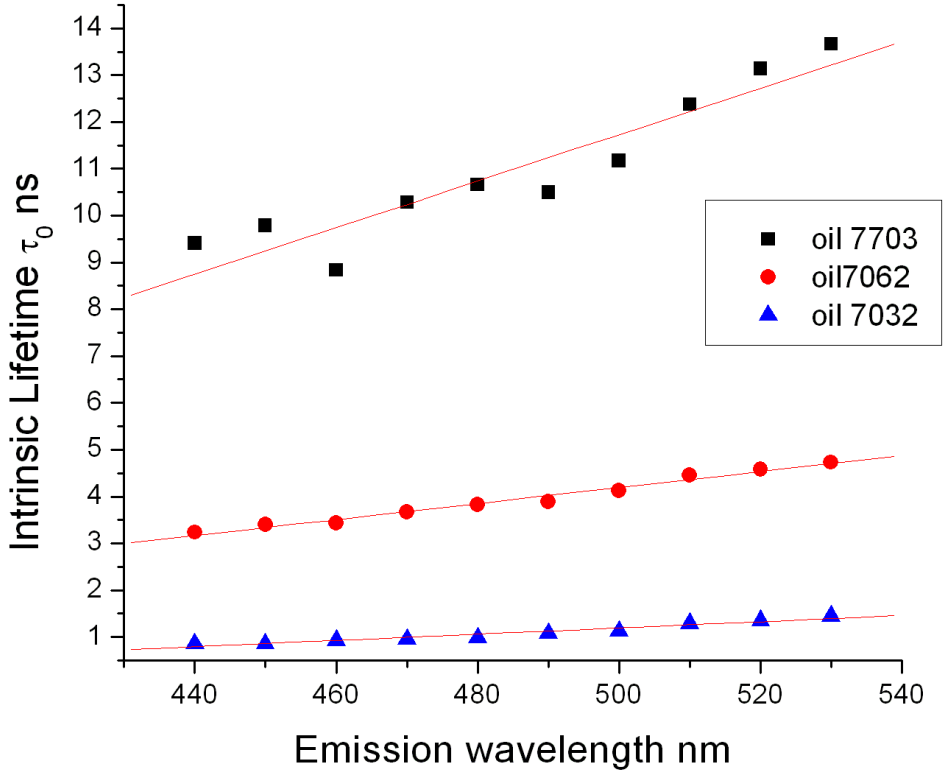

Figure 5.15: *Variation of intrinsic lifetime with emission wavelength for three crude oils representing the full API gravity range.*

Though the data presented in Table 5.4 represents a summation of the physical processes resulting in approximated Arrhenius terms, it is interesting that the pre-exponential factors and activation energies are in the same order of magnitude for a temperature based lifetime study on methyl anisoles [209]. This study attempted to provide mechanistic details of various isomers of methyl anisole based on low temperature lifetime measurements and concluded that for these compounds, the very small temperature effect (low values for the Arrhenius terms) was primarily due to activated intersystem crossing being the dominant temperature dependent

[¶] Non-linear least squares fitting minimizes the value of χ^2 representing the deviations of the theoretical curve from the experimental data. Depending on the number of parameters used, a series of partial differential equations are found which must be solved by an iterative method (i.e. no explicit solution exists for these equations). In this case, the Levenberg-Marquardt (LM) algorithm is used to provide estimations for the parameter values. The errors on the fitted parameters are derived during LM iteration.

process. Table 5.4 shows the Arrhenius parameters determined for all the oils in Batch 1. As questioned in [209], can reliable values for Arrhenius parameters be obtained using temperature-dependent de-excitation from the S_1 state? Equation 5.1 simply assumes that only the non-radiative pathways of de-excitation of the S_1 state are temperature independent. It would seem more likely that in the context of crude oil fluorescence, non-radiative pathways are also dependent on temperature as indicated by the low activation energy values ($\sim$ 6 to $\sim$ 24 kJconc^{-1}). The low values of activation energy could also imply that deactivation of the excited state of the fluorophores in crude oils is primarily diffusion controlled [204].

Table 5.4: *Arrhenius parameters calculated for neat crude oils as determined by the non-linear least squares fitting of the data to Equation 5.1. Measurements were recorded at* 500 *nm. The fitting errors for the data are as follows:* τ_0 *(*$\sim$ 0.2 *ns),* E_{act} *(*$5-8\%$*)and A (*$\sim 1-2\%$*).*

Oil	API	Arrhenius Parameters			R^2
		τ_0 ns	A $\times 10^{10} s^{-1}$	E_{act} $(kJconc^{-1})$¶	
7033	12.8	0.8	0.15	5.35	0.982
7188	13.3	1.43	0.06	4.6	0.961
7321	14.1	2.56	0.8	5.92	0.930
7130	15.6	1.62	1.54	8.95	0.940
7032	19.1	1.13	3.50	10.87	0.927
7169	21.6	1.87	0.04	5.79	0.980
7633	24.8	11.56	4.46	17.03	0.998
7187	29.4	7.86	98.1	24.42	0.986
7093	30.9	5.37	1.31	12.16	0.968
7324	32.3	3.44	1.46	12.31	0.936
7632	32.7	6.59	171.3	22.91	0.996
7186	34.3	8.21	300.0	27.18	0.987
7062	36.0	4.12	22.9	16.91	0.964
7193	36.0	6.87	6.2	17.21	0.948
7090	36.8	6.76	22.0	19.24	0.977
7086	39.5	6.96	1.29	12.92	0.999
7058	40.1	9.22	1.94	14.06	0.998
7098	44.6	14.59	1.41	13.32	0.997
7197	45.1	9.9	0.55	10.81	0.997
7703	50.6	11.17	0.47	10.37	0.982

In Table 5.4, oils 7186, 7187 and 7632 are clear outliers with the highest values of activation energies and pre-exponential factors across the set of oil samples. These oils follow similar behaviour leading to higher Arrhenius parameters, whereby these oils quickly reach a point where no further changes in temperature influence the lifetime. In comparison, the other oils show a more gradual change in lifetime with temperature. This is shown in Figure 5.16 where oil 7632 represents an example of the Arrhenius behaviour of these outliers. In comparison oil 7197 shows a gradual change in lifetime with temperature. In both cases the Arrhenius equation fits the data and the correlation coefficients are similar (see Table 5.4).

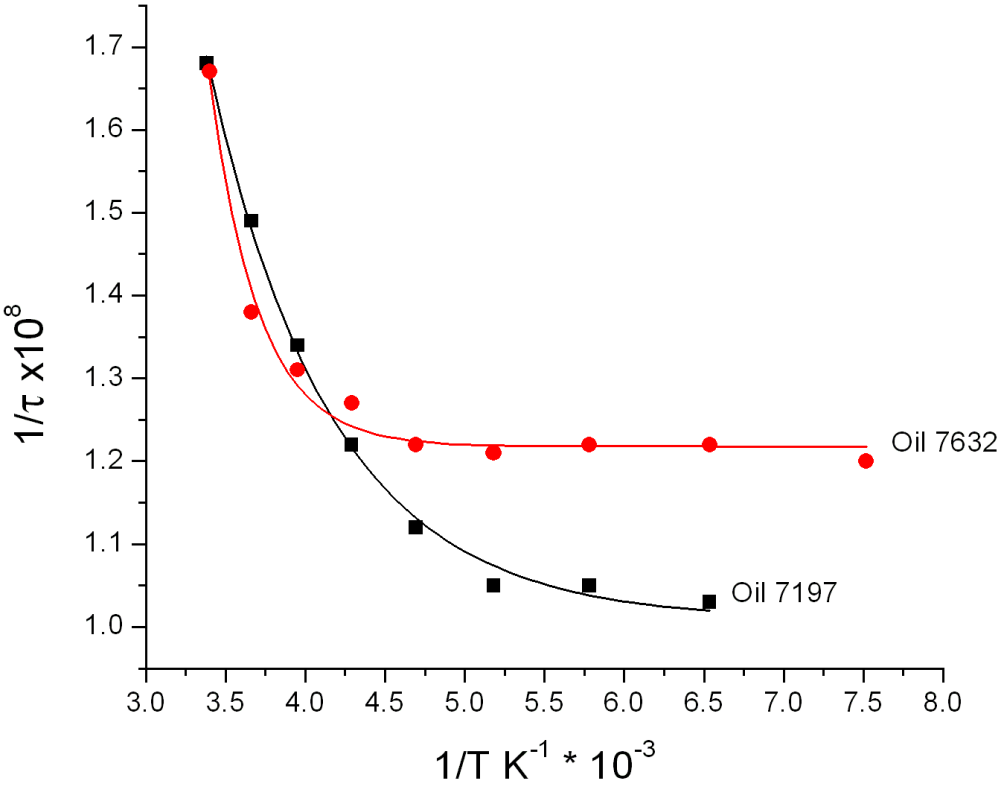

Figure 5.16: *Arrhenius plots for oils 7197 (black points and fitted curve) and 7062 (red points and fitted curve). Emission recorded at 500 nm.*

As for average lifetime correlations with physical and chemical properties, τ_0 also varies with oil density (Figure 5.17). In this figure, oils 7098 and 7633 stand out as outliers to this trend, which is similar to the correlations based on measured average lifetimes; the reasons for this (abnormally high wax and low polar content) have

been previously described. Similarly correlations with corrected alkane and polar concentrations can be made (Figure 5.18). Comparison of the correlation coefficients shows a small improvement in fitting using the intrinsic lifetime data as shown by the values in Table 5.5.

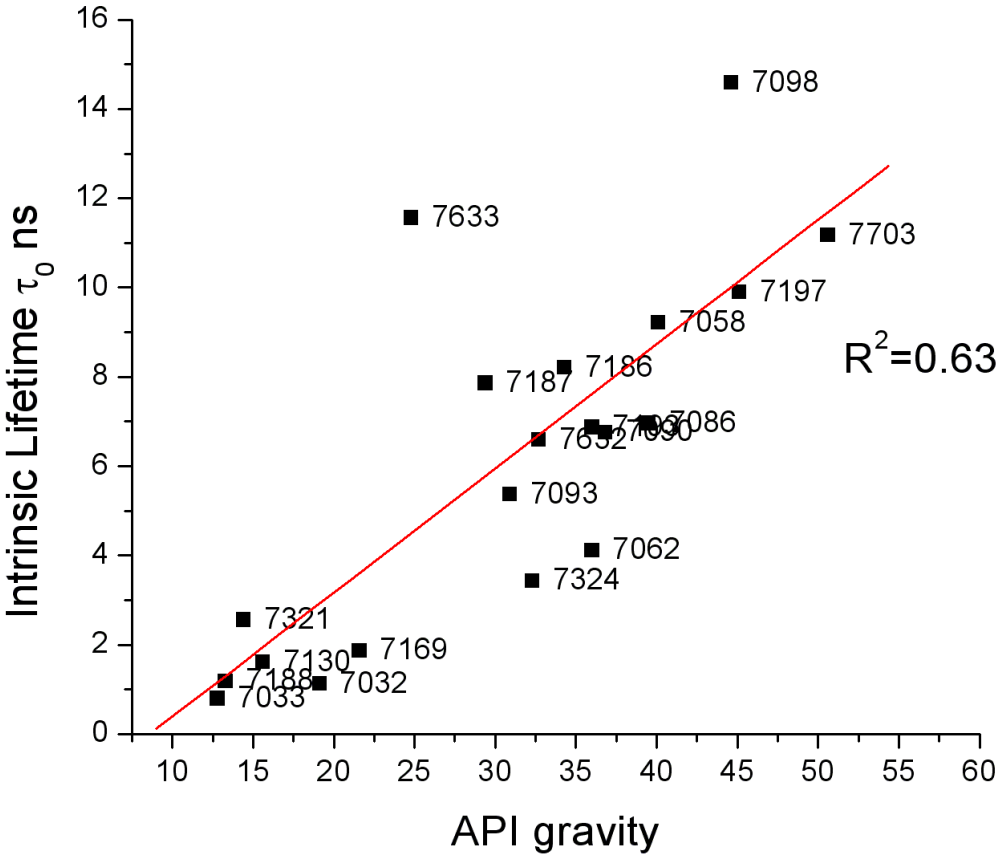

Figure 5.17: *Correlation of intrinsic lifetimes with* API *gravity. A general positive trend with a high degree of scatter is observed.*

Table 5.5: *Comparison between correlations based on discrete average lifetime experiments (500 nm emission wavelength) and those made using the intrinsic lifetime.*

Property	R^2 based on τ_0	R^2 based on τ_{av} (500 nm)
Polar	0.77	0.74
Corrected Alkane	0.61	0.56
API	0.63	0.56

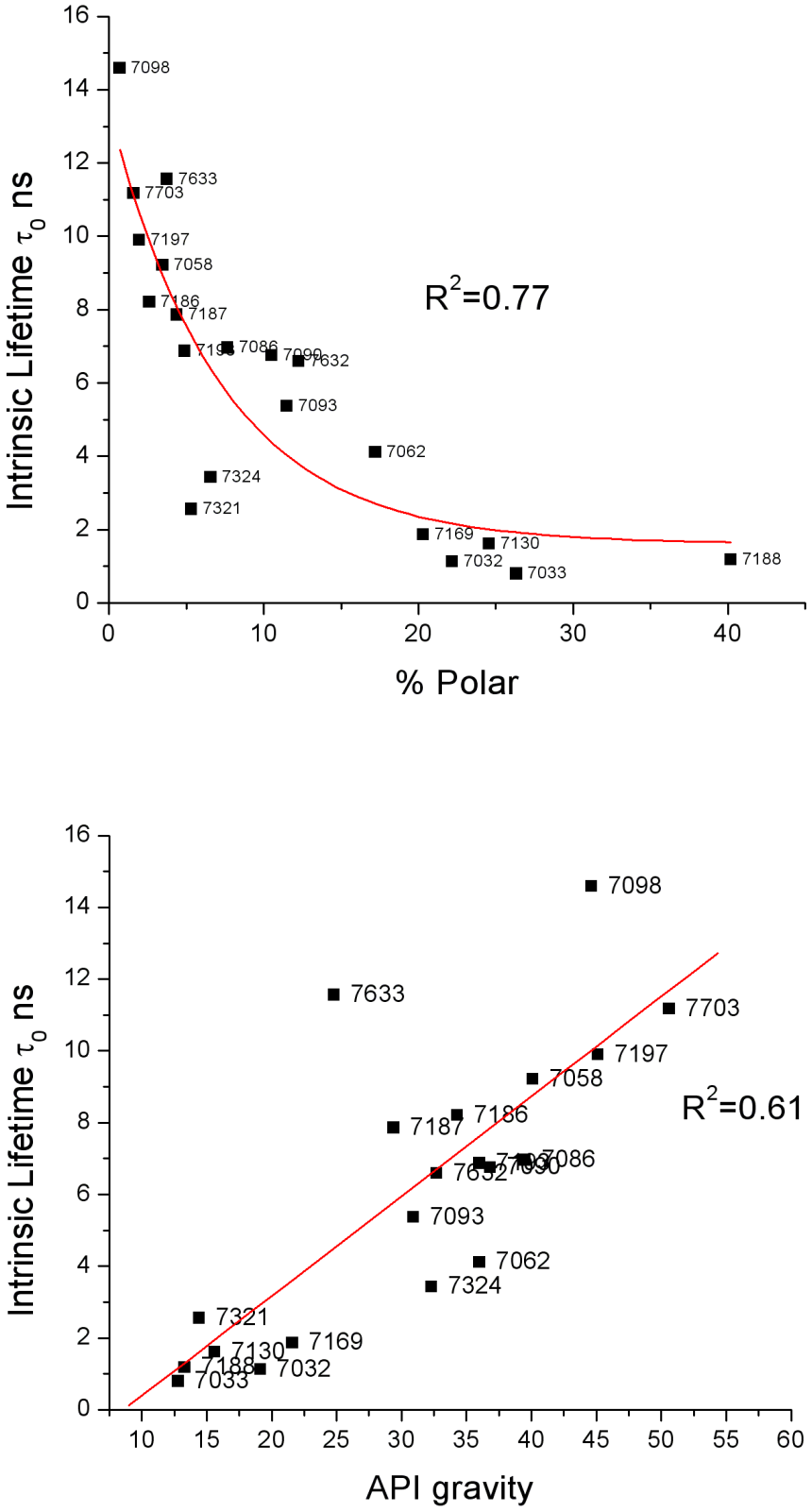

Figure 5.18: *Correlations between intrinsic lifetimes and gross chemical composition parameters (%Corrected alkane and %Polar) for Batch* 1 *crude oils.*

In comparison to this temperature study on neat oils, an Arrhenius analysis has also been applied to a sub-set of 6 oils diluted with the MeCH:MeCP solvent mix (Table 5.6) along with the values for the neat crude oils (units of E_{act} for neat crude oils are kJ conc^{-1}). For neat oils there are more collisional processes occurring (quenching and energy transfer) leading to lower lifetimes. On dilution, the greatest change in the value of τ_0 occurs on initial dilution of 1:10; for more dilute samples τ_0 then reaches a maximum value. At low dilutions, oils follow the Arrhenius model but for some higher dilutions, Arrhenius parameters could not be recovered due to poor fitting of the model to the data (as indicated by NC in Table 5.6). At highly dilute samples, temperature has a reduced effect where collisional effects are already minimised by dilution. For the light oils 7062 and 7197, since lifetimes were unchanged after dilutions of 1:50, temperature data were not recorded (NR) for dilutions from 1:500. The Arrhenius model could not be applied at high dilutions since small changes in lifetime with temperature resulted in a large degree of scatter in the Arrhenius plots. For the cases where the Arrhenius model is followed, the calculated values of τ_0 are consistent with average lifetimes determined at the lowest temperatures. But for E_{act} and A values, a large spread in magnitudes is found with no discernable trend with dilution. The low confidence in the values of E_{act} and A values are reflected by the R^2 values.

Table 5.6: *Arrhenius parameters for dilute crude oils as determined by the non-linear least squares fitting of the data to Equation 5.1. Measurements were recorded at 500 nm. The calculated errors for the data are as follows: τ_0 (~ 0.2 ns), $E_{act}(5-8\%)$ and A ($\sim 1-2\%$).* NR *indicates Not Recorded and* NC *indicates where there was too much scatter in the data to generate the appropriate values.*

Oil	API	Dilution	Arrhenius Parameters			R^2
			τ_0 ns	A $\times 10^{10} s^{-1}$	E_{act} $(kJconc^{-1})$	
7033	12.8	neat	0.8	0.77	4.8	0.982
		1:10	5.1	0.15	5.4	0.984
		1:50	4.9	0.065	5.4	0.981
		1:100	5.5	0.086	5.1	0.983
		1:500	5.4	0.033	3.1	0.996
		1:5000	4.5	0.26	8.8	0.958
7188	13.3	neat	1.43	0.058	4.6	0.961
		1:10	10.6	0.14	7.0	0.997
		1:50	11.0	0.24	12.1	0.986
		1:100	11.1	0.51	8.8	0.987
		1:500	11.2	0.78	10.2	0.938
		1:5000	10.9	0.11	6.0	0.859
7130	15.6	neat	1.62	1.54	8.95	0.938
		1:10	13.8	0.04	3.9	0.983
		1:50	11.2	0.53	14.0	0.970
		1:100	12.0	0.03	7.1	0.998
		1:500	11.3	0.03	7.50	0.967
		1:5000	NC	NC	NC	-
7169	21.6	neat	1.87	0.043	5.8	0.980
		1:10	9.1	0.04	6.2	0.996
		1:50	10.4	0.04	9.0	0.973
		1:100	10.5	0.05	10.4	0.970
		1:500	10.5	0.05	12.3	0.870
		1:5000	10.1	0.01	6.5	0.931
7062	36.0	neat	4.12	22.92	16.91	0.964
		1:10	9.0	0.23	9.9	0.983
		1:50	9.4	0.03	7.1	0.987
		1:100	9.3	0.01	5.0	0.944
		1:500	NR	NR	NR	-
		1:5000	NR	NR	NR	-
7197	45.1	neat	9.9	0.55	10.81	0.997
		1:10	13.0	0.74	9.9	0.968
		1:50	NC	NC	NC	-
		1:100	NC	NC	NC	-
		1:500	NR	NR	NR	-
		1:5000	NR	NR	NR	-

5.5 Quenching of crude oil fluorescence

The temperature dependence of fluorescence quenching of selected crude oils was investigated between 293K and 153K. Figure 5.19 shows the modified Stern-Volmer plot for the heavy oil 7033, where the slope of the high concentration part (or dynamic region) reduces with decreasing temperature. This shows that for crude oils, collisional quenching processes in diluted oils is the dominant mechanism over static effects. The associated Stern-Volmer data from these plots can be found in Table 5.7.

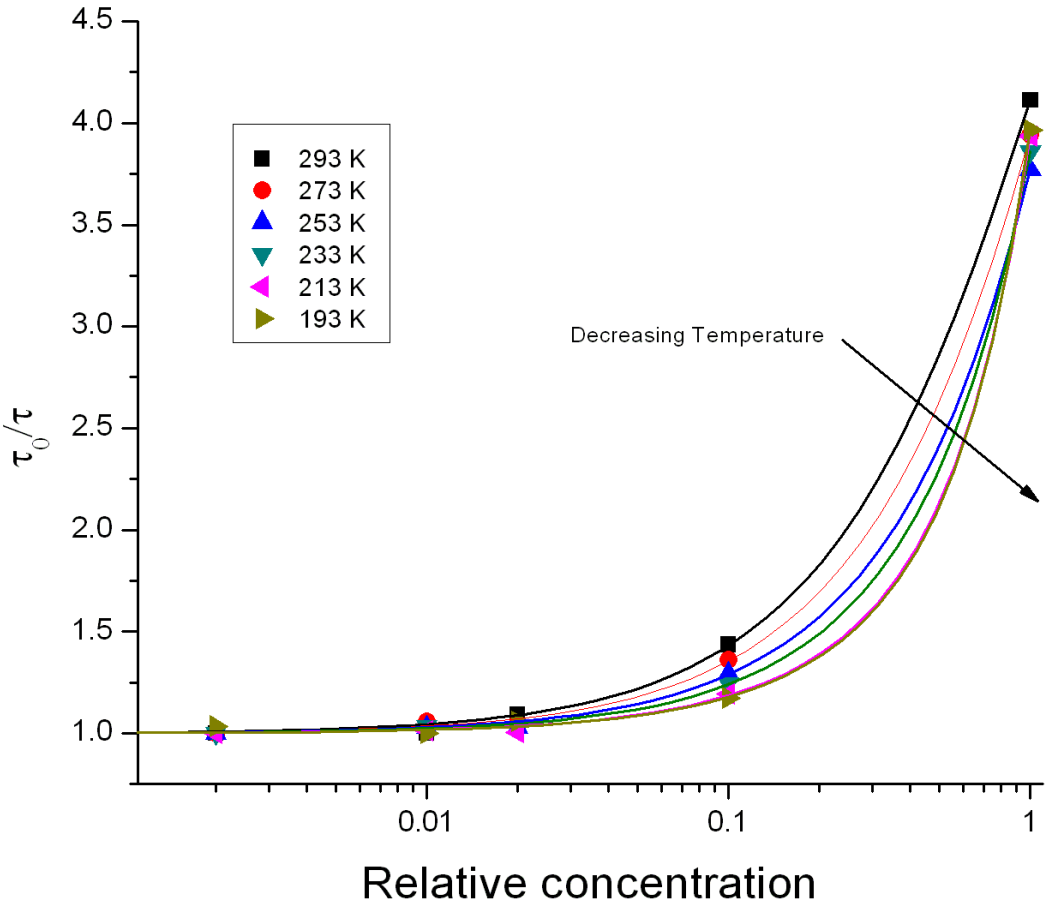

Figure 5.19: *Modified Stern-Volmer plots for heavy oil* 7033 *over a range of temperatures, data measured at* 500 *nm. As the temperature decreases the slope decreases indicating that collisional quenching is the dominant mechanism. Deoxygenated solutions were used throughout.*

Table 5.7: *Quenching parameters from fitting of lifetime data for oil 7033 recorded at 500 nm to the modified Stern-Volmer Equation 4.7. Dilutions were made using a 3:2 Methlycyclohexane:Methylcyclopentane mix at room temperature. Errors calculated for the collisional quenching constant are also given in brackets.*

Temp K	K_{sv}	K_{st}	R^2	τ_0	$k_q \times 10^8 s^{-1}$
293	4.81	0.35	0.9954	3.99	12.1 (3.11)
273	3.84	0.21	0.9997	3.90	9.85 (0.85)
253	2.94	0.04	0.9998	3.96	7.42 (0.63)
233	2.17	0.20	0.9998	4.13	5.25 (0.59)
213	1.16	0.59	0.9996	4.29	2.71 (1.12)
193	1.02	0.67	0.9985	4.64	2.20 (2.17)
173	NC	1.99	0.9975	4.86	NC
153	NC	1.99	0.9996	5.07	NC

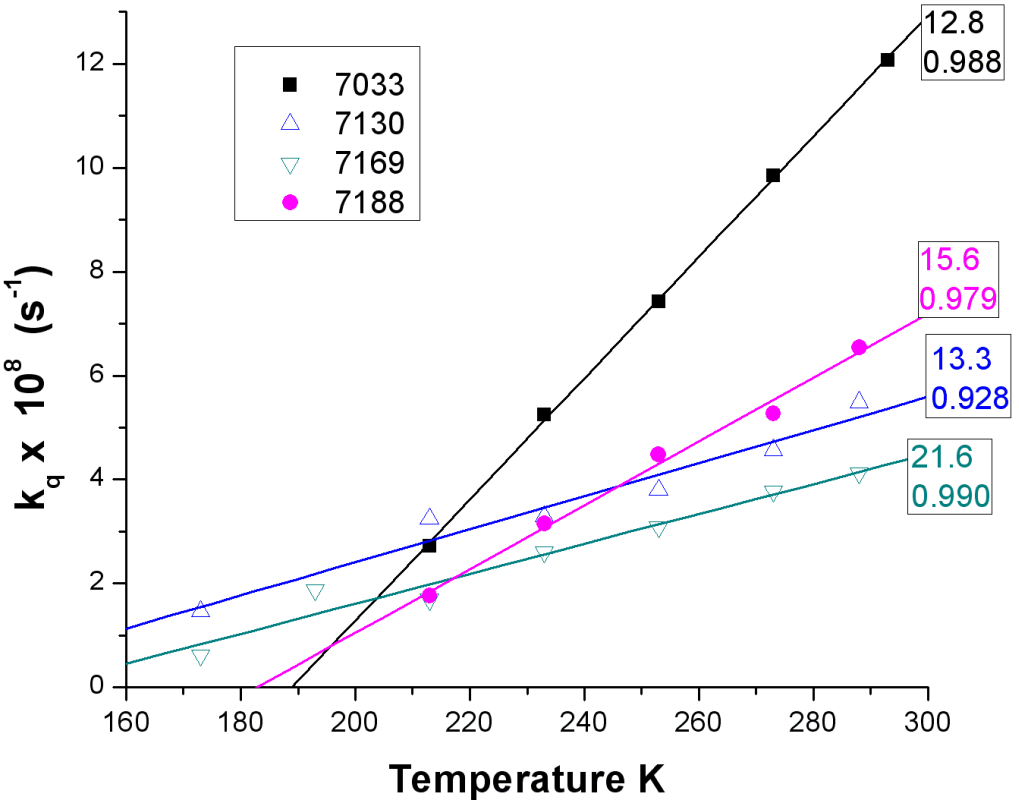

Figure 5.20: *Collisional quenching constant as a function of temperature for several oils. Data was measured at 500 nm. API gravity values and correlation coefficients (r^2)are also given.*

At the lowest temperatures (173-153 K), fitting of Equation 4.7 does not return a value for K_{sv} as indicated by NC. This failure of the model is caused by the small change in lifetimes between high and low dilutions at low temperature. For all the other temperatures sampled, the Stern-Volmer constant reduces as the temperature reduces and hence the value of the collisional quenching constant k_q (as calculated from $K_{sv} = k_q \times \tau_0$) decreases linearly with decreasing temperature as shown in Figure 5.20. This figure shows the data for the set of diluted oils and implies that collisional quenching rates depend linearly with temperature and that at high or low temperatures, the collisions that effectively reduce the fluorescence in crude oils are similar. The type of oil also has a strong influence on this mechanism as the slope of the linear fits to the quenching constants decreases with API gravity.

5.6 Viscosity effect on crude oil fluorescence

In order to examine the effect of temperature on the viscosity of crude oils, it is useful to make comparisons to diffusion processes in simple systems. The diffusion constant of a molecule depends on both its size and on the properties of the surrounding media. For example, taking a hard sphere in a solvent with a temperature dependent viscosity $\eta_S(T)$, the translational diffusion constant for a single species is calculated by the Stokes-Einstein relation [36]: $D = \frac{k_B T}{6\pi\eta_s(T)r}$ where r is the radius of the sphere and k_B is Boltzmann's constant. For a single species, diffusion controlled rate constants (k_d) can be approximated using the Stokes-Einstein diffusion equation [39]: $k_d = \frac{8RT}{3\eta_s}$ where R is the gas constant, T is the temperature and η_s is the solvent viscosity at each temperature. An increase in viscosity leads to a slowing of the rate of collisions between fluorophores and quenchers, and thus to a reduction in the rate of quenching.

To make observations of the effect of viscosity on crude oil fluorescence, it was necessary to record/calculate the viscosity of the diluted oils as a function of temperature. As a simplification, the viscosity of diluted crude oils was assumed to be equivalent to the viscosity of the solvent mixture used for dilution. Individual viscosity values as a function of temperature, of solvents MeCH and MeCP, were obtained from the online database http://www.fiz-chemie.de/infotherm/.

Using the Arrhenius mixing law [211] the viscosity of the solvent mixture can be found using:

$$\ln \eta_{mix} = X_1 \ln \eta_1 + X_2 \ln \eta_2 \tag{5.2}$$

where η_{mix} is the viscosity of the mixture, X_1 and X_2 are the volume fractions of the liquids, and η_1 , η_2 are the viscosities of the neat liquids (MeCH and MeCP) respectively[‖]. Equation 5.2 was used to calculated the solvent mixture at a range of temperatures and this value was assumed to be equivalent to the viscosity of the diluted crude oil samples. Using these viscosity values, the theoretical rate constant for diffusion can be calculated at each temperature from the Stokes-Einstein diffusion equation (at room temperature this is approximately $10^7 m^3 mol^{-1} s^{-1}$). In comparison, the experimental values for the quenching coefficients derived for crude oils are of the order $10^8 s^{-1}$ (Table 5.7 and Figure 5.20).

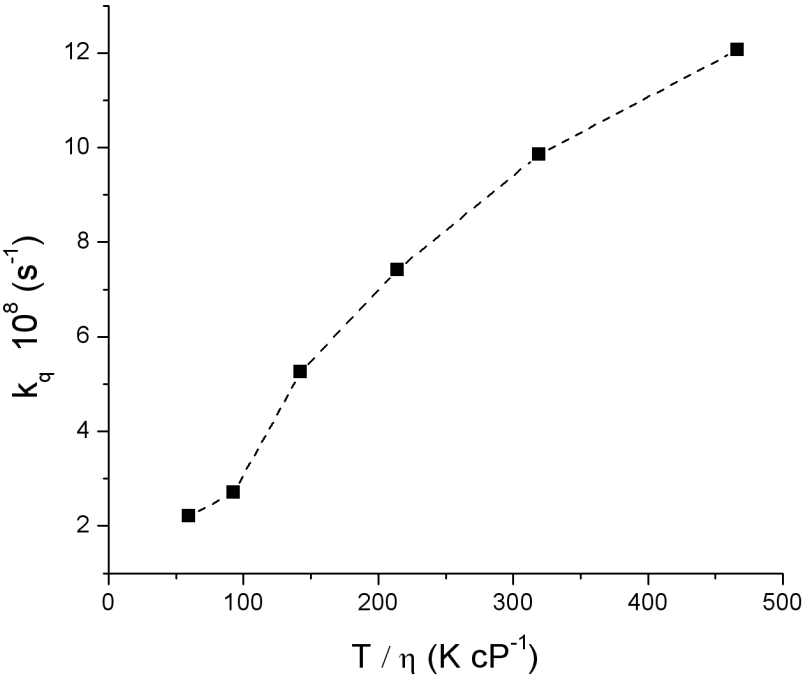

Figure 5.21: *Stokes-Einstein plot for diluted heavy oil* 7033 *measured at an emission wavelength of 500 nm.*

[‖] Enhancements to this model have been made subsequently [211, 212] but for simplicity the original form has been used for this work.

It has been postulated that the Stokes-Einstein model is not adequate for describing diffusion in crude oils [213] as evidenced by the fact that plots of $\log D$ versus $\log \frac{k_B T}{\eta_S}(T)$ are linear despite a large variance of the molecular radii that can occur. Similarly, if the quenching constant $k_q(T)$ (obtained by modified Stern-Volmer analysis) is plotted versus T / $\eta_S(T)$, a linear plot would demonstrate agreement with the Stokes-Einstein relation. For the crude oil samples, an example is shown in Figure 5.21, a curved plot is obtained for oil 7033, showing that collisional quenching and energy transfer are not diffusion-limited processes, and do not follow Stokes-Einstein behaviour.

5.7 Thermodynamic Considerations of crude oil photophysics

The Eyring equation represents the transition-state theory whose central idea is also based on a quasi-thermodynamic equilibrium between the ground state and the activated complex ($K^{\ddagger}$): the reaction rate at any given temperature depends only on the concentration of the activated complex and the rate of crossover of this activated complex. It takes the form [39]:

$$\ln\left(\frac{k_f}{T}\right) = -\frac{\triangle H^{\ddagger}}{RT} + \frac{\triangle S^{\ddagger}}{R} + \ln\left(\frac{k_B}{h}\right) \tag{5.3}$$

where k_f is the rate constant for fluorescence and is given by $1/\tau$, $\triangle H^{\ddagger}$ is the enthalpy ($kJmol^{-1}$), $\triangle S^{\ddagger}$ is the entropy ($Jmol^{-1}K^{-1}$), R is the gas constant ($JK^{-1}mol^{-1}$), k_B is Boltzmann's constant, and h is Planck's constant. $\frac{\triangle S^{\ddagger}}{R} + \ln\left(\frac{k_B}{h}\right)$ corresponds to the Arrhenius pre-exponential term A. $\triangle H^{\ddagger}$ and $\triangle S^{\ddagger}$ are quasi-thermodynamic quantities of the equilibrium between the ground state and the activated complex ($\triangle H^{\ddagger} = E_{act} - RT$). Whereas $\triangle S^{\ddagger}$ can be either positive or negative, generally $\triangle H^{\ddagger}$ is positive as energy is required to create the partly broken bonds of an activated complex. There are cases such as protein-folding reactions where positive $\triangle H^{\ddagger}$ values occur [214]. Fluorescence lifetimes of crude oils can also be shown to follow Eyring behaviour (using Equation 5.3) from which quasi-thermodynamic

information can be evaluated. A reverse Eyring behaviour is found for crude oils, where positive slopes in the plots of $ln(k_f/T)$ versus $1/T$ are obtained. This is in comparison to the normal case where reaction rates increase with increasing temperature leading to negative slopes in an Eyring plot. A positive Eyring plot occurs for crude oils because lifetimes increase with decreasing temperature. While this treatment results in quasi-thermodynamic parameters for crude oils it is important to note that viscosity based lifetime changes are responsible rather than complex formation. Figure 5.22 shows Eyring plots for selected neat crude oils and the associated linear fits. For most heavy immobile crude oils, Eyring behaviour is followed over the full range of temperatures sampled and a single domain is observed. A visual inspection of the slope of these plots shows similarities across the samples (apart from the heaviest oil tested) and indicate that the Eyring-derived enthalpic contributions are independent of oil type (Table 5.8).

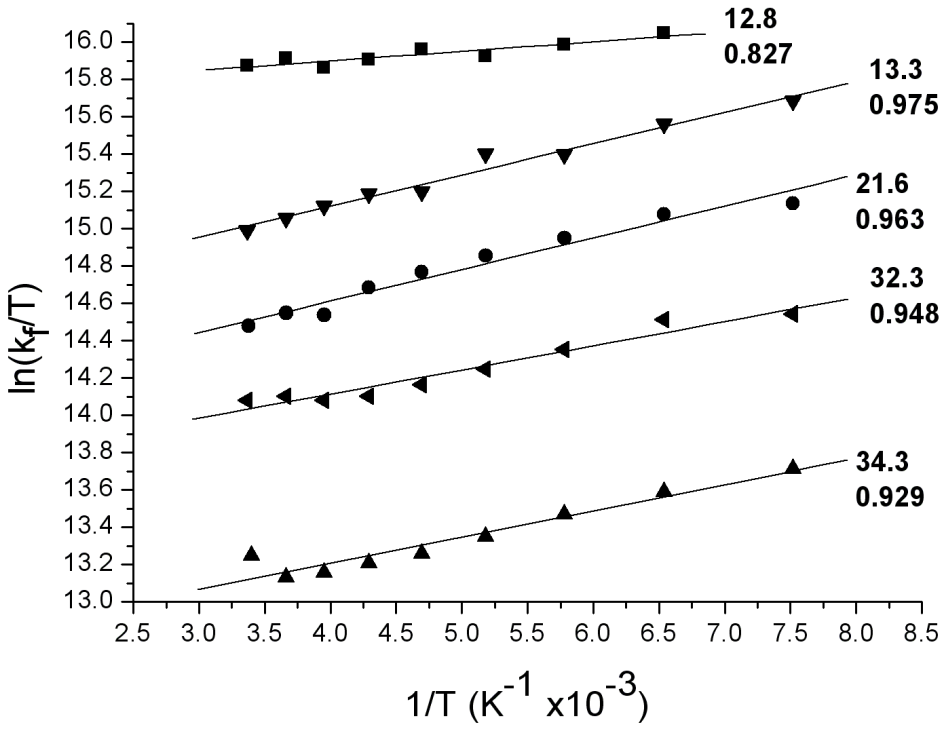

Figure 5.22: *Eyring plots for neat heavy crude oils and associated linear fits.* ■*:* 7033,▼*:* 7188, ●*:* 7169, ◄*:* 7324, ▲*:* 7186. API *gravity and correlation coefficients* (r^2) *are also shown for each plot. Lifetime data recorded at* 500 *nm.*

For lighter crude oils, deviation from the linear behaviour occurs and this is shown in Figure 5.23 where a separation into two domains or mechanisms at $\sim 212K$ becomes evident. For the low temperature domain, similar slopes are found which compare to the heavy oils. Because of the similarity in the slopes, there is very little difference in the $\triangle H^{\ddagger}$ values for the crude oils sampled despite the high variation in fluorophore concentrations or oil types. The quasi-thermodynamic data for all crude oils in Batch 1 is given in Table 5.8. The data in the table represent the linear fitting of the lifetime data to Equation 5.3 over the full temperature range for heavy oils and the partial fitting over the low temperature part for the lighter oils.

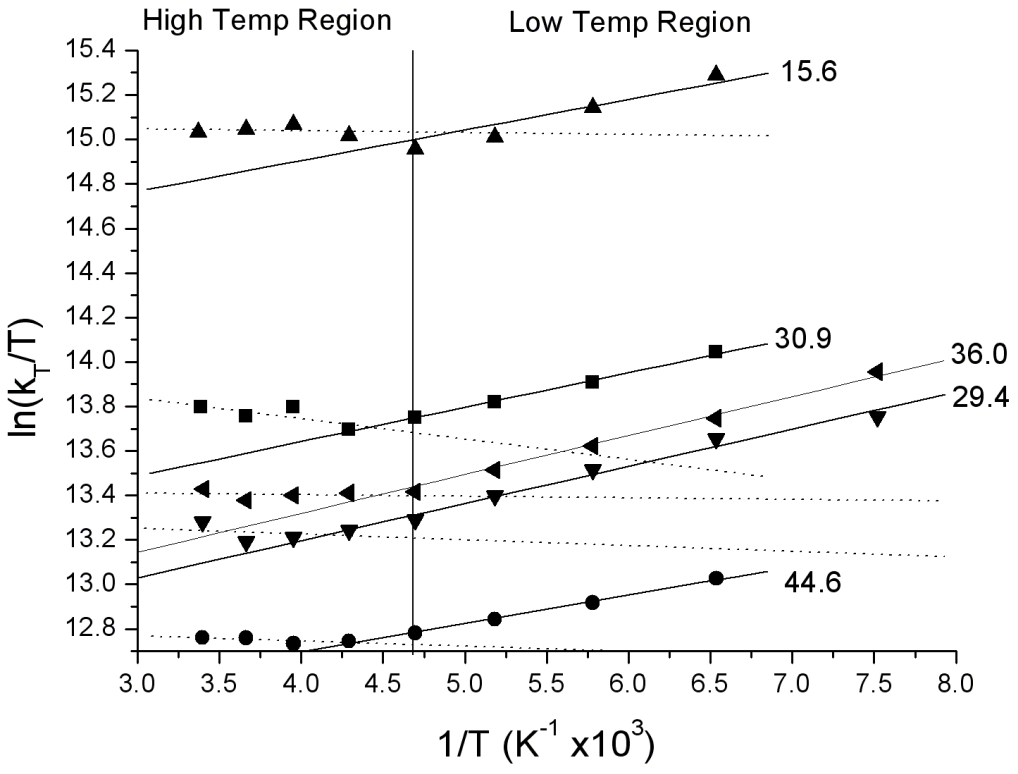

Figure 5.23: *Eyring plots for selected neat crude oils and associated linear fits.* ▲*:* 7130*,* ■*:* 7093*,* ◄*:* 7193*,* ▼*:* 7187*,* ●*:* 7098 *and the associated* API *gravity values. The vertical line separates the higher and lower temperature domains at* $\sim 212K$*.*

Table 5.8: *Eyring activation parameters (errors in $\triangle H^{\ddagger}(\sim 10-20\%)$, $\triangle S^{\ddagger}(\sim 10\%)$) for neat crude oils (plot of $ln(k_f/T)$ vs $1/T$). Measurements were recorded at* 500 *nm.*

Oil	API	Eyring Parameters	
		$\triangle H^{\ddagger}$ $(kJconc^{-1})$	$\triangle S^{\ddagger}$ $(kJconc^{-1})^{**}$
7033	12.8	-0.4	-67.2
7188	13.3	-1.4	-77.4
7321	14.1	-0.7	-77.8
7130	15.6	-1.1	-78.2
7032	19.1	-0.8	-73.7
7169	21.6	-1.4	-81.7
7633	24.8	-1.3	-95.9
7187	29.4	-1.4	-93.4
7093	30.9	-1.3	-89.3
7324	32.3	-1.1	-84.5
7632	32.7	-1.2	-92.4
7186	34.3	-1.2	-92.4
7062	36.0	-1.6	-88.8
7193	36.0	-1.5	-92.6
7090	36.8	-1.2	-90.7
7086	39.5	-1.5	-92.6
7058	40.1	-1.2	-93.1
7098	44.6	-1.1	-96.2
7197	45.1	-1.0	-92.6
7703	50.6	-1.0	-93.3

** The units of activation energy of kJ per unit concentration take into account the fact that the fluorophore concentration could not be determined accurately for neat crude oils and for the purposes of this work is left as an arbitrary concentration unit.

Though small in magnitude, the calculated values for $\triangle H^{\ddagger}$ are all negative, which derives from the positive slope of the Eyring plots in Figures 5.22 and 5.23. The values of $\triangle H^{\ddagger}$ also do not vary significantly across all the oils tested and because of this the physical meaning for the values determined is not clear. The values of $\triangle S^{\ddagger}$ give an indication on the extent of collisions occurring; the more negative the value of $\triangle S^{\ddagger}$, the greater amount of collisions. This is shown in Figure 5.24 where lighter oils have more negative $\triangle S^{\ddagger}$ values. Higher API gravity/ alkane content leads to higher $\triangle S^{\ddagger}$ values. Higher alkane content is akin to higher dilution or lighter oils.

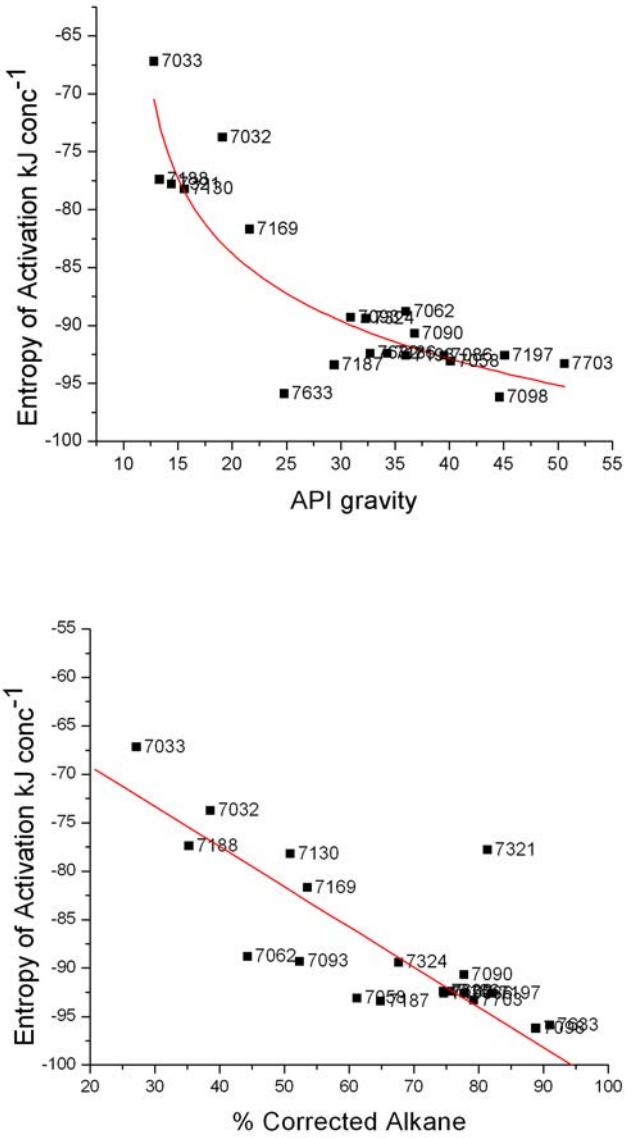

Figure 5.24: *Correlation between the calculated activation entropy values and the parameters, % corrected alkane and* API.

Table 5.9 gives the quasi-thermodynamic data obtained from the Eyring plots for a selection of the crude oils from Batch 1.

Table 5.9: *Eyring parameters for dilute crude oils as determined by the non-linear least squares fitting of the data to Equation 5.3. Eyring activation parameters (errors in* $\triangle H^{\ddagger}(\sim \pm 10-20\%)$, $\triangle S^{\ddagger}(\sim \pm 10\%)$*) were determined from the fluorescence rate constant (plot of* $ln(k_T/T)$ *vs 1/T).* NR *indicates Not Recorded and* NC *indicates where there was too much scatter in the data to generate the appropriate values. Emission recorded at* 500 *nm.*

Oil	API	Dilution	Eyring Parameters	
			$\triangle H^{\ddagger}$ $(kJconc^{-1})$	$\triangle S^{\ddagger}$ $(kJconc^{-1})$
7033	12.8	1:10	-1.0[¶]	-86.1[¶]
		1:50	-1.0	-86.5
		1:100	-0.8	-85.8
		1:500	-0.9	-86.1
		1:5000	-1.1	-87.0
7188	13.3	1:10	-0.9	-91.9
		1:50	-1.3	-95.6
		1:100	-1.4	-96.0
		1:500	-1.5	-96.6
		1:5000	-1.5	-96.7
7130	15.6	1:10	NC	NC
		1:50	-1.3	-96.0
		1:100	-1.3	-96.0
		1:500	-1.3	-96.0
		1:5000	-1.6	-97.4
7169	21.6	1:10	-1.1	-92.5
		1:50	-1.4	-95.9
		1:100	-1.5	-96.4
		1:500	-1.7	-97.3
		1:5000	-1.6	-96.6
7062	36.0	1:10	-1.0	-91.9
		1:50	-1.4	-94.5
		1:100	-1.3	-94.2
		1:500	NR	NR
		1:5000	NR	NR
7197	45.1	1:10	-1.4	-97.3
		1:50	-1.6	-98.5
		1:100	-1.6	-98.6
		1:500	NR	NR
		1:5000	NR	NR

[¶] Data calculated from the linear part of the Eyring plot (i.e. the low temperature part).

In all cases, the value of $\triangle S^{\ddagger}$ for the dilute oils is greater than $\triangle S^{\ddagger}$ for the neat oil. Also, the value of $\triangle S^{\ddagger}$ gradually increases on dilution. The $\triangle S^{\ddagger}$ values obtained are related to fluorophore mobility; high dilutions have greater mobility and greater incidence of collisions. Some plots had too much scatter (reflecting the difficulty of lifetime measurement for low concentrations) and the Eyring parameters could not be recovered. For oil 7062 and 7197, dilutions 1 to 500 and 1 to 5000 were not recorded due to the very weak emission of fluorescence from these light oils at low concentrations. Figure 5.25 shows Eyring plots for a selection of oils, at a dilution factor of 1:100. As the density of the oil reduces, the data fits the Eyring model more closely as indicated by the correlation coefficients.

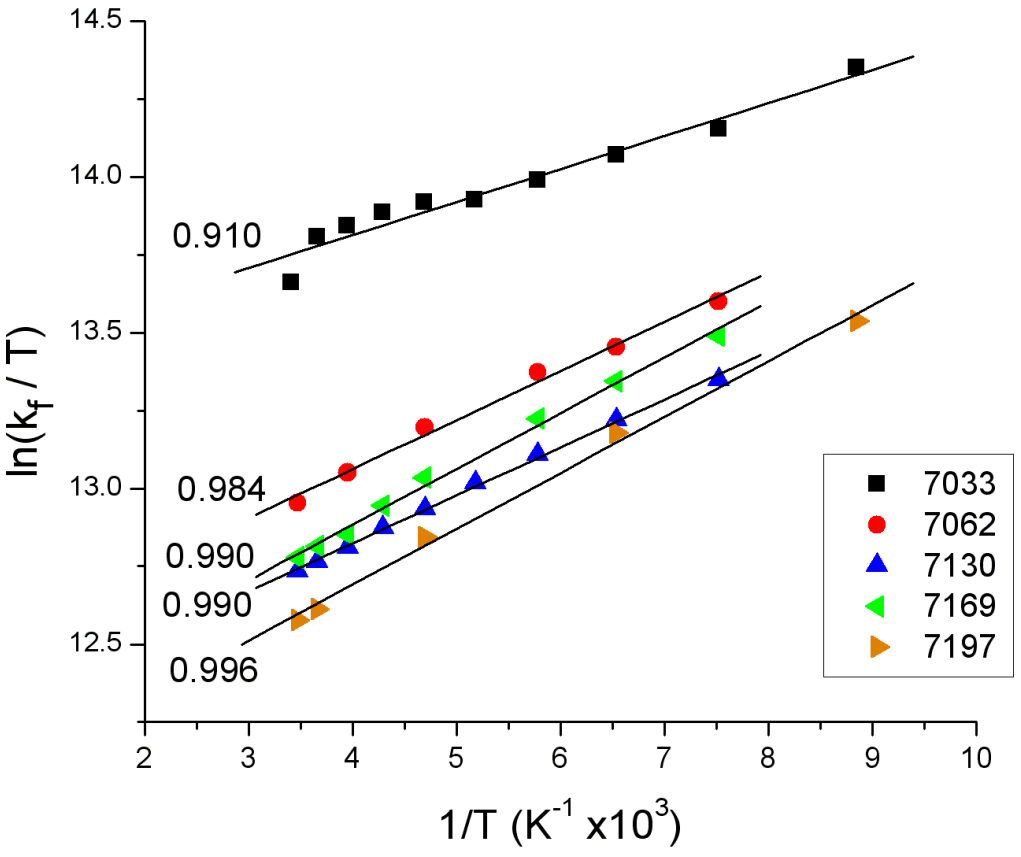

Figure 5.25: *Eyring plots for a selection of diluted oils* $(1:100)$ *and the associated linear fits and correlation coefficients* (r^2)*. Data recorded at 500 nm.*

Figure 5.26 shows the Eyring plots for oil 7169 at a range of dilutions. The model applies for all dilutions.

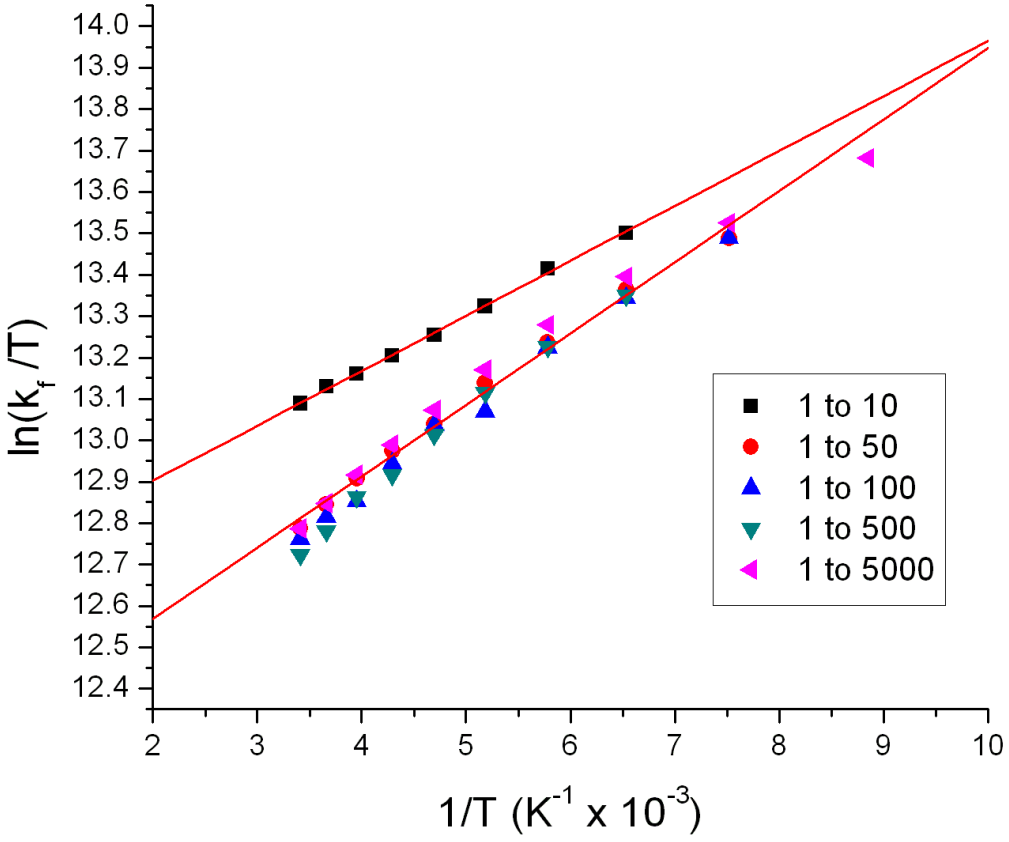

Figure 5.26: *Eyring plots for oil* 7169 *for a range of dilutions up to* 1 : 5000. *Linear fits are also shown for the 1:10 and 1:50 dilutions. Data recorded at 500 nm.*

5.8 Conclusions

The fluorescence emission of crude oils is governed by composition and concentration. Lowering the temperature of the oil increases its viscosity and reduces molecular collisions, leading to an increase in the fluorescence intensity. The lifetime reported for an oil sample is also governed by composition and it is influenced by the extent of energy transfer and quenching that occurs post excitation. As for fluorescence emission, lifetimes also increase on lowering the temperature. Dilution changes the photophysics of crude oils considerably but lowering the temperature does not in-

fluence the interplay between energy transfer and quenching processes as shown by the linear plot between $\delta\tau$ (difference between neat and dilute oil lifetime) versus T. At low temperatures, lifetimes increase due as the sample viscosity increases until a point where no further increases occur. For heavy oils, small changes in lifetime are found due to low temperature. For light oils with higher inherent mobilities, temperature influences the lifetime to a greater extent. Similarly, the rate of energy transfer and quenching for heavy oils does not change much from high to low temperatures. For lighter oils, the rate of energy transfer and quenching changes to a greater degree. Quenching occurs mainly by a dynamic/collisional mechanism with a smaller static contribution as shown by a modified Stern-Volmer analysis. Lowering the temperature influences the Stern-Volmer plots in turn influencing the quenching constants obtained. Stern-Volmer quenching constants were found to be linear with temperature. Since dynamic quenching is the dominant process, it follows that energy transfer is weakly influenced by temperature, which is also shown by small red shifts in the emission spectra of crude oils as the temperature is lowered. The Arrhenius model can be applied to temperature induced lifetime changes, leading to determination of activation parameters; E_{act}, A and τ_0. The latter parameter represents the lifetime in the absence of non-radiative (collisional) processes, which varies linearly with emission wavelength as opposed to the curved lifetime-emission wavelength response based on average lifetime values. The lifetime data was also found to follow reverse Eyring behaviour shown by positive plots of $ln(k_f/T)$ versus T. This reverse behaviour is due to the increasing lifetimes with decreasing temperature as opposed to classic Eyring analysis where reaction rates increase with increasing temperature. Values of the enthalpy and entropy of activation were calculated; the entropy values becoming more negative as the oil was diluted and also as the oil density decreased. As the oil mobility decreases the entropy becomes more negative. This chapter has brought together many concepts originally derived for simple systems such as Arrhenius and Eyring behaviour; and applied them to crude oil fluorescence. Surprisingly though heterogeneous in nature and comprising of a multitude of fluorescing components, the behaviour at low temperature can be modeled by simple models using fluorescence lifetime data.

Chapter 6

Conclusions and Future Work

Fluorescence Spectroscopy offers the possibility to make qualitative and quantitative analysis of crude oils [41, 91]. However, in its application to complex systems, the selectivity of conventional fluorescence techniques appears to be insufficient and instead, three dimensional fluorescence spectroscopy can be used to improve resolution [116, 120, 215, 216]. Time resolved methods offer new diagnostics for complex systems giving increased sensitivity and rapid analysis times. Real-time fluorescence analysis of crude oils then has the potential to be a distinct possibility [124, 126, 129, 131, 217]. However crude oils display an enormous variation in chemistry ranging from low molecular weight alkane mixtures to oils containing a broad array of high molecular weight compounds. All crude oils fluoresce and this emission can be quantified by an average lifetime. But due to the large variation in crude oil chemistry, a fully quantitative time resolved method has yet to be found.

This thesis has detailed the FD method for determining the fluorescence lifetime of crude oils. As found for TD based average lifetimes [126, 126, 130], FD based average lifetimes follow a curved trend with emission wavelength. The average lifetime reported for crude oils is subjective to the model used. To date, the discrete intensity based average lifetime of crude oils and HCFI has been reported in the literature [112, 124, 126, 178]. In this work I have compared discrete average lifetimes with the lifetimes obtained from the Gaussian and Lorentzian distribution models. For most cases, the multiple distribution models gave average lifetimes close to the multiple discrete model. It was found that a simpler single decay term distribution

model (based on a Gaussian or Lorentzian function) also fits the data. The long distribution of lifetimes modeled by the Lorentzian function was deemed to be closest to the real distribution. The center of the distribution and the distribution width values output from the model provide an alternative way to examine crude oils. Center lifetimes increase with emission wavelength and the width of distribution follows a curved trend with emission wavelength as found for average lifetimes.

In terms of correlations to physico-chemical properties of crude oils, FD lifetimes followed similar trends as for TD lifetimes. No improvement in these correlations was made with a high degree of scatter still present in API gravity and Polar plots (representing the best correlations). The FD method was successfully applied to the determination of lifetimes of oil within HCFI [178, 218] enabling quantitative distinction of oil from geochemically different populations. However, there are difficulties associated with linking crude oil fluorescence and composition. It is hard to obtain quantities of crude oils that will statistically validate any of the fluorescence methods to date. With larger data sets, multivariate analysis techniques could be used more successfully. One way of overcoming the limitations of small data sets is to share fluorescence data between laboratories but a standard fluorescence based method is not available and currently measurement conditions vary widely. Perhaps in this regard we should think of lifetime data for crude oils in the same way as the 'Petroleome', a phase coined by Mullins [219]. The Petroleome (analogous to the human genome project) is a complete listing of the chemical constituents in a crude oil and Petroleomics being the study of the structure-function relations of a library of these oils. As a means to developing a quantitative prediction model for crude oils based on fluorescence, the concept of the Petroleome should be extended to include fluorescence lifetime data. Nevertheless, a standard method to determine fluorescence lifetimes in crude oils must also be universally accepted.

While a large percentage of the investigation on crude oil fluorescence (primarily spectral methods) has been focused on quantitative analytical methods [107, 112, 122, 126, 215, 216], less attention has been placed on the the mechanisms and factors controlling fluorescence in crude oils [108, 113, 124, 125]. The second goal of this thesis was to contribute to our understanding of crude oil fluorescence by investigating the influence of energy transfer and quenching on fluorescence behaviour of

neat and diluted oils at room and low temperature. While spectral changes in crude oil emission spectra can be used to determine the relative change in energy transfer, lifetime measurements can be used to determine the change due to energy transfer *and* quenching. The rate of energy transfer and quenching was found to vary with oil type (in this case API gravity is used as an indicator of oil type). Lifetime-emission wavelength curves are similar for neat and diluted oils showing that the interplay between energy transfer *and* quenching is not influenced by dilution. As a future project, the temperature dependent spectral shifts at low temperature could be studied in more detail by recording the emission spectra at specific time intervals (Time Resolved Emission Spectra (TRES [131])).

Models developed for simple fluorophore systems (one species) turn out to apply to crude oils. A modified Stern-Volmer plot that incorporates static and dynamic parts was found to model quenching in crude oils allowing quantitative analysis. The dominant process is dynamic quenching and the calculated Stern-Volmer quenching constants decrease exponentially with emission wavelength showing that the quenching is less effective for larger red emitting fluorophores. Heavy oils with high molecular weight compounds have greater Stern-Volmer quenching rates. The dynamic quenching rate varies linearly with temperature and this mechanism is dependent on oil type. The temperature behaviour of crude oils follows a simple Arrhenius model giving a procedure to calculate the intrinsic lifetime. Also linear (positive) Eyring plots are found giving an opportunity to evaluate quasi-thermodynamically the change of lifetime with temperature. Heavy oils have less negative entropy meaning more collisions, the converse true for lighter oils. Dilution acts to increase the entropy value. These models show that the fluorescence of many emitting species in a complex mixture such as crude oils can be summated or approximated by simple fluorophore models.

Finally, the methods described in this thesis show that a large amount of information can be obtained for crude oils using spectral and time-resolved methods. While a quantitative method for property estimation is still in progress, the methods used are also applicable to any other complex mixture of fluorophores such as PAH's and biomolecules such as proteins.

Appendix A

Reference Lifetime Standards

A.1 Standards for FD lifetime measurements

Fluorophores are generally compared according to their absorption and emission properties such as spectral profiles, wavelengths of maximum absorbance, lifetime, and their quantum yield. In the context of the FD analysis of oils, a series of reference fluorophores with reproducible lifetimes were required. The following fluorophores were all commercially available in solid form from Sigma-Aldrich. Stock solutions of 10^{-3} or 10^{-4}M were made up using the appropriate solvent and further diluted for fluorescence measurement. All solutions were kept in the dark before measurement. Samples were placed in conventional 10 mm path length quartz cuvettes. UV-VIS spectra were recorded by Shimadzu UV-1601 spectrophotometer, using the solvent placed in a 10 mm quartz cuvette as blank. Fluorescence emission spectra were recorded on a Cary Eclipse spectrophotometer (Varian), using right-angled geometry on 10 mm path length quartz cells to collect the emission. Fluorescence lifetimes for each of the test standards were performed using the FD instrument and were also verified by TCSPC measurements. For all lifetime measurements, 1 mm pathlength quartz cells were used as it was more convenient to use 1 mm pathlength cuvettes with the FD system due to the nature of the upright microscope.

A.2 HPTS: 8-hydroxypyrene-1,3,6-trisulphonic acid trisodium salt (common name: Pyranine)

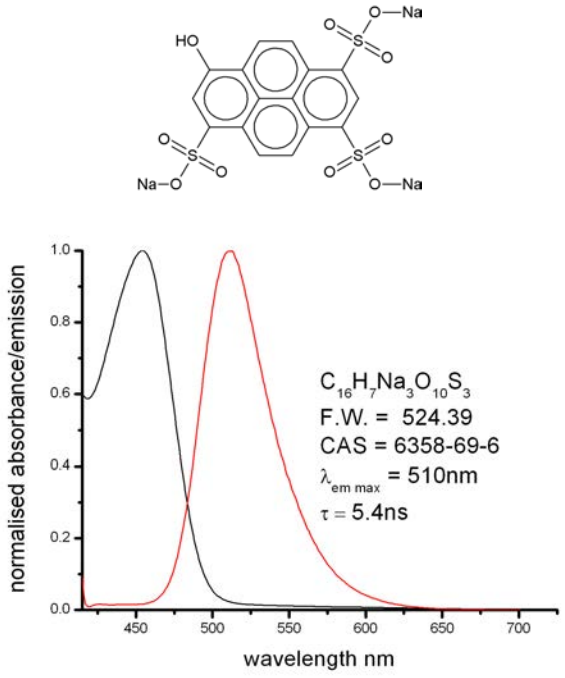

Figure A.1: *Normalised absorbance (black) / emission (red) spectra for HPTS* 10^{-5} *M in* 0.2 *M Phosphate Buffer. Excitation/emission slit widths* 5 *nm, excitation filter:* 335-620 *nm, emission filter:* 360-1100 *nm.*

10^{-5} M HPTS was made up in 0.2 M phosphate buffer (pH 7.6). This pH sensitive dye belongs to a family of aromatic alcohols and have been widely studied by Förster [220] and Weller [221]. Fluorescence emission from the anionic form of the dye (pH>7.5) has a lifetime of 5.3 ± 0.1 ns and is centered around 515 nm [222, 223]. Using UV excitation (283 nm), the quantum yield of HPTS in alkaline solution has been measured to be 78% [224]. At 496 nm and calculated in reference to Fluoroscein in 0.1M NaOH, the standard quantum yield value is 95% [36]. Figure A.1 show the structure and spectral characteristics of HPTS respectively. The high absorbance at 405 nm and the large Stokes shift is apparent, making this dye a suitable lifetime standard. HPTS also has other favourable characteristics: its solutions are very photostable and also remain un-degraded for long periods of time when kept in the dark. The phase and demodulation response is given in Figure A.2.

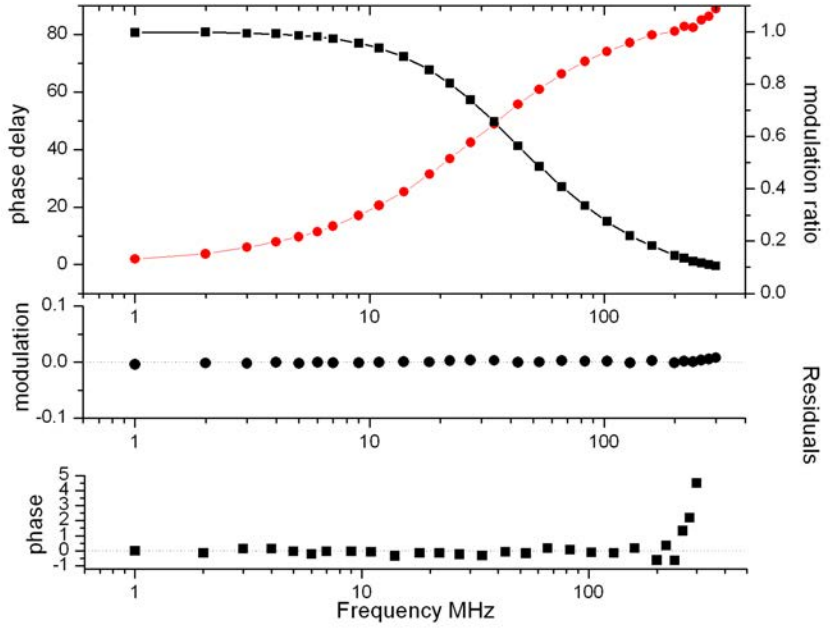

Figure A.2: FD *response for* HPTS *standard fluorophore along with the residuals from the fitting process. (λ_{ex}=405nm), λ_{em}=465 to 500nm, number of frequencies = 27, from 1 to 300* MHz*). Results: τ= 5.44 ± 0.1 ns, χ^2_R = 0.54.*

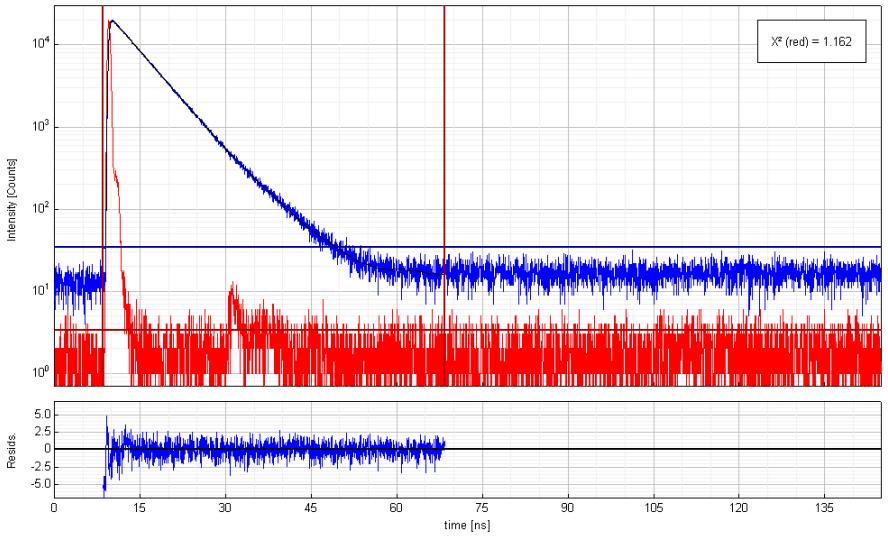

Figure A.3: *HPTS ($10^{-5}M$) decay curve by* TCSPC *and associated IRF (glass slide at 405 nm). Repetition Frequency = 5 MHz, Resolution = 35 ps, Number of channels used in the fitting = 2142, λ_{ex} = 405 nm),λ_{em} = 510 nm). Results: τ = 5.40 ± 0.06 ns, χ^2_ν = 1.16.*

An increase in the residuals for both phase and demodulation data above 200

MHz is noticeable. The TCSPC decay curve for HPTS is shown in A.3, using a glass slide to generate the IRF. The single exponential decay is found for both the FD and TD methods giving lifetime values of 5.44 and 5.40 ns respectively, which compare exactly to literature values [225] and with previous studies at the Nanoscale Biophotonics Laboratory [226].

A.3 SPA N-(3-sulfopropyl) acridinium salt

The lifetime of this chloride sensitive probe [36] is the longest of all the fluorophores tested (31 ns [227]). It absorbed strongly at 405 nm and emits over a wide wavelength range (Figure A.4). Measurement by FD recovers a single exponential decay of 30 ns (Figure A.5, slightly shorter than previously published lifetime of 31.5 ns [227]. The fitting of the TCSPC decay showed two lifetimes indicating the presence of an impurity that was not observed by FD (Figure A.6). The fractional amplitude of the short lifetime second component is 0.62%. This highlights the fact that the FD method, in some cases, can not resolve low amplitude components. Though the original solid could have been purified by recrystalisation, the lifetime was ultimately too long to use as a standard for the measurement of crude oils, whose average lifetimes were generally 1 to 10 ns.

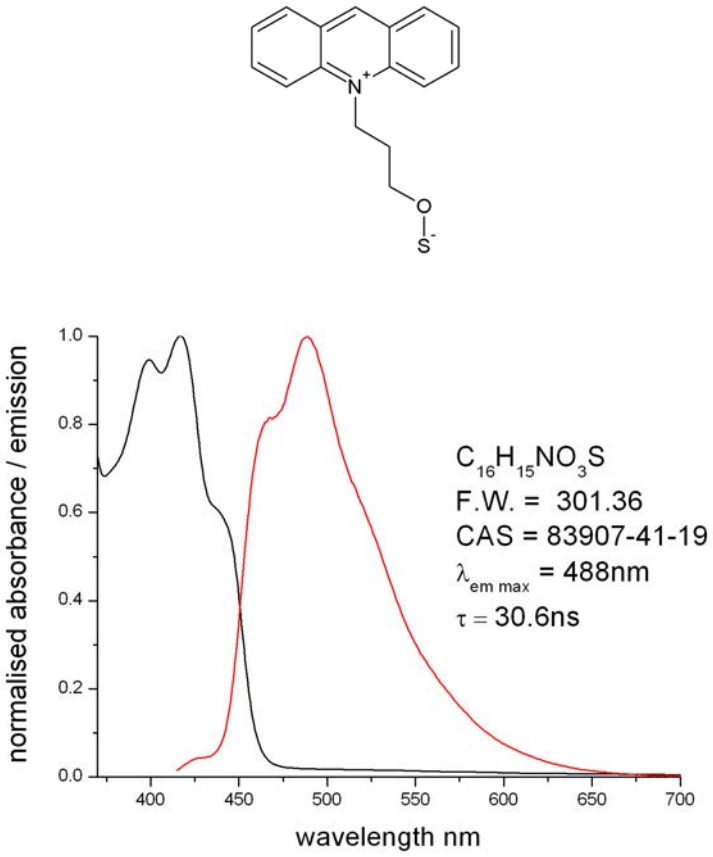

Figure A.4: *Normalised* SPA$(10^{-4}M)$ *absorbance(black) / emission(red) spectra, excitation/emission slit widths* $= 5$ *nm, excitation filter:* $335 - 620$ *nm, emission filter:* $360 - 1100$ *nm.*

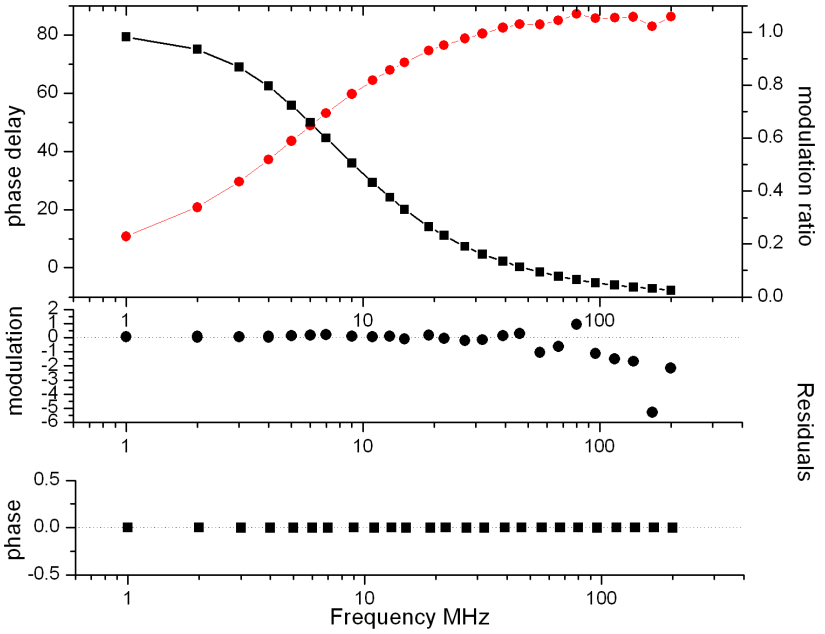

Figure A.5: FD *response for* SPA (10^{-6}M) *along with the residuals from the fitting process.* (λ_{ex}=*405nm*),λ_{em}=*465 to 500nm, number of frequencies = 30, from 1 to 200* MHz*). Results:* τ= *30.1*$\pm$0.3*ns,* χ^2_R = *0.71.*

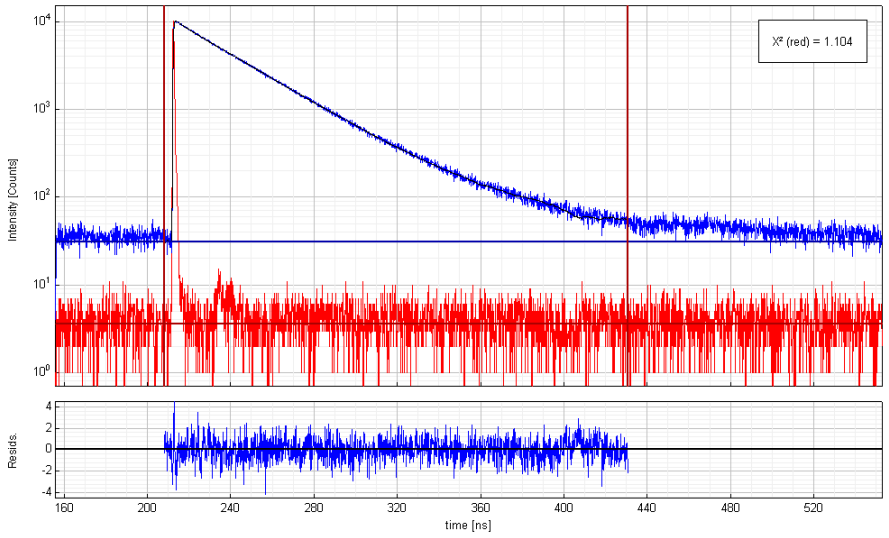

Figure A.6: *SPA* ($10^{-6}M$) *decay curve by* TCSPC *and associated IRF (by Ludox at* 405 *nm,* 1 *mm slit width to* PMT*). Repetition Frequency =* 2.5 *MHz, Resolution =* 140 *ps, Number of channels used in the fitting =* 3045*,* λ_{ex} = 405 *nm),* λ_{em} = 488 *nm). Results:* τ_1 = 30.66 ± 0.1 *ns,* τ_2 = 3.2 *ns (fraction =* 0.62%*),* χ^2_ν = 1.10.

A.4 Rhodamine B

Rhodamine B is a derivative of the xanthene dye class, which are among the oldest synthetic dyes in use [228] and is potentially useful because of its short lifetime (1.7 ns [229]). The absorbance emission spectra for Rhodamine B (10^{-6}M in H_2O) is shown in Figure A.7. Rhodamine B absorbs weakly at 405 nm but lifetime data could still be acquired. For FD measurements a single decay gives the best fit resulting in a lifetime of 1.5 ns. As for SPA, the solution of this dye shows two decay terms when measured by TCSPC (two lifetimes of 1.6 and 13.3 ns), although the fractional amplitude of the long lifetime component is very low (0.37% of the total amplitude). Rhodamine B in water readily forms aggregates (even at very low concentrations) [228] leading to a second (albeit a very small fraction) decay term. As for the SPA results, the FD system was not able to resolve low amplitude components and gave just a single term of lifetime 0.2 ns shorter than the literature value.

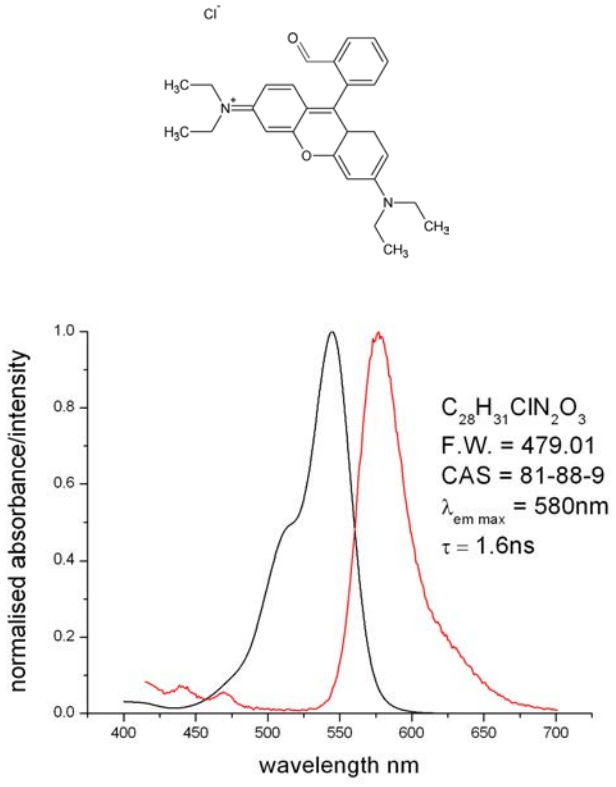

Figure A.7: *Normalised RhodamineB $10^{-6}M$ in H_2O absorbance(black) / emission(red) spectra, excitation/emission slit widths = 5 nm, excitation filter:* 335-620 *nm, emission filter:* 360-1100 *nm.*

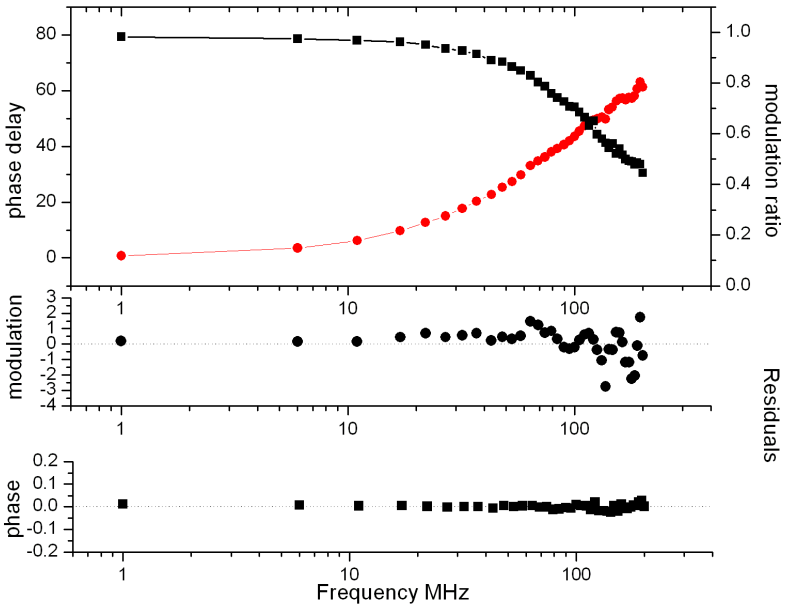

Figure A.8: FD *response for Rhodamine B* ($10^{-6}M$) *standard fluorophore along with the residuals from the fitting process.* ($\lambda_{ex} = 405$ *nm*),$\lambda_{em} = 465$ *to* 500 *nm, number of frequencies* $= 39$, *from* 1 *to* 200 MHz. *Results:* $\tau = 1.54 \pm 0.1$ *ns,* $\chi^2_R = 0.45$.

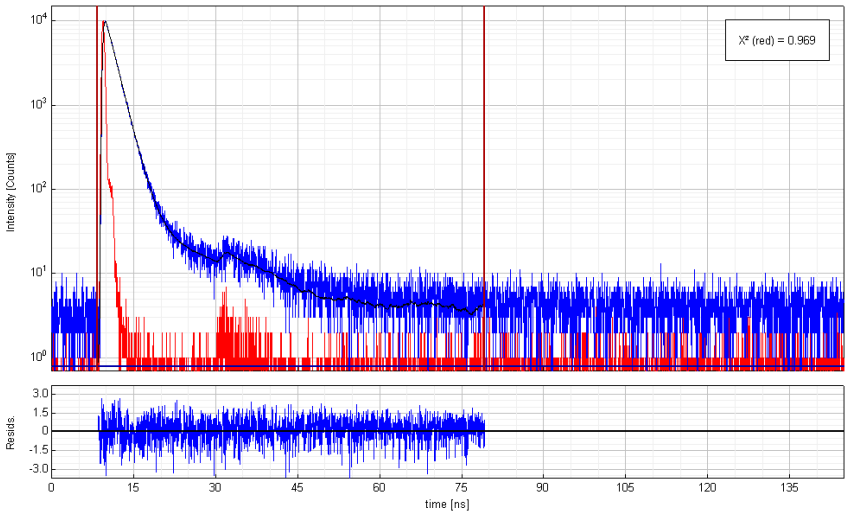

Figure A.9: *RhodamineB* ($10^{-6}M$) *decay curve by* TCSPC *and associated* IRF *(by glass slide at* 405 *nm,* 1 *mm slit width to* PMT*). Repetition Frequency* $= 5$ MHz, *Resolution* $= 35$ *ps, Number of channels used in the fitting* $= 2238$, $\lambda_{ex} = 405$ *nm,* $\lambda_{em} = 580$ *nm). Results:* $\tau_1 = 1.6 \pm 0.01$ *ns,* $\tau_2 = 13.3$ *ns (fraction* $= 0.37\%$ *by amplitude),* $\chi^2_\nu = 0.97$.

A.5 Acridone

The highly photostable yet poorly water-soluble probe Acridone has high absorbance at 405 nm and emits up to 550nm (Figure A.10. Time resolved decays are fitted with a single exponential (lifetime = 14.9 ns, quantum yield = 0.8 in water [183]. Figures A.11 and A.12 show the FD and TCSPC plots respectively. At higher modulation the error on the phase increases dramatically. The short lifetime fluorophore DASPI of lifetime approximately 150 ps [230] is used in this case to produce the IRF. Acridone was used in section 2.2.3.1 as a long lifetime probe to test the ability of the system to resolve fluorophore mixtures. It was hoped to obtain a fluorescence lifetime that was close to the longer lifetimes of light crude oils and for Acridone, very good lifetime data was obtained with excellent fits but due to it's poor water solubility, it was difficult to make up standards of exact concentrations and was not chosen as a reference standard.

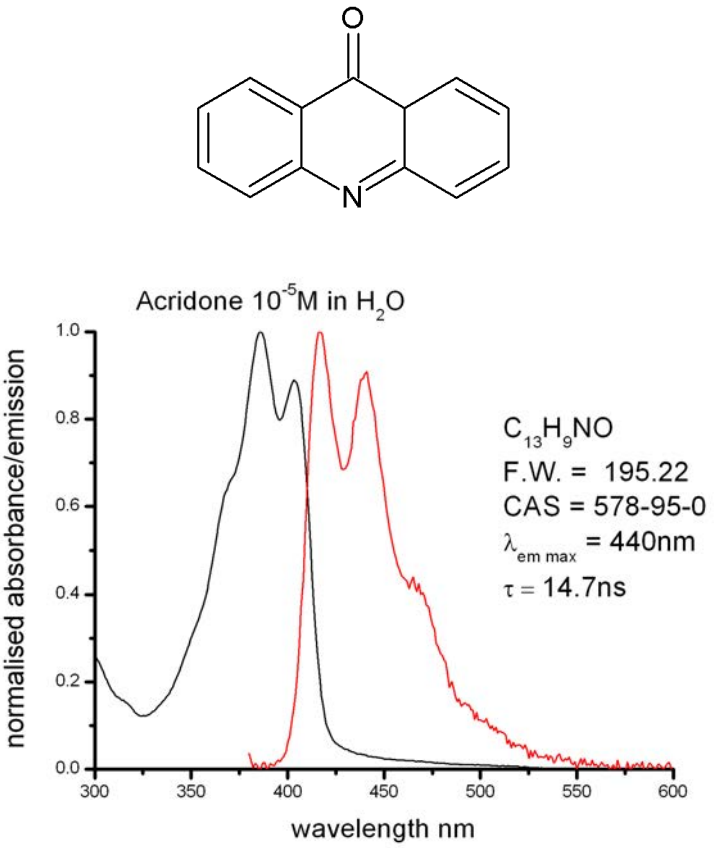

Figure A.10: *Normalised Absorbance Emission spectra of Acridone* $10^{-5}M$ *in* H_2O *absorbance(black) / emission(red) spectra, excitation/emission slit widths* $= 5$ *nm, excitation filter:* 335-620 *nm, emission filter:* 295-1100 *nm.*

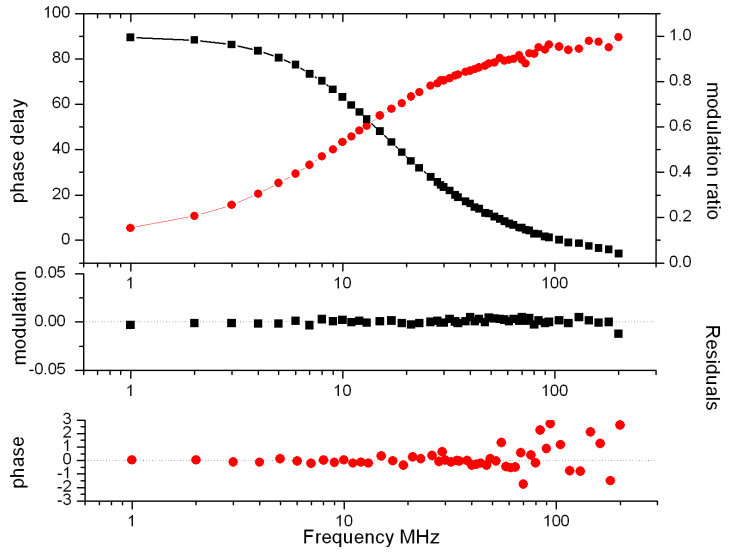

Figure A.11: FD *response for Acridone* ($10^{-5}M$ *in water) standard fluorophore along with the residuals from the fitting process. (Reference standard* HPTS $10^{-5}M$ *in* $0.2M$ *phosphate buffer* $\lambda_{ex} = 405$ *nm),*$\lambda_{em} = 410$ *nm Long Pass Filter, number of frequencies* $= 15$*, from* 1 *to* 97 MHz*). Results:* $\tau = 14.6 \pm 0.2$ *ns,* $\chi^2_R = 0.31$.

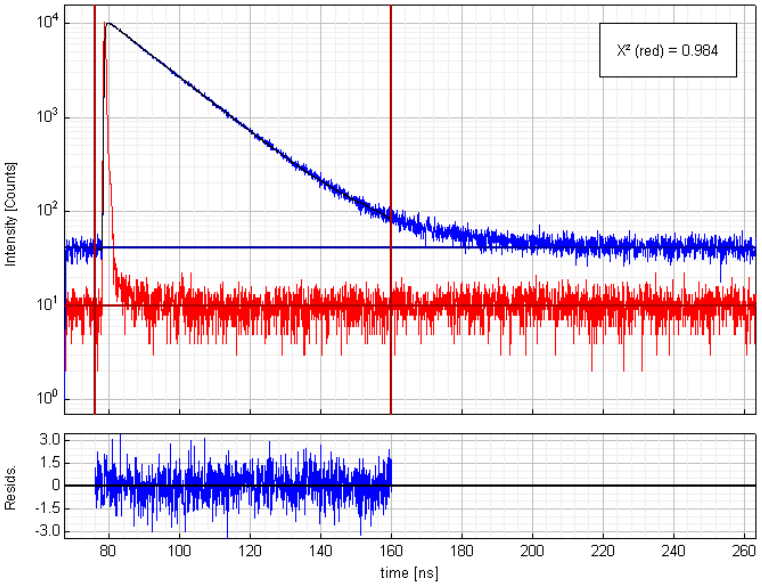

Figure A.12: *Acridone* ($10^{-5}M$ *in water) decay curve by* TCSPC *and associated* IRF *using DASPI* (10^{-6} *M in Methanol at* 405 *nm),* 1 *mm slit width to* PMT*). Repetition Frequency* $= 5$ *MHz, , Resolution* $= 70$ *ps, Number of channels used in the fitting* $= 1188$*,* $\lambda_{ex} = 405$ *nm,* $\lambda_{em} = 580$ *nm). Results:* $\tau_1 = 14.7 \pm 0.05$ *ns,* $\chi^2_\nu = 0.98$.

A.6 Coumarin 6

Widely used in dye lasers, this dye gives a strong emission in the green spectral region. A large Stokes shift and large emission range are observed as shown in A.13. It displays a high quantum yield (0.78) [231] when excited at 450 nm. The reported lifetime of Coumarin 6 (10^{-5} M) in ethanol varies from 2.4 ns in [231] and 2.5 in [232] although instrumental conditions were not described in both references and thus the figure compares reasonably to the measurements obtained in this work (2.6 ns). Coumarin 6 was dissolved in Ethanol (spectroscopic grade) to 10^{-6}M. Figure A.14 shows a high error on the phase and modulation fit at higher modulation frequencies yet this does not significantly impact the quality of the fit. The TCSPC data shows a very good fit based on a single exponential decay (Figure A.15).

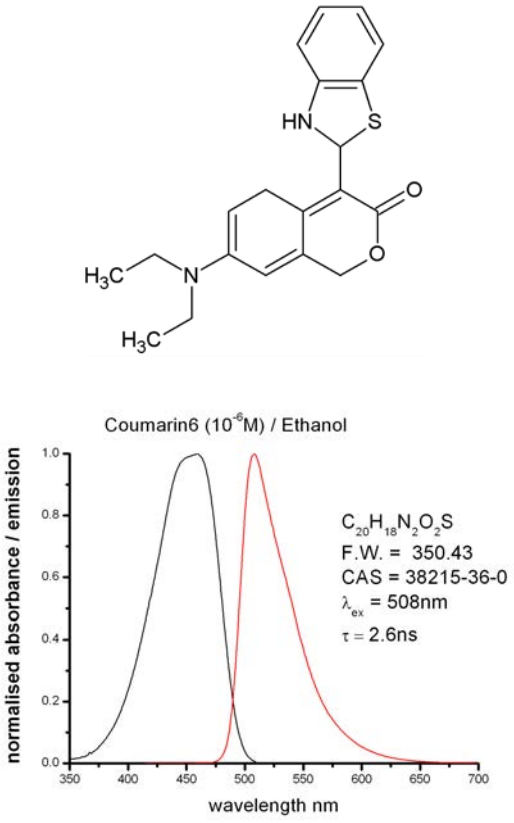

Figure A.13: *Normalised Coumarin* 6 10^{-6} *M in Ethanol (spectroscopic grade), absorbance(black) / emission(red) spectra, excitation/emission slit widths*= 5 *nm, excitation filter:* 335-620 *nm, emission filter:* 295-1100 *nm.*

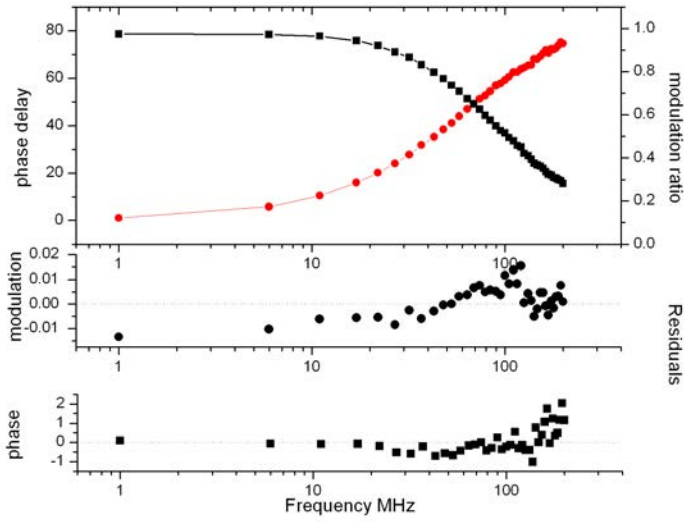

Figure A.14: FD *response for Coumarin 6 ($10^{-6}M$ in Ethanol) standard fluorophore along with the residuals from the fitting process. (Reference standard Fluoroscein* 10^{-6} *M in* 0.1 *M NaOH* λ_{ex} = 405 *nm),*λ_{em} = 465-500 *nm, number of frequencies* = 39*, from* 1 *to* 200 MHz*). Results:* $\tau = 2.69 \pm 0.02$ *ns,* $\chi^2_\nu = 0.35$.

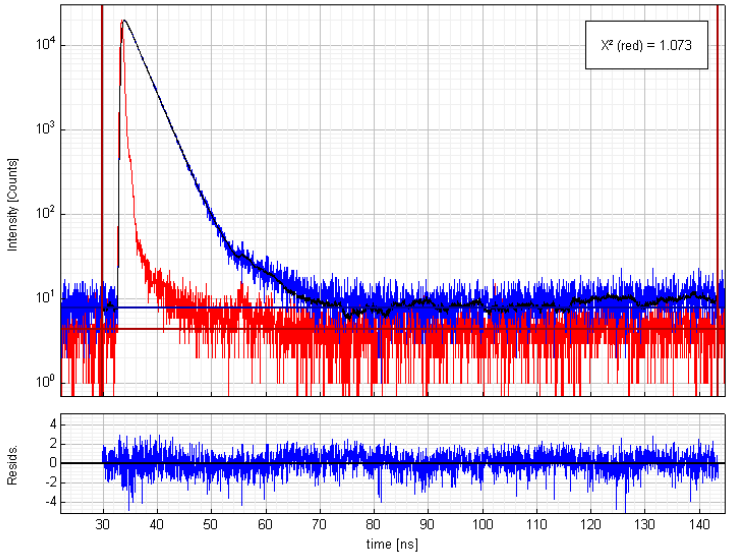

Figure A.15: *Coumarin 6 ($10^{-6}M$ in Ethanol) decay curve by* TCSPC *and associated* IRF *using* DASPI *(10^{-6} M in Methanol at* 405 *nm - recorded at open monochromator,* 405 *nm stopline filter,* 410 *nm long pass filter),* 1*mm slit width to* PMT*). Repetition Frequency* = $10MHz$*, Resolution* = 35 *ps, Number of channels used in the fitting* = 1209*,* λ_{ex} = 405 *nm,* λ_{em} = 508 *nm). Results:* $\tau_1 = 2.57 \pm 0.01$ *ns,* $\chi^2_\nu = 1.073$.

A.7 Coumarin 30

Coumarin 30 (3-(2-N-Methylbenzimidazolyl)-7-N,N-diethylaminocoumarin) is another dye from the 7-amino coumarin family, which gives a strong emission in the blue-green spectral region. The reported fluorescence lifetime of Coumarin 30 is 2.57 ns [233] in Acetonitrile (determined by TCSPC) which is comparable to measurements in this work (2.6 ns). Figures A.17 and A.18 show that single exponential decays are found for both the FD and TD methods (2.67 and 2.6 ns respectively). Coumarin 30 was made up in Acetonitrile(spectroscopic grade) to 10^{-6} M. A reasonable Stokes shift and emission range is shown in Figure A.16.

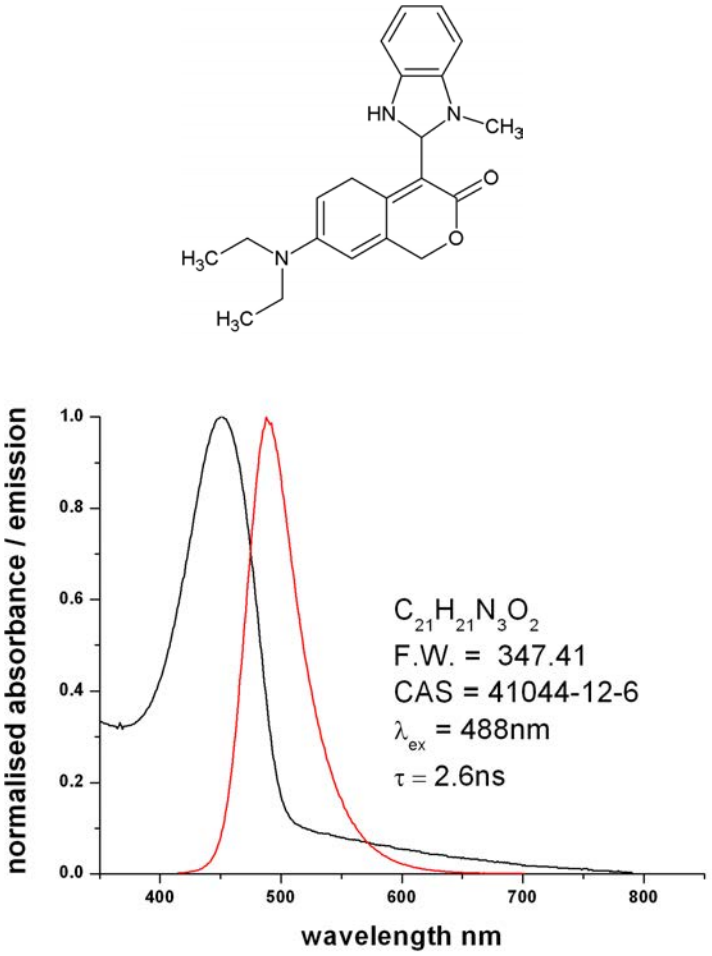

Figure A.16: *Normalised Coumarin 30 $10^{-6}M$ in Acetonitrile (spectroscopic grade), absorbance(black) / emission(red) spectra, excitation/emission slit widths = 5nm, excitation filter: 335-620nm, emission filter: 295-1100nm.*

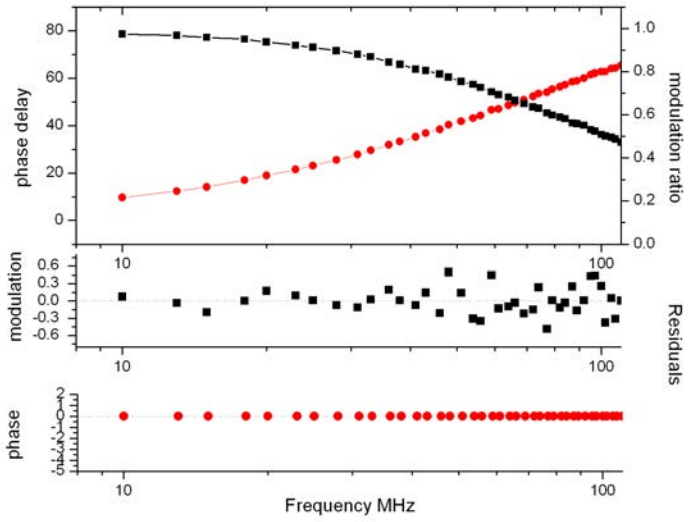

Figure A.17: FD *response for Coumarin 30 (10^{-6} M in Acetonitrile) standard fluorophore along with the residuals from the fitting process. (Reference standard* HPTS10^{-5} *M in phosphate buffer $\lambda_{ex} = 405$ nm), $\lambda_{em} = 465 - 500$ nm, number of frequencies= 40, from 1 to 110* MHz*). Results: $\tau = 2.67 \pm 0.02$ ns, $\chi^2_\nu = 0.62$.*

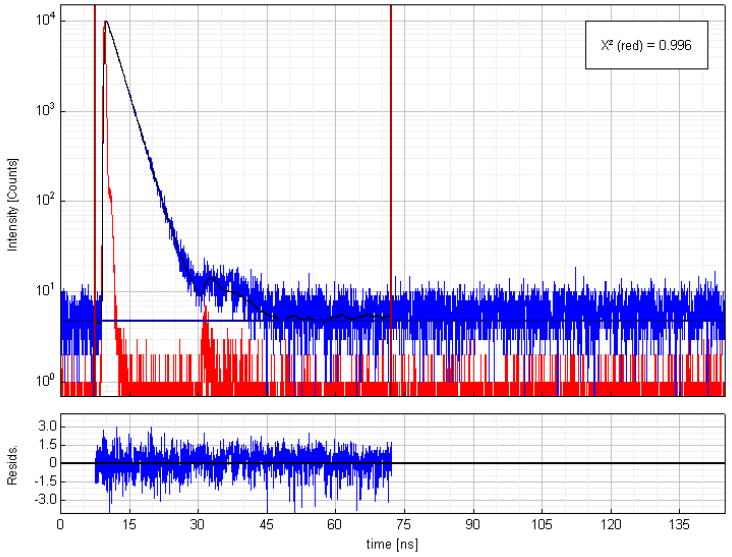

Figure A.18: *Coumarin30 (10^{-6} M in Acetonitrile) decay curve by* TCSPC *and associated* IRF *using glass slide recorded at 405 nm. Decay recorded using 405 nm stopline filter, 410 nm long pass filter), 1 mm slit width to* PMT*). Repetition Frequency = $5MHz$, Resolution= 35 ps, Number of channels used in the fitting= 1824, $\lambda_{ex} = 405$ nm, $\lambda_{em} = 488$ nm. Results: $\tau_1 = 2.6 \pm 0.02$ ns, $\chi^2_\nu = 0.996$.*

A.8 Coumarin 314

Though this dye has a broad absorption range, it gives a slightly narrow emission band, again in the blue-green region (Figure A.19). The reported fluorescence lifetime of Coumarin 314 is 3.46 ns [234] in ethanol which compares well to measurements in this work (Figures A.20 and A.21 show good fitting to a single decay term yielding lifetimes of 3.33 ns by FD and 3.55 ns by TD. Coumarin 314 was dissolved in Ethanol (spectroscopic grade) to 10^{-6} M.

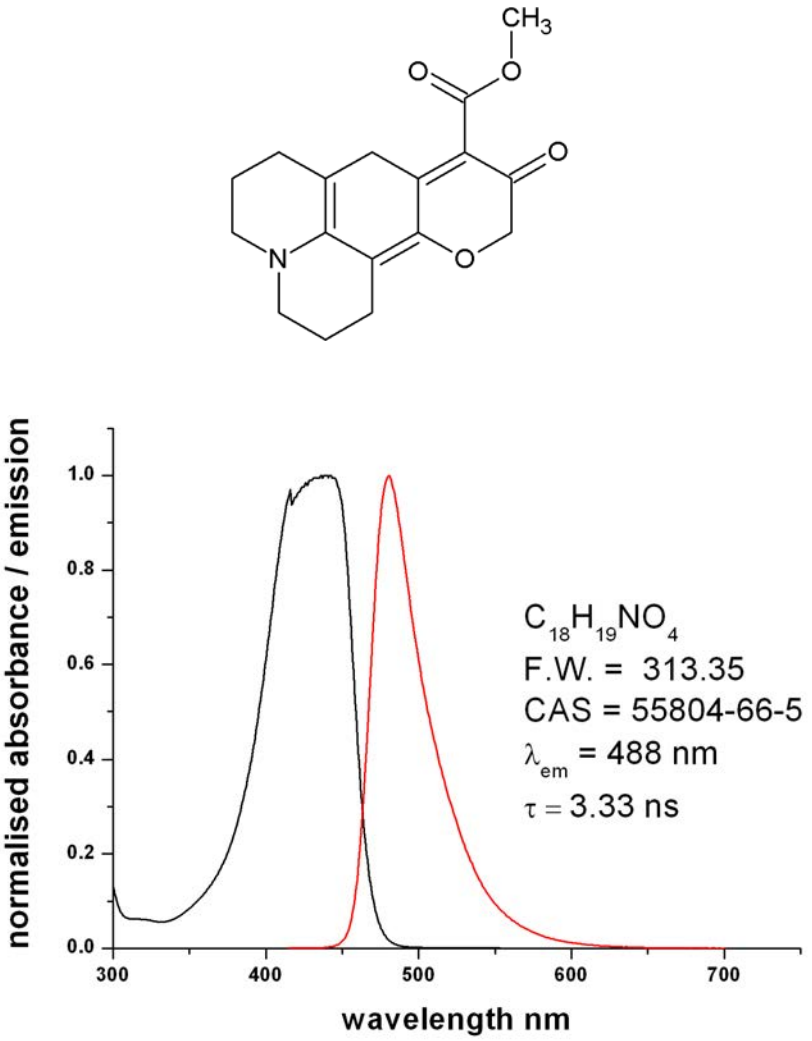

Figure A.19: *Normalised Coumarin 314* 10^{-6} *M in Ethanol (spectroscopic grade), absorbance(black) / emission(red) spectra, excitation/emission slit widths*= 5 *nm, excitation filter:* 335-620 *nm, emission filter:* 295-1100 *nm.*

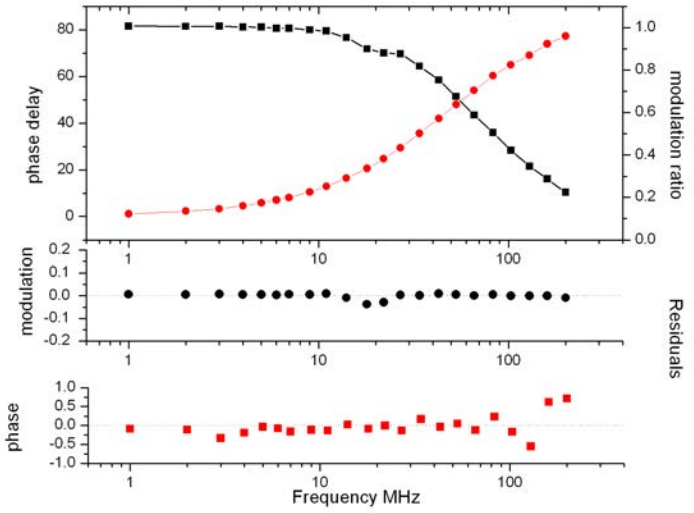

Figure A.20: FD *response for Coumarin 314 (*10^{-5} *M in ethanol) standard fluorophore along with the residuals from the fitting process. (Reference standard* HPTS 10^{-5} *M in phosphate buffer* λ_{ex}*=405 nm),* λ_{em} *=open window, number of frequencies=* 22*, from* 1 *to* 200 MHz*). Results:* $\tau = 3.33 \pm 0.04$ *ns,* $\chi^2_\nu = 0.04$*.*

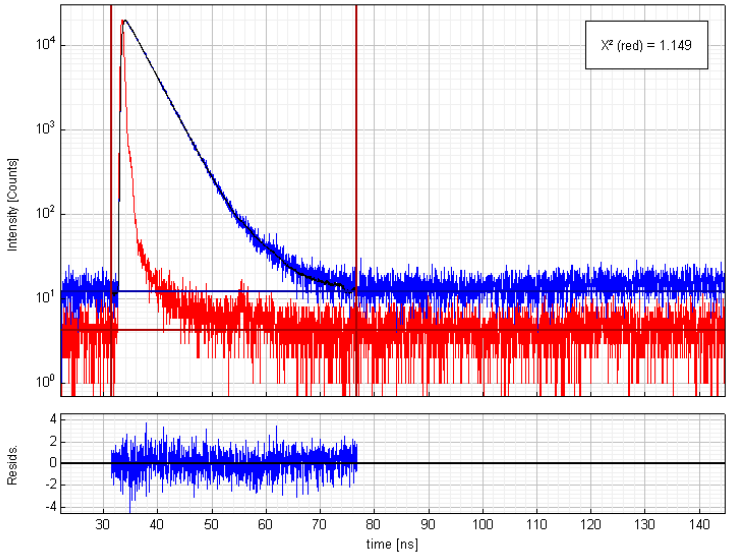

Figure A.21: *Coumarin 314 (*10^{-6} *M in ethanol) decay curve by* TCSPC *and associated* IRF *using* DASPI *recorded at* 405 *nm. Decay recorded using* 405 *nm stopline filter,* 410 *nm long pass filter),* 1 *mm slit width to* PMT*). Repetition Frequency =* 5 MHz*, Resolution=* 35 *ps, Number of channels used in the fitting=* 1587*,* λ_{ex} *=* 405 *nm,* λ_{em} *=* 481 *nm). Results:* $\tau = 3.55 \pm 0.01$ *ns,* χ^2_ν *= 1.134.*

A.9 Lucifer Yellow CH di-potassium salt

Lucifer yellow salts are based on a sulphonated 4-amino-1,8-naphthalimide core with variable substituents on the imide nitrogen. It has long been a popular probe for studying neuronal morphology because it contains a carbohydrazide group that allows it to be covalently linked to surrounding biomolecules [235, 236]. They are also used as selective metal reagents for the fluorimetric determination of Copper [237]. Lucifer Yellow salts have good water solubility, quantum yields in the order of 0.25 and a large Stokes shift which gives applications in biological tracing [236, 238]. Figure A.22 shows the large emission range making it a suitable reference compound for lifetime measurments at longer emission wavelengths. Lucifer Yellow decays can be fit with a single exponential with a high goodness of fit as shown in Figures A.23 and A.24. Our experimental lifetime values (Lucifer Yellow was dissolved in distilled water to 10^{-5} M.) of 5.1 ns in water compares exactly to literature values [238].

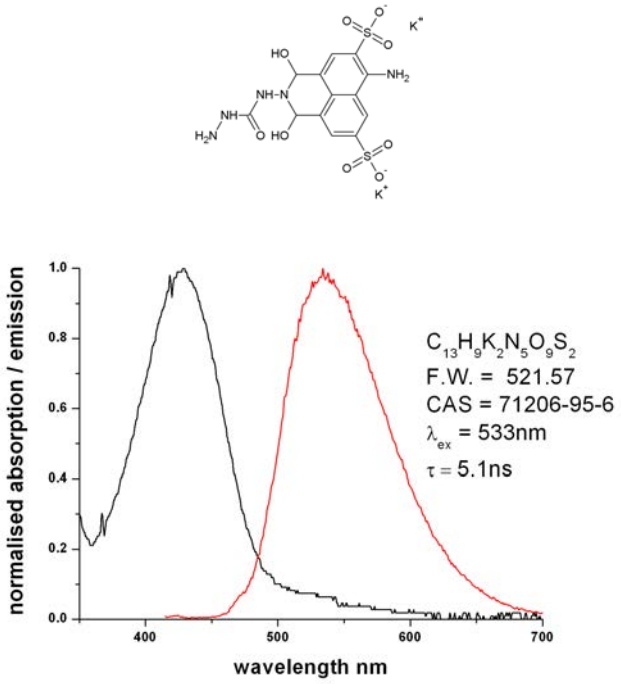

Figure A.22: *Normalised Lucifer Yellow* 10^{-6} *M in distilled water, absorbance(black) / emission(red) spectra, excitation/emission slit widths*= 5 *nm, excitation filter:* 335-620 *nm, emission filter:* 360-1100 *nm.*

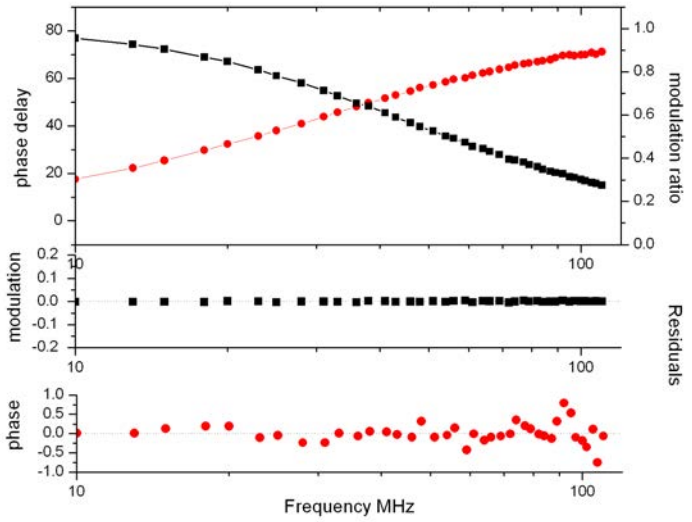

Figure A.23: FD *response for Lucifer Yellow* (10^{-5} *M in water) standard fluorophore along with the residuals from the fitting process. (Reference standard* HPTS 10^{-5} *M in phosphate buffer* $\lambda_{ex} = 405$ *nm),* $\lambda_{em} = 465 - 500$ *nm, number of frequencies* $= 40$*, from* 10 *to* 110 MHz*). Results:* $\tau = 5.1 \pm 0.06$ *ns,* $\chi^2_\nu = 0.03$.

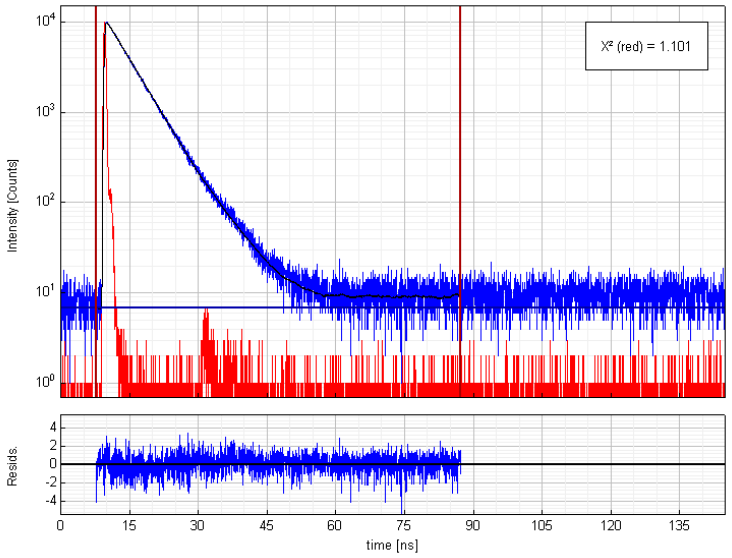

Figure A.24: *Lucifer Yellow* (10^{-5} *M in water) decay curve by* TCSPC *and associated* IRF *using glass slide. Decay recorded using* 405 *nm stopline filter,* 410 *nm long pass filter),* 2*mm slit width to* PMT*). Repetition Frequency* $= 5$ MHz*, Resolution* $= 35$ *ps, Number of channels used in the fitting* $= 2264$*,* $\lambda_{ex} = 405$ *nm,* $\lambda_{em} = 533$ *nm). Results:* $\tau_1 = 5.1 \pm 0.02$ *ns,* $\chi^2_\nu = 1.10$.

Appendix B

Supplementary Data

B.1 Frequency Domain Lifetime Data

The following tables give supplementary FD lifetime data for all the emission wavelength ranges sampled. A listing of the emission wavelength of maximum intensity is also given.

Table B.1: *Frequency Domain average lifetime data for Batch 1 oils - Discrete Fitting.*

Oil	API	426-477 nm	465-500 nm	480-520 nm	510-560 nm	542-582 nm	573-613 nm	600-650 nm	575-650 nm
198	31.5	2.90	3.41	4.35	5.00	5.93	5.86	6.28	5.76
199	30.4	2.40	4.45	4.65	5.33	6.16	6.34	6.76	6.43
201	29.8	2.83	3.28	3.77	5.30	6.21	5.98	6.63	5.26
207	38.0	2.76	3.45	4.24	4.45	5.70	5.59	5.83	5.48
7032	19.1	0.15	0.38	0.54	0.80	0.98	1.50	1.36	1.19
7033	12.7	0.14	0.41	0.55	0.46	0.60	0.74	0.93	0.69
7058	40.1	3.25	4.18	4.4	5.58	5.3	5.5	5.62	5.15
7062	36.0	1.20	1.52	1.76	2.30	2.17	2.32	2.32	2.31
7086	39.5	2.56	3.46	3.68	4.93	4.63	4.87	5.15	5.04
7090	36.8	2.35	3.11	3.83	4.84	4.92	5.08	5.21	5.01
7093	30.9	1.79	2.57	2.84	4.03	3.27	3.05	3.66	3.21
7098	44.6	6.91	7.18	7.15	7.66	7.08	9.84	9.26	7.82
7130	15.6	0.53	0.73	0.70	1.06	1.04	0.94	1.11	1.40
7169	21.6	0.81	1.18	1.47	1.59	1.91	1.96	1.97	1.83
7186	34.3	3.74	4.87	5.58	6.23	6.78	6.74	7.17	6.60
7187	29.4	3.45	5.49	5.14	5.59	6.09	6.25	6.62	6.40
7188	13.3	0.38	0.75	0.82	1.06	1.28	1.46	1.71	1.59
7193	36.0	3.28	3.79	4.42	4.32	5.16	5.05	5.02	4.76
7197	45.1	3.90	4.32	5.39	6.14	6.49	6.21	6.32	6.08
7321	14.1	0.39	0.67	0.72	1.04	1.08	1.29	1.19	1.15
7324	32.3	1.29	1.8	2.22	2.6	3.16	3.42	3.67	3.45
7632	32.7	1.7	2.55	2.81	3.35	3.6	3.76	3.88	3.65
7633	24.8	5.85	6.88	7.34	7.97	8.16	8.22	7.86	8.03
7703	50.6	4.78	6.10	5.78	6.87	7.11	7.26	7.51	5.79

Table B.2: *Frequency Domain lifetime data for Batch 2 oils - Discrete fitting. Also included is the lifetime data for connemara crude oil.*

Oil	API	426-477 nm	465-500 nm	480-520 nm	510-560 nm	542-582 nm	573-613 nm	600-650 nm	575-650 nm
ME1	32.7	1.48	2.30	3.09	3.23	4.00	4.56	4.60	4.43
ME2	28.9	1.49	2.14	2.39	4.06	3.59	4.08	4.55	3.98
ME3	30.8	2.16	2.86	2.93	4.67	3.98	3.46	4.17	3.70
ME4	39.2	3.47	4.96	5.05	6.91	7.07	7.00	7.80	6.56
ME5	44.1	4.09	4.91	5.48	7.49	7.98	8.34	7.60	7.98
ME6	39.6	3.80	5.72	5.66	7.00	8.86	8.06	9.10	8.74
ME7	42.1	5.34	5.23	5.77	6.30	8.11	8.32	7.52	6.40
ME8	44.2	3.80	5.94	5.06	6.32	7.54	7.53	7.00	5.58
ME9	47.8	4.11	4.95	5.06	5.67	6.40	6.42	6.24	5.64
ME10	24.7	0.67	1.12	1.31	1.98	1.74	1.76	2.00	1.93
Connemara Crude *	~ 35	2.80	3.95	4.42	4.87	5.62	5.74	5.87	5.84

* The oil labeled Connemara Crude is a stand alone crude oil with the following properties: water 0.03%, sulphur 0.13%, alkane $\sim 65\%$, aromatics $\sim 30\%$ and polar $\sim 2.0\%$.

Table B.3: *Emission λ_{max} values for the crude oils sampled. 405 nm excitation. Spectra measured on a Cary Eclipse spectrophotometer. Excitation filter: 335-620 nm. Emission filter: 360-1100 nm.*

Oil	λ_{max} nm
198	473
199	476
201	474
207	474
7032	473
7033	484
7058	457
7062	466
7086	467
7090	540
7093	467
7098	435
7130	465
7169	535
7186	463
7187	441
7188	496
7193	467
7197	463
7321	481
7324	470
7632	464
7633	464
7703	438
ME1	477
ME2	480
ME3	473
ME4	474
ME5	467
ME6	473
ME7	466
ME8	441
ME9	437
ME10	480
Conn Crude	469

Table B.4: *Frequency Domain lifetime data by Single Gaussian Fitting Batch 1 oils. For each oil the lifetime in ns (top figure), the distribution width in ns (middle figure) and the χ^2_ν value (bottom figure). DNF: Did not fit.*

Oil	API	426-477 nm	465-500 nm	480-520 nm	510-560 nm	542-582 nm	573-613 nm	600-650 nm	575-650 nm
198	31.5	DNF	2.11	2.54	4.17	4.84	5.54	5.85	5.40
			5.45	7.19	5.06	8.50	8.39	7.17	8.41
			1.73	1.08	2.51	0.30	0.22	0.44	0.2
199	30.4	DNF	1.67	2.19	4.79	5.37	5.92	6.53	6.0
			7.70	9.91	6.16	9.46	10.6	8.36	9.30
			0.4	0.15	0.51	0.06	0.08	0.10	0.05
201	29.8	DNF	2.27	2.82	3.91	4.72	5.62	6.07	5.50
			3.09	3.97	4.14	6.28	8.34	6.85	7.74
			2.19	2.42	2.20	0.99	0.24	0.46	0.31
207	38.0	DNF	1.83	DNF	3.58	4.59	4.69	5.46	5.29
			4.63		5.42	11.3	12.2	7.36	8.48
			1.89		1.62	0.19	0.56	0.43	0.48
7032	19.1	0.15	0.55	DNF	DNF	DNF	DNF	DNF	DNF
		0	0.55						
		0.09	0.18						
7033	12.7	0.14	0.40	0.32	0.54	DNF	DNF	DNF	DNF
		0	0	0	0				
		1.85	3.26	1.07	2.52				
7058	40.1	DNF	3.11	3.63	5.19	5.65	6.29	6.74	5.60
			7.34	8.90	7.33	11.6	11.7	9.81	11.8
			0.48	0.2	0.38	0.04	0.12	0.2	0.06
7062	36.0	DNF	DNF	DNF	DNF	DNF	DNF	DNF	DNF
7086	39.5	DNF	0.89	1.57	4.27	4.58	5.0	5.86	5.1
			8.76	10.2	6.84	10.9	11.6	9.47	10.6
			0.41	0.17	0.4	0.06	0.09	0.11	0.075

Table B.5: *Frequency Domain lifetime data by Single Gaussian Fitting Batch 1 oils. For each oil the lifetime in ns (top figure), the distribution width in ns (middle figure) and the χ^2_ν value (bottom figure). DNF: Did not fit.*

Oil	API	426-477 nm	465-500 nm	480-520 nm	510-560 nm	542-582 nm	573-613 nm	600-650 nm	575-650 nm
7090	36.8	DNF	DNF	DNF	4.09 6.93 0.33	3.42 13.5 0.03	4.98 10.5 0.10	5.50 9.74 0.09	5.1 10.6 0.10
7093	30.9	0.64 2.83 1.44	1.50 1.73 2.45	1.81 2.83 2.60	2.46 2.5 3.66	DNF	DNF	3.04 11.0 0.53	DNF
7098	44.6	6.41 8.56 0.13	6.36 6.82 0.29	6.64 7.94 0.25	7.24 9.06 0.28	8.01 11.5 0.30	7.91 11.9 0.14	7.68 10.3 0.36	7.16 8.83 0.16
7130	15.6	0.27 0.13 0.23	0.43 0.1 0.49	DNF 1.41 0.39	0.70 0.85 1.10	DNF	DNF	DNF	DNF
7169	21.6	DNF	DNF	DNF	DNF	DNF	DNF	DNF	DNF
7186	34.3	0.81 1.08 0.17	3.18 6.5 0.32	3.91 8.32 0.08	5.31 8.21 0.11	6.53 11.4 0.13	6.78 11.5 0.16	6.86 8.5 0.16	6.41 9.72 0.08
7187	29.4	DNF	2.28 7.62 0.42	2.98 9.35 0.13	4.74 8.44 0.15	5.73 11.8 0.16	6.13 11.2 0.11	6.28 8.92 0.14	5.95 8.93 0.12
7188	13.3	DNF	DNF	DNF	DNF	DNF	DNF	DNF	DNF
7193	36.0	DNF	2.03 3.24 2.41	2.28 5.42 1.32	3.24 3.87 2.56	3.54 7.89 0.41	2.47 13.0 0.60	4.29 7.87 0.27	4.0 7.95 0.33

Table B.6: *Frequency Domain lifetime data by Single Gaussian Fitting Batch 1 oils. For each oil the lifetime in ns (top figure), the distribution width in ns (middle figure) and the χ^2_ν value (bottom figure). DNF: Did not fit.*

Oil	API	426-477 nm	465-500 nm	480-520 nm	510-560 nm	542-582 nm	573-613 nm	600-650 nm	575-650 nm
	45.1	0.78	3.12	3.65	4.71	6.43	6.01	6.39	6.69
7197		7.85	5.49	8.67	5.38	12.6	13.1	8.89	10.7
		1.0	1.68	0.66	2.03	0.69	0.88	0.17	0.69
	14.1	DNF	DNF	DNF	0.51	DNF	DNF	DNF	DNF
7321					2.29				
					0.09				
	32.3	DNF	DNF	DNF	0.36	DNF	DNF	DNF	DNF
7324					0.71				
					0.30				
	32.7	DNF	DNF	DNF	0.33	DNF	DNF	DNF	DNF
7632					9.51				
					0.25				
	24.8	2.87	3.78	4.76	5.56	7.84	8.40	8.74	8.17
7633		6.13	3.45	5.93	3.43	12.5	17.1	13.5	15.8
		2.86	5.83	2.60	6.08	0.39	0.87	0.76	0.62
	50.6	3.75	4.21	4.70	5.56	6.47	6.87	7.33	5.05
7703		5.21	4.07	4.70	5.56	6.47	6.87	7.33	5.05
		0.63	1.91	1.18	1.18	0.69	0.52	0.72	0.51

Table B.7: *Frequency Domain lifetime data by Single Lorentzian Fitting Batch* 1 *oils. For each oil the lifetime in ns (top figure), the distribution width in ns (middle figure) and the* χ^2_ν *value (bottom figure). DNF: Did not fit.*

Oil	API	426-477 nm	465-500 nm	480-520 nm	510-560 nm	542-582 nm	573-613 nm	600-650 nm	575-650 nm
	31.5	0.7	1.89	2.30	3.80	4.20	4.90	5.34	4.74
198		2.99	3.38	4.58	3.31	6.06	5.85	4.53	5.92
		0.46	1.05	0.58	2.37	0.18	0.16	0.42	0.12
	30.4	0.25	1.92	2.38	4.29	4.69	5.15	5.93	5.27
199		3.96	4.36	5.98	4.28	6.85	7.78	5.53	6.84
		0.03	0.17	0.04	0.32	0.05	0.11	0.06	0.07
	29.8	0.67	2.04	2.53	3.67	4.26	4.98	5.58	4.92
201		3.03	2.14	2.81	2.45	4.28	5.87	3.88	5.33
		0.33	1.78	2.02	2.26	0.89	0.19	0.44	0.24
	38.0	0.24	1.63	1.60	3.17	3.92	4.01	4.91	4.64
207		2.93	3.07	5.67	3.90	8.37	9.02	4.95	6.10
		0.44	1.33	0.36	1.30	0.35	0.73	0.39	0.45
	19.1	0.15	0.32	DNF	0.46	DNF	DNF	DNF	DNF
7032		0	0.17	DNF	0.79	DNF	DNF	DNF	
		0.09	0.18		0.16				
	12.7	0.14	0.40	0.32	0.54	DNF	DNF	DNF	DNF
7033		0	0	0	0				
		1.85	3.26	1.07	2.52				
	40.1	1.53	2.76	3.20	4.64	4.88	5.46	6.01	4.84
7058		4.97	4.86	6.08	5.05	8.59	8.73	6.87	8.70
		0.04	0.23	0.07	0.28	0.10	0.18	0.22	0.11
	36.0	DNF	0.83	0.28	1.04	DNF	DNF	DNF	DNF
7062			1.57	2.15	2.47				
			0.14	0.14	0.15				
	39.5	0.51	1.71	2.13	3.76	3.98	4.33	5.16	4.40
7086		3.97	4.52	5.82	4.75	7.81	8.42	6.8	7.73
		0.04	0.18	0.06	0.25	0.11	0.15	0.13	0.11

Table B.8: *Frequency Domain lifetime data by Single Lorentzian Fitting Batch 1 oils. For each oil the lifetime in ns (top figure), the distribution width in ns (middle figure) and the χ^2_ν value (bottom figure). DNF: Did not fit.*

Oil	API	426-477 nm	465-500 nm	480-520 nm	510-560 nm	542-582 nm	573-613 nm	600-650 nm	575-650 nm
	36.8	DNF	0.14	0.71	3.58	3.31	4.31	4.80	4.39
7090			4.12	5.82	4.81	9.06	7.61	7.08	8.01
			0.08	0.07	0.19	0.09	0.08	0.08	0.12
	30.9	0.76	1.38	1.60	2.34	DNF	DNF	2.79	1.68
7093		1.47	1.14	1.97	1.54			2.79	1.68
		0.97	2.10	2.06	3.55			0.64	1.26
	44.6	5.82	5.93	6.11	6.63	7.21	7.07	6.96	6.56
7098		5.89	3.94	5.07	5.98	8.33	8.75	7.09	5.73
		0.11	0.33	0.26	0.29	0.29	0.15	0.36	0.16
	15.6	0.27	0.43	0.37	0.64	DNF	DNF	DNF	DNF
7130		0.06	0.03	0.53	0.49				
		0.23	0.49	0.31	0.18				
	21.6	DNF	0.23	DNF	0.66	DNF	DNF	0.73	0.24
7169			1.16		1.80			3.0	2.95
			0.14		0.11			0.09	0.1
	34.3	1.72	2.79	3.44	4.70	5.70	5.94	6.27	5.69
7186		4.69	4.3	5.77	5.79	8.47	8.45	5.43	6.92
		0.02	0.15	0.02	0.06	0.18	0.21	0.16	0.09
	29.4	0.62	2.23	2.78	4.14	4.95	5.34	5.63	5.29
7187		4.82	4.64	6.07	6.01	8.72	8.28	6.16	6.30
		0.05	0.19	0.03	0.07	0.25	0.18	0.15	0.11
	13.3	0.16	0.33	DNF	0.45	DNF	DNF	DNF	DNF
7188		0.29	0.45		1.03				
		0.06	0.11		0.11				
	36.0	0.86	1.79	1.99	2.99	3.03	2.61	3.70	3.44
7193		2.74	2.28	3.74	2.58	5.73	8.53	5.75	5.82
		0.6	1.84	0.81	2.37	0.20	0.79	0.23	0.24

Table B.9: *Frequency Domain lifetime data by Single Lorentzian Fitting Batch 1 oils. For each oil the lifetime in ns (top figure), the distribution width in ns (middle figure) and the χ^2_ν value (bottom figure). DNF: Did not fit.*

Oil	API	426-477 nm	465-500 nm	480-520 nm	510-560 nm	542-582 nm	573-613 nm	600-650 nm	575-650 nm
	45.1	1.40	2.71	3.13	4.36	5.51	5.12	5.71	5.86
7197		4.31	3.99	6.30	3.34	9.40	9.88	8.02	7.65
		0.55	1.26	0.43	2.09	0.91	1.09	0.16	0.75
	14.1	DNF	0.18	0.15	0.72	DNF	DNF	0.70	0.58
7321			0.52	0.90	0.89	DNF	DNF	1.56	1.39
			0.09	0.06	0.06			0.10	0.09
	32.3	DNF	0.67	DNF	1.34	DNF	DNF	1.48	DNF
7324			2.03		3.27			1.48	
			0.17		0.16			0.14	
	32.7	DNF	0.55	DNF	1.61	DNF	DNF	DNF	0.51
7632			3.02		4.65				0.51
			0.14		0.13				0.32
	24.8	2.46	3.64	4.37	5.23	6.90	7.18	7.70	7.02
7633		4.48	1.81	3.99	0.69	9.10	13.10	9.64	12.0
		2.10	6.23	2.50	6.55	0.39	1.05	0.80	0.77
	50.6	3.34	3.99	4.31	5.01	5.68	5.93	6.51	4.46
7703		3.45	2.20	3.41	4.94	7.71	9.92	7.88	5.26
		0.39	2.06	1.09	1.06	0.60	0.57	0.71	0.32

Appendix C

HCFI analysis - an application of crude oil fluorescence lifetime analysis

HCFI are tiny droplets of oil encapsulated in defects during crystallisation of minerals such as quartz, fluorite or calcite. Hydrocarbon-bearing fluid inclusions (HCFI) commonly occur within petroleum reservoirs and along migration pathways. They generally vary in size from submicron to 50 μm and preserve the oil in a closed system [166, 239]. Geological information from HCFI has been used to model hydrocarbon deposition and transport within petroleum reservoirs. This can been achieved by estimating the pressure-temperature conditions of fluid entrapment but the precise elucidation of these conditions requires knowledge of the chemical composition of the oil within the HCFI [166, 169, 240]. With accurate oil composition data, geologists can estimate the pressure and temperature behaviour of the oil, which can then be used to predict locations of hydrocarbon deposits. Traditionally, the analysis of HCFI by is time-consuming and uses destructive methods. The application of use of non-destructive methods for the analysis of HCFI is therefore very appealing [109, 131, 177]. It is hoped that by studying the fluorescence properties of bulk crude oils and applying the findings to HCFI data, that a quantitative method

for the determination of the entrapped petroleum fluid composition can be found.

C.1 FD analysis of HCFI

Using the protocol described in Chapter 2, the lifetimes of HCFI can be determined by either single point measurement taken at a specific location on the inclusion or by scanning the entire inclusion. An example of the fluorescence intensity image of a large inclusion (F10) of diameter 50 μm is given in Figure C.1 (right). In comparison the left hand figure shows a transmitted image of the inclusion taken with plain white light illumination giving detail of a gas bubble in the center and wax deposits along the periphery. The fluorescence intensity image recorded at a modulation frequency of 26 MHz is shown in the right hand figure, where no fluorescence is observed from the gas or wax parts.

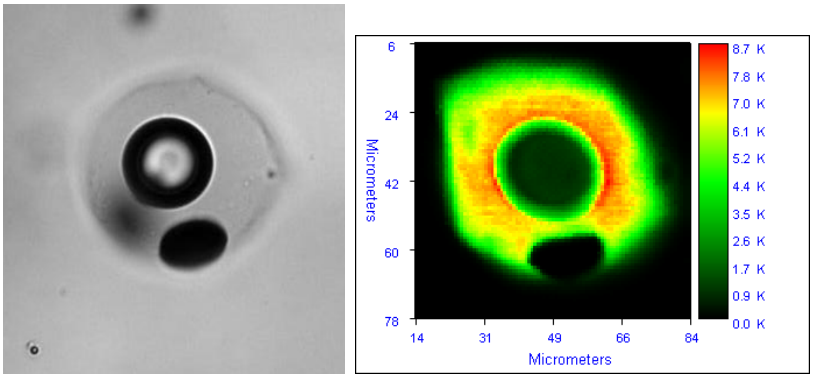

Figure C.1: *Left: Plain light illumination of the F10* HCFI *from the Cave in Rock mining district Illinois, USA. Inclusion diameter is* 50 μm. *The gas bubble in the center and the dark wax deposit are clearly seen. Right: Fluorescence intensity image recorded at* 26*MHz modulation frequency of the same fluid inclusion.*

The modulation (top left) and phase (bottom left) FLIM images for the F10 inclusion (calculated at a single frequency 26 MHz) are given in Figure C.2. To generate these images, the sample was scanned and the lifetime calculated on a per-pixel basis using the reference standard phase and demodulation data. The colour bars on the right side of the FLIM images are calibrated in terms of lifetime and the associated histograms (top right: demodulation based and bottom right: phase based) show the distribution of calculated lifetimes for the sample. Demodulation

and Phase based lifetimes were found to be 10.5 ns for the modulation and 6.5 ns respectively. The reason for this difference in phase and modulation based lifetime in heterogeneous samples such as the F10 inclusion is as follows. At a single frequency, the 'apparent' phase and demodulation fluorescence lifetimes measured are a weighted average of all the individual lifetime components. At low modulation frequencies, longer lifetime components have a greater weighting and conversely at higher modulation frequencies, shorter lifetimes have a greater weighting. As the modulation frequency increases, the relative contribution of the short lived components increases leading to shorter values of the phase based lifetime. For the demodulation based lifetimes, the relative contribution of short lived components is smaller at higher modulation frequencies leading to longer lifetimes (Also see FD theory in Chapter 1). The net result is that the phase based lifetime is shorter than the modulation based lifetime [36, 241].

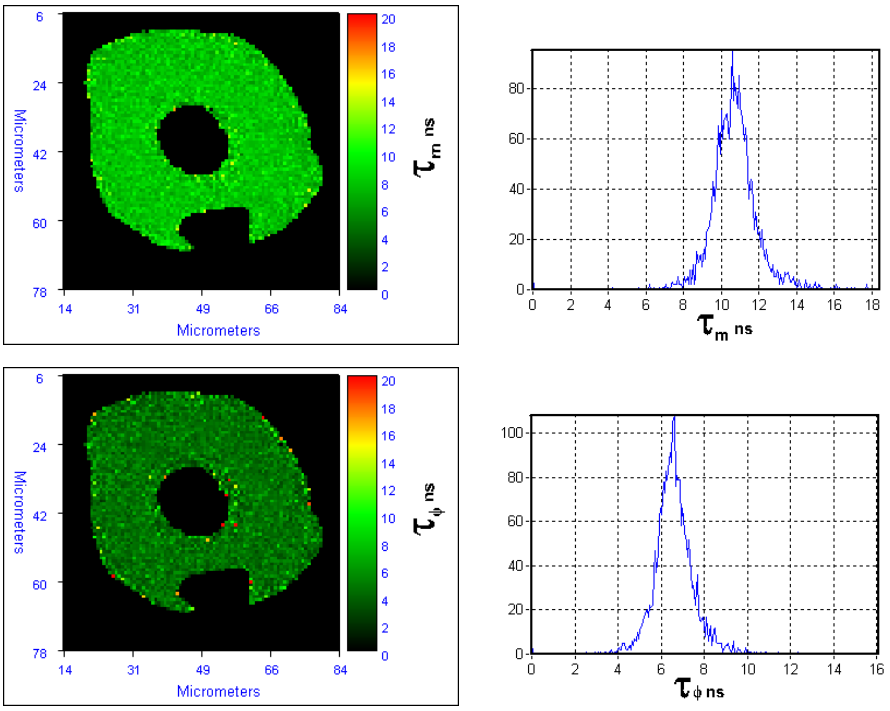

Figure C.2: *FLIM lifetime images (top and bottom left) recorded at a single frequency 26 MHz for the F10 fluid inclusion. Lifetimes are calculated based on the reference calibration modulation (top left) and phase (bottom left) values at that modulation frequency. Lifetime histograms show a gaussian distribution of the lifetimes around center mean of* ~ 10.5 *and* ~ 6.5 *ns respectively.*

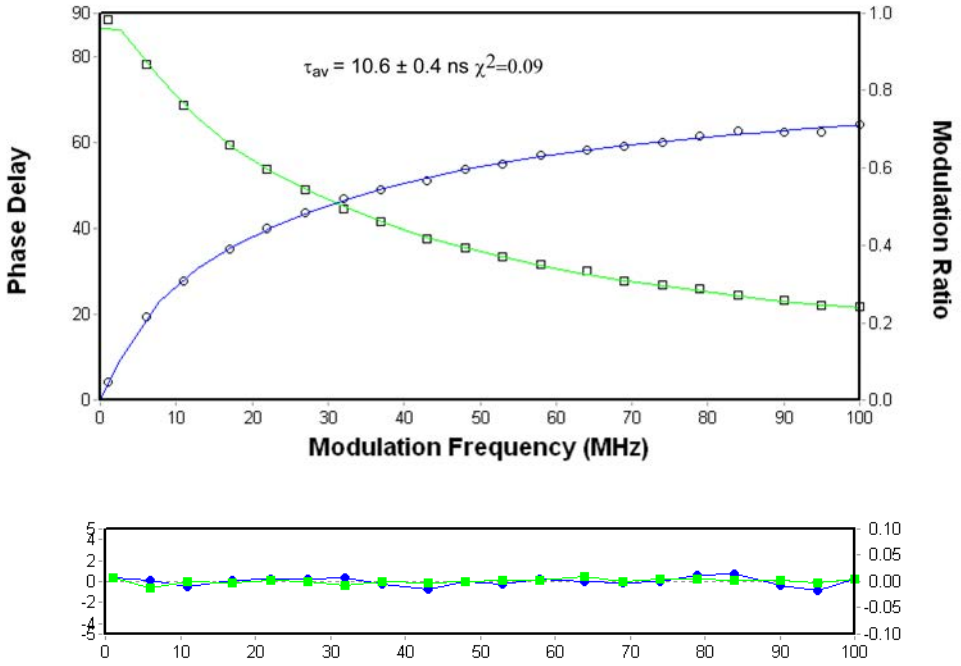

Figure C.3: *Multifrequency FLIM fitting of phase and modulation data from the F10 fluid inclusion.*

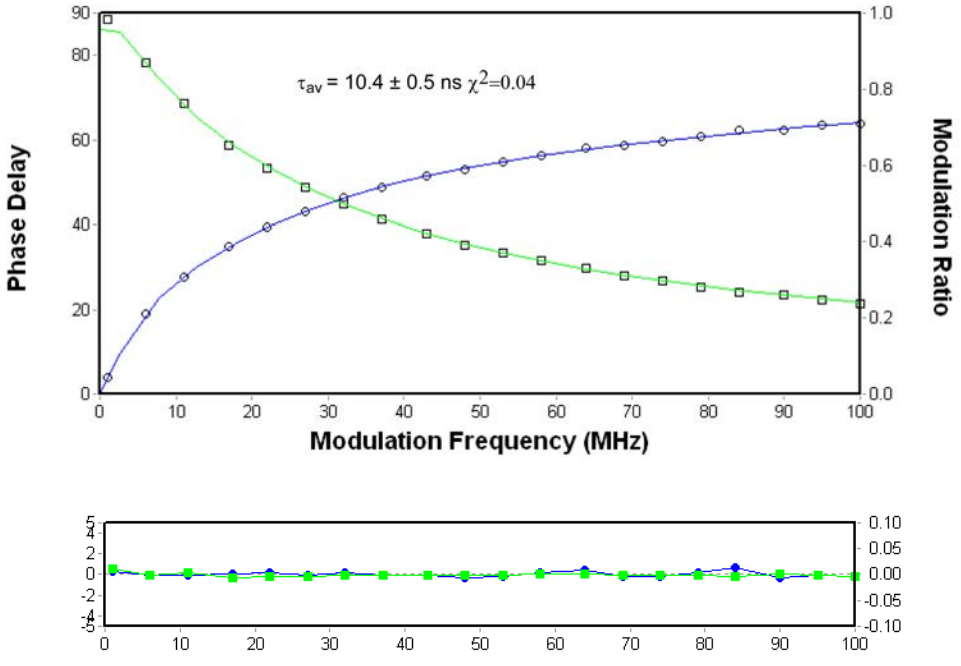

Figure C.4: *Single point measurement (at multiple modulation frequencies) fitting of phase and modulation data from the F10 fluid inclusion.*

While using a single modulation frequency is adequate for fast imaging and contrast, in order to average out the weighting of individual contributions at single frequencies, and thus give the closest fit for an average lifetime, the phase and modulation must be recorded at multiple frequencies. For FLIM images, a selected area can be chosen (in the case of the F10 inclusion, an area within the fluorescent region) and the mean phase and modulation values for that selected area are calculated and used in a multi-frequency fit (Figure C.3). However, multi-frequency fitting of FLIM images is slow to perform and an alternatively accurate lifetimes can also be obtained from a single point multiple modulation frequency measurement. An example of a single point multi-frequency fitting is given in Figure C.4 . A lifetime of 10.6 ± 0.4 ns was obtained using multi-frequency fitting from the FLIM images recorded which is very close to the single point measurement of 10.4 ± 0.5 ns. Single point measurements (at a range of modulation frequencies) were much faster to perform than multi-frequency fitting of FLIM images and thus this method was chosen for HCFI analysis. In practice, lifetimes were recorded in triplicate, using three separate single point locations within the HCFI.

C.1.1 Distinguishing HCFI by lifetime

The average fluorescence lifetimes of individual HCFI can be readily determined using the FD method and can be used to quantitatively discriminate generations of inclusions within the same sample. In a geological context, this means differentiation between oils of different sources. To date HCFI have been primarily distinguished by their colour though there are reported problems with this method [68, 242]. In general, red fluorescence indicates the presence of heavy immature oils and white/blue indicates lighter, more mature oils. This practice is not quantitative and can easily lead to misinterpretation and variable results between different observers. In contrast, discrimination by lifetime is accurate and can easily distinguish between hydrocarbon inclusions within the same sample. This can be shown by comparing Figures C.5 with the FLIM images in Figures C.6 and C.7, where two types of HCFI are distinguishable by their lifetime images (for both modulation and phase data).

In Figure C.5, the fluorescence intensity image of a Tunisian HCFI sample

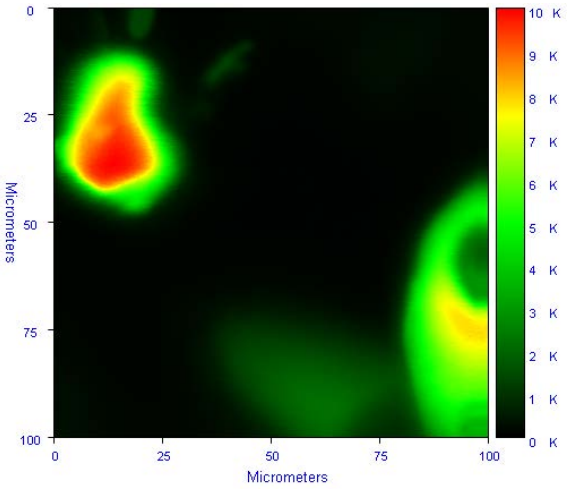

Figure C.5: *FLIM intensity image of multiple types of inclusions within a Tunisian HCFI (BJ95c) sample. Measurements were recorded at* 465-500 *nm emission and at a frequency of 30 MHz. Image courtesy of Dr. Nigel Blamey, Nanoscale Biophotonics Laboratory,* NUIG.

(BJ95c, hosted in Fluorite, Frequency 30 MHz, 465-500 nm emission wavelength) is shown. The corresponding modulation and phase basedFLIM images (Figures C.6 and C.7) enables distinction of different regions in terms of lifetime. In Figure C.6, modulation based lifetimes of 6.5 and 8.5 ns are obtained for regions A and B respectively. Phase based lifetimes from Figure C.7 are 3.8 and 5.5 ns for regions A and B. Both figures show a clear distinction between each region in terms of lifetime value. This distinction between lifetime regions may indicate multiple oil generations but also could be caused by trapping of a single oil generation under slightly different conditions. In contrast to the phase and modulation lifetimes given above, multi-frequency single point measurements on this sample gives an average lifetime of 10.1 ns and by evaluation of the lifetime-emission wavelength curves [243] it was found that the inclusions did originate from the different sources (not shown).

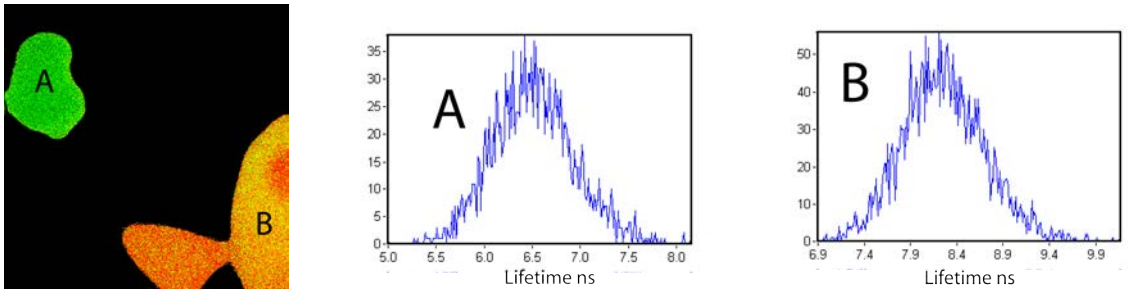

Figure C.6: *Modulation based lifetime map of the BJ95c Tunisian HCFI sample. Measurements were recorded at* 465-500 *nm emission and at a frequency of 30 MHz. The modulation based FLIM image shows two distinct lifetime regions; this variation in lifetime could infer different oil generations or a variation in the trapping conditions. Also shown are the lifetime histograms for each region.*

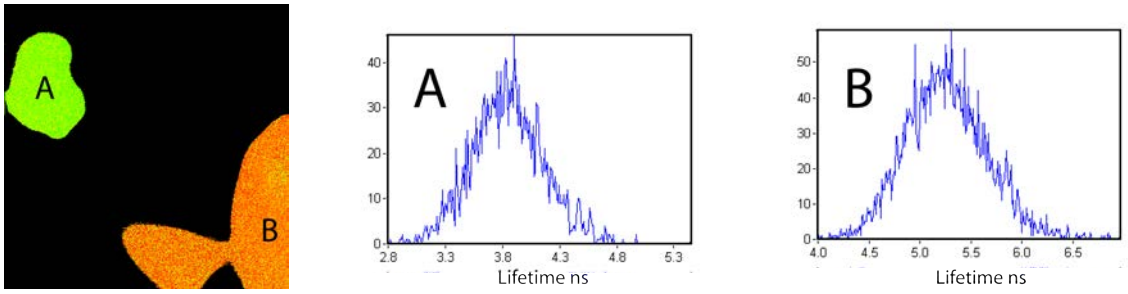

Figure C.7: *Phase based lifetime map (left figure) of the BJ95c Tunisian HCFI sample. Measurements were recorded at* 465-500 *nm emission and at a frequency of 30 MHz. As for the modulation based image, two distinct lifetime regions are shown. Also shown are the lifetime histograms for each region.*

As part of a co-current study on fluid inclusions [243], the lifetimes of a series of fluid inclusion samples were determined using the methodology outlined in Chapter 2. The lifetimes of the oil present in the fluid inclusions were generally similar to those found for the bulk oils (Table C.1) and inclusions from the same locations can have very different properties as shown by the spread of lifetimes. Heavy, medium and light oils within individual HCFI can be distinguished based on lifetime comparisons but it was found that certain included light oils gave lifetimes much longer than any of the bulk oils sampled in this work, sometimes up to 20 ns.

Table C.1: *Fluorescence lifetimes of selected* HCFI *. All data is from single point measurements recorded at* $542 - 582$ *and the discrete three decay term model was used.*

Inclusion	Location	Discrete Lifetime (ns)
1	West Shetland	7.9
2	West Shetland	2.5
3	Porcupine Basin (NW Ireland)	0.9
4	Porcupine Basin (NW Ireland)	8.8
5	Porcupine Basin (NW Ireland)	10.6
6	Greenland	17.3
7	Laghy (NW Ireland)	20.5
8	Jean D'Arc Basin (New Foundland)	5.5
9	Jean D'Arc Basin (New Foundland)	3.2
10	Cave In Rock (Illinois,USA)	1.7
11	Cave In Rock (Illinois,USA)	13.1
12	Tunisia	18.1
13	Tunisia	20.1

The longer fluorescence lifetimes observed for HCFI may be due to the light alkanes still trapped within the inclusion. However, dilution of light neat oils did not increase the fluorescence lifetime to levels close to the those found for some HCFI. For example the lightest oils (7197 and 7703) in the Batch 1 crude oil set diluted with either Toluene or a mixture of MeCH:MeCP gives a lifetime of ~ 11.4 ns which does not approach the long lifetime values obtained for some inclusions. This indicates that the photophysical processes occurring within the inclusions are not purely dictated by the alkane content.

C.2 A final word

Using the methods developed for bulk oil analysis, FD FLIM can be used to determine the lifetimes of HCFI and also distinguish between different generations. These measurements are repeatable, quantitative, and have a low sensitivity to photobleaching and electronic fluctuations. However, care is needed to determine if the lifetime differences are really due to generational changes and not trapping variations. In some cases, the lifetimes determined by single point measurements on HCFI were considerably longer than those determined for bulk oils, even surpass-

ing diluted bulk oils indicating that the photophysical behaviour of the oil within the inclusion is not purely dictated by alkane content. Because of this, correlation between HCFI lifetimes and those from the bulk oil samples has so far not been possible. HCFI have been synthesised [244] and to allow comparison between the lifetime data from HCFI and that of bulk oils, synthetic inclusions must be made from diluted crude oils.

Appendix D

Published Work

J Fluoresc (2008) 18:997–1006
DOI 10.1007/s10895-008-0330-5

ORIGINAL PAPER

Frequency Domain Fluorescence Lifetime Study of Crude Petroleum Oils

Peter Owens · Alan G. Ryder · Nigel J. F. Blamey

Received: 11 December 2007 / Accepted: 22 January 2008 / Published online: 7 February 2008

Abstract Frequency domain (FD) fluorescence lifetime data was collected for a series of 20 crude petroleum oils using a 405 nm excitation source and over a spectral range of ~426 to ~650 nm. Average fluorescence lifetimes were calculated using three different models: discrete multi-exponential, Gaussian distribution, and Lorentzian distribution. Fitting the data to extract accurate average lifetimes using the various models proved easier and less time consuming for the FD data than with Time Correlated Single Photon Counting (TCSPC) methods however the analysis of confidence intervals to the computed average lifetimes proved cumbersome for both methods. The uncertainty in the average lifetime was generally larger for the discrete lifetime multi-exponential model when compared to the distribution-based models. For the lifetime distributions, the data from the light crude oils with long lifetimes generally fit to a single decay term. Heavier oils with shorter lifetimes required multiple decay terms. The actual value for the average lifetime is more dependant on the specific fitting model employed than the data acquisition method used. Correlations between average fluorescence lifetimes and physical and chemical parameters of the crude oils were made with a view to developing a quantitative model for predicting the gross chemical composition of crude oils. It was found that there was no significant benefit gained by using FD over TCSPC other than more rapid data analysis in the FD case. For the FD data the Gaussian distribution model for fluorescence lifetime gave the best correlations with chemical composition allowing a qualitative correlation to some bulk oil parameters.

Keywords Fluorescence · Petroleum · Crude oil · Fluorescence lifetime · Frequency domain · Phase modulation

P. Owens · A. G. Ryder (✉) · N. J. F. Blamey
Nanoscale Biophotonics Laboratory, School of Chemistry,
National University of Ireland-Galway,
Galway, Ireland
e-mail: alan.ryder@nuigalway.ie

A. G. Ryder
National Centre for Biomedical Engineering Science,
National University of Ireland—Galway,
Galway, Ireland

Introduction

Petroleum oils are complex mixtures of aliphatic, aromatic, and high molecular weight organic compounds and due to this heterogeneity, chemical analysis is complex and time consuming. Petroleum oils are typically characterised using liquid chromatography, separating into four major component classes based on differences in solubility and polarity: saturates, aromatics, resins, and asphaltenes (SARA). Details on ASTM standard methods and improvements on the determination of SARA components can be found in the literature [1, 2]. Each of the major SARA components can be further characterised by the use of Gas Chromatography–Mass Spectrometry (GC–MS) which provides unambiguous identification of individual components. These chromatographic techniques are however, time consuming, expensive, and destructive.

Molecular spectroscopy techniques such as Mid Infra-Red (MIR), Near Infra-Red (NIR) absorption, and Fluorescence emission have been used for many years as a fast and non-destructive tool in the analysis of crude oils [3–6]. For crude oils, the fluorescence emission is due to the presence of a multitude of aromatic hydrocarbons in varying concentrations. Factors such as the specific chemical composition (concentration of fluorophores and quenching

species) and physical (viscosity and optical density) influence emission properties such as intensity, wavelength of emission, and lifetimes. For heavy oils, fluorescence emission is generally broad, very weak, and has short lifetimes, whereas lighter oils have narrower more intense emission bands, and longer lifetimes (Fig. 1) [7, 8]. The nature of the emission is governed by the complex interplay between energy transfer and quenching caused by the high concentrations of fluorophores and quenchers in petroleum oils. The complexity of crude oils usually prevents the resolution of any specific chemical component in terms of emission parameters.

Fluorescence lifetimes are potentially more useful for characterising crude oils than steady-state fluorescence data as the measurements are relatively insensitive to excitation intensity fluctuations, sample optical density and turbidity. Previous studies in our laboratory using Time Correlated Single Photon Counting (TCSPC) methods have shown that one can correlate various aspects of oil composition with lifetime changes [9–14]. Unfortunately, these studies also showed that accurate quantitative measurements were not possible using intensity averaged lifetimes calculated from TCSPC data. Another complicating factor with the TCSPC method was the time consuming nature of data analysis when fitting multi exponential decays to complex decay curves. This arises from a tendency in the fitting algorithms to return an abnormally high long lifetime component when using multi-exponential fit models on complex petroleum decay curves. This in turn, can generate a longer average lifetime which can skew results. Since there are an unknown number of emitting fluorophores represented by each decay measurement (at any emission wavelength) one cannot use techniques like global analysis to rectify the situation. In practice, the solution required the refitting of the data multiple times and undertaking a support plane analysis to find the true minimum average lifetime.

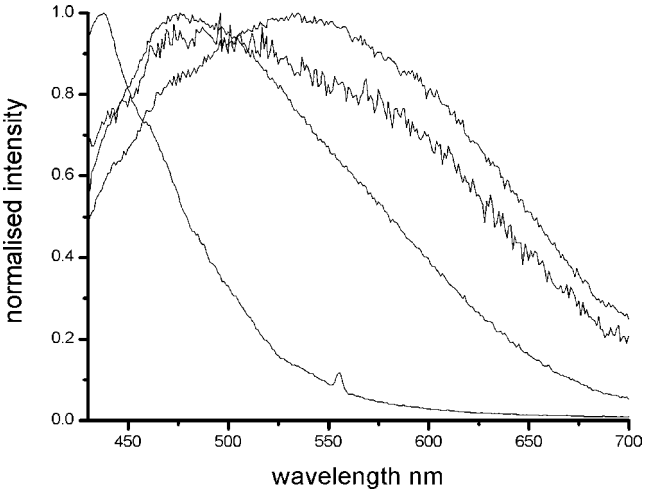

Fig. 1 Normalised steady state fluorescence emission spectra of a selection of crude petroleum oils excited at 405 nm. Light oils display a narrow yet strong fluorescence emission as opposed to medium to heavy oils which emit weakly over a broad emission range

The major alternative to the TCSPC method for lifetime determination is the widely used Frequency Domain (FD) methodology [15–17]. This method is potentially more useful for complex fluid analysis, since the data analysis can be more straightforward and rapid than for TCSPC. Using multiple modulation frequencies, the FD method can resolve fluorescence lifetimes in simple heterogeneous systems [18–20]. For complex systems comparable to petroleum oils, there are fewer examples in the literature, the most relevant being the Total Lifetime distribution analysis [21] which was used to characterise coal derived liquids. Here we report an initial FD lifetime based study of crude petroleum oils to evaluate the method for the qualitative and quantitative analysis of crude petroleum oils. We compare the FD and TCSPC methods in terms of analysis time, rapidity, and correlations to physical and chemical parameters. An evaluation of the FD data fitting models is also made in terms of correlating the resultant average lifetimes with the physical and chemical parameters of the crude oils.

Materials and methods

The phase and modulation data were obtained using an Alba Fluorescence Lifetime Imaging (FLIM) system (ISS Inc, Champaign, Ill., USA) based on an upright Olympus BX51 microscope fitted with a modulated (10 to 200 MHz) 405 nm laser diode excitation source. The fluorescence emission was wavelength separated into two wavelength ranges using pairs of bandpass filters in each of four different filter cubes (Table 1). The experimental setup enabled the simultaneous recording of phase and modulation data at two narrow wavelength ranges defined by the particular emission filters. The instrument was calibrated by the determination of the phase and modulation responses over a range of frequencies for a number of different standards of known fluorescence lifetime (reference stand-

Table 1 Dichroic cube and filter characteristics

Cube	Dichroic mirror	Filter1 (nm)	Filter2 (nm)	Reference standard
1	495 m	542–582	426–477	Coumarin 30
2	505 m	573–613	465–500	HPTS
3	562 m	480–520	600–650	LuciferYellow CH
4	570 m	510–560	575–650	Lucifer Yellow CH

ards, Table 2). Acetonitrile (spectrophotometric grade), Coumarin30, and Lucifer Yellow CH were obtained from Sigma Aldrich. HPTS (8-hydroxypyrene-1,3,6 trisulfonic acid trisodium salt) was obtained from Invitrogen. All materials were used without further purification. The choice of standard was predicted on the ability for excitation at 405 nm, a broad emission spectra which overlapped the bandpass filters of the lifetime system, a mono-exponential fluorescence lifetime in the range of the crude oil samples (1–10 ns), good solubility and photostability, and a reasonably large Stokes shift. Single exponential non-linear least squares fitting for each standard was performed using the instrument software and the quality of fit as judged by the proximity of the calculated lifetime (±0.1 ns) and the goodness of fit (χ^2_R) value. Fluorescence lifetimes for the three standards were also verified by TCSPC measurements using a Fluotime 200 lifetime spectrometer (PicoQuant, Germany) and compared favourably to the literature values [22–24], and with previous studies in this laboratory [25]. All measurements were made at room temperature and the standard solutions were not degassed or deoxygenated. Lifetimes were calculated from phase and modulation responses relative to the phase and modulation responses from the chosen standard fluorophore.

The 20 crude oils tested had a wide chemical variance and were sourced from diverse geographical locations and rock types [12]. For the bulk crude oils, the FLIM system was operated in non-confocal mode (for higher throughput) and the neat, non-degassed crude oils were placed directly into a 1 mm path length quartz cuvette and then placed normal to the excitation source on the sample stage. All measurements were made in triplicate at room temperature (20–22 °C). The physical and chemical properties of these oils have previously been published in detail [12, 14].

Due to the large number of different emitting fluorophores at every emission wavelength the calculation of a fluorescence lifetime value is not a trivial task. Here the data were fit to discrete exponential, Gaussian and Lorentzian distribution models using a non-linear least squares fitting method as implemented by the instrument software (Vista, ISS, ver. 3.6). A single decay time was attempted for the distribution models; however, in most cases 2 or 3 individual decay times were required for all model types to achieve a satisfactory fit. For all cases the intensity based average lifetime ($\overline{\tau}$) was reported [26].

Table 2 Reference standards used for lifetime calibration

Standard	Solvent	Concentration	λ_{em}(max)	τ (ns)
Coumarin30	CH_3CN	10^{-5} M	488 nm	2.6
HPTS	0.2 M (phosphate buffer)	10^{-6} M	510 nm	5.4
Lucifer yellow CH	Water	10^{-5} M	533 nm	5.1

The goodness of fit in each case was described by χ^2_Rwhich is defined as:

$$\chi^2_{\mathrm{R}} = \frac{1}{\nu}\sum_{\omega}\left[\frac{\phi_\omega - \phi_{c\omega}}{\delta\phi}\right]^2 + \frac{1}{\nu}\sum_{\omega}\left[\frac{m_\omega - m_{c\omega}}{\delta m}\right]^2 \quad (1)$$

where ν is the number of degrees of freedom (twice the number of sampled frequencies minus the number of variable parameters). The subscript c indicates calculated values of phase and modulation based on the chosen values of α_i (fractional contribution of the ith component) and τ_i (lifetime of the ith component). α_i and τ_i are varied in order to give a minimum value of χ^2_{R}. $\delta\phi$ and δm are the uncertainties in the phase and modulation values respectively. The goodness of the model is judged on the minimisation of the value of χ^2_{R} and also on the number of decay terms used [19, 26].

In order to determine the confidence limits on the average lifetimes reported, it is necessary to prepare a χ^2_{R} surface plot, or Support Plane Analysis [26, 27]. This plots the value of $\left(\chi^2_{\mathrm{R}}/\chi^2_{\mathrm{Rmin}}\right)$ versus the average lifetime obtained and the F_χ statistic (appropriate for ρ and ν degrees of freedom of the measurement method) is then used to determine the confidence interval.

$$F_\chi = \frac{\chi^2_{\mathrm{R}}(\mathrm{par})}{\chi^2_{\mathrm{R}}(\mathrm{min})} = 1 + \frac{\rho}{\nu}F(\rho,\nu,P) \quad (2)$$

where, $\chi^2_{\mathrm{R}}(\mathrm{par})$ is the value of χ^2_{R} with a fixed parameter value, $\chi^2_{\mathrm{R}}(\mathrm{min})$ is the minimum value of χ^2_{R}, ρ is the number of parameters, and F (ρ, ν, P) is the F statistic with ρ parameters and ν degrees of freedom with a probability of P. The F statistic values needed to calculate F_χ are described in Lakowicz [26]. A value of P=0.32 was used, representing one standard deviation. When dealing with complex decays and average lifetime values, the most facile means of generating a plot of $\left(\chi^2_{\mathrm{R}}/\chi^2_{\mathrm{Rmin}}\right)$ versus the average lifetime is to systematically change the longest lifetime value only. This procedure is carried out in triplicate for each oil and the mean values of average lifetime are reported. We have observed that in practice [9–14], when studying complex systems, small changes in this long lifetime have the greatest impact on the average lifetime and χ^2_{R} values. The situation is exacerbated as more lifetime terms are included in the fit model. An increase in the number of parameters increases the uncertainty significantly and thus there is a larger confidence interval range as shown in Table 3. An example of the support plane plots used to generate this data is shown in Fig. 2. The response of the χ^2_{R} surface to change in the average lifetime is generally much broader for the discrete model than for the

Table 3 Average lifetime and single decay distribution lifetimes calculated for the 542–582 nm emission band (empty cells indicate unable to fit)

Model		Gaussian (single)	Gaussian (multiple)	Lorentzian (single)	Lorentzian (multiple)	Discrete (multiple)
Oil	API	Average lifetime (ns)				
7703	50.6	6.47±0.07	6.72±0.30 (2)	5.67±0.06	6.14±0.21 (2)	7.42±0.86 (3)
7197	45.1	6.37±0.10	6.24±0.39 (3)	5.44±0.10	6.18±0.42 (3)	6.21±0.44 (3)
7098	44.6	7.89±0.17	7.89±0.17 (1)	7.25±0.16	7.14±0.28 (2)	10.80±1.64 (3)
7058	40.1	5.67±0.05	6.58±0.26 (3)	4.90±0.05	6.58±0.16 (3)	6.40±0.23 (3)
7086	39.5	4.98±0.06	5.77±0.38 (3)	4.32±0.05	5.74±0.38 (3)	5.66±0.32 (3)
7090	36.8	3.44±0.07	5.72±0.23 (3)	3.33±0.05	5.94±0.39 (3)	5.68±0.25 (3)
7193	36.0	3.11±0.04	5.16±0.24 (3)	3.00±0.04	5.04±0.94 (3)	5.18±0.26 (3)
7062	36	–	2.80±0.39 (3)	–	2.11±0.09 (2)	2.70±0.15 (3)
7186	34.3	6.53±0.07	7.57±0.50 (3)	5.71±0.07	8.19±0.74 (3)	6.78±0.33 (3)
7632	32.7	–	3.21±0.09 (2)	–	3.17±0.07 (2)	3.60±0.14 (3)
7324	32.3	–	2.85±0.06 (2)	–	2.72±0.06 (2)	3.16±0.15 (3)
7093	30.9	–	3.23±0.15 (2)	–	3.28±0.15 (3)	4.13±0.22 (3)
7187	29.4	5.75±0.06	6.04±0.23 (3)	4.97±0.08	5.38±0.11 (2)	6.09±0.22 (3)
7633	24.8	7.92±0.13	8.40±0.72 (3)	6.88±0.09	8.50±0.53 (3)	8.30±0.56 (3)
7169	21.6	–	1.90±0.10 (3)	–	1.96±0.10 (3)	1.91±0.13 (3)
7032	19.1	–	0.98±0.11 (2)	–	0.98±0.06 (2)	0.98±0.10 (2)
7130	15.6	–	1.04±0.07 (2)	–	1.03±0.08 (2)	1.36±0.21 (3)
7321	14.1	–	1.10±0.06 (2)	–	1.08±0.05 (2)	1.08±0.05 (2)
7188	13.3	–	1.27±0.08 (3)	–	1.29±0.09 (3)	1.28±0.10 (3)
7033	12.8	–	0.52±0.10 (2)	–	0.38±0.10 (2)	0.51±0.05 (2)

The number in brackets indicates the number of individual decay times used to achieve an accurate fit. The lifetimes reported here are the averages of fitting results from three separate fits

Gaussian or Lorentzian distribution models. Three decay parameters give the greatest uncertainty on the average lifetime reducing to a minimum when using a single decay. Although the quickest to fit, the discrete model gives the greatest temporal uncertainty range for long and middle average lifetimes while for short average lifetimes, all models show similarly small temporal confidence intervals.

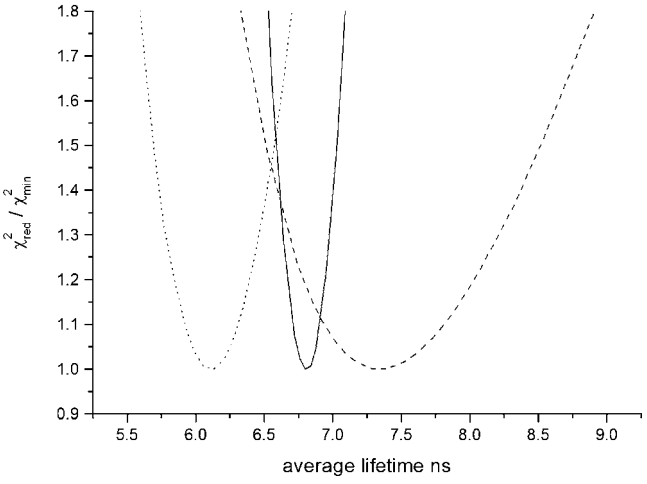

Fig. 2 Sample surface plot (Oil 7703 542–582 nm emission data) used to calculate the confidence interval in the average lifetime for the three fitting models: Discrete (*dashed line*), Lorentzian (*dotted line*), and Gaussian (*line*). The broader curve of the discrete model case indicates a much less precise determination of lifetime than for the narrower intervals determined for the single decay time distribution models

If the uncertainty is expressed as a percentage of the average lifetime then the relative error is larger for the short lifetime oils. The intervals reported in Table 3 are comparable with those obtained for the TCSPC results and in each case the production of surface analysis plots for average lifetimes is a laborious manual process.

Results and discussion

In order to judge the average lifetimes obtained from the two methods, the TD lifetimes measured at a centre wavelength of 480 nm (approximately 13 nm bandpass) were compared to the FD lifetimes obtained using the 465–500 nm emission filter (Fig. 3). The TCSPC measurements covered ~473–487 nm, while the filter on the FLIM system sampled 465 to ~500 nm. This suggests that the TCSPC lifetimes originate from a sampled fluorophore population with a slightly greater fraction of bluer emitting, longer lived fluorophores than the population sampled by the FD instrumentation. For oils with a relatively long lifetime the FD data generated slightly longer lifetime values than the TCSPC data. However, there does not seem to be any consistent pattern, and one should therefore exercise caution when comparing lifetimes of complex fluids collected on different instrumentation.

In practical terms, data collection times for each method are comparable, although the shorter acquisition times for single

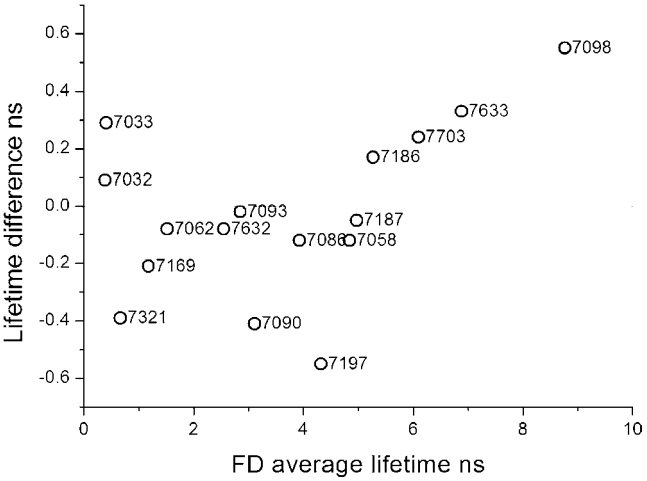

Fig. 3 Plot of the average lifetimes determined by Frequency Domain (FD) method and the difference with the TD average lifetimes determined using TCSPC. Both lifetimes calculated using discrete average lifetime model. Data recorded at a centre wavelength of 480 nm using 405 nm excitation. Positive lifetime differences indicate the oils whose FD average lifetimes are longer that the TCSPC measured average lifetimes

frequency phase and modulation measurements is a distinct advantage for rapid imaging or sensing applications. The greater sensitivity of TCSPC is an advantage with weakly emitting heavy crude oils however; the majority of oils are strongly fluorescent and are therefore better suited to FD analysis. The most significant difference between the two methods was fitting of the data to extract average lifetimes which were found to be faster for FD than for TCSPC although the evaluation of the parameter uncertainty was similar in both cases.

The phase modulation responses for a selection of the crude oils at different emission wavelengths are shown in Fig. 4. All show an increase in the modulation frequency at which a phase shift of 45 degrees occurs as the oils get heavier and the lifetimes shorten. Another point of note is the fact that a minimum of 40 frequencies (that are within the phase-dependent frequency range of sample) were required for accurate fits to the complex decay profiles. Heavy crude oils exhibit noisy phase modulation responses because they tend to be weak emitters, leading to low signal to noise ratios. An additional factor is the fact that the lifetimes are very short (tending to 1 ns or less) due to quenching, and the FLIM system we used is only capable of generating accurate modulation frequencies up to ~200 MHz. The phase and modulation data therefore do not span a wide enough range; leading to relatively poor data fitting. It would be possible to obtain better quality data with a system capable of higher modulation frequencies (up to 1 GHz).

The choice of model used to calculate an average fluorescence lifetime of these complex fluids is critical. The fact that there are very large numbers of interacting fluorophores produces very complex decay behaviour. In previous work from this laboratory [9–14] the intensity averaged lifetime calculated from a multiple discrete lifetime model was used. However, it should be noted that while this model is not an accurate descriptor of the emitting species, it had utility in describing general trends in the photophysics of crude oils. Part of the reason for undertaking this study was to evaluate the different models available for FD lifetime calculations.

All phase-modulation data were fitted using the discrete and distribution models with multiple lifetime components. The normalised distributions from three representative oils are shown in Fig. 5. As one would expect the Lorentzian distribution gives a narrower distribution of lifetimes when compared to the Gaussian case. In some cases the Lorentzian model fits incorporate very narrow peak widths as can be seen in the top distribution of Fig. 5. Intrinsically one would expect that a broader distribution would be a better description of the photophysical behaviour and because of this, determination of average lifetime for the distribution of lifetimes in the oil may not be valid. A detailed analysis of all the fit data for the oils (Table 3) shows some interesting features.

First, most of the light to medium oils can be fitted to a simple mono-modal Gaussian (or Lorentzian) distribution, i.e., when the API[1] gravity is above 36, or where the average lifetime is ~ 3 ns or longer). The mono-modal lifetime values are all reasonably short compared to the average lifetimes generated from a multi-exponential discrete decay model. This can be very significant in some cases up to ~2 ns. A comparison of the confidence intervals from the surface plot-derived limits, indicate that the lifetimes from the mono-modal distribution are more accurate than the discrete lifetime models. This may directly represent the simpler distribution of fluorophores found in the lighter crude oils. These results indicate that this simpler distribution model is a more accurate representation of the oil photophysics and should be used in preference to the average lifetimes generated by multi-exponential models.

The shorter lifetime oils in general required multi-modal distributions (Gaussian or Lorentzian) to accurately model the fluorescence decay. This introduced significant variances in the calculated average fluorescence lifetimes, and in certain oils this difference was as much as 3.0 ns. A comparison of the confidence intervals provides no guidance as to which is the correct lifetime. The uncertainty in the average lifetime value is generally greater for the multimodal distribution models and the long lifetime component has the most significant impact on this value. These results confirm that extreme caution should be applied in comparing fluorescence lifetimes of complex fluids such as crude oils.

[1] API gravity is defined as: ((141.5/specific gravity at 15.6 °C)−131.5).

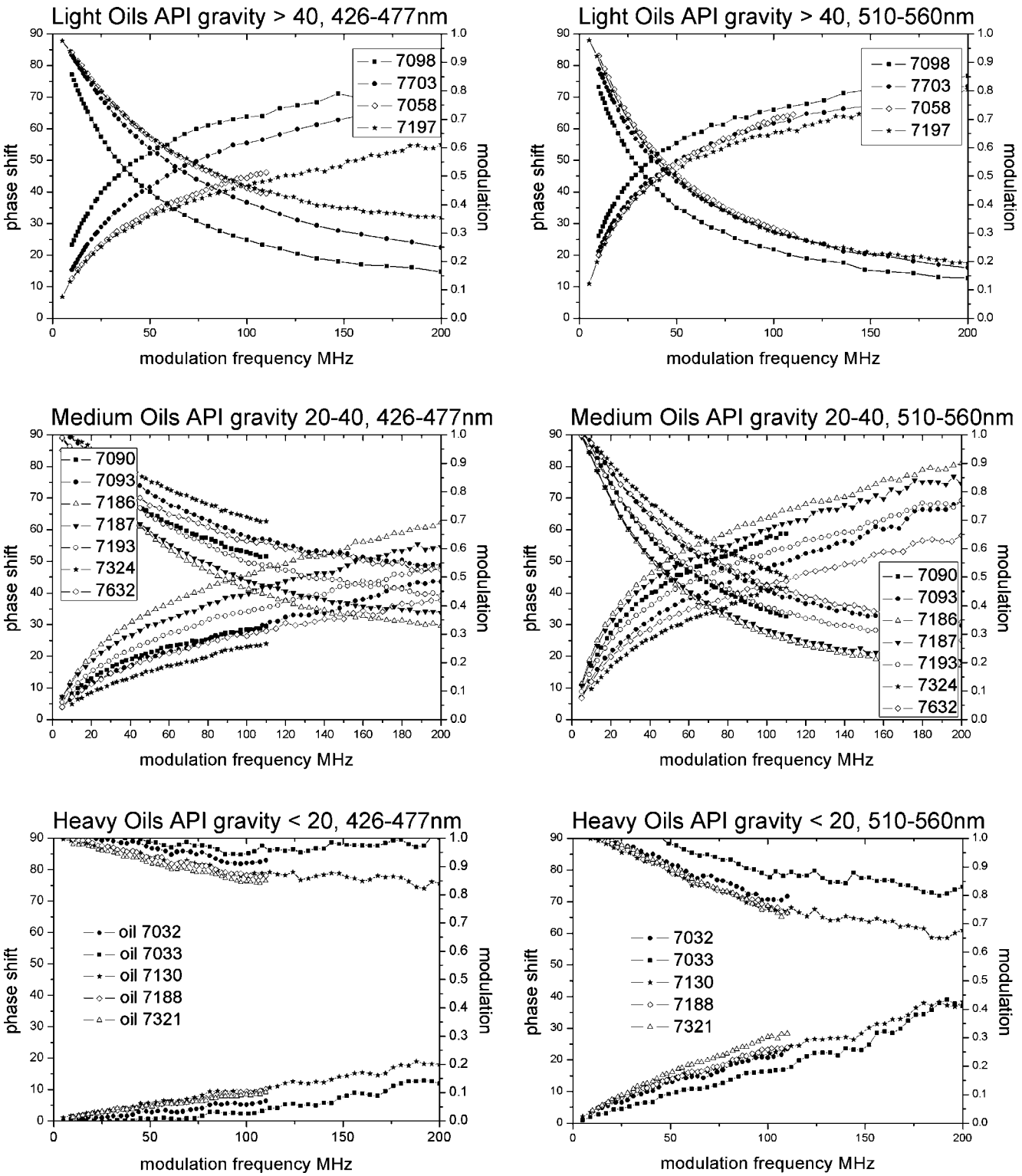

Fig. 4 Phase and modulation responses for light (*top*), medium (*middle*), and heavy (*bottom*) crude oils at two different emission wavelength bands. The increased noise in the data from the heavy oils is due to the much lower signal to noise ratios resulting from the weak emission and from the very short lifetimes (near to 1 ns)

In essence the average lifetime value is only valid for a particular model and measurement method.

The average lifetime (irrespective of the fit model) increases with increasing emission wavelength which is in agreement with literature studies [9, 12] (Fig. 6). This curved lifetime/wavelength response is due to the fact that fluorescence lifetimes are affected by processes such as collisional quenching, energy transfer, and excited state complex

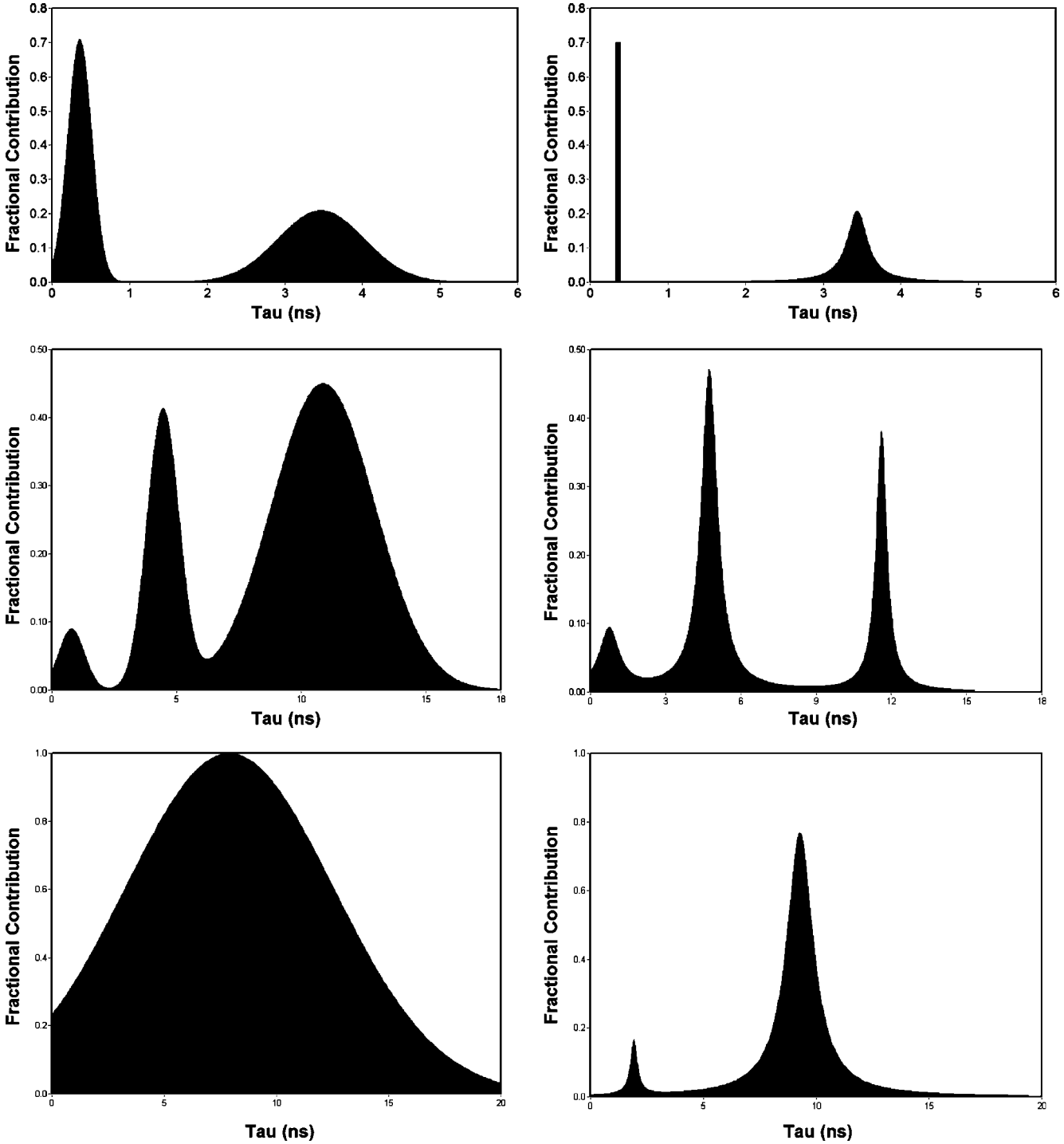

Fig. 5 Gaussian (*left*) and Lorentzian (*right*) lifetime distributions for a heavy oil, 7032 (*top*), a medium density oil, 7058 (*middle*), and a light crude oil, 7098 (*bottom*). The *single bar* in the top right figure indicates a peak width too narrow to display

formation. Each emission wavelength range represents a different population of emitting fluorescent species. At shorter wavelengths the emission largely occurs from smaller aromatics with relatively large HOMO–LUMO band gaps. At longer wavelengths the emission is largely due to the response of larger molecules with smaller HOMO–LUMO band gaps. There is a net decrease in the quantity of energy transfer at longer wavelengths and hence the lifetime increases. Lifetimes are generally shorter for heavy oils and longer for low density oils because heavy oils contain greater proportions of polar and asphaltic compounds which cause fluorescence quenching leading to shorter lifetimes. Lighter

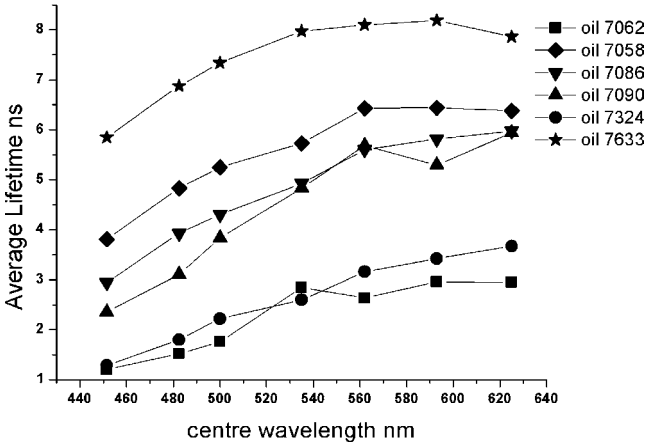

Fig. 6 Average lifetimes (discrete lifetime model) for some selected medium density crude oils. A general increase in lifetime is observed with increasing emission wavelength. A similar trend occurs with heavy and light crude oils

oils have higher alkane content and less heavy asphaltic molecules which give rise to longer lifetimes.

In order to test the lifetime values obtained from the different models, correlations were made with bulk composition parameters of the oils. Previous studies at this laboratory [14] have showed that there was a positive linear correlation between average fluorescence lifetime and API gravity but with a high degree of scatter. Figure 7 plots the API gravity–lifetime correlation for the FD and TCSPC data, showing a similar degree of scatter and no major improvement in correlation. Following on from this, a comparison in correlations of the FD average lifetimes across the emission wavelength range is shown in Table 4,

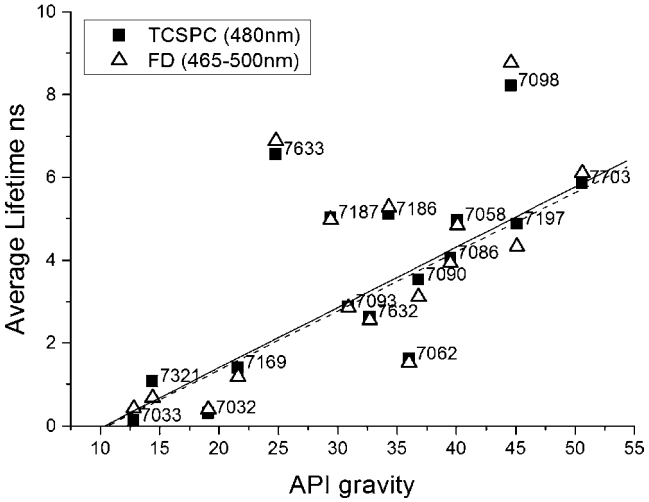

Fig. 7 Correlation between API gravity and TCSPC/FD average lifetimes. All data was measured at a *centre wavelength* of 480nm and average lifetimes were calculated using the discrete multiple decay model. Correlation coefficients were calculated without the outliers 7633 and 7098. (*line* TCSPC linear fit r^2=0.73; *dashed line* FD linear fit, r^2=0.74)

where the 542–582 nm range shows marginally better correlations. In [14], it was determined that the TCSPC average lifetimes recorded in the 540 nm emission range gave the best correlations (in terms of r^2 values) to the bulk oil composition parameters. Thus the 542–582 nm data set was selected for comparison of average lifetimes between the fitting models (Fig. 8).

The alkane and aromatic plots (not shown) showed a high degree of scatter and no clear trend. A better correlation was made with corrected (normalised in order to take account of the column losses) alkane and the best correlations were obtained with % Polar and also with API gravity. The outliers evident in Fig. 8 are oils with unusual characteristics such as abnormally high water, wax, or polar concentrations relative to their API gravity [9–14]. This highlights the difficulties in dealing with crude oil samples, namely the large non-linear variations in chemical composition encountered. The correlation coefficients determined from the plots in Fig. 8 are shown in Table 5 which indicate that there is no significant improvement over previously reported correlations [14]. This indicates that the compositional parameters of crude petroleum oils generated by conventional SARA analyses do not correlate linearly with fluorescence lifetime irrespective of measurement method and analysis model.

Conclusions

Frequency Domain (FD) methods were used to measure the fluorescence lifetimes of a series of crude oils. It was found that the calculated average lifetimes vary significantly depending on the fit model used. For light crude oils with long fluorescence lifetimes, a relatively simple mono-modal Gaussian or Lorentzian distribution was sufficient to accurately describe the fluorescence decay. For heavier oils, with shorter lifetimes, more complex multi-modal distributions were required to adequately fit the data. This

Table 4 Correlation coefficients (r^2) associated with best linear fits for the 20 crude oils recorded at varying wavelength ranges

Emission wavelength (nm)	Corrected alkane	Polar	Corrected polar	API gravity
426–477	0.66	0.77	0.77	0.72
465–500	0.72	0.81	0.86	0.74
510–560	0.72	0.83	0.88	0.76
542–582	0.76	0.86	0.85	0.79
573–613	0.76	0.81	0.81	0.81
575–650	0.74	0.83	0.85	0.74

All values have been determined using the discrete multi exponential model with outliers removed

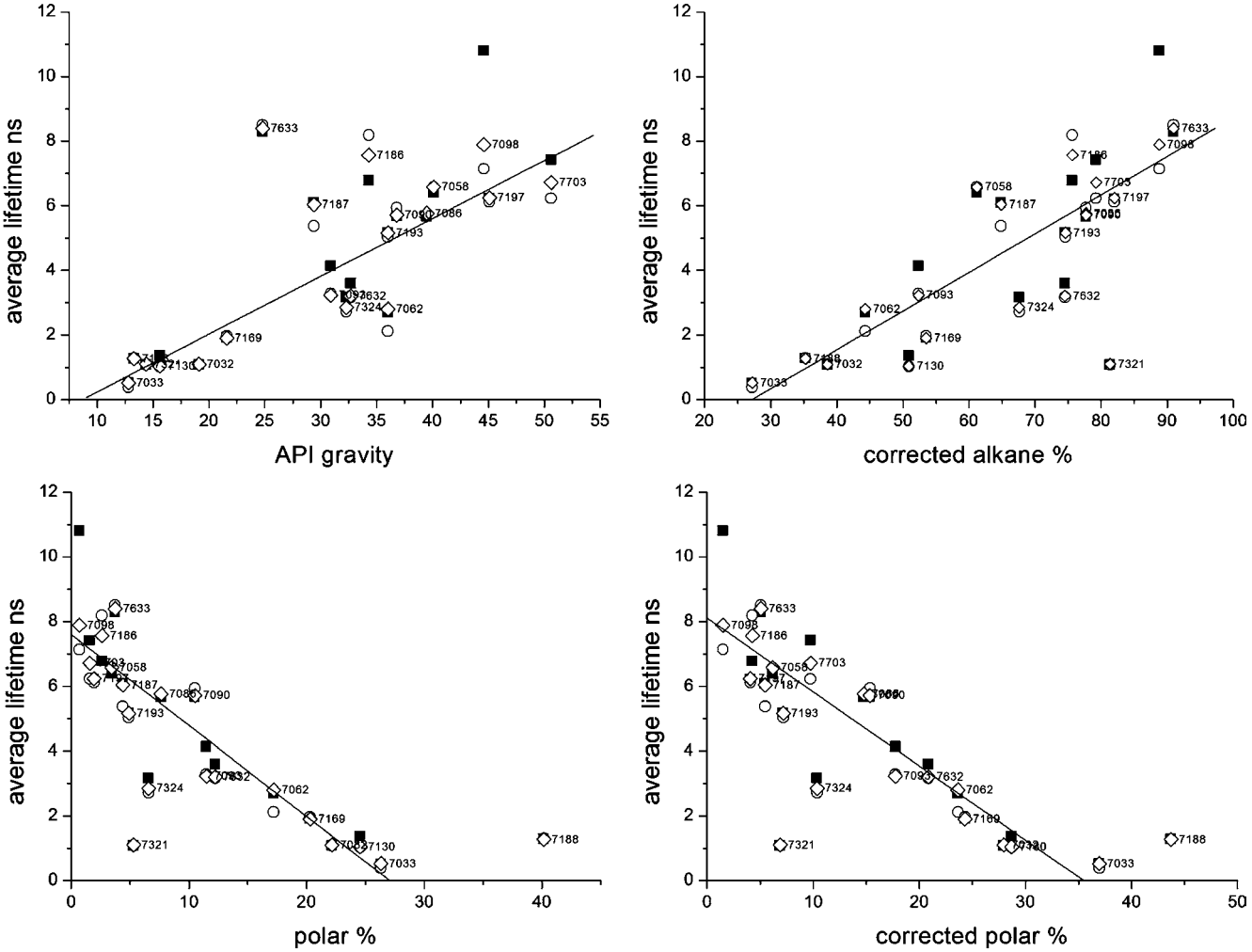

Fig. 8 Correlations between average lifetimes and gross chemical composition parameters (%corrected alkane, polar and corrected polar %) and API gravity for the 20 crude oils. The regression lines are based on the Gaussian model average lifetimes. Emission wavelength was 542–582 nm (*filled square* Discrete, *empty circle* Lorentzian, *empty diamond* Gaussian)

may mirror the increased complexity of the composition and photophysical processes underway. When a discrete multi-exponential decay model was used to fit the FD data it was found that the majority of lifetimes differed significantly (by at least 0.2 ns) from the values obtained using TCSPC methods. This underlines the need to specify precisely both the data acquisition method and the exact fit model when quoting fluorescence lifetimes of complex fluids such as crude petroleum oils. In practical terms, data collection times for both FD and TCSPC methods are comparable, although the shorter acquisition times for single frequency phase and modulation measurements is a distinct advantage for rapid imaging or sensing applications. Data fitting in this particular case of complex crude oils was on balance, found to be quicker for FD than for TCSPC. It is also concluded, that neither TCSPC nor FD derived fluorescence lifetimes correlate quantitatively with gross chemical compositional parameters as generated by SARA analysis.

Table 5 Correlation coefficients (r^2) associated with best linear fits for the 20 crude oils recorded at 542–582 nm as shown in Fig. 8

Fitting method	Corrected alkane	Polar	Corrected polar	API gravity
Discrete	0.76 (0.77)	0.86 (0.86)	0.85 (0.81)	0.79 (0.7)
Lorentzian	0.76	0.86	0.86	0.83
Gaussian	0.76	0.90	0.90	0.86

Figures in brackets indicate the best reported correlation coefficients from [12]

Acknowledgements This work was funded under a Science Foundation Ireland Research Frontiers Programme, grant (05/RFP/GEO0002) to AGR and an SFI equipment grant (02/IN.1/M231S1). Also many thanks to Dr. D.M. Togashi for his help and advice.

References

1. Fan T, Buckley JS (2002) Rapid and accurate SARA analysis of medium gravity crude oils. Energ Fuel 16(6):1571–1575
2. Barman B, Cebolla VL, Membrado L (2000) Chromatographic techniques for petroleum and related products. Crit Rev Anal Chem 30(2):75–120
3. Ryder AG (2005) Analysis of crude petroleum oils using fluorescence spectroscopy. In: Geddes CD, Lakowicz JR (eds) Annual Reviews in Fluorescence. Springer, London, pp 169–198
4. Aske N, Kallevick H, Sjoblom J (2001) Determination of saturate, aromatic, resin and asphaltenic (SARA) components in crude oils by means of Infrared and Near-Infrared spectroscopy. Energ Fuel 15(5):1304–1312
5. Sastry MIS, Chopra A, Sarpal AS, Jain SK, Srivastava SP, Bhatnagar AK (1998) Determination of physicochemical properties and carbon-type analysis of base oils using mid-IR spectroscopy and partial least-squares regression analysis. Energ Fuel 12 (2):304–311
6. Falla FS, Larini C, Le Roux GAC, Quina FH, Moro LFL, Nascimento CAO (2006) Characterization of crude oil by NIR. J Petrol Sci Eng 51(1–2):127–137
7. Downare TD, Mullins OC (1995) Visible and rear-infrared fluorescence of crude oils. Appl Spectrosc 49(6):754–764
8. Ralston CY, Wu X, Mullins OC (1996) Quantum yields of crude oils. Appl. Spectrosc 50(12):1563–1568
9. Ryder AG (2002) Quantitative analysis of crude oils by fluorescence lifetime and steady state measurements using 380 nm excitation. Appl Spectrosc 56(1):107–116
10. Ryder AG, Glynn TJ, Feely M, Barwise AJG (2002) Characterization of crude oils using fluorescence lifetime data. Spectrochim Acta (A) 58(5):1025–1038
11. Ryder AG, Glynn TJ, Feely M (2003) Influence of chemical composition on the fluorescence lifetimes of crude petroleum oils. Proc SPIE-Int Soc Opt Eng 4876:1188–1195
12. Ryder AG (2004) Time resolved spectroscopic study of crude petroleum oils: influence of chemical composition. Appl Spectrosc 58(5):613–623
13. Ryder AG (2004) Assessing the maturity of crude petroleum oils using total synchronous fluorescence scan spectra. J Fluor 14 (1):99–104
14. Ryder AG, Przyjalgowski MA, Feely M, Szczupak B, Glynn TJ (2004) Time resolved fluorescence microspectroscopy for characterizing crude oils in bulk and hydrocarbon bearing fluid inclusions. Appl Spectrosc 58(9):1106–1115
15. Lakowicz JR, Laczko G, Cherek H, Gratton E, Limkeman M (1984) Analysis of fluorescence decay kinetics from variable-frequency phase shift and modulation data. Biophys J 46(4):463–477
16. Bright FV, Munson CA (2003) Time-resolved fluorescence spectroscopy for illuminating complex systems. Anal Chim Acta 500(1):71–104
17. Lakowicz JR, Gryczynski I (1991) In Lakowicz JR (ed) Topics in Fluorescence Spectroscopy Volume I: Techniques. Plenum Press, New York, pp. 293–331
18. Weber G (1981) Resolution of the fluorescence lifetimes in a heterogeneous system by phase and modulation measurements. J Phys Chem 85(8):949–953
19. Gratton E, Limkeman M, Lakowicz JR, Maliwal BP, Cherek H, Laczko G (1984) Resolution of mixtures of fluorophores using variable frequency phase and modulation data. Biophys J 46 (4):479–486
20. Alcala JR, Gratton E, Prendergast FG (1987) Resolvability of fluorescence lifetime distributions using phase fluorometry. Biophys J 51(4):587–596
21. McGown LB, Hemmingsen SL, Shaver JM, Geng L (1995) Total lifetime distribution analysis for fluorescence fingerprinting and characterization. Appl Spectrosc 49(1):60–66
22. Jones G, Jackson WR, Choi CY (1985) Solvent effects on emission yield and lifetime for Coumarin laser dyes. Requirements for a rotary decay mechanism. J Phys Chem 89:294–300
23. Chaudhury NK, Bhardwaj R, Murari BM (2003) Fluorescence spectroscopic study to characterize and monitor TEOS based sol–gel process for development of optical sensors. Curr Appl Phys 3 (2–3):177–184
24. Mishra PP, Koner AL, Datta A (2004) Interaction of lucifer yellow with cetyl trimethyl ammonium bromide micelles and the constant suppression of its non-radiative process. Chem Phys Lett 400:128–132
25. Ryder AG, Power S, Glynn TJ, Morrison JJ (2001) Time-domain measurement of fluorescence lifetime variation with pH. Proc SPIE-Int Soc Opt Eng 4259:102–109
26. Lakowicz JR (2006) Principles of Fluorescence Spectroscopy 3rd ed. Springer, New York
27. Straume M, Frasier-Cadoret SG, Johnson ML (1991) In Lakowicz JR (ed) Topics in Fluorescence Spectroscopy Volume 2. Plenum, New York, pp. 177–240

Bibliography

[1] J. Lopez-Gejo, P. A. Pantoja, F. Falla, G. A. Soteloa, C. L. Roux, F. H. Quina and C. A. O. d. Nascimento (2008), Electronic and vibrational spectroscopy for remote and on-line analysis and classification of petroleum, in K. L. Montclaire (Editor), Petroleum Science Research Progress Chapter 10, Nova Science Publishers, Inc., 187–233

[2] T. Fan and J. Buckley (2002), Rapid and Accurate SARA analysis of Medium Gravity Crude Oils, *Energy Fuels*, 16(6):1571–1575

[3] A. A. Herod, K. D. Bartle and R. Kandiyoti (2007), Characterization of heavy hydrocarbons by chromatographic and mass spectrometric methods: An overview, *Energy Fuels*, 21(4):2176–2203

[4] S. Betancourt, G. Fujisawa, O. C. Mullins and A. Carnegie (2003), Analysing hydrocarbons in the borehole, *Oilfield Review*, 15(3):54–61

[5] P. Gateau, I. Henaut, L. Barre and J. F. Argillier (2004), Heavy oil dilution, *Oil Gas Sci Technol*, 59(5):503–509

[6] J. G. Speight (1999), The chemistry and technology of petroleum, Marcel Dekker, New York

[7] J. M. Hunt (1979), Petroleum Geochemistry and Geology, W.H Freeman and Company

[8] R. C. Selley (1997), Elements of Petroleum Geochemistry, American Association of Petroleum Geologists, 2nd edition

[9] M. Vandenbroucke and C. Largeau (2007), Kerogen origin, evolution and structure, *Org Geochem*, 38(5):719–833

[10] W. G. Dow (1977), Kerogen Studies and Geological Interpreations, *J Geochem Explor*, 7(2):79–99

[11] M. Vandenbroucke (2003), Les kerogenes : de la notion de types aux modeles de structure chimique, *Rev Inst Fr Pet*, 58(2):243–269

[12] K. E. Peters, C. C. Walters and J. M. Moldowan (2005), Biomarkers and Isotopes in Petroleum Systems and Earth History, volume 2 of *The Biomarker Guide*, Cambridge University Press

[13] K. Stojanovic, B. Jovancicevic, D. Vitorovic, Y. Golovko, G. Pevneva and A. Golovko (2007), Evaluation of saturated and aromatic hydrocarbons oil-oil maturity correlation parameters (SE Pannonian Basin, Serbia), *J Serb Chem Soc*, 72(12):1237–1254

[14] J. G. Speight (2001), Handbook of Petroleum Analysis, Wiley

[15] J. L. Creek (2004), Freedom of action in the state of asphaltenes: Escape from conventional wisdom, *Energy Fuels*, 19(4):1212–1224

[16] E. Lundanes and T. Greibrokk (1994), Separation of fuels, heavy fractions, and crude oils into compound classes - a review, *J High Resolut Chrom*, 17(4):197–202

[17] B. Barman, V. L. Cebolla and L. Membrado (2000), Chromatographic techniques for petroleum and related products, *Crit Rev Anal Chem*, 30(2):75–120

[18] D. Jones and P. P. Pujad (2006), Handbook of Petroleum Processing, Springer, New York

[19] S. L. Sah (2003), Encyclopaedia of Petroleum Science and Engineering, Gyan Publishing House

[20] S. I. Andersen and J. G. Speight (2001), Petroleum resins: Separation, character, and role in petroleum, *Pet Sci Technol*, 19(1-2):1–34

[21] H. Groenzin and O. C. Mullins (1999), Asphaltene Molecular Size and Structure, *J Phys Chem A*, 103(50):11237 – 11245

[22] H. Groenzin and O. C. Mullins (2006), Asphaltene molecular size and weight by time-resolved fluorescence depolarization, in Asphaltenes, Heavy Oils, and Petroleomics, Springer, New York

[23] J. G. Speight (2004), Petroleum asphaltenes - Part 1 - Asphaltenes, resins and the structure of petroleum, *Rev Inst Fr Pet*, 59(5):467–477

[24] S. Badre, C. C. Goncalves, K. Norinaga, G. Gustavson and O. C. Mullins (2006), Molecular size and weight of asphaltene and asphaltene solubility fractions from coals, crude oils and bitumen, *Fuel*, 85(1):1–11

[25] Y. Ruiz-Morales and O. C. Mullins (2007), Polycyclic aromatic hydrocarbons of asphaltenes analyzed by molecular orbital calculations with optical spectroscopy, *Energy Fuels*, 21(1):256–265

[26] A. B. Andrews, R. E. Guerra, O. C. Mullins and P. N. Sen (2006), Diffusivity of asphaltene molecules by fluorescence correlation spectroscopy, *J Phys Chem A*, 110(26):8093–8097

[27] M. H. Schneider, A. B. Andrews, S. Mitra-Kirtley and O. C. Mullins (2007), Asphaltene molecular size by fluorescence correlation Spectroscopy, *Energy Fuels*, 21(5):2875–2882

[28] A. Hammami and J. Ratulowski (2008), Precipitation and deposition of Asphaltenes in production systems: A flow assurance overview., in O. C. Mullins, E. Y. Sheu, A. Hammami and A. G. Marshall (Editors), Asphaltenes, Heavy Oils and Petroleomics, Springer, New York, 617–660

[29] ASTMD2007-93, Standard Test Method for Characteristic Groups in Rubber Extender and Processing Oils and Other Petroleum-Derived Oils by the Clay-Gel Absorption Chromatographic Method, Technical report, American Society for Testing and Materials

[30] ASTMD4124-91, Standard Test Methods for Separation of Asphalt into Four Fractions, Technical report, American Society for Testing and Materials

[31] M. A. Ali and W. A. Nofal (1994), Application of high performance liquid chromatography for hydrocarbon group type analysis of crude oils, *Fuel Sci Tech Int*, 12(1):21–33

[32] S. L. S. Sarowha, B. K. Sharma, C. D. Sharma and S. D. Bhagat (1997), Characterization of petroleum heavy distillates using HPLC and spectroscopic methods, *Energy Fuels*, 11(3):566–569

[33] C. A. Islas-Flores, E. Buenrostro-Gonzalez and C. Lira-Galeana (2005), Comparisons between open column chromatography and HPLC SARA fractionations in petroleum, *Energy Fuels*, 19(5):2080–2088

[34] A. Hannisdal, P. V. Hemmingsen and J. Sjoblom (2005), Group-type analysis of heavy crude oils using vibrational spectroscopy in combination with multivariate analysis, *Ind Eng Chem Res*, 44(5):1349–1357

[35] J. Sjoblom, P. V. Hemmingsen and H. Kallevik (2007), The Role of Asphaltenes in Stabilizing Water-in-Crude Oil Emulsions, in Asphaltenes, Heavy Oils and Petroleomics, Springer, New York, 549–587

[36] J. R. Lakowicz (2006), Principles of Fluorescence Spectroscopy, Springer, New York, 3rd edition

[37] J. W. Lichtman and J. A. Conchello (2005), Fluorescence microscopy, *Nature Methods*, 2(12):910–919

[38] B. Valeur (2002), Molecular Fluorescence, Wiley-VCH, Weinheim

[39] P. W. Atkins and J. D. Paula (2002), Physical Chemistry, Oxford University Press, Oxford, UK, 8th edition

[40] J. N. Miller (2006), Some recent advances in fluorescence spectroscopy, *Anal Lett*, 39(5):851–862

[41] G. Ellingsen and S. Fery-Forgues (1998), Application of fluorescence spectroscopy to the study of petroleum: Challenging complexity, *Rev Inst Fr Pet*, 53(2):201–216

[42] T. Forster (1948), Zwischenmolekulare Energiewanderung und Fluoreszenz, *Ann Phys-Berlin*, 2(1-2):55–75

[43] F. V. Bright and C. A. Munson (2003), Time-resolved fluorescence spectroscopy for illuminating complex systems, *Anal Chim Acta*, 500(1-2):71–104

[44] D. J. S. Birch and R. E. Imhof (1991), Time-domain fluorescence spectroscopy using time-correlated single-photon counting, in Topics in Fluorescence Spectroscopy Volume 1 Techniques, Plenum Press, New York

[45] A. Grinvald and I. Steinber (1974), Analysis of fluorescence decay kinetics by method of least squares, *Anal Biochem*, 59(2):583–598

[46] D. F. Eaton (1990), Recommended methods for fluorescence decay analysis, *Pure Appl Chem*, 62(8):1631–1648

[47] P. R. Bevington and D. K. Robinson (2003), Data reduction and error analysis for the physical sciences, McGraw-Hill, New York

[48] A. G. Ryder, T. J. Glynn, M. Przyjalgowski and B. Szczupak (2002), A compact violet diode laser-based fluorescence lifetime microscope, *J Fluoresc*, 12(2):177–180

[49] N. Chaudhury, R. Bhardwaj and B. Murari (2003), Fluorescence spectroscopic study to characterize and monitor TEOS based sol-gel process for development of optical sensors, *Curr Appl Phys*, 3:177–184

[50] C. Hille, M. Berg, L. Bressel, D. Munzke, P. Primus, H. G. Lohmannsroben and C. Dosche (2008), Time-domain fluorescence lifetime imaging for intracellular pH sensing in living tissues, *Anal Bioanal Chem*, 391(5):1871–1879

[51] E. Gratton, D. M. Jameson and R. Hall (1984), Multifrequency Phase and Modulation Fluorometry, *Ann Rev Biophys Bioeng*, 13:105–124

[52] J. R. Lakowicz, G. Laczko, H. Cherek, E. Gratton and M. Limkeman (1984), Analysis of Fluorescence Decay Kinetics From Variable-Frequency Phase Shift and Modulation Data, *Biophys J*, 46:463–477

[53] R. D. Spencer and G. Weber (1969), Measurements of subnanosecond fluorescence lifetimes with a cross-correlation phase fluorometer, *AnnNY AcadSci*, 158(A1):368–

[54] D. M. Jameson, E. Gratton and R. D. Hall (1984), The measurement and analysis of heterogeneous emissions by multifrequency phase and modulation fluorometry, *Appl Spectrosc Rev*, 20(1):55–106

[55] G. Weber (1981), Resolution of the fluorescence lifetimes in a heterogeneous system by phase and modulation measurements, *J Phys Chem*, 85(8):949–953

[56] E. Gratton, M. Limkeman, J. R. Lakowicz, B. P. Maliwal, H. Cherek and G. Laczko (1984), Resolution of mixtures of fluorophores using variable frequency phase and modulation data, *Biophys J*, 46(4):479–486

[57] A. Sillen and Y. Engelborghs (1998), The Correct Use of Average Fluorescence Parameters, *Photochem Photobiol*, 67(5):475–486

[58] J. R. Alcala, E. Gratton and F. G. Prendergast (1987), Resolvability of fluorescence lifetime distributions using phase fluorometry, *Biophys J*, 51:587–596

[59] J. R. Alcala, E. Gratton and F. J. Prendergast (1987), Interpretation of fluorescence decays in proteins using continuous lifetime distributions, *Biophys J*, 51:925–936

[60] J. R. Alcala, E. R. Gratton and F. G. Prendergast (1987), Fluorescence Lifetime Distributions in Proteins, *Biophys J*, 51:597–604

[61] K. C. B. Lee, J. Siegel, S. E. D. Webb, S. Leveque-Fort, M. J. Cole, R. Jones, K. Dowling, M. J. Lever and P. M. W. French (2001), Application of the stretched exponential function to fluorescence lifetime imaging, *Biophys J*, 81(3):1265–1274

[62] J. Siegel, D. S. Elson, S. E. D. Webb, K. C. B. Lee, A. Vlanclas, G. L. Gambaruto, S. Leveque-Fort, M. J. Lever, P. J. Tadrous, G. W. H. Stamp, A. L. Wallace, A. Sandison, T. F. Watson, F. Alvarez and P. M. W. French (2003), Studying biological tissue with fluorescence lifetime imaging: microscopy, endoscopy, and complex decay profiles, *Appl Optics*, 42(16):2995–3004

[63] D. V. O'Connor and D. Phillips (1984), Time Correlated Single-Photon Counting, Academic Press, London

[64] W. Becker (2005), Advanced Time-Correlated Single-Photon Counting Techniques, Springer-Verlag, Hiedelberg

[65] M. Wahl (2000), Time-Correlated Photon Counting Tech Note TCSPC 1.2, *Picoquant web site wwwpicoquantcom*

[66] J. R. Lakowicz and I. Gryczynski (1991), Frequency Domain Fluorescence Spectroscopy, Topics in fluorescence spectroscopy Volume I: Techniques, Plenum Press, New York

[67] F. S. Wouters (2006), The physics and biology of fluorescence microscopy in the life sciences, *Contemp Phys*, 47(5):239–255

[68] S. C. George, T. E. Ruble, A. Dutkiewicz and P. J. Eadington (2001), Assessing the maturity of oil trapped in fluid inclusions using molecular geochemistry data and visually-determined fluorescence colours, *Appl Geochem*, 16(4):451–473

[69] R. S. Davidson (1996), Application of fluorescence microscopy to a study of chemical problems, *Chem Soc Rev*, 25(4):241–253

[70] R. H. Webb (1996), Confocal optical microscopy, *Rep Prog Phys*, 59(3):427–471

[71] Z. Földes-Papp, U. Demel and G. P. Tilz (2003), Laser scanning confocal fluorescence microscopy: an overview, *Int Immunopharmacol*, 3(13-14):1715–1729

[72] N. Claxton, T. Fellers and M. Davidson (2009), http://www.olympusfluoview.com/theory/LSCMIntro.pdf

[73] B. Menendez, C. David and A. M. Nistal (2001), Confocal scanning laser microscopy applied to the study of pore and crack networks in rocks, *Comput Geosci*, 27(9):1101–1109

[74] R. Yuste (2005), Fluorescence microscopy today, *Nat Methods*, 2(12):902–904

[75] K. Konig (2000), Multiphoton microscopy in life sciences, *J Microsc-Oxf*, 200:83–104

[76] R. M. Clegg, O. Holub and C. Gohlke (2003), Fluorescence lifetime-resolved imaging: Measuring lifetimes in an image, in Biophotonics, Pt A, volume 360 of *Methods in Enzymology*, Academic Press Inc, San Diego, 509–542

[77] K. Suhling, P. M. W. French and D. Phillips (2005), Time-resolved fluorescence microscopy, *Photochem Photobiol Sci*, 4(1):13–22

[78] P. C. Schneider and R. M. Clegg (1997), Rapid acquisition, analysis, and display of fluorescence lifetime-resolved images for real-time applications, *Rev Sci Instrum*, 68(11):4107–4119

[79] R. Cubeddu, D. Comelli, C. D'Andrea, P. Taroni and G. Valentini (2002), Time-resolved fluorescence imaging in biology and medicine, *J Phys D-Appl Phys*, 35(9):R61–R76

[80] P. J. Verveer, A. Squire and P. Bastiaens (2000), Global analysis of fluorescence lifetime imaging microscopy data, *Biophys J*, 78(4):2127–2137

[81] S. E. D. Webb, Y. Gu, S. Leveque-Fort, J. Siegel, M. J. Cole, K. Dowling, R. Jones, P. M. W. French, M. A. A. Neil, R. Juskaitis, L. O. D. Sucharov, T. Wilson and M. J. Lever (2002), A wide-field time-domain fluorescence lifetime imaging microscope with optical sectioning, *Rev Sci Instrum*, 73(4):1898–1907

[82] D. Elson, J. Requejo-Isidro, I. Munro, F. Reavell, J. Siegel, K. Suhling, P. Tadrous, R. Benninger, P. Lanigan, J. McGinty, C. Talbot, B. Treanor, S. Webb, A. Sandison, A. Wallace, D. Davis, J. Lever, M. Neil, D. Phillips, G. Stamp and P. French (2003), Time-domain fluorescence lifetime imaging applied to biological tissue, in 10th Congress of the European-Society-for-Photobiology, Royal Soc Chemistry, Vienna, Austria, 795–801

[83] A. Squire, P. J. Verveer and P. I. H. Bastiaens (2000), Multiple frequency fluorescence lifetime imaging microscopy, *J Microsc-Oxf*, 197:136–149

[84] S. Pelet, M. J. R. Previte, D. Kim, K. H. Kim, T. T. J. Su and P. T. C. So (2006), Frequency domain lifetime and spectral imaging microscopy, *Microsc Res Tech*, 69(11):861–874

[85] M. J. Booth and T. Wilson (2004), Low-cost, frequency-domain, fluorescence lifetime confocal microscopy, *J Microsc-Oxf*, 214:36–42

[86] J. J. Kelly and J. B. Callis (1990), Nondestructive analytical procedure for simultaneous estimation of the major classes of hydrocarbon constituents of finished gasolines, *Anal Chem*, 62(14):1444–1451

[87] M. Sasry, A. Chopra, A. Sarpal, S. Jain, S. Srivastava and A. Bhatnagar (1998), Determination of Physicochemical Properties and Carbon-Type Analysis of Base Oils Using Mid-IR Spectroscopy and Partial Least-Squares Regression Analysis, *Energy Fuels*, 12:304–311

[88] O. C. Mullins, T. Daigle, C. Crowell, H. Groenzin and N. B. Joshi (2001), Gas-oil ratio of live crude oils determined by near-infrared spectroscopy, *Appl Spectrosc*, 55(2):197–201

[89] N. Aske, H. Kallevick and J. Sjoblom (2001), Determination of Saturate, Aromatic, Resin and Asphaltenic (SARA) Components in Crude Oils by means of Infrared and Near-Infrared Spectroscopy, *Energy Fuels*, 15(5):1304–1312

[90] N. Batina, A. Reyna-Cordova, Y. Trinidad-Reyes, M. Quintana-Garcia, E. Buenrostro-Gonzalez, C. Lira-Galeana and S. I. Andersen (2005), Qualitative analysis of thin films of crude oil deposits on the metallic substrate by Fourier transform infrared (FTIR) microscopy, *Energy Fuels*, 19(5):2001–2005

[91] O. Abbas, N. Dupuy, C. Rebufa, L. Vrielynck, J. Kister and A. Permanyer (2006), Prediction of Source Rock Origin by Chemometric Analysis of Fourier Transform InfraredAttenuated Total Reflectance Spectra of Oil Petroleum: Evaluation of Aliphatic and Aromatic Fractions by Self-Modeling Mixture Analysis, *Appl Spectrosc*, 60(3):304–314

[92] F. Falla, C. Larini, G. LeRoux, F. Quina, L. Moro and C. Nascimento (2006), Characterization of crude oil by NIR, *J Petrol Sci Eng*, 51(1-2):127–137

[93] C. Pasquini and A. F. Bueno (2007), Characterization of petroleum using near-infrared spectroscopy: Quantitative modeling for the true boiling point curve and specific gravity, *Fuel*, 86(12-13):1927–1934

[94] S. A. Asher and C. R. Johnson (1984), Raman spectroscopy of a coal liquid shows that fluorescence interference is minimized with ultraviolet excitation, *Science*, 225(4659):311–313

[95] G. R. Loppnow, L. Shoute, K. J. Schmidt, A. Savage, R. H. Hall and J. T. Bulmer (2004), UV Raman spectroscopy of hydrocarbons, *Phil Trans R Soc A*, 362(1824):2461–2476

[96] G. Fujisawa and O. C. Mullins (2008), Live Oil Sample Acquisition and Downhole fluid Analysis, in Asphaltenes, heavy oils and petroleomics, Chapter 22, Springer, New York

[97] M. Blanco, S. Maspoch, I. Villarroya, X. Peralta, J. M. Gonzalez and J. Torres (2001), Determination of physical properties of bitumens by use of near-infrared spectroscopy with neural networks. Joint modelling of linear and non-linear parameters, *Analyst*, 126(3):378–382

[98] O. C. Mullins, S. Mitra-Kirtley and Y. Zhu (1992), The electronic absorption-edge of petroleum, *Appl Spectrosc*, 46(9):1405–1411

[99] A. Barbaro, G. Cecchi and P. Mazzinghi (1991), Oil UV extinction coefficient measurement using a standard spectrophotometer, *Appl Optics*, 30(7):852–857

[100] I. N. Evdokimov and A. P. Losev (2007), Potential of UV-Visible Absorption Spectroscopy for characterizing crude petroleum oils, *Oil and Gas Business (online journal)*, http://www.ogbus.ru/eng/

[101] I. N. Evdokimov and A. P. Losev (2007), On the nature of UV/VIS absorption spectra of asphaltenes, *Pet Sci Technol*, 25(1-2):55–66

[102] K. Gautam, X. H. Jin and M. Hansen (1998), Review of spectrometric techniques for the characterization of crude oil and petroleum products, *Appl Spectrosc Rev*, 33(4):427–443

[103] A. G. Ryder (2005), Analysis of Crude Petroleum Oils Using Fluorescence Spectroscopy, in Reviews in Fluorescence 2005, 169–198

[104] F. L. Staplin (1969), Sedimentary organic matter, organic metamorphism, and oil and gas occurence, *Canadian Petrol Geol Bull*, 17(1):47–66

[105] R. C. Buruss (1981), Hydrocarbon fluid inclusions in studies of sedimentary diagenesis, in L. S. Hollister and M. L. Crawford (Editors), Short Course in Fluid Inclusions: Applications to Petrology, volume 6, Mineralogical Association of Canada, 138–156

[106] P. Bertrand, J. L. Pittion and C. Bernaud (1986), Fluorescence of sedimentary organic matter in relation to its chemical composition, *Org Geochem*, 10(1-3):641–647

[107] H. W. Hagemann and A. Hollerbach (1986), The fluorescence behaviour of crude oils with respect to their thermal maturation and degradation, *Org Geochem*, 10(1-3):473–480

[108] T. Downare and O. Mullins (1995), Visible and near-infrared fluoresecence of crude oils, *Appl Spectrosc*, 49(6):754–764

[109] L. D. Stasiuk and L. R. Snowdon (1997), Fluorescence micro-spectrometry of synthetic and natural hydrocarbon fluid inclusions: crude oil chemistry, density and application to petroleum migration, *Appl Geochem*, 12(3):229–233

[110] W. Schade and J. Bublitz (1996), On-site laser probe for the detection of petroleum products in water and soil, *Environ Sci Technol*, 30(5):1451–1458

[111] D. E. Nicodem, M. C. Z. Fernandes, C. L. B. Guedes and R. J. Correa (1997), Photochemical processes and the environmental impact of petroleum spills, *Biogeochemistry*, 39(2):121–138

[112] P. Owens, A. Ryder and N. Blamey (2008), Frequency Domain Fluorescence Lifetime Study of Crude Petroleum Oils, *J Fluoresc*, 18(5):997–1006

[113] C. Ralston, X. Wu and O. Mullins (1995), Quantum yields of crude oils, *Appl Spectrosc*, 50(12):1563–1568

[114] D. A. Nicodem, M. F. V. D. Cuhna and C. L. B. Guedes (2000), Time-Resolved Single Photon Counting Study of the Quenching of Fluorescent Probes by Petroleum: Probing the Energy Distribution of the Nonaliphatic Components, *Appl Spectrosc*, 54(9):1409–1411

[115] H. Groenzin, O. C. Mullins and W. W. Mullins (1999), Resonant fluorescence quenching of aromatic hydrocarbons by carbon disulfide, *J Phys Chem A*, 103(11):1504–1508

[116] A. Ryder (2004), Assessing the maturity of crude petroleum oils using total synchronous fluorescence scan spectra, *J Fluoresc*, 14(1):99–104

[117] D. Patra and A. K. Mishra (2002), Study of diesel fuel contamination by excitation emission matrix spectral subtraction fluorescence, *Anal Chim Acta*, 454(2):209–215

[118] T. A. Taylor and H. H. Patterson (1987), Excitation resolved synchronous fluorescence analysis of aromatic compounds and fuel oil, *Anal Chem*, 59(17):2180–2187

[119] D. Patra and A. K. Mishra (2001), Concentration dependent red shift: qualitative and quantitative investigation of motor oils by synchronous fluorescence scan, *Talanta*, 53(4):783–790

[120] D. Patra and A. K. Mishra (2002), Total synchronous fluorescence scan spectra of petroleum products, *Anal Bioanal Chem*, 373(4-5):304–309

[121] V. G. van Mispelaar, A. K. Smilde, O. E. de Noord, J. Blomberg and P. J. Schoenmakers (2005), Classification of highly similar crude oils using data sets from comprehensive two-dimensional gas chromatography and multivariate techniques, *J Chromatogr A*, 1096(1-2):156–164

[122] O. Abbas, C. Rebufa, N. Dupuy, A. Permanyer, J. Kister and D. A. Azevedo (2006), Application of chemometric methods to synchronous UV fluorescence spectra of petroleum oils, *Fuel*, 85(17-18):2653–2661

[123] P. V. Hemmingsen, A. Silset, A. Hannisdal and J. Sjoblom (2005), Emulsions of heavy crude oils. I: Influence of viscosity, temperature, and dilution, *J Dispersion Sci Technol*, 26(5):615–627

[124] X. Wang and O. C. Mullins (1994), Fluorescence Lifetime Studies of Crude Oils, *Appl Spectrosc*, 48(8):977–984

[125] G. C. Smith and J. F. Sinski (1999), The red-shift cascade: Investigations into the concentration-dependent wavelength shifts in three-dimensional fluorescence spectra of petroleum samples, *Appl Spectrosc*, 53(11):1459–1469

[126] A. Ryder (2002), Quantitative analysis of crude oils by fluorescence lifetime and steady state measurements using 380 nm excitation, *Appl Spectrosc*, 1(56):107–116

[127] M. F. Quinn, S. Joubian, F. Albahrani, S. Alaruri and O. Alameddine (1988), A deconvolution technique for determining the intrinsic fluorescence decay lifetimes of crude oils, *Appl Spectrosc*, 42(3):406–410

[128] M. F. Quinn, A. S. Al-Otaibi, A. Abdullah, P. S. Sethi, F. Al-Bahrani and O. Alameddine (1995), Determination of Intrinsic Fluorescence Lifetime Parameters of Crude Oils Using a Laser Fluorosensor with a Streak Camera Detection System, *Instrum Sci Technol*, 23(3):201 – 215

[129] A. Ryder, T. Glynn, M. Feely and A. Barwise (2002), Characterization of crude oils using fluorescence lifetime data, *Spectroc Acta Pt A-Molec Biomolec Spectr*, 58(5):1025–1038

[130] A. Ryder, T. Glynn and M. Feely (2003), Influence of chemical composition on the fluorescence lifetimes of crude petroleum oils, *Proc SPIE Int Soc Opt Eng*, 4876:1188–1195

[131] A. G. Ryder, M. A. Przyjalgowski, M. Feely, B. Szuczpak and T. Glynn (2004), Time Resolved Fluorescence Microspectroscopy for Characterizing Crude Oils in Bulk and Hydrocarbon Bearing Fluid Inclusions, *Appl Spectrosc*, 58(9):1106–1115

[132] A. Ryder (2004), Time Resolved Spectroscopic Study of Crude petroleum Oils: Influence of Chemical Composition, *Appl Spectrosc*, 58(5):613–623

[133] L. B. McGown and D. W. Millican (1988), Fluorescence lifetime selectivity in multifrequency phase-resolved fluorescence spectroscopy, *Appl Spectrosc*, 42(6):1084–1089

[134] P. M. R. Hertz and L. B. McGown (1991), Phase-resolved fluorescence spectral fingerprinting of petrolatums, *Appl Spectrosc*, 45(1):73–79

[135] J. M. Shaver and L. B. McGown (1994), Generation of a new spectral format, the lifetime synchronous spectrum (LiSS), using phase-resolved fluorescence spectroscopy., *Appl Spectrosc*, 48(6):755–760

[136] E. Gratton and D. M. Jameson (1985), New approach to phase and modulation resolved spectra, *Anal Chem*, 57(8):1694–1697

[137] L. B. McGown, S. L. Hemmingsen, J. M. Shaver and L. Geng (1995), Total lifetime distribution analysis for fluorescence fingerprinting and characterization, *Appl Spectrosc*, 49(1):60–66

[138] A. Livesey and J. Brochon (1987), Analyzing the Distribution of Decay Constants in Pulse Fluorimetry Using the Maximum Entropy Method, *Biophys J*, 52(5):693–706

[139] H. M. Marwani, M. Lowry, P. Keating, I. M. Warner and R. L. Cook (2007), Segmented frequency-domain fluorescence lifetime measurements: Minimizing the effects of photobleaching within a multi-component system, *J Fluoresc*, 17(6):687–699

[140] H. Marwani, M. Lowry, B. Xing, I. Warner and R. Cook (2009), Frequency-Domain Fluorescence Lifetime Measurements via Frequency Segmentation and Recombination as Applied to Pyrene with Dissolved Humic Materials, *J Fluoresc*, 19(1):41–51

[141] M. Arlk, N. Celebi and Y. Onganer (2005), Fluorescence quenching of fluorescein with molecular oxygen in solution, *Photochem Photobiol*, 170(2):105–111

[142] C. Canuel, S. Badre, H. Groenzin, M. Berheide and O. C. Mullins (2003), Diffusional fluorescence quenching of aromatic hydrocarbons, *Appl Spectrosc*, 57(5):538–544

[143] X. P. Li and V. L. McGuffin (2004), Selective fluorescence quenching of nitrogen-containing polycyclic aromatic hydrocarbons by aliphatic amines, *Anal Chim Acta*, 526(2):155–162

[144] D. Patra and A. K. Mishra (2001), Excitation dependent fluorescence quantum yield in hydrocarbon fuels containing polycyclic aromatic compounds, *Polycycl Aromat Compd*, 18(4):381–396

[145] Z. Wasylewski, P. Kaszycki, A. Guz and W. Stryjewski (1988), Fluorescence Quenching resolved spectra of fluorophores in mixtures and micellar solutions, *Eur J Biochem*, 178(2):471–476

[146] E. Bowen (1959), Viscosity and temperature effects in fluorescence, *Faraday Discuss*, 27:40–42

[147] D. F. Futoma, S. R. Smith and J. Tanaka (1982), Spectroscopic methods of analysis for polycycycli aromatic hydrocarbons in the aqeuous environment, *Crit Rev Anal Chem*, 13(2):117 – 154

[148] C. Gooijer, I. Kozin and N. Velthorst (1997), Shpol'skii Spectrometry, a Distinct Method in Environmental Analysis, *Mikrochim Acta*, 127:149–182

[149] P. Garrigues and M. Ewald (1985), Application of High Resolution Shpol'skii Luminescence Spectroscopy to the Analysis of Polycyclic Aromatic Hydrocarbons (PAH) in the Environmental Samples, *Int J Environ Anal Chem*, 21(3):185 – 197

[150] P. Garrigues, J. Bellocq and S. A. Wise (1990), Determination of methylbenzo[a]pyrene isomers in a coal tar standard reference material using liquid chromatography and Shpol'skii spectrometry, *Fresenius' Journal of Analytical Chemistry (now titled Anal Bioanal Chem)*, 336(2):106–110

[151] W. Zhang, D. Lin, Z. Zou and Y. Li (2008), A novel approach for simultaneous determination of polycyclic aromatic hydrocarbons by Shpol'skii non-linear

variable-angle synchronous fluorescence spectrometry, *Talanta*, 71(4):1481–1488

[152] R. B. Dickinson and E. L. Wehry (1979), Time-resolved matrix isolation fluorescence spectrometry of mixtures of polycyclic aromatic hydrocarbons, *Anal Chem*, 51(6):778–780

[153] K. M. Bark and R. K. Force (1990), Analysis of Polynuclear Aromatic Hydrocarbon Mixtures Desorbed from Particulate Matter in a Low-Temperature Matrix by Shpol'skii Time-Resolved Fluorescence Spectroscopy, *Appl Spectrosc*, 44(8):1373–1376

[154] A. J. Bystol, S. Yu and A. D. Campiglia (2003), Analysis of polycyclic aromatic hydrocarbons in HPLC fractions by laser-excited time-resolved Shpolskii spectrometry with cryogenic fiber-optic probes, *Talanta*, 60:449–458

[155] S. H. Fortier and D. Eastwood (1978), Identification of fuel oils by low temperature luminescence spectrometry, *Anal Chem*, 50(2):334–338

[156] J. B. F. Lloyd (1980), Examination of petroleum-products of high relative molecular mass for forensic purposes by synchronous fluorescence spectroscopy. 1. Appraisal of experimental factors, *Analyst*, 105(1247):97–109

[157] M. M. Corfield, H. L. Hawkins, P. John and I. Soutar (1981), Assessment of phosphorescence spectroscopy for crude oil identification, *Analyst*, 106(1259):188–197

[158] O. Chukova, O. Krut, S. Nedilko, V. Sakun and V. Scherbatskyi (2005), Luminescent determination of automobile petrol in hexane solutions, *Ann Chim-Rome*, 95(11-12):885–895

[159] S. A. Stout and R. Lin (1990), Lasers in organic petrology and organic geochemistry. 1. Laser-Induced fluorescence, thermal extraction and pyrolysis, in 7th Annual Meeting of the Soc for Organic Petrology, Pergamon-Elsevier Science Ltd, Calgary, Canada, 229–239

[160] Y. Zhu and O. C. Mullins (1992), Temperature Dependence of Fluorescence of Crude Oils and Related Compounds, *Energy Fuels*, 6(12):545–552

[161] R. Michels, E. Langlois, O. Ruau, L. Mansuy, M. Elie and P. Landais (1996), Evolution of asphaltenes during artificial maturation: A record of the chemical processes, *Energy Fuels*, 10(1):39–48

[162] W. L. Huang and G. A. Otten (1997), Oil generation kinetics determined by DAC-FS/IR pyrolysis: technique development and preliminary results, *18th International Meeting on Organic Geochemistry*:1119–1137

[163] W. L. Huang and G. A. Otten (2001), Cracking kinetics of crude oil and alkanes determined by diamond anvil cell-fluorescence spectroscopy pyrolysis: technique development and preliminary results, *Org Geochem*, 32(6):817–830

[164] Y. J. Chang, W. L. Huang, A. Hsu and S. Y. L. Huang (2008), Characterization of kerogens and coals using fluorescence measured in situ at elevated temperatures, *Int J Coal Geol*, 75(2):63–75

[165] Y. J. Chang and W. L. Huang (2008), Simulation of the fluorescence evolution of live oils from kerogens in a diamond anvil cell: Application to inclusion oils in terms of maturity and source, *Geochim Cosmochim Acta*, 72(15):3771–3787

[166] I. A. Munz (2001), Petroleum inclusions in sedimentary basins: systematics, analytical methods and applications, *Lithos*, 55:195–212

[167] D. Hall (2008), Fluid inclusion images from http://www.fittulsa.com/

[168] H. Volk, S. C. George, H. Middleton and S. Schofield (2005), Geochemical comparison of fluid inclusion and present-day oil accumulations in the Papuan Foreland - evidence for previously unrecognised petroleum source rocks, *Org Geochem*, 36(1):29–51

[169] J. Kihle (1995), Adaptation of fluorescence excitation-emission microspectroscopy for characterization of single hydrocarbon fluid inclusions, *Org Geochem*, 23(11-12):1029–1042

[170] P. F. Greenwood, S. C. George, M. A. Wilson and K. J. Hall (1996), A new apparatus for laser micropyrolysis gas chromatography mass spectrometry, *J Anal Appl Pyrolysis*, 38:101–118

[171] R. K. McLimans (1987), The application of fluid inclusions to migration of oil and diagenesis of petroleum reservoirs, *Appl Geochem*, 2:585–603

[172] J. Pironon, R. Thiery, M. A. Ougougal, S. Teinturier, G. Beaudoin and F. Walgenwitz (2001), FT-IR measurements of petroleum fluid inclusions: methane, n-alkanes and carbon dioxide quantitative analysis, *Geofluids*, 1:2–10

[173] E. A. J. Burke (2001), Raman microspectrometry of fluid inclusions, *Lithos*, 55(1-4):139–158

[174] N. J. F. Blamey and A. G. Ryder (2009), Hydrocarbon Fluid Inclusion Fluorescence: A review, in Reviews in Fluorescence 2007, 299–334

[175] R. Thiery, J. Pironon, F. Walgenwitz and F. Montel (2002), Individual characterization of petroleum fluid inclusions (composition and P-T trapping conditions) by microthermometry and confocal laser scanning microscopy: inferences from applied thermodynamics of oils, *Mar Pet Geol*, 19(7):847–859

[176] R. J. Bodnar (1990), Petroleum migration in the miocene-monterey-formation, California, USA - Constraints from fluid inclusion studies, *Mineral Mag*, 54(375)

[177] M. A. Przyjalgowski, A. G. Ryder, M. Feely and T. J. Glynn (2005), Analysis of hydrocarbon-bearing fluid inclusions (HCFI) using time-resolved fluorescence spectroscopy, *Proc SPIE Int Soc Opt Eng*, 5826:173–184

[178] N. J. F. Blamey, J. Conliffe, J. Parnell, A. G. Ryder and M. Feely (2009), Application of fluorescence lifetime measurements on single petroleum-bearing fluid inclusions to demonstrate multicharge history in petroleum reservoirs, *Geofluids*, 9(4):330–337

[179] Hamamatsu R928 specification sheet http://sales.hamamatsu.com

[180] AHF analysentechnik AG www.ahf.de

[181] (2009), http://www.oceanoptics.com/technical/detectorsonyILX511.pdf, Sony CCD specification sheet

[182] D. Marquardt (1963), An algorithm for least-squares estimation of nonlinear parameters, *SIAM J Appl Math*, 11:431–441

[183] C. Gonzalez-Blanco, M. Velazquez, S. M. Costa and P. Barreleiro (1997), Fluorescence Study of Acridone in W/O Microemulsions Perturbed by the Addition of Water-Soluble Polymers, *J Colloid Interface Sci*, (189):43–50

[184] M. Straume, F. G. Frasier-Cadoret and M. L. Johnson (1991), Least Squares Analysis of Fluorescence Data, volume 2 of *Topics in Fluorescence Spectroscopy*, Plenum Press, New York

[185] A. J. Macdonald and E. T. C. Spooner (1981), Calibration of a Linkam TH 600 programmable heating-cooling stage for microthermometric examination of fluid inclusions, *Econ Geol*, 76(5):1248–1258

[186] M. Montalti (2006), Handbook of Photochemistry, CRC Press LLC, Boca Raton, USA

[187] C. M. McGraw, G. Khalil and J. B. Callis (2008), Comparison of time and frequency domain methods for luminescence lifetime measurement, *J Phys Chem C*, 112(21):8079–8084

[188] A. T. N. Kumar, S. B. Raymond, B. J. Bacskai and D. A. Boas (2008), Comparison of frequency-domain and time-domain fluorescence lifetime tomography, *Opt Lett*, 33(5):470–472

[189] M. K. Helms, C. E. Petersen, N. V. Bhagavan and D. M. Jameson (1997), Time-resolved fluorescence studies on site-directed mutants of human serum albumin, *FEBS Lett*, 408(1):67–70

[190] E. Terpetschnig and D. Jameson (2009), Fluorescence Lifetime http://www.iss.com/resources/tech1/index.html

[191] S. Asomaning (2003), Test methods for determining asphaltene stability in crude oils, *Pet Sci Technol*, 21(3-4):581–590

[192] L. Riveros, B. Jaimes, M. A. Ranaudo, J. Castillo and J. Chirinos (2006), Determination of asphaltene and resin content in Venezuelan crude oils by

using fluorescence spectroscopy and partial least squares regression, *Energy Fuels*, 20(1):227–230

[193] O. C. Mullins (1998), Optical interrogation of aromatic moieties in crude oils and asphaltenes, in O. C. Mullins and E. Y. Sheu (Editors), Symposium on Asphaltene and Resin Characterization, Plenum Press Div Plenum Publishing Corp, San Francisco, USA, 21–77

[194] F. J. V. Santos, C. A. N. de Castro, J. H. Dymond, N. K. Dalaouti, M. J. Assael and A. Nagashima (2006), Standard reference data for the viscosity of toluene, *J Phys Chem Ref Data*, 35(1):1–8

[195] M. Dominguez-Perez, C. Franjo, J. Pico, L. Segade, O. Cabeza and E. Jimnez (2009), Experimental Study of the Dynamic Viscosity Deviations in the Binary Systems: Hexane + Ethylbenzene, + o-Xylene, + m-Xylene, + p-Xylene at 298.15 K, *Int J Thermophys*, 30(4):1197–1201

[196] A. M. A. Dias, R. P. Bonifacio, I. M. Marrucho, A. A. H. Padua and M. F. C. Gomes (2003), Solubility of oxygen in n-hexane and in n-perfluorohexane. Experimental determination and prediction by molecular simulation, *Phys Chem Chem Phys*, 5(3):543–549

[197] A. R. Li, S. W. Tang, P. H. Tan, C. J. Liu and B. Liang (2007), Measurement and prediction of oxygen solubility in toluene at temperatures from 298.45 K to 393.15 K and pressures up to 1.0 MPa, *J Chem Eng Data*, 52(6):2339–2344

[198] T. Moriya (1984), Excited-state reactions of Coumarins in Aqueous Solutions. II. The Fluorescence Quenching of 7-Ethoxycoumarins by Halide ions., *Bull Chem Soc Jpn*, 57(7):1723–1730

[199] T. L. Nemzek and W. R. Ware (1975), Kinetics of diffusion-controlled reactions - transient effects in fluorescence quenching, *J Chem Phys*, 62(2):477–489

[200] J. Keizer (1983), Nonlinear fluorescence quenching and the origin of positive curvature in Stern-Volmer plots, *J Am Chem Soc*, 105(6):1494–1498

[201] K. Mauring, J. Deich, F. I. Rosell, T. B. McAnaney, W. E. Moerner and S. G. Boxer (2005), Enhancement of blue fluorescence of blue fluorescent proteins by high pressure or low temperature, *J Phys Chem*, 109:12976–12981

[202] B. Zelent, T. Troxler and J. Vanderkooi (2007), Temperature Dependence for Fluorescence of β-NADH in Glycerol/Water Solution and in Trehalose/Sucrose Glass, *J Fluoresc*, 17(1):37–42

[203] N. Mataga, Y. Kaifu and M. Koizumi (1956), Solvent effects upon fluorescence spectra and the diploe moments of excited molecules, *Bull Chem Soc Jpn*, 29(4):465–470

[204] N. J. Turro, V. Ramamurthy and J. C. Scaiano (2009), Principles of molecular photochemistry: an introduction, University Science Books

[205] F. Barrigelletti, S. Dellonte and G. Orlandi (1984), Effect of temperature on the photophysical properties of styrylpyridines, *J Chem Soc Faraday Trans*, 1(80):1123–1129

[206] N. L. Boens, L. D. Janssens, L. V. Dommelen, F. C. D. Schryver and J. Gallay (1992), Photophysics of tryptophan : global analysis of the fluorescence decay surface as a function of pH, temperature, quencher concentration, excitation and emission wavelengths, timing calibration and deuterium isotope effect, *SPIE*, 1640:58–69

[207] K. Sahu, S. K. Mondal, S. Ghosh, D. Roy and K. Bhattacharyya (2006), Temperature dependence of solvation dynamics and anisotropy decay in a protein: ANS in bovine serum albumin, *Chem Phys*, 124(12):7

[208] S. L. C. Moors, M. Hellings, M. D. Maeyer, Y. Engelborghs and A. Ceulemans (2006), Tryptophan Rotamers as Evidenced by X-Ray, Fluorescence Lifetimes, and Molecular Dynamics Modeling, *Biophys J*, 91(3):816–823

[209] C. Gonzalez and J. Pincock (2006), Temperature effects, arrhenius activation parameters and rate constants for the photochemical reactivity of cyano, boronato, trifluoromethyl and methoxy substituted toluenes in the excited singlet state, *Photochem Photobiol*, 82(1):301–309

[210] H. Mishra, S. Pant and H. B. Tripathi (2008), Temperature-dependent time-resolved fluorescence study of cinchonine alkaloid dication, *J Fluoresc*, 18(1):17–27

[211] L. Grunberg and A. H. Nissan (1949), Mixture law for viscosity, *Nature*, 164(4175):799–800

[212] A. Jouyban, M. Khoubnasabjafari, Z. Vaez-Gharamaleki, Z. Fekari and W. E. Acree (2005), Calculation of the viscosity of binary liquids at various temperatures using Jouyban-Acree model, *Chemical and Pharmaceutical Bulletin*, 53(5):519–523

[213] D. E. Freed, N. V. Lisitza, P. N. Sen and Y.-Q. Song (2007), Molecular Composition and Dynamics of Oils from Diffusion Measurements, in O. C. Mullins, E. Y. Sheu, A. Hammami and A. G. Marshall (Editors), Asphaltenes, Heavy Oils, and Petroleomics, Springer, New York , USA, 279–299

[214] M. Oliveberg, Y. J. Tan and A. R. Fersht (1995), Negative Activation Enthalpies in the kinetics of Protein-Folding, *Proc Natl Acad Sci U S A*, 92(19):8926–8929

[215] J. H. Christensen, A. B. Hansen, J. Mortensen and O. Andersen (2005), Characterization and Matching of Oil Samples Using Fluorescence Spectroscopy and Parallel Factor Analysis, *Anal Chem*, 77(7):2210–2217

[216] Y. Liu, J. He, C. W. Song, Y. Li, S. Wang, Y. L. Han and H. X. Wang (2009), Oil Fingerprinting by Three-Dimensional (3D) Fluorescence Spectroscopy and Gas Chromatography-Mass Spectrometry (GC-MS), *Environ Forensics*, 10(4):324–330

[217] E. Hegazi, A. Hamdan and J. Mastromarino (2005), Remote fingerprinting of crude oil using time-resolved fluorescence spectra, *Arab J Sci Eng*, 30(1B):3–12

[218] N. J. F. Blamey and A. G. Ryder (2009), Hydrocarbon Fluid Inclusion Fluorescence: A Review, in Reviews in Fluorescence 2007, 299–334

[219] O. C. Mullins (2007), Petroleomics and Structure Function Relations of Crude Oils and Asphaltenes, in Asphaltenes, Heavy Oils, and Petroleomics, Springer, pages 1–16

[220] T. Forster (1950), Die pH-Abhangigkeit der fluoreszenz von naphthalinderivaten, *Zeitschrift Fur Elektrochemie*, 54(7):531–535

[221] A. Weller (1958), Protolytic reactions of excited hydroxy compounds, *Z Phys Chem*, (17):224–

[222] O. S. Wolfbeis, E. Furlinger, H. Kroneis and H. Marsoner (1983), Fluorimetric Analysis 1. A study on fluorescent indicators for measuring near neutral (physiological) pH-values, *Fresen Z Anal Chem*, (314):119–124

[223] T. H. Tran-Thi, T. Gustavsson, C. Prayer, S. Pommeret and J. T. Hynes (2000), Primary ultrafast events preceding the photoinduced proton transfer from pyranine to water, *Chem Phys Lett*, 329(5-6):421–430

[224] A. Suwaiyan, F. Al-Adel, A. Hamdan, A. Klein and K. A. Uwe (1990), Dynamics of Proton Transfer from Photon-Initiated Acids in Alcohol/Water Mixtures, *J Phys Chem*, (94):7423–7429

[225] V. Orlien, A. K. Happe, H. Stapelfeldt and L. H. Skibsted (2008), In situ pH measurement in partly frozen aqueous solution using the fluorescent probe 8-hydroxypyrene-1,3,6-trisulfonic acid, *Food Biophys*, 3(1):94–99

[226] A. G. Ryder, S. Power, T. J. Glynn and J. J. Morrison (2001), Time-domain measurement of fluorescence lifetime variation with pH, in G. H. Bearman, D. J. Bornhop and R. M. Levenson (Editors), Proceedings of SPIE - Biomarkers and Biological Spectral Imaging, volume 2, 102–109

[227] R. B. Thompson and E. Gratton (1988), Phase Fluorometric Method for determination of Standard Lifetimes, *Anal Chem*, (60):670–674

[228] J. Ghasemi, A. Niazi and M. Kubista (2005), Thermodynamics study of the dimerization equilibria of rhodamine B and 6G in different ionic strengths by photometric titration and chemometrics method, *Spectroc Acta Pt A-Molec Biomolec Spectr*, 62(1-3):649–656

[229] N. Boens, W. W. Qin, N. Basaric, J. Hofkens, M. Ameloot, J. Pouget, J. P. Lefevre, B. Valeur, E. Gratton, M. Vandeven, N. D. Silva, Y. Engelborghs, K. Willaert, A. Sillen, G. Rumbles, D. Phillips, A. Visser, A. van Hoek, J. R. Lakowicz, H. Malak, I. Gryczynski, A. G. Szabo, D. T. Krajcarski, N. Tamai and A. Miura (2007), Fluorescence lifetime standards for time and frequency domain fluorescence spectroscopy, *Anal Chem*, 79(5):2137–2149

[230] K. Dowling, M. J. Dayel, M. J. Lever, P. M. W. French, J. D. Hares and A. K. L. Dymoke-Bradshaw (1998), Fluorescence lifetime imaging with picosecond resolution for biomedical applications, *Opt Lett*, 23(10):810–812

[231] D. M. Li, J. L. Zhang and M. Anpo (2006), The luminescence properties of coumarin-6 within Ti-HMS, *J Lumines*, 116(1-2):73–78

[232] http://www.iss.com/resources/tech1/, Lifetime of Coumarin 6

[233] S. Senthilikumar, S. Nath and H. Pal (2004), Photophysical properties of coumarin-30 dye in aprotic and protic solvents of varying polarities, *Photochem Photobiol*, 80(1):104–111

[234] M. J. Cole, J. Siegel, S. E. D. Webb, R. Jones, K. Dowling, M. J. Dayel, D. Parsons-Karavassilis, P. M. W. French, M. J. Lever, L. O. D. Sucharov, M. A. A. Neil, R. Juskaitis and T. Wilson (2001), Time-domain whole-field fluorescence lifetime imaging with optical sectioning, *J Microsc-Oxf*, 203:246–257

[235] W. W. Stewart (1978), Functional connections between cells as revealed by dye-coupling with a highly fluorescent naphthalimide tracer, *Cell*, 14(3):741–759

[236] W. W. Stewart (1981), Lucifer Dyes - Highly Fluorescent Dyes for Biological Tracing, *Nature*, 292(5818):17–21

[237] T. Mayr, D. Wencel and T. Werner (2001), Fluorimetric determination of copper(II) in aqueous solution using lucifer yellow CH as selective metal reagent, *Fresenius J Anal Chem*, 371(1):44–48

[238] P. P. Mishra, A. L. Koner and A. Datta (2004), Interaction of Lucifer Yellow with cetyltrimethyl ammonium bromide micelles and the constant suppression of its non-radiative process, *Chem Phys Lett*, (400):128–132

[239] S. C. George, H. Volk and M. Ahmed (2004), Oil-bearing fluid inclusions: geochemical analysis and geological applications, *Acta Petrologica Sinica*, 20(6):1319–1332

[240] G. X. Chi, I. M. Chou and H. Z. Lu (2003), An overview on current fluid-inclusion research and applications, *Acta Petrol Sin*, 19(2):201–212

[241] A. Esposito, H. C. Gerritsen and F. S. Wouters (2005), Fluorescence lifetime heterogeneity resolution in the frequency domain by lifetime moments analysis, *Biophys J*, 89(6):4286–4299

[242] N. H. Oxtoby (2002), Comments on: Assessing the maturity of oil trapped in fluid inclusions using molecular geochernistry data and visually-determined fluorescence colours, *Appl Geochem*, 17(10):1371–1374

[243] N. Blamey, A. G. Ryder, P. Owens and M. Feely (2009), Accurate characterisation of hydrocarbon bearing fluid inclusiosn using frequency domain lifetime measurements., *Manuscript in preparation*

[244] J. Pironon (1990), Synthesis of hydrocarbon fluid inclusions at low temperature, *Am Miner*, 75(1-2):226–229